ARMY RESEARCH LABORATORY

Extended Grassland Calculation Results With Comparisons to PRISCILLA Experimental Data and a Near-Ideal Calculation

Robert G. Ekler
Charles E. Needham
Lynn W. Kennedy

ARL-CR-236 July 1995

prepared by

S-Cubed, a Division of Maxwell Laboratories, Inc.
2501 Yale Boulevard, SE, Suite 300
Albuquerque, NM 87106

under contract

DAAL01-94-P-2257

NOTICES

Destroy this report when it is no longer needed. DO NOT return it to the originator.

Additional copies of this report may be obtained from the National Technical Information Service, U.S. Department of Commerce, 5285 Port Royal Road, Springfield, VA 22161.

The findings of this report are not to be construed as an official Department of the Army position, unless so designated by other authorized documents.

The use of trade names or manufacturers' names in this report does not constitute endorsement of any commercial product.

REPORT DOCUMENTATION PAGE

Form Approved
OMB No. 0704-0188

1. AGENCY USE ONLY *(Leave blank)*	2. REPORT DATE	3. REPORT TYPE AND DATES COVERED
	July 1995	Final, Oct 1993–Mar 1995

4. TITLE AND SUBTITLE

Extended Grassland Calculation Results With Comparisons to PRISCILLA Experimental Data and a Near-Ideal Calculation

5. FUNDING NUMBERS

C: DAAL01-94-P-2257
4G061-415-U2
4G061-515-U2

6. AUTHOR(S)

Robert G. Ekler, Charles E. Needham, and Lynn W. Kennedy

7. PERFORMING ORGANIZATION NAME(S) AND ADDRESS(ES)

S-Cubed, a Division of Maxwell Laboratories, Inc.
2501 Yale Boulevard, SE, Suite 300
Albuquerque, NM 87106

8. PERFORMING ORGANIZATION REPORT NUMBER

SSS-DFR-94-14920

9. SPONSORING / MONITORING AGENCY NAME(S) AND ADDRESS(ES)

U.S. Army Research Laboratory
ATTN: AMSRL-WT-NC
Aberdeen Proving Ground, MD 21005-5066

10. SPONSORING / MONITORING AGENCY REPORT NUMBER

ARL-CR-236

11. SUPPLEMENTARY NOTES

The point of contact for this report is Richard E. Lottero, U.S. Army Research Laboratory, ATTN: AMSRL-WT-NC, Aberdeen Proving Ground, MD 21005-5066. Computer time supplied by HQ, Defense Nuclear Agency.

12a. DISTRIBUTION / AVAILABILITY STATEMENT

Approved for public release; distribution is unlimited.

12b. DISTRIBUTION CODE

13. ABSTRACT *(Maximum 200 words)*

An extended calculation of the non-ideal airblast environment resulting from a PRISCILLA-like nuclear detonation has been completed. This calculation used the results of the S-CUBED THRML[1] code to determine the structure of the preshock turbulence, surface roughness, and material lofted during the burning process in determining the near-surface blast environment. No dust sweep-up was used. The argument is that the roots of the grass will remain intact and prevent the erosion and entrainment of large amounts of dust. Full hydrodynamic definition of the precursor environment is now available from ground zero to a distance of nearly 2 km. Information includes full spatial definition at about 25 selected times and full time-resolved waveforms at over 1,000 locations. The results of the calculation are compared to experimental data from the PRISCILLA shot and show the influence of the more intense thermal layer created by the burning grassland. An accompanying calculation without a thermal layer was also extended over a 2-km range. This calculation served as the "ideal" case. The "ideal" calculation included the effects of surface roughness and turbulence but not an interaction with a thermal layer or dust sweep-up. Results of this calculation are used to quantify the differences specifically caused by thermal interactions.

The enhancement and extent of the precursor effects of this calculation relative to the experiment demonstrate that precursors over desert surfaces do not result in the worst-case environments for detonations over real surfaces. The definition and understanding of the free-field environment is the necessary first step to predicting loads and response of vehicles or other targets subjected to such an environment.

14. SUBJECT TERMS	15. NUMBER OF PAGES
non-ideal blast, dynamic pressure impulse, nuclear blast, airblast, dust, turbulence, thermal precursor	174
	16. PRICE CODE

17. SECURITY CLASSIFICATION OF REPORT	18. SECURITY CLASSIFICATION OF THIS PAGE	19. SECURITY CLASSIFICATION OF ABSTRACT	20. LIMITATION OF ABSTRACT
UNCLASSIFIED	UNCLASSIFIED	UNCLASSIFIED	UL

INTENTIONALLY LEFT BLANK.

FOREWORD

This work was performed for the U.S. Army Research Laboratory (ARL) under contract DAAL01-94-P-2257. The calculations were made using the latest version of the S-Cubed Hydrodynamic Advanced Research Code (SHARC). This code has been upgraded to include a version of a K–ϵ turbulence model, which has been modified by S-Cubed[2] for non-steady, compressible fluid flow. The turbulence model has a rough law of the wall boundary layer model[3] and a dust sweep-up model,[4] both of which were used for the desert calculation; however, no dust sweep-up has been used in the grassland calculation. The K–ϵ model and the rough law-of-the-wall were also used in the near-ideal calculation. It is the combination of high-order differencing, efficient computer algorithms, and realistic physical models that have made the results of these calculations credible.

A conversion table has been provided in Appendix D for the reader's use.

INTENTIONALLY LEFT BLANK.

ACKNOWLEDGMENTS

We would like to acknowledge the efforts of Rich Lottero, Klaus Opalka, and Bud Raley of ARL for making this work possible, and John Keefer and Noel Ethridge of ARA for their guidance in matters of thermal layer development and experimental data interpretation.

INTENTIONALLY LEFT BLANK.

TABLE OF CONTENTS

INTENTIONALLY LEFT BLANK.

LIST OF FIGURES

SECTION 1

BACKGROUND

This calculation is the product of over four decades of research into thermally-precursed airblast. It has been made possible by significant advances in numerical differencing techniques, physical modeling development, and computer hardware improvement. The importance of turbulence and a good boundary layer model were demonstrated during the DIAMOND ARC experiments in 1989[5].

The role of pre-shock dust has been debated for many years. The thermal layer generated over a grassland is significantly different from that over a desert surface[6a,6b, 7, 8]. The role of preshock dust is significantly reduced. The mass of ash from pyrolyzed or burned organic material, along with some dust particulates from the soil lofted prior to shock arrival, far exceeds the mass of preshock dust over a desert surface. The energy released by the oxidation of organic material increases the sound speed in the thermal layer far above that over a desert surface. The cloud of ash and dust creates an optically-dense layer which absorbs incoming radiation before it reaches the ground. This energy, combined with that released by the burning organic material, produces a complex structure within the thermal layer which can be more than two meters thick. In general, the part of the layer near the surface is cooler with the maximum temperature (and sound speed) at some distance above the surface (Figure 1). The relative timing of the energy release by organic material, which is partially controlled by turbulent mixing of oxygen from above, along with incident radiant energy from the fireball and the arrival time of the shock all play a role in the structure within the layer and the height of the layer. The resultant layer is thicker, more intense, and extends further than the thermal layer generated over a desert surface.

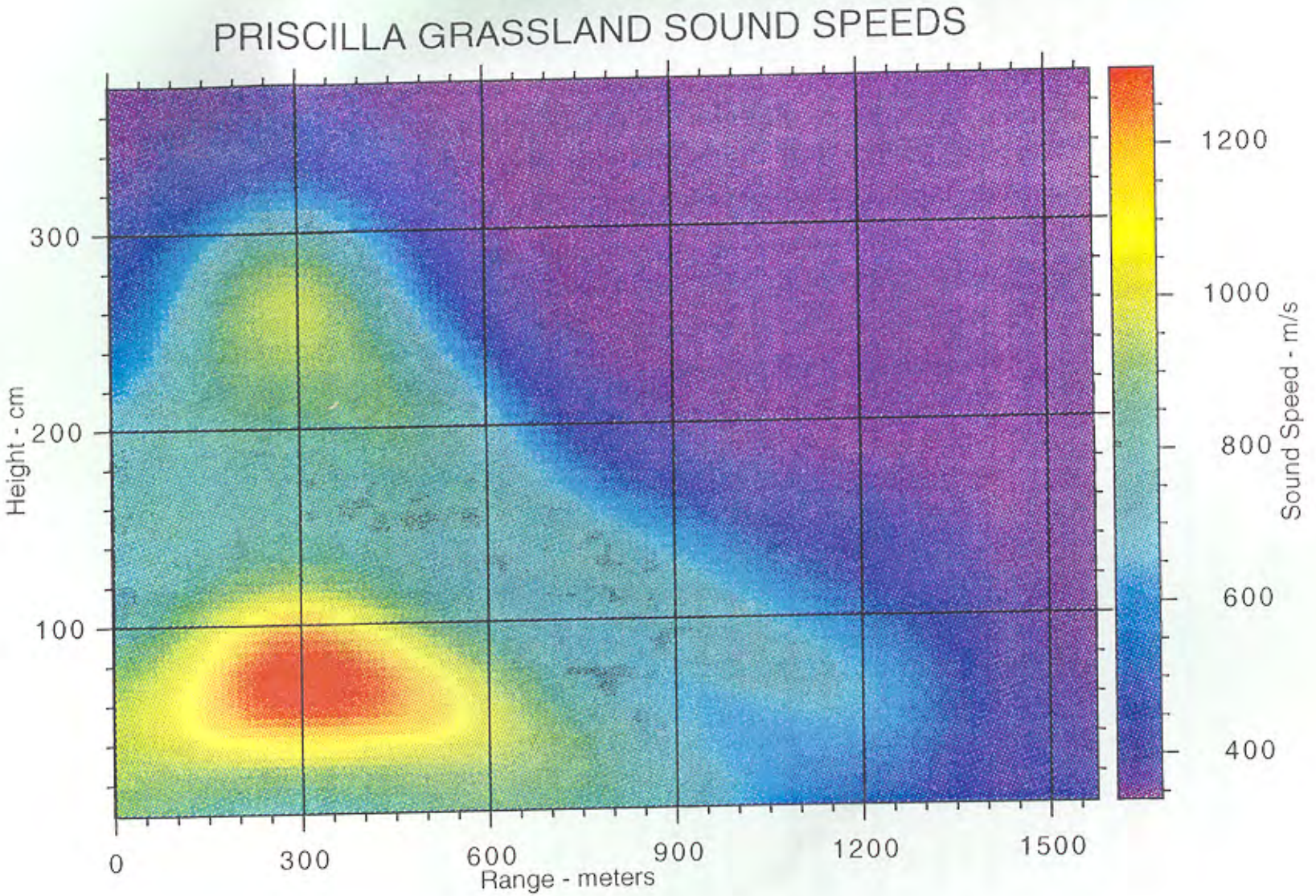

Figure 1. Contour of thermal layer.

SECTION 2

INITIAL CONDITIONS

The calculations described in Reference 9 were used as initial conditions for the extended calculations reported here. The "ideal" calculation was started from a time of two seconds and run to a time of four seconds.

The grassland thermal layer calculation was restarted at a time of 0.23393 seconds when the shock had reached about 390 meters in ground range. The thermal layer temperature distribution was nearly identical to that of the earlier calculation of Reference 9. The zoning in the earlier calculation was 10 cm in the constant subgrid but could not be continued for practical cost reasons. The minimum zone size used in the extended calculation was increased to 15 cm, which meant that average temperatures over the new zone size were slightly different from those averaged over 10 cm. This change in zone size also made it necessary to stabilize the thermal layer for the zone size of this calculation. The thermal layer was modified by averaging the results of the THRML code over the 15 cm zoning of the SHARC calculational mesh. The average density was determined and the energy modified until the zone was in pressure equilibrium with the ambient atmosphere. This modification was necessary to prevent the thermal layer from moving prior to shock arrival. The resulting maximum sound speed as a function of ground range is shown in Figure 2.

Both calculations (ideal and grassland) used the S-CUBED K–ε turbulence model. This model is an extension of the usual K–ε model, which uses a variable coefficient for formation and dissipation of turbulence, based on local conditions and the history of the flow. The S-CUBED modifications extend the K–ε model to compressible, non-steady flows. Both calculations used a law-of-the-wall for real surfaces in conjunction with the turbulence model. The ideal calculation used a smooth wall Clauser law-of-the-wall and the grassland used a rough law-of-the-wall to represent the surface interaction.

The ideal calculation used a shock-following subgrid with 10-centimeter zones throughout most of the calculation. The precursor calculation used a similar shock following subgrid, but had 15-centimeter zones for most of the calculation duration.

PRISCILLA DESERT CALCULATION
THERMAL LAYER REVISITED

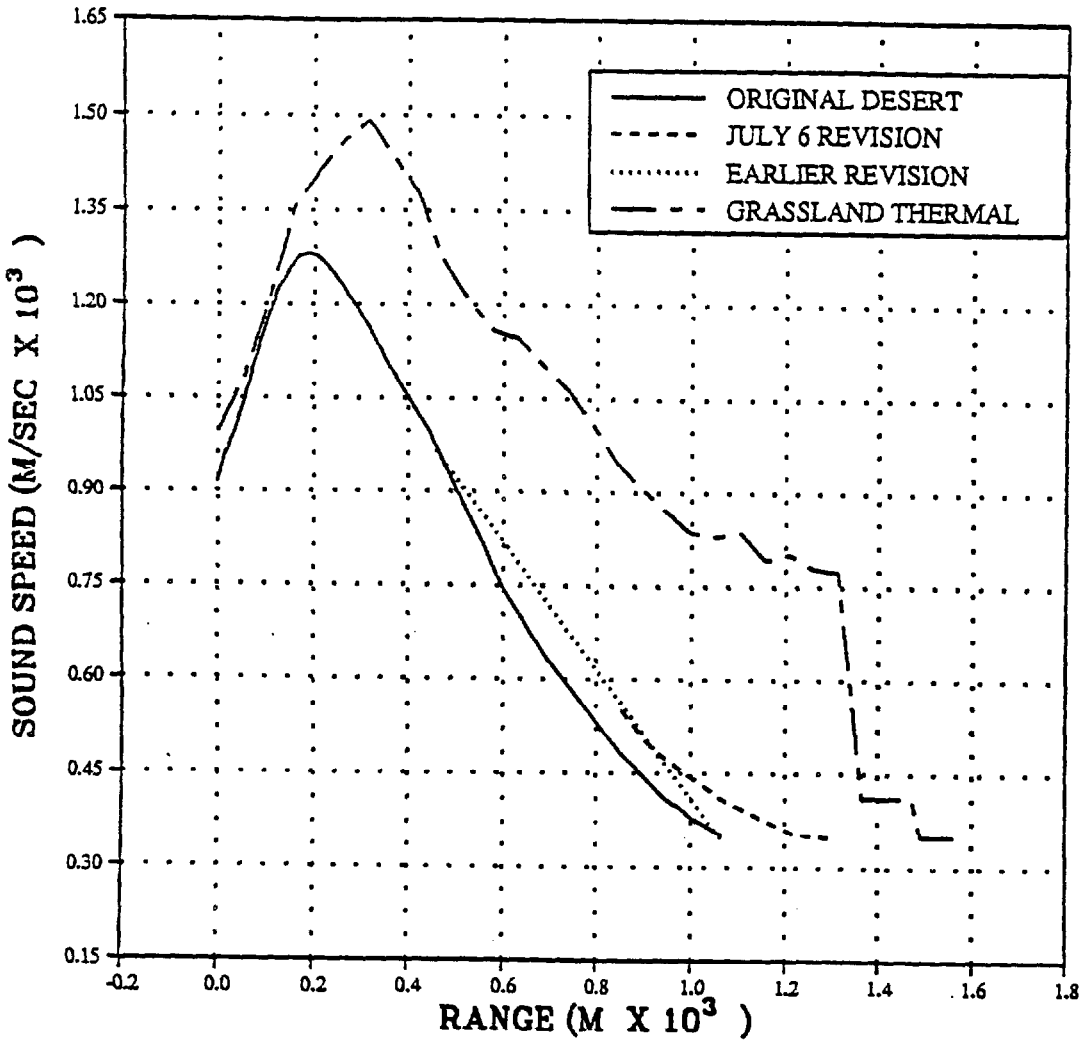

THIS PLOT SHOWS THE GRASSLAND'S THERMAL LAYER MAXIMUM VALUE. THE CALCULATION WAS REMAPPED WHEN THE PRECURSOR TOE WAS JUST SHORT OF 1.5 KILOMETERS IN ORDER TO EXPEDITE RESOLUTION OF A PROBLEM WITH PRESSURE INSTABILITY. FOR THIS REASON THE SOUND SPEED DROPS ABRUBTLY TO AMBIENT.

Figure 2. PRISCILLA grassland maximum sound speed vs. range.

SECTION 3

CALCULATED IDEAL RESULTS

The results of the extended ideal calculation are discussed in the previous volume of this report[10]. Results of the ideal calculation are included here to provide a basis of comparison.

Summary plots of arrival time, overpressure, overpressure impulse, dynamic pressure, and dynamic pressure impulse are contained in Appendix A for the results of the ideal calculation. These results are compared to the results from the grassland calculation and to experimental data from the PRISCILLA event. Waveform comparisons at a number of selected ranges are included in Appendix B. The waveforms are compared to the grassland calculation results and to experimental waveforms where possible.

We have also included a number of parameter-versus-height plots at selected ground ranges. These extend from ground level to 50 feet above the ground. Comparisons are made with the results from the thermal layer calculation. These plots are included in Appendix C. Overpressure, arrival time, and impulse for the ideal calculation show very little variation in altitude. At large distances (those beyond 4,000 feet), the rough surface has a small effect in reducing the near surface dynamic pressure.

SECTION 4

CALCULATED GRASSLAND SURFACE RESULTS

A summary of the initial conditions is given in Section 2. Because the same thermal layer was used for this calculation as that reported in Reference 9, the results for distances less than 400 meters are the same as those of Reference 9 and will not be discussed here.

No dust sweep-up model was used in the grassland calculation. We felt that the roots of the grass would remain intact and prevent the erosion of significant amounts of soil during the passage of the blast wave. The preshock thermal layer was loaded with the mass of the organic material and any preshock lofted dust. These combined materials were carried throughout the calculation and treated as fully interactive fluid dust.

The calculation was carried to a time of 3.6 seconds and a distance of just under two kilometers. At the end of the calculation, the positive duration of the overpressure and dynamic pressure were complete for all ranges having overpressures greater than or equal to five psi.

The dynamic pressures reported are the result of both air and dust contributions. The dust contribution has been assigned a "registry coefficient" of 0.5. The dust and air were treated as fluids and dynamic pressure was calculated as:

$$DP = 0.5 * rho * u * |u|, \quad (1)$$

where rho is the total density (air plus dust) of the zone.

4.1. SUMMARY PLOT DESCRIPTION.

The arrival-time curves on the first figure in Appendix A show that the precursor separates from the ideal at a distance of less than the height-of-burst (~200 m) and remains ahead of the ideal arrival throughout the two-kilometer ground range. The maximum separation between precursor arrival and ideal is just over 200 meters at a time of about 1 second and a distance of about one kilometer. The waveforms of Appendix B show that the precursor arrives before the ideal at ranges as small as 200 meters.

The summary plots of Appendix A show that the maximum overpressure in the grassland case is as little as one-third of the ideal overpressure. The overpressure at the precursor front may be less than a tenth of the peak pressure occurring later in the waveform. The overpressure impulse differs by less than ten percent from the ideal over the entire range of comparison.

The maximum dynamic pressure is, at some ranges (*e.g.*, 900 m), as much as a factor of four greater than the ideal. The peak dynamic pressure curve shows that the precursor peak dynamic pressure is greater than the ideal to a range of over 1.4 kilometers. The dynamic pressure impulse exceeds the ideal by as much as a factor of eight between ground ranges of 600 and 850 meters, then falls below the ideal values at ranges greater than 1.4 km.

4.2. WAVEFORM COMPARISON DESCRIPTION.

The waveforms of Appendix B show the details of many of the features described above. At a range of 762 meters, the ground-level overpressure waveform has a rounded front, with a negative overpressure between the front and the peak overpressure. The peak pressure occurs nearly 300 ms after first arrival. The peak overpressure is about one-half of that for the ideal calculation. Overpressures at three and ten feet are very close to those at ground level. The dynamic pressure waveform shows that the maximum pressure occurs in a secondary peak some 200 milliseconds behind the precursor wave. The peak is about more than four times the ideal peak. A tertiary peak occurs about 500 ms after arrival with a peak dynamic pressure about three times the ideal. The dynamic pressure impulse at this range is nearly an order of magnitude greater than the ideal.

At a range of 914 meters, the overpressure waveforms are similar and the non-ideal peak remains about half that of the ideal. A negative phase still occurs between the precursor arrival and the peak overpressure. The precursor arrives nearly 600 ms prior to the peak overpressure. The dynamic pressure waveform at this range is complex with the maximum occurring over half a second after first arrival but before the arrival of the peak overpressure. Several rounded peaks are evident, with the fifth peak being the maximum. The peak is about six times that of the ideal. The increase in separation time between first arrival and the peak shows that the precursor is still growing at this range. The dynamic pressure impulse remains about an order of magnitude greater than the ideal.

By 1,067 meters, the grassland calculation shows a rounded front, an inflection, a long plateau, and a rounded rise to a peak overpressure which is about one-third that of the ideal. The slow rise to the peak is an indication of strong precursor development. The dynamic pressure waveform shows multiple peaks and a rapid rise after first arrival. The peak dynamic pressure is twice the ideal peak. The decay after the peak is reached is much more rapid than in the ideal case and is followed by secondary peaks a full second after first arrival, whichhis leads to a dynamic pressure impulse of about eight times the ideal.

At a range of 1,219 meters, the overpressure waveform retains the precursor form with over a half second between arrival and peak overpressure. The major difference between precursed and ideal at this range is the long, slow rise to the peak overpressure, with the peak about two-thirds of the ideal. The dynamic pressure waveform shows that the peak of the precursed waveform is only about 50 percent greater than the ideal. The impulse still exceeds the ideal by a factor of three.

By a range of 1,524 meters, the ideal and desert precursor waveforms were nearly identical. The grassland overpressure waveform is starting to clean up. The time between first arrival and peak overpressure has been reduced to about 300 ms. The peak of the main wave has a sharp rise, indicating that clean-up has begun. This is nearly 50 meters beyond the end of any significant heated layer. The extent to which precursor waveforms can be propagated beyond the thermal layer is the result of both the growth of the distance between the precursor and main wave during precursor formation and the suddenness with which the organic thermal layer terminates.

4.3. VARIATION OF PARAMETERS WITH HEIGHT.

Appendix C contains comparisons of various parameters as functions of height at selected ground ranges. The plots cover the variation with altitude from ground level to 15 meters above the ground. At the 640-meter ground range, the peak precursor overpressure is about one-half that of the ideal with the near ground-level pressure only about 10 percent greater than that above 10 meters in altitude. The ideal varies with altitude to less than one percent.

At 701 meters, some variation in peak overpressure is seen, but the variations are less than 15 percent in the precursor case. In general, the precursed maximum overpressures are about one-half those of the ideal. The ideal shows no variation with altitude.

The comparison at 777 meters shows the precursor pressures to be less than half those of the ideal case. Variations with altitude are about 20 percent for the precursor and less than one percent for the ideal. The precursor peak remains about half of the ideal peak. This trend continues through the 899 meter ground range.

The temperature and sound speed in the thermal layer decrease rapidly beyond a range of 1.3 kilometers. This marks the beginning of the clean-up phase of precursor propagation. The variation with height at 0.99 to 1.11 kilometers shows little variation with height as the layer cools. At 0.99 kilometers, the peak overpressure at 15 meters above the surface is only about 15 percent less than near the surface, but is about one-third that of the ideal. The ideal remains unchanged with height. By 1.11 kilometers, the overpressure is nearly constant with height and differs from the ideal by more than a factor of two.

The thermal layer terminated at the 1.3 kilometers range; very little pre-shock heating was present beyond this range. The variations with height beyond the end of the thermal layer are caused by residual differences in energy distribution in the shock and transient flows which are attempting to equilibrate along the shock front. Variations in height are small, of the order of twelve percent, and the differences between precursed and ideal are of the same order.

The arrival time as a function of height plots show no surprises; the curves are very smooth and show that the arrival at ground level is earlier than at any other height. This is in agreement with observed arrival times on structures from the PRISCILLA event. The precursor arrival times are earlier than the ideal for all ground ranges. Beyond the 4,300-foot range, the arrival time does not change with height.

The dynamic pressure plots of Appendix C show that the dynamic pressure nearest ground level is about a factor of two lower than at an elevation of three feet at the 640-meter ground range. This is the opposite of what was observed in the desert case and is the result of the temperature distribution within the layer. For the desert case, the highest temperatures were at or very near ground level, whereas the peak temperatures in the grassland case are found one to two meters above the surface. By 777 meters, the maximum dynamic pressure occurs one to two meters above the ground. For all ground ranges less than about 1.5 kilometers, the precursed dynamic pressure exceeds that of the ideal near ground level. At 1.49 kilometers, the dynamic pressure near ground level is more than twice the ideal and remains above the ideal to a height exceeding 15 meters above the surface.

As with the overpressure, several oscillations are present in dynamic pressure as the precursor cleans up. Apparently, energy is exchanged between dynamic pressure and overpressure as the shock front adjusts to the absence of a thermal layer.

The most dramatic effect is seen in the dynamic pressure impulse. At a range of 701 meters, the near-surface dynamic pressure impulse from the precursor calculation exceeds the ideal by about a factor of three, while at the two meter elevation, the ideal is exceeded by about an order of magnitude. The impulse remains greater than the ideal for all heights. Some effect of the boundary layer can be seen in the reduction of dynamic pressure impulse for the ideal case also. The effect of the boundary layer is evident at all ranges. The ideal impulse is also reduced near ground level.

The maximum impulse of the precursor is greater than the ideal at all heights, but approaches the ideal near the 15 meter height throughout the clean-up phase, to a distance of nearly 1.2 kilometers. The impulse drops sharply beyond 1.2 km and falls below the ideal above a height of 6 meters at the 1.25-kilometer ground range. By 1.5 kilometers, the dynamic pressure impulse has fallen below that of the ideal for all heights and remains below the ideal at all greater ground ranges.

SECTION 5

COMPARISONS OF CALCULATIONS WITH EXPERIMENTAL DATA

The summary plots of Appendix A contain comparisons of calculations with nearly all available data from the PRISCILLA event.

The arrival-time curve shows that the grassland arrival is earlier than the vast majority of the data. In general, the desert calculation shows good agreement with the measured data, and its wave front always arrives earlier at any given range than does that of the ideal case. The grassland precursor arrives over 0.4 seconds prior to the ideal at a range of 1 kilometers. The density contour plot (Figure 3) at a time of 700 ms, shows that the precursor extends 200 meters ahead of the free-field shock. The upward-moving precursor shock intersects the Mach stem at a height of over 100 meters. The vortex, which contains the highest dynamic pressures and gradients, is over 250 meters in extent and 30 meters in height. The highest velocities are found about 200 meters behind the precursor front and at a height of 5 meters above the surface (Figure 4). The upward-moving precursor shock is somewhat curved, indicating the beginnings of cleanup at this time. The angle it forms with the ground is between 25 and 30 degrees. All of these characteristics indicate a stronger, more extensive precursor than was observed in the PRISCILLA experiment.

Figure 5 shows the structure of the precursor at a time of 1.5 seconds. The precursor shock is continuously curved from ground surface to its intersection with the Mach stem. The precursor continues into the cleanup phase. It is still about 200 meters ahead of the free air shock; the intersection of the upward moving shock with the Mach stem is over 200 meters above the surface. A number of vortices have been shed from the ground-level vortex as cleanup has progressed. One large vortex is centered 400 meters behind the precursor and 50 meters above the surface. A second vortex near 950 meters is about to be shed. Velocities near ground level are on the order of three to four hundred meters per second. This is all occurring at distances at which the desert precursor had nearly cleaned up.

At a distance of 1.9 kilometers, the precursor is still over 100 ms ahead of the ideal. The Mach number of the shock at this distance is only 1.14. The distance by which the precursor leads the ideal can never be overcome because the shocks always travel faster than Mach 1 and the ideal and precursed shocks have essentially the same overpressure as a function of distance for distances beyond 1.5 kilometers.

The overpressure summary plot includes experimental data from ground level, three-foot and ten-foot heights. The three- and ten-foot elevation data agree better with the ideal overpressures than with the precursor values. The calculated overpressures are for ground level only. Two overpressures are plotted for each calculation: the first peak and the maximum. The only range for which these curves differ in the ideal case is during double and complex Mach reflection. This limited region extends from about 200 to 300 meters. For the precursor calculation, the peak overpressure falls below the ideal almost immediately. As the precursor forms and generates a double peaked waveform, the two curves diverge. At a range of 350 feet, only one peak is present, but by 500 feet a weak shock having a peak of about 10 percent[1] of the maximum leads the so-called

[1] The agreement of the computation with the BRL waveform at 1650 feet is apparently fortuitous. The timing on the BRL waveform is now believed to be in error; the BRL waveform should be expanded so that the maximum peak coincides with that on the SRI peak. The BRL self-recording gages used in PRISCILLA did not have a timing-mark generator.

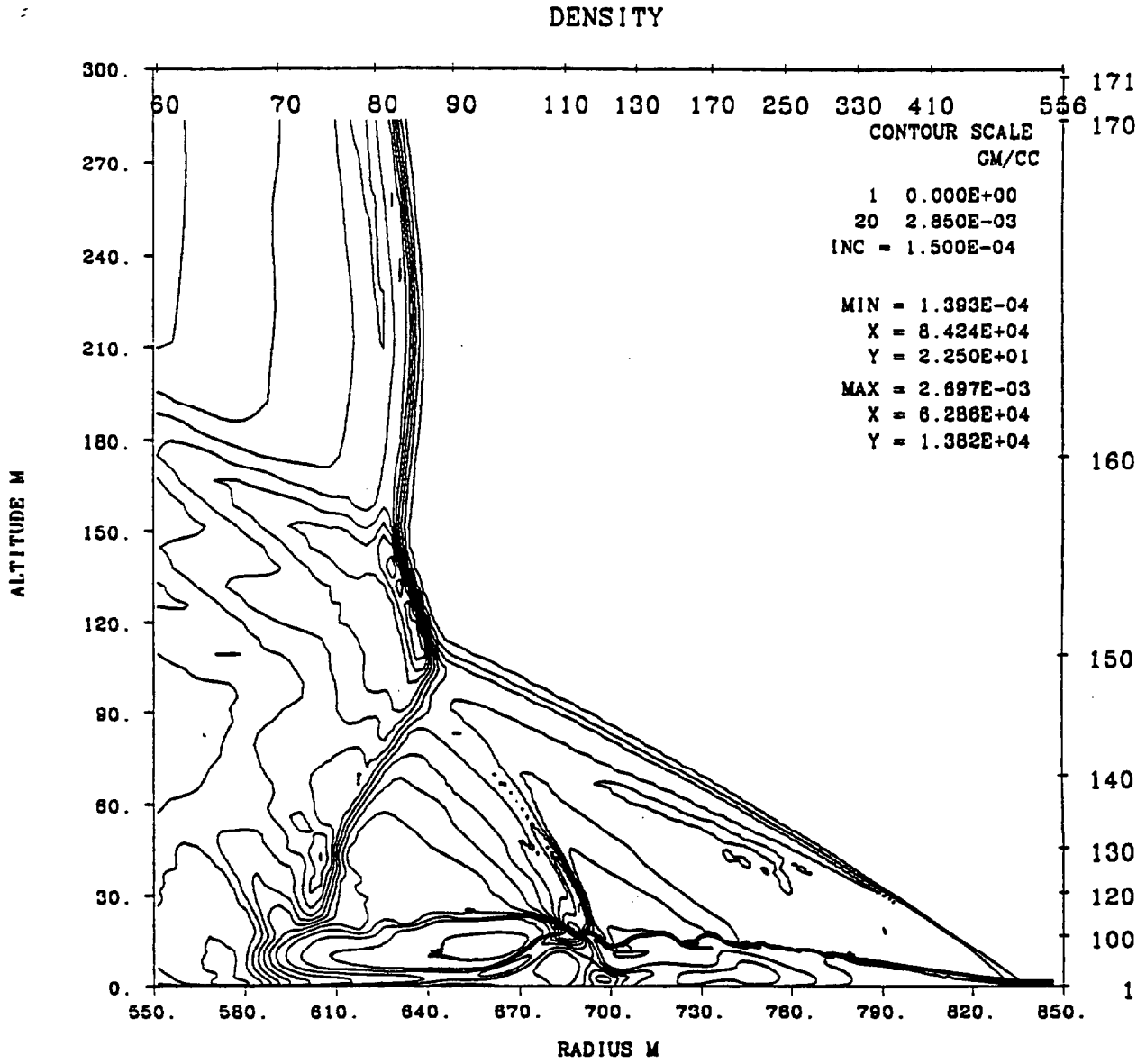

Figure 3. Density contour at 700 msec.

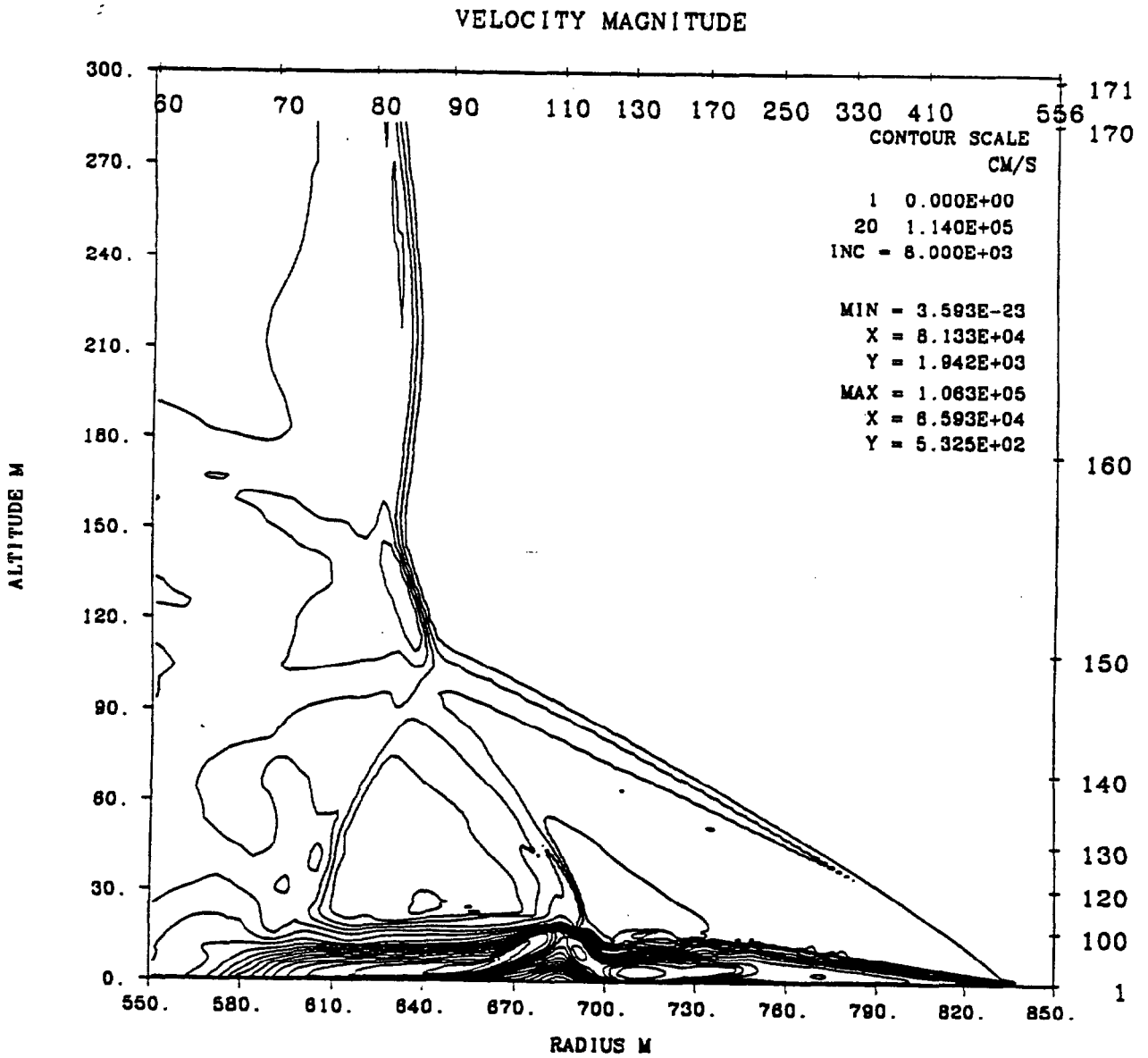

Figure 4. Velocity magnitude at 700 msec.

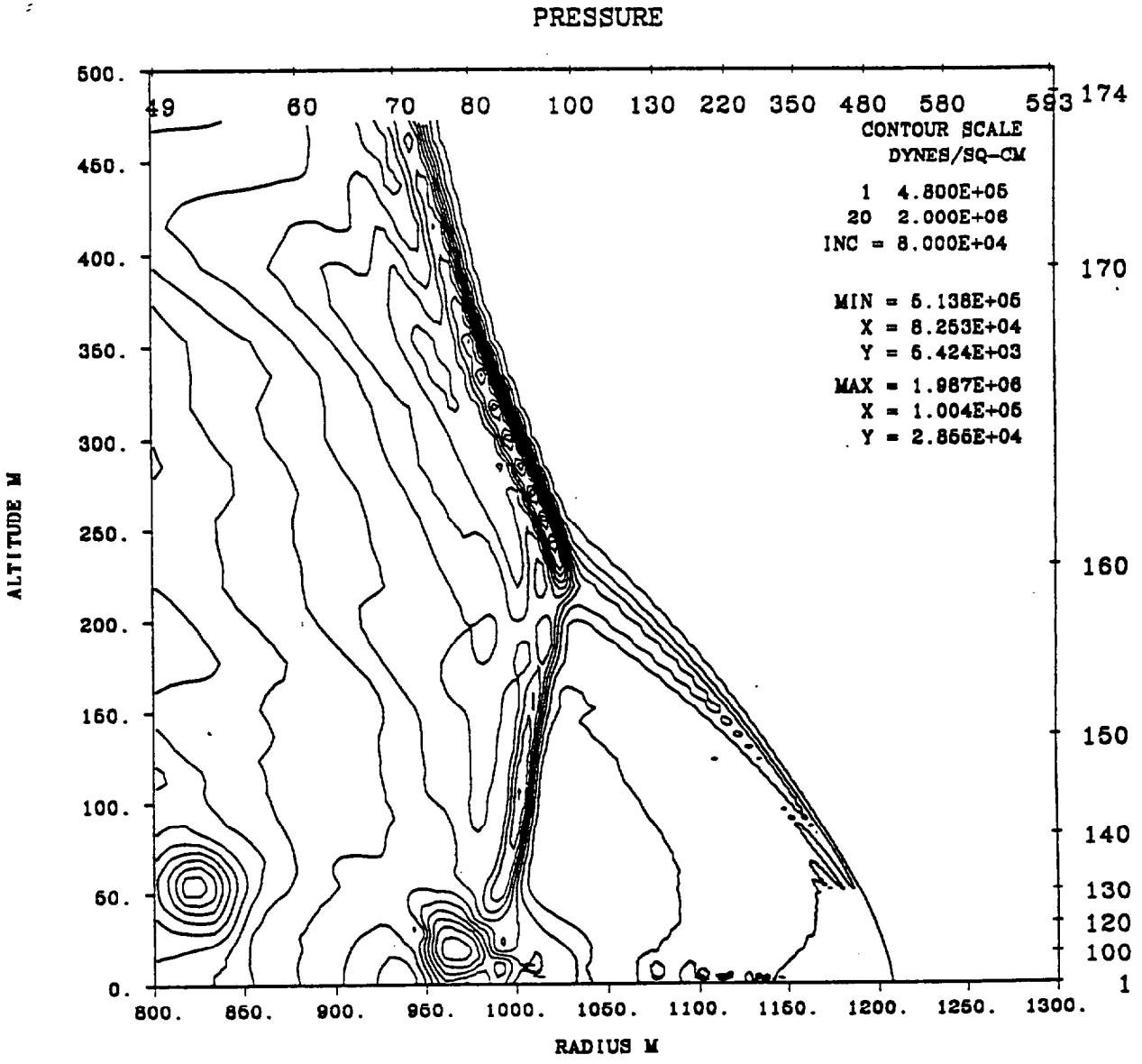

Figure 5. Pressure contour at 1.5 seconds.

"main wave". The precursed overpressure peaks fall below those of the ideal to a range of just over 4,000 feet, the end of the thermal layer. The first peak may be as little as 10 percent of the maximum overpressure at a given range.

The calculated precursor overpressure falls below nearly all of the experimental data beyond a range of 700 meters. It should be noted that the overpressure reaches a relative minimum at a range of just over 1.1 kilometers, then rises to a relative maximum at about 1.45 kilometers. This maximum is slightly higher than the ideal at this range. The peak then falls back to the ideal level for the remainder of the calculated ranges. This behavior is in agreement with the experimental data from several nuclear shots, including PRISCILLA.

The increase in overpressure as a function of ground range, beyond the 1.3-kilometer range, has been observed experimentally and is now confirmed by calculation. The rise and fall of the overpressure with range leads to a triple-valued function for the range of a given overpressure; *e.g.*, there are three ranges at which 40 KPa occurs. The calculation indicates 900 meters, 1.4 kilometers, and 1.6 kilometers all had a peak overpressure of 40 KPa. This triple-valued function is the cause of the non-ideal height-of-burst curves having loops and multiple values as a function of ground range and height of burst. These characteristics are real, calculable, and we believe that we now understand them.

The overpressure impulse data have considerably more scatter than the peaks. The calculations fall near the high side of the data. Both the ideal and precursed overpressure impulses are within a few percent of one another. The causes for the data scatter can be seen in the waveforms of Appendix B. Some waveforms fall below ambient at a relatively early time after shock arrival, while others do not return to ambient for an extended period. Such scatter is an indication of the difficulty of making measurements in the nuclear environment and the variety of waveforms measured at the same ground range. The waveforms depend on the integrated history of the interaction of the shock with the thermal layer, and surface irregularities contribute significantly to variations in this history.

The peak dynamic pressure summary plot shows that the peak measured values differ, in general, by about a factor of two to three from the ideal. The grassland calculation is above the ideal for all ground ranges beyond 150 meters.

The dynamic pressure impulse data, taken three feet above the surface, fall below the grassland precursor calculated results. The data and the calculation indicate that for some ranges the dynamic pressure impulse may exceed the ideal by more than an order of magnitude.

The waveforms of Appendix B include all available desert line waveforms. No effort has been made to edit, delete, or emphasize any particular waveform or comparison. Many of the gages did not have associated arrival times, but times were given as relative to first signal arrival. We have shifted all grassland waveforms so that the first signal arrives at the time of the calculated precursor waveform. Because the data was gathered over a dusty desert surface and the calculation represents the thermal environment over a grassland, we did not expect detailed agreement with the waveforms.

The calculated waveforms of Appendix B represent the mean flow parameters at the positions given. The calculations include the turbulent contribution as a separate parameter. Waveforms using a combination of the mean parameters and the turbulent contribution can be reconstructed from the calculations. This reconstruction includes a full frequency distribution of the Kolmogorov spectrum. The resulting waveforms must

then be low-pass filtered to the characteristics of a given gage before comparisons can be made; this has not been done here. The calculated waveforms are therefore somewhat smoother than the data because of the lack of the turbulent component. The turbulence will add oscillations on the waveforms, but impulse values will not be changed.

As early as 107 meters the effect of the intense thermal layer can be seen on the grassland waveform. The rise is not sharp and the peak overpressure is very rounded. At 137 meters the beginnings of precursor separation can be seen with a first peak of less than 400 KPa and a rounded peak of nearly 4 MPa. This is not seen in the desert precursor data.

By a distance of 168 meters the precursor extends over 10 ms ahead of the "main wave," in surprisingly good agreement with the desert data. At 198 meters the precursor leads the main wave by nearly twice as much as measured during PRISCILLA. This is a good indication of how much hotter this layer is than was present in the experiment.

The precursor continues to grow with distance and by 320 meters is so far extended that a negative phase begins to build between the precursor and the peak. This negative phase grows in depth and duration. At a distance of 686 meters the precursor arrives nearly 450 ms prior to the peak overpressure. A strong negative phase continues to exist. The negative phase persists to a distance of over 900 meters.

The first indication of clean-up is after the 900-meter range where the separation of the precursor has grown to nearly 700 ms. By 1.067 kilometers the negative phase has filled in and the separation of the precursor has just begun to decrease.

The clean-up continues, as seen at the 1.2-kilometer range. The calculation has a shorter separation, a rounded front, and a higher second peak. The peak is well below that of the experimental data, indicating that the grassland thermal layer is significantly warmer than observed in PRISCILLA at this range. The experimental waveform falls on the ideal curve just after the peak.

The extended clean-up of the calculation is further demonstrated in the waveforms compared at 1.5 kilometers. The experimental data shows no separation while the calculation has over 250 ms between the first and second peaks.

SECTION 6

CONCLUSIONS

The results of the "ideal" calculation serve as a benchmark for the definition of the entire airblast flowfield over a realistic surface. Noel Ethridge of ARA is currently making detailed comparisons of the results of this calculation with previous calculations and with height-of-burst curves. The preliminary indications are that the current results show excellent agreement with previous work. More details of this comparison will be included in the ARA volume of this report.

The ideal calculation is being and will be used to compare and quantify the effects of dust and thermal layers. The zone size remained at 10 centimeters in the shock-following sub-grid to a distance of over 1.2 kilometers. The zone size in the subgrid was then gradually increased to a maximum of 30 centimeters as the shock approached two kilometers. The resolution is adequate for this calculation to be considered state-of-the-art.

The grassland calculation required some compromise on resolution. The moving subgrid contained zones with dimensions of 15 centimeters throughout the calculation. This compromise was necessary in order to assure completion of the calculation within cost constraints. A grassland thermal layer calculation with 10-centimeter resolution at the PRISCILLA scale is still a very desirable goal. The very small zoning required for the desert calculation is not as critical for the grassland case because the thermal layer is upwards of two meters thick, whereas the desert layer is the order of 15 centimeters thick. This calculation has sufficient resolution to answer many of the questions about thermal layer temperature distribution and the role of temperature inversions within the thermal layer on the overall flowfield. A higher resolution calculation will require careful reconsideration of the temperature distribution in the thermal layer, the extent of the high sound-speed region, and the consequences of temperature gradients on precursor cleanup.

The grassland precursor calculation results, presented here, show that the grassland layer generates a more severe environment than a desert surface. This comparison includes arrival times, overpressures, dynamic pressures, impulses, and waveform details. We now have defined the flowfield for a more severe case than the PRISCILLA event in sufficient detail to provide high quality environment descriptions. The non-ideal effects extend well beyond those measured over the desert surface and have significant implications for equipment deployed over vegetated surfaces.

The results of this calculation are being transferred to magnetic media and will be available for further detailed analysis in the future. The large enhancements in dynamic pressure and dynamic pressure impulse were achieved without the entrainment of large amounts of dust. The dust contribution to the dynamic pressure in this case was minimal. The growth of a boundary layer and the interaction of the precursor with the boundary layer can be more fully examined. The role of turbulence in vortex generation and separation behind the precursor is yet to be addressed in detail. Many insights into these phenomena and some answers are now available, but further analysis is required to exploit fully this pair of computations.

REFERENCES

1 Rogers, S.H., "Stressing Thermal Layer Sensitivity to Parameters in the THRML Code Model," Defense Nuclear Agency Report DNA-TR-90-10, June 1990.

2 Pierce, T.H., "Numerical Boundary Layer Analysis with K-E Turbulence Model and Wall Functions," Defense Nuclear Agency Report DNA-TR-87-15, September 1986.

3 Barthel, J.R., et. al., "A Computational Model for Precursed Airblasts Over Rough Surfaces," S-Cubed Report SSS-R-89-10003, August 1989.

4 Pierce, T.H., "Turbulence and Real-Surface Sub-Models in S-Cubed Hydrocodes," S-Cubed Draft Report DTR-91-12671, 1991.

5 Needham, C.E., et. al., "Theoretical Calculations for Precursor Definition," Defense Nuclear Agency Report DNA-TR-90-18, September 1990.

6a Swift, L.M., Sachs, D.C., and Kriebel, A.R., "Operation PLUMBBOB, Project 1.3: Air-Blast Phenomena in the High Pressure Region," WT-1043, Stanford Research Institute, Menlo Park, CA, December 1960.

6b Bryant, E.J., Keefer, J.H., Swift, L.M., and Sachs, D.C., "Operation PLUMBBOB, Projects 1.8a and 1.8c: Effects of Rough and Sloping Terrain on Airblast Phenomena", WT-1407, Ballistic Research Laboratories, Aberdeen, MD, July 1962.

7 Operation PLUMBBOB, Event PRISCILLA, documentary photography, available from DASIAC film archives, Kaman Sciences, Corp., P.O. Box 1479, Santa Barbara, CA 93102-1479.

8 Banister, J.R., and L.J. Vortman, "Operation PLUMBBOB, Project 34.1: Effects of a Precursor Shock Wave on Blast Loading of a Structure," WT-1472, Sandia Corporation, Albuquerque, NM, October 1960.

9 Crepeau, J.E., et. al., "SHARC Hydrocode Calculations of the PRISCILLA Event," S-Cubed Report SSS-DFR-93-14283, October 1993.

10 Needham, C.E., Ekler, R.G., and Kennedy, L.W., "Extended Desert Calculation Results with Comparisons to PRISCILLA Experimental Data and a Near-Ideal Calculation (Draft Report)," S-Cubed Report SSS-DTR-94-14802, September 1, 1994.

INTENTIONALLY LEFT BLANK.

APPENDIX A
PARAMETER SUMMARY PLOTS

This Appendix contains summary plots of hydrodynamic parameters as a function of ground range. Each plot contains the results of the ideal calculation, the grassland calculation, and desert experimental data. No dynamic pressure measurements were made at ground level. All the experimental dynamic pressure data were taken at least three feet above the surface. Many of the dynamic pressures from the experiment were derived from stagnation pressure measurements at a 3-foot elevation and the overpressure measurements at ground level. The results from the PRISCILLA calculation show that the overpressure varies between ground level and three feet in the region of strong precursor and the assumption of equal overpressures may be in error by 10 percent or so.

All measured dynamic pressures are taken without regard to the type of gage or its dust registry coefficient. The calculated dynamic pressures include the dust dynamic pressure contribution. In the plots from these calculations, the dust is treated as a fluid and has a registry coefficient of 0.5.

PRISCILLA
ARRIVAL TIME VS RANGE
AT GROUND LEVEL

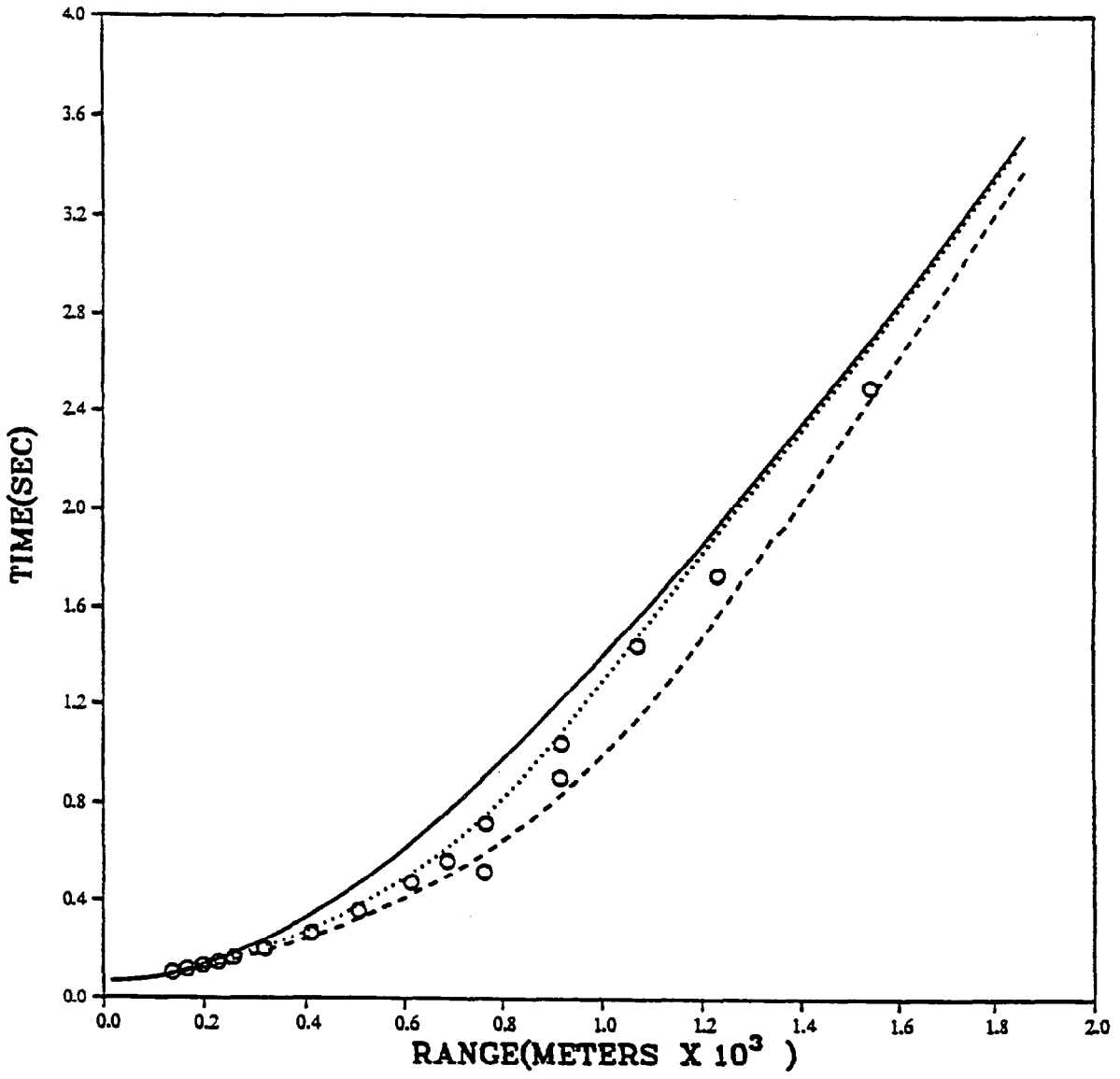

PRISCILLA
ARRIVAL TIME AT GROUND LEVEL

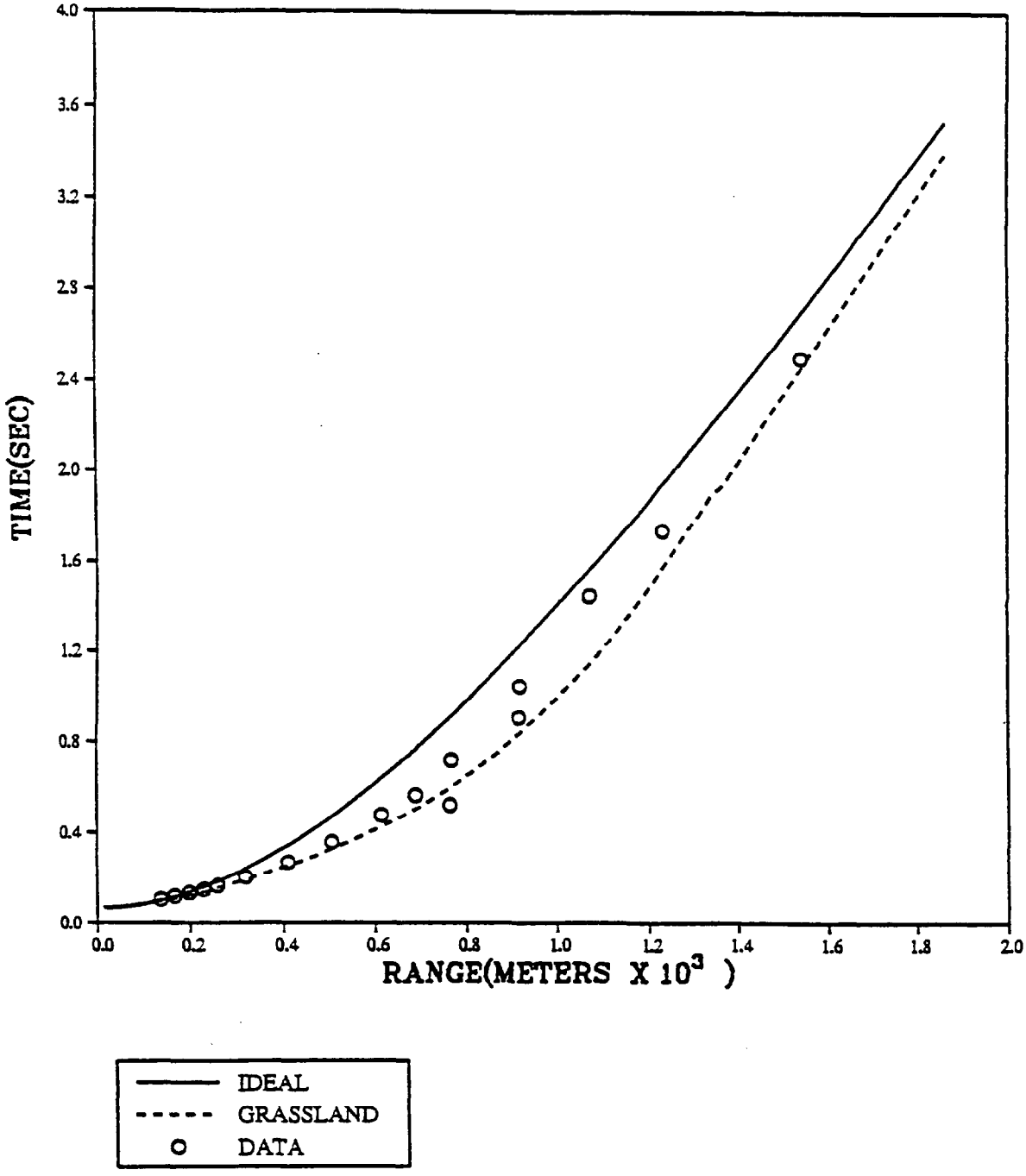

PRISCILLA GRASSLAND
PEAK OVERPRESSURE VS RANGE
AT GROUND LEVEL

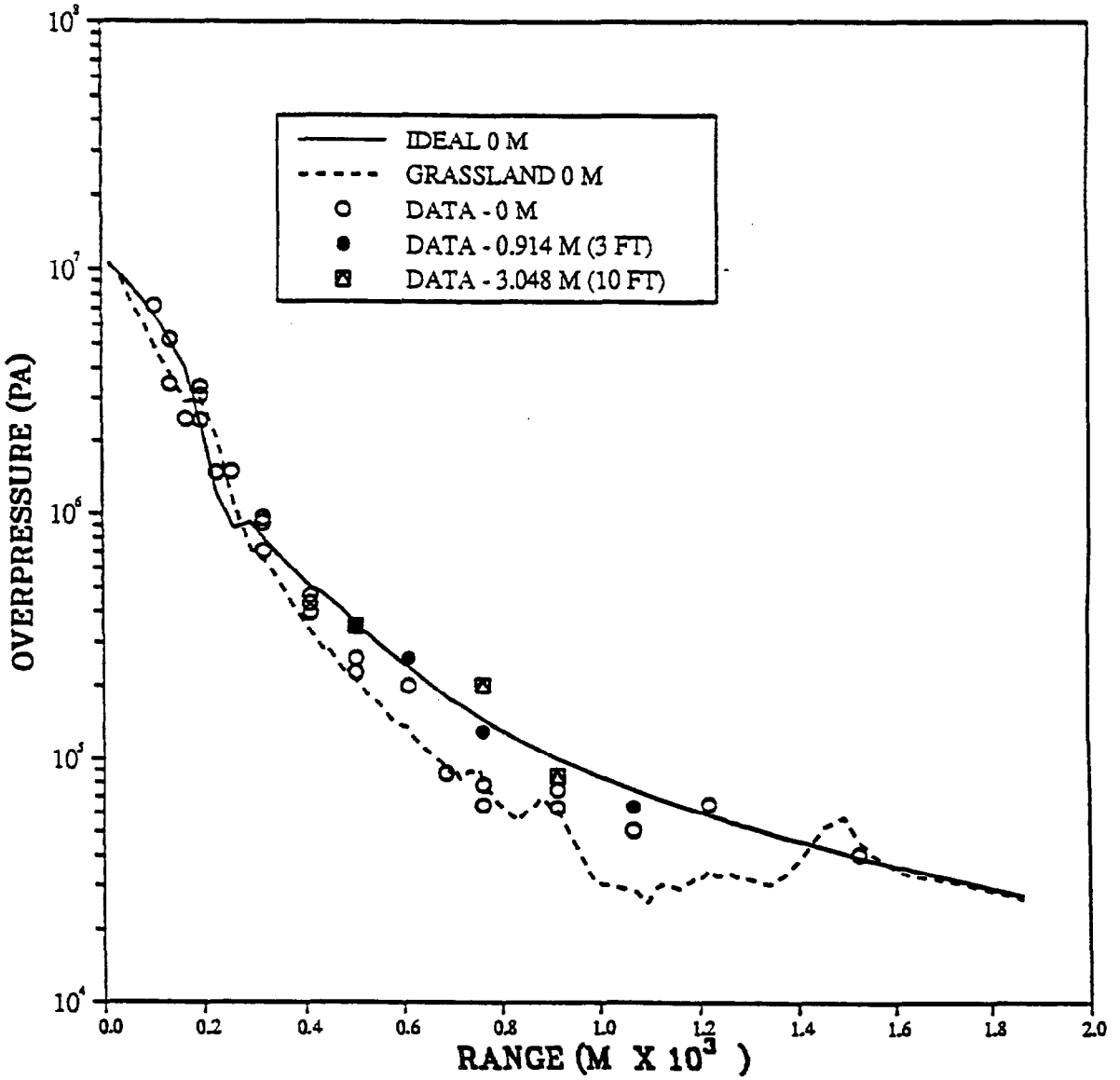

PRISCILLA GRASSLAND
PEAK OVERPRESSURE VS RANGE
AT GROUND LEVEL

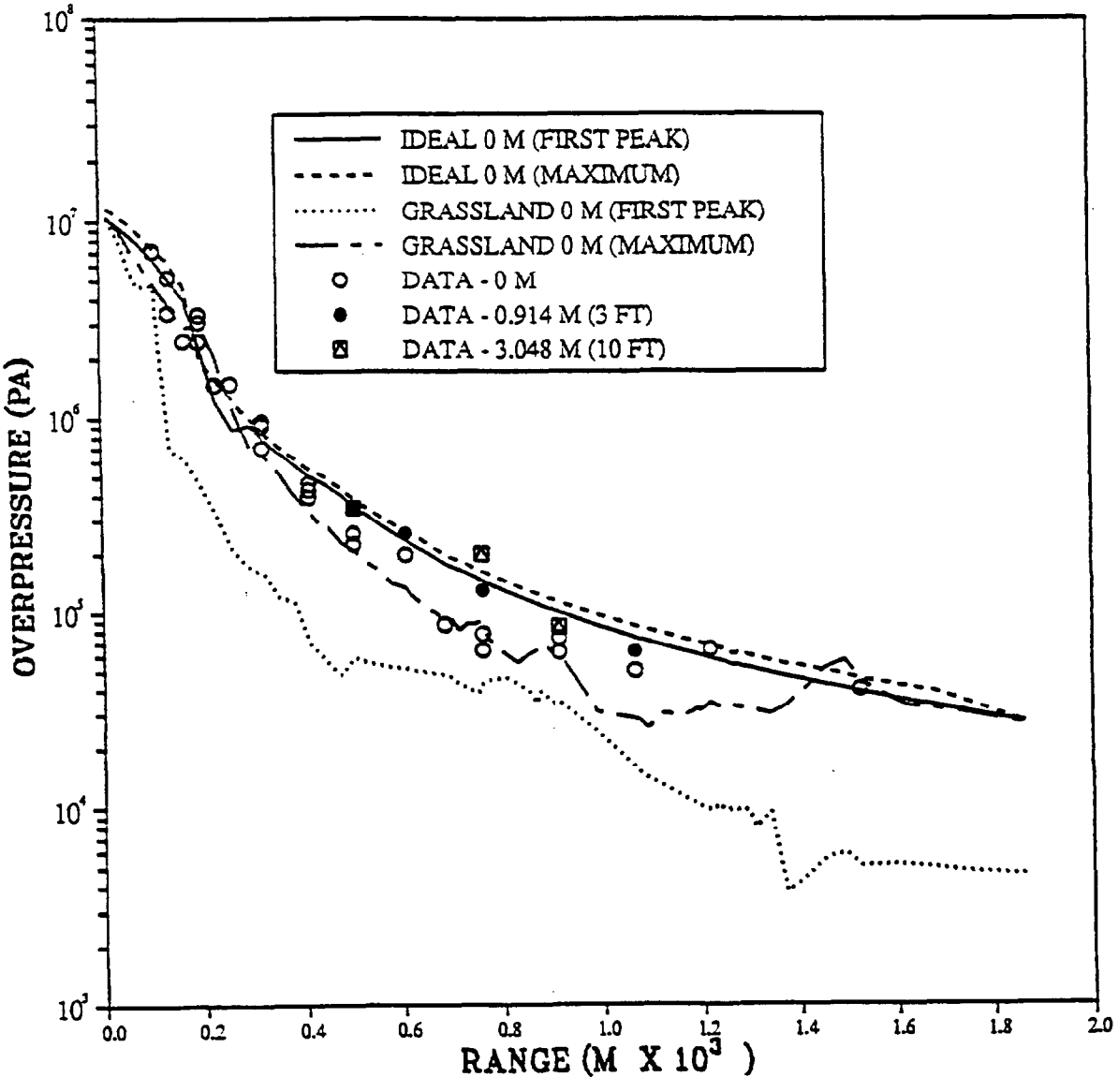

PRISCILLA GRASSLAND
PEAK OVERPRESSURE IMPULSE VS RANGE
GROUND LEVEL

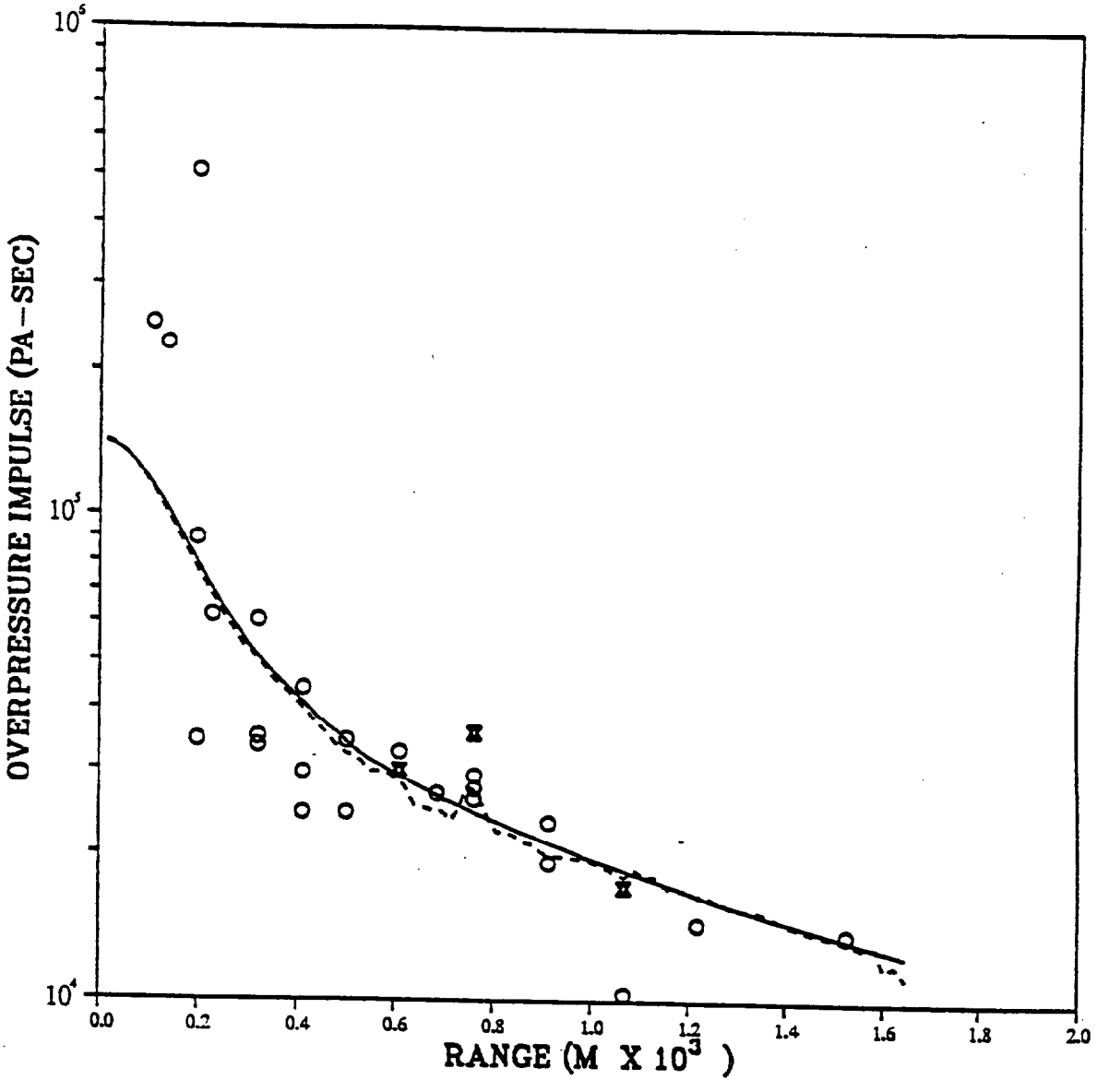

IDEAL - 0M
GRASSLAND - 0 M
DATA - 0 M
DATA - 0.914 M (3FT)

PRISCILLA GRASSLAND
PEAK OVERPRESSURE VS RANGE
AT 0.914 METER (3 FT) ABOVE SURFACE

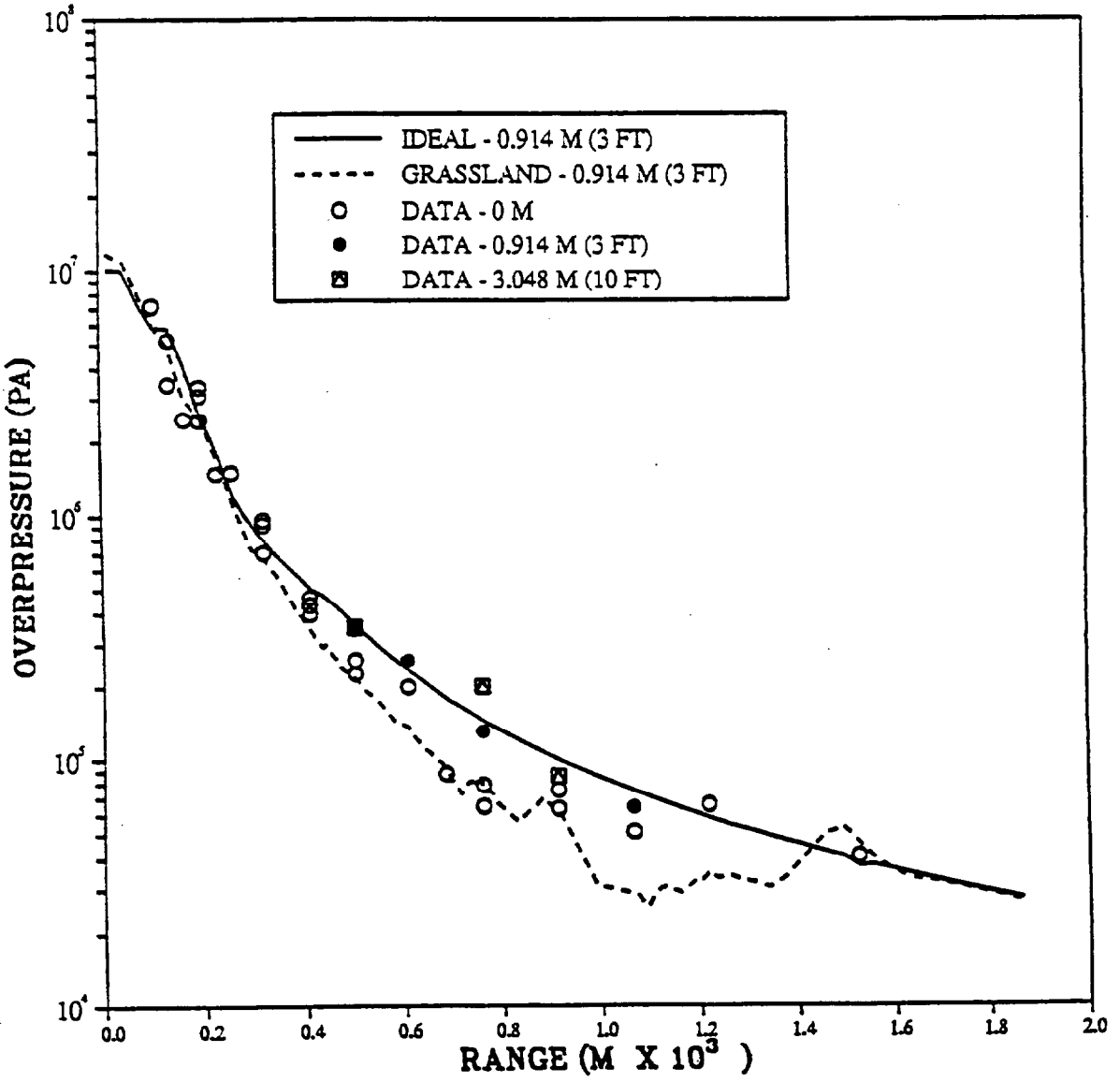

PRISCILLA GRASSLAND
PEAK OVERPRESSURE IMPULSE VS RANGE
0.914 METERS (3FT) ABOVE SURFACE

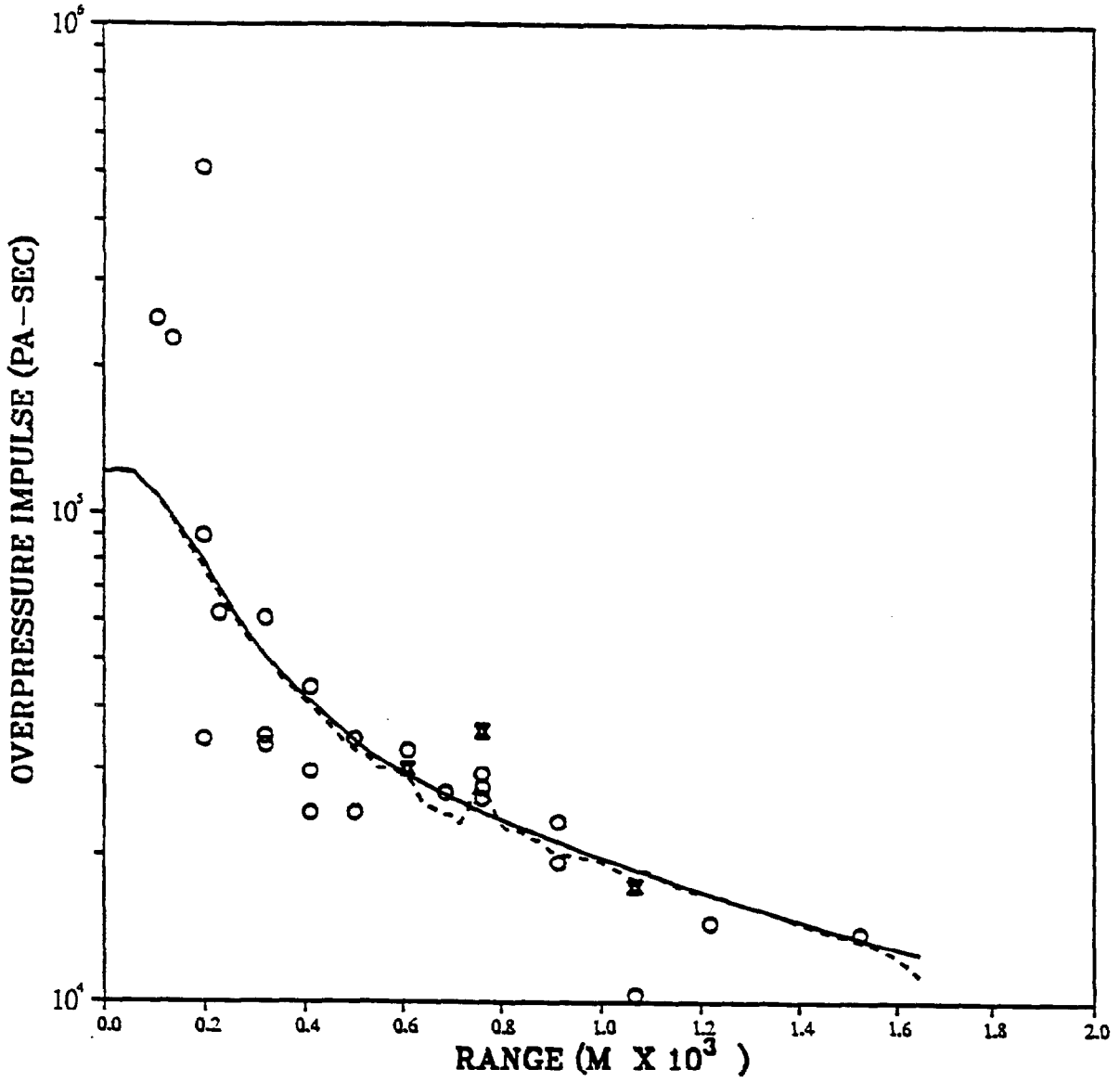

PRISCILLA GRASSLAND
PEAK OVERPRESSURE VS RANGE
AT 3.048 METERS (10 FT) ABOVE SURFACE

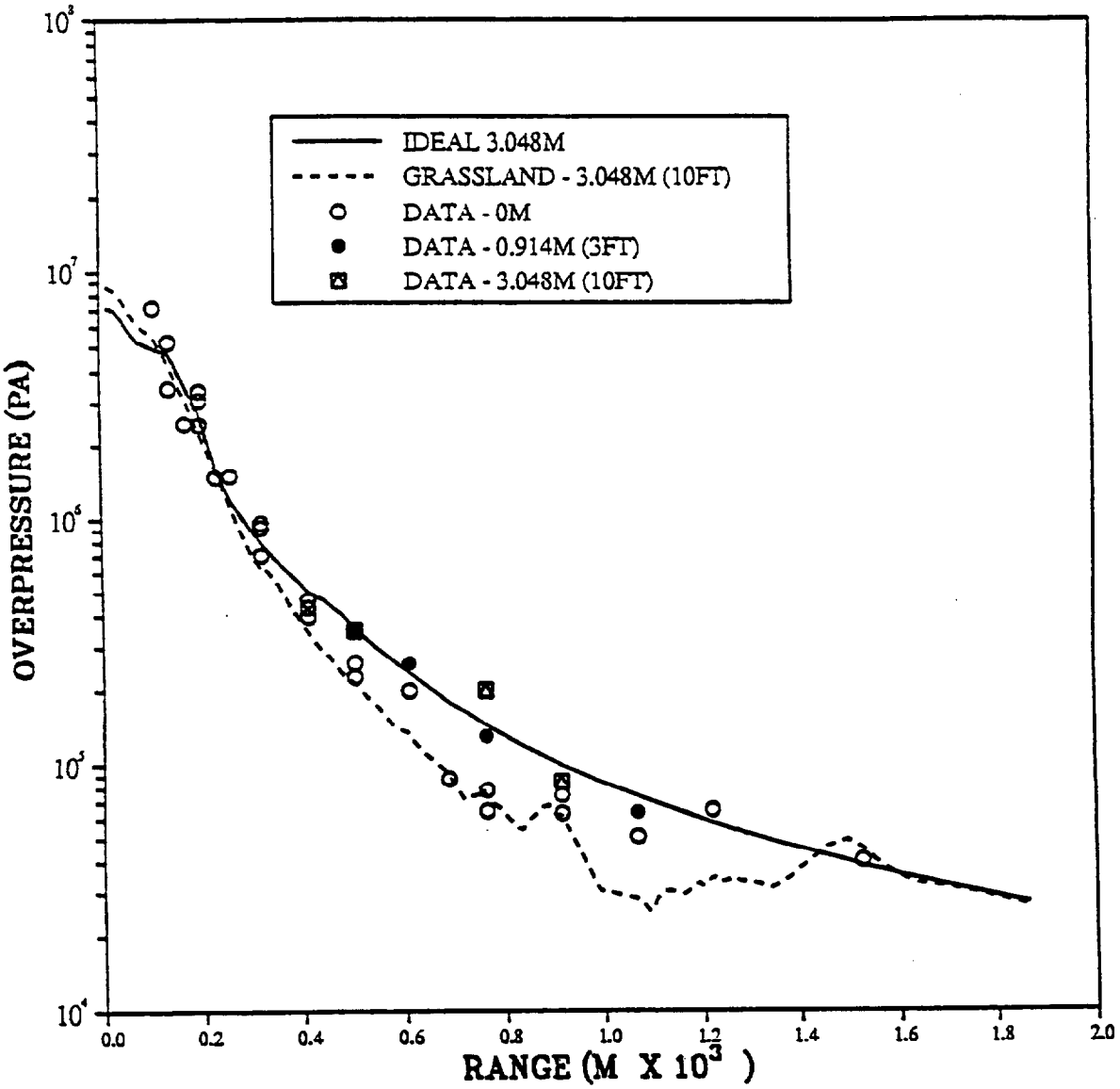

PRISCILLA GRASSLAND
PEAK OVERPRESSURE IMPULSE VS RANGE
3.048 METERS (10FT) ABOVE SURFACE

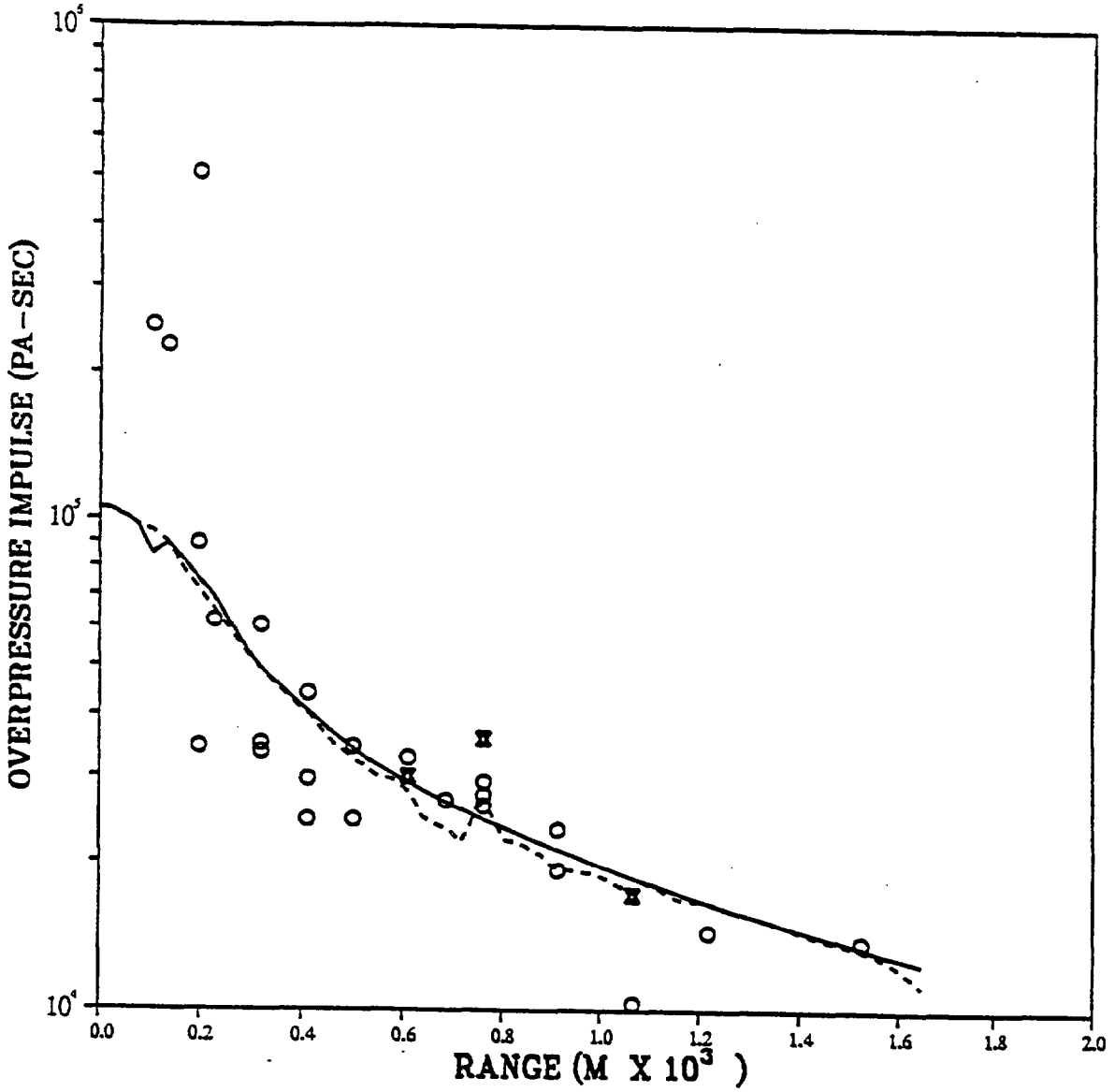

IDEAL - 3.048 M (10FT)
GRASSLAND - 3.048 M (10FT)
DATA - 0 M
DATA - 0.914 M (3FT)

PRISCILLA GRASSLAND
HORIZONTAL DYNAMIC PRESSURE PEAKS
GROUND LEVEL

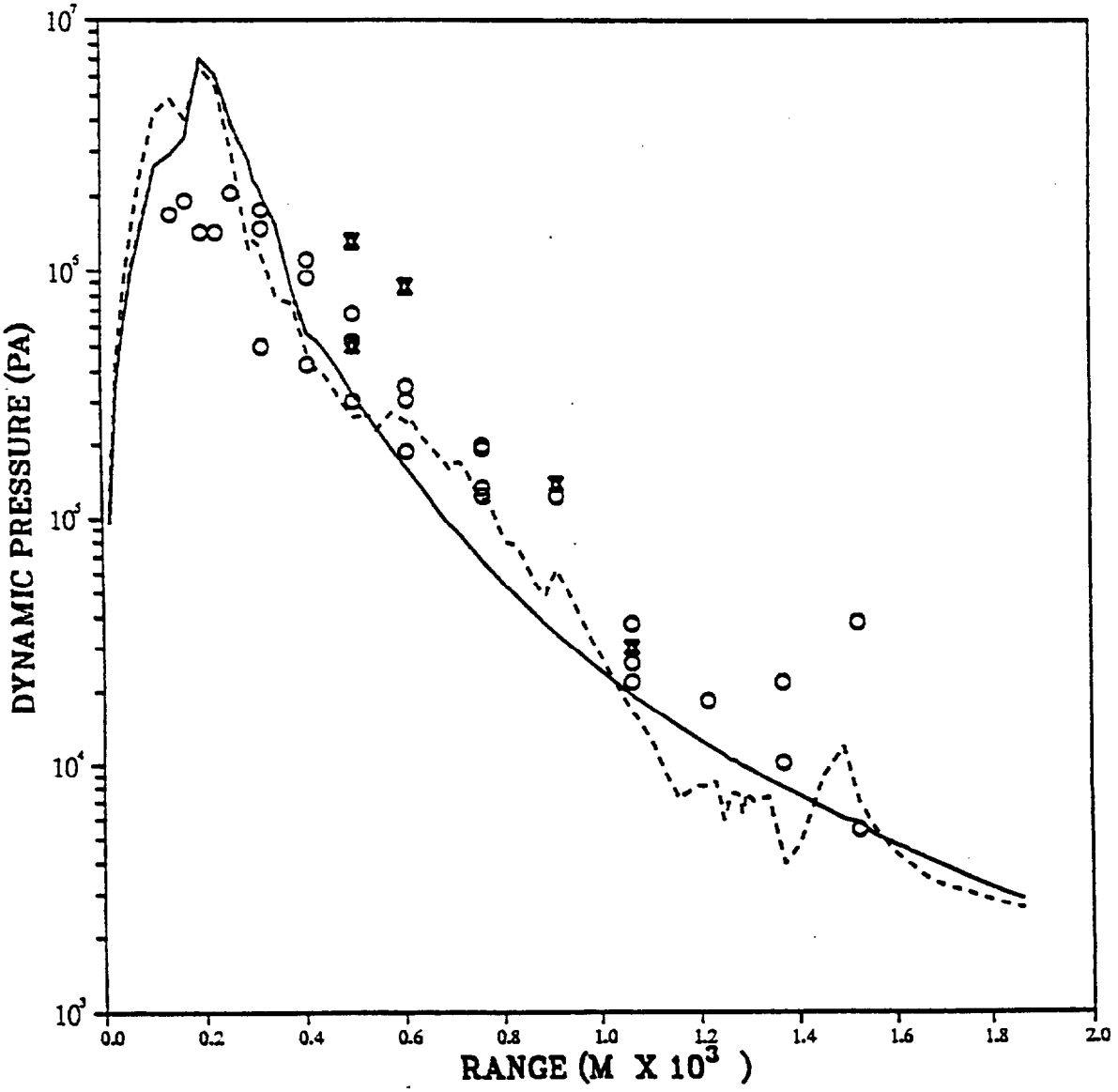

IDEAL - 0 M LEVEL
GRASSLAND - 0 M
DATA - 0.914 M (3FT)
DATA - 3.048 M (10FT)

PRISCILLA GRASSLAND
HORIZONTAL DYNAMIC PRESSURE IMPULSE
GROUND LEVEL

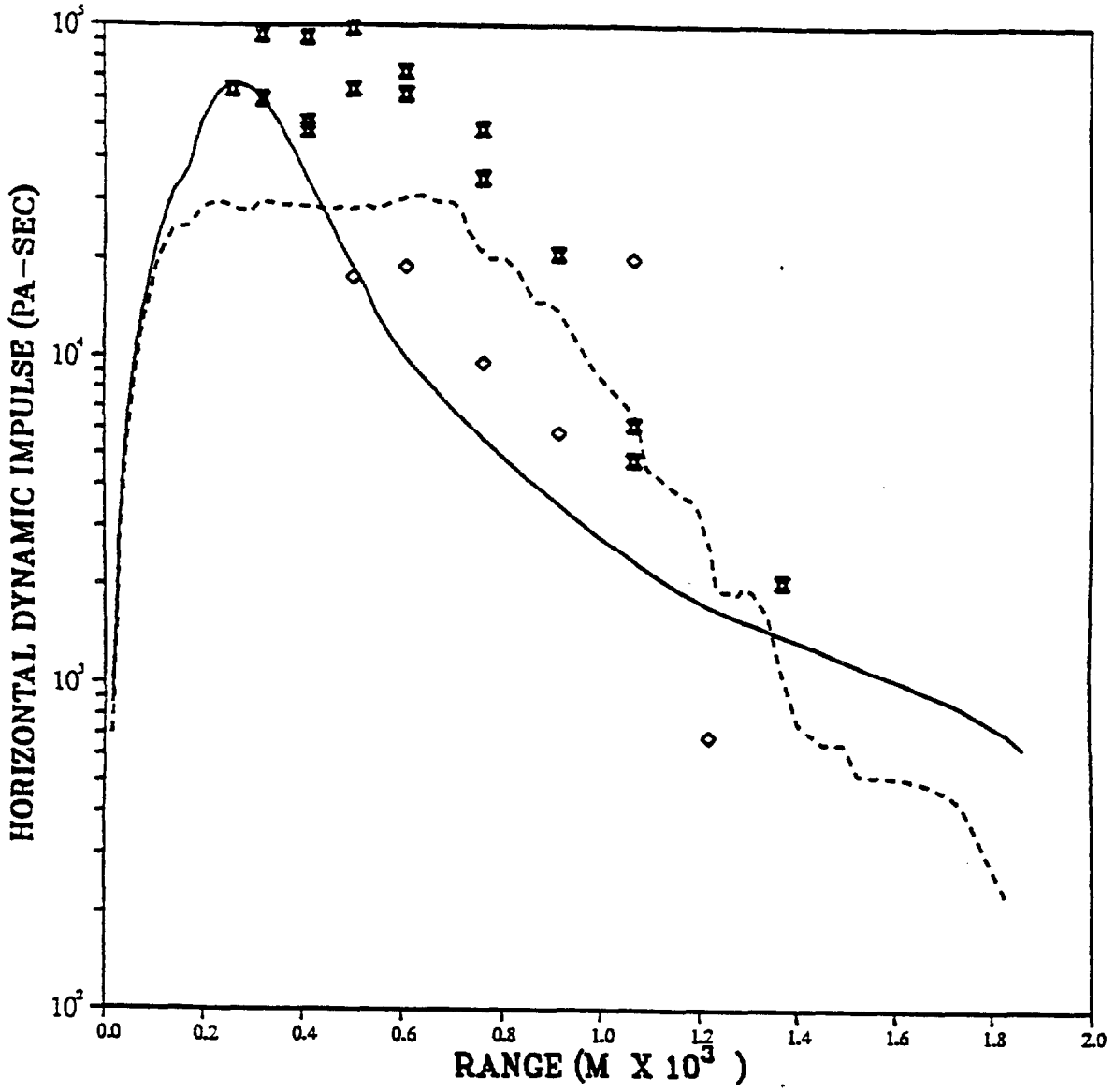

IDEAL - 0 M
GRASSLAND - 0 M
DATA - 0.914 M (3FT)
DATA - 0.914 M (3FT) (QUESTIONABLE RECORD)

PRISCILLA GRASSLAND
HORIZONTAL DYNAMIC PRESSURE PEAKS
0.914 CM (3FT) ABOVE SURFACE

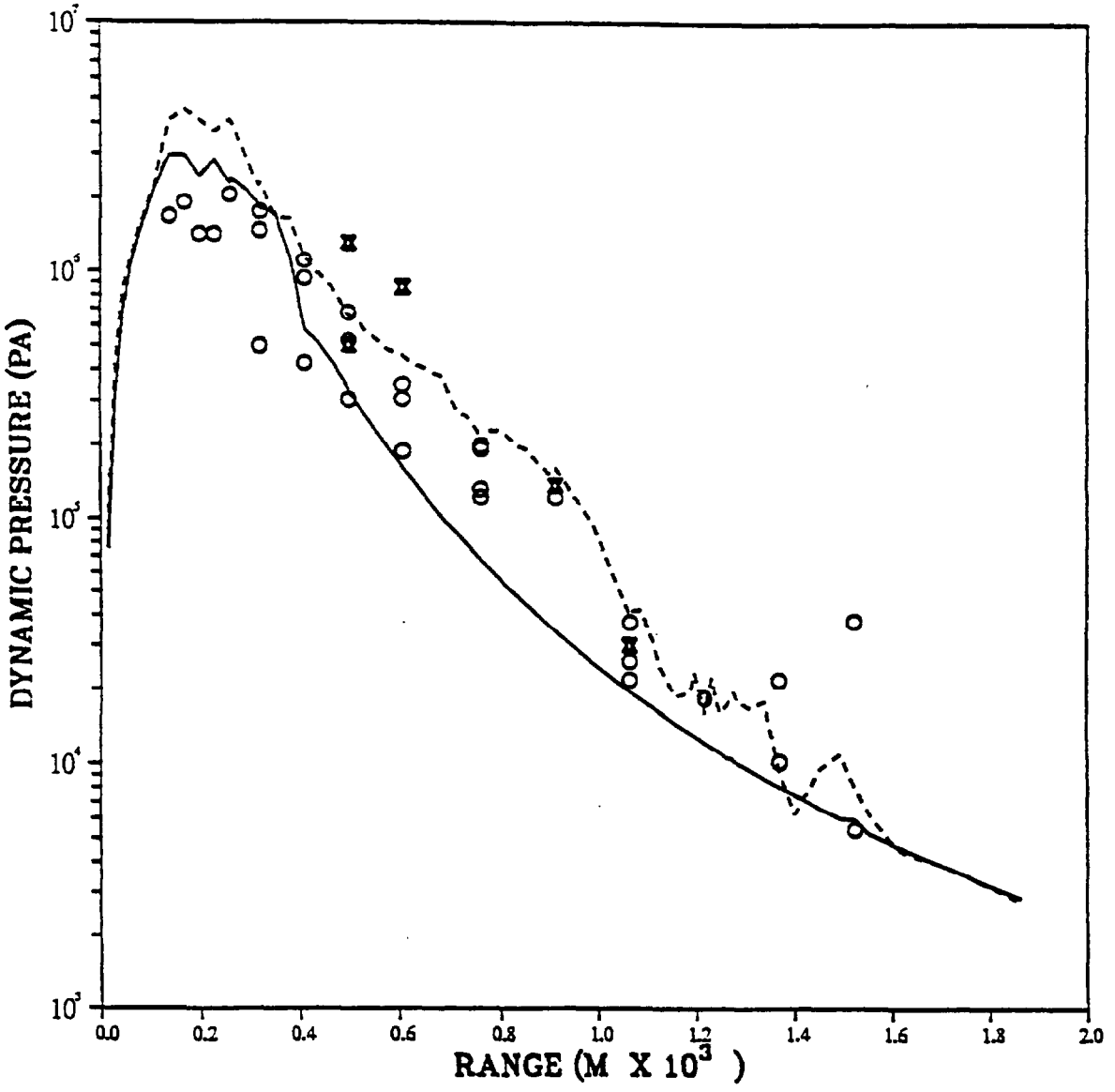

PRISCILLA GRASSLAND
HORIZONTAL DYNAMIC PRESSURE IMPULSE
0.914 M (3FT) ABOVE SURFACE

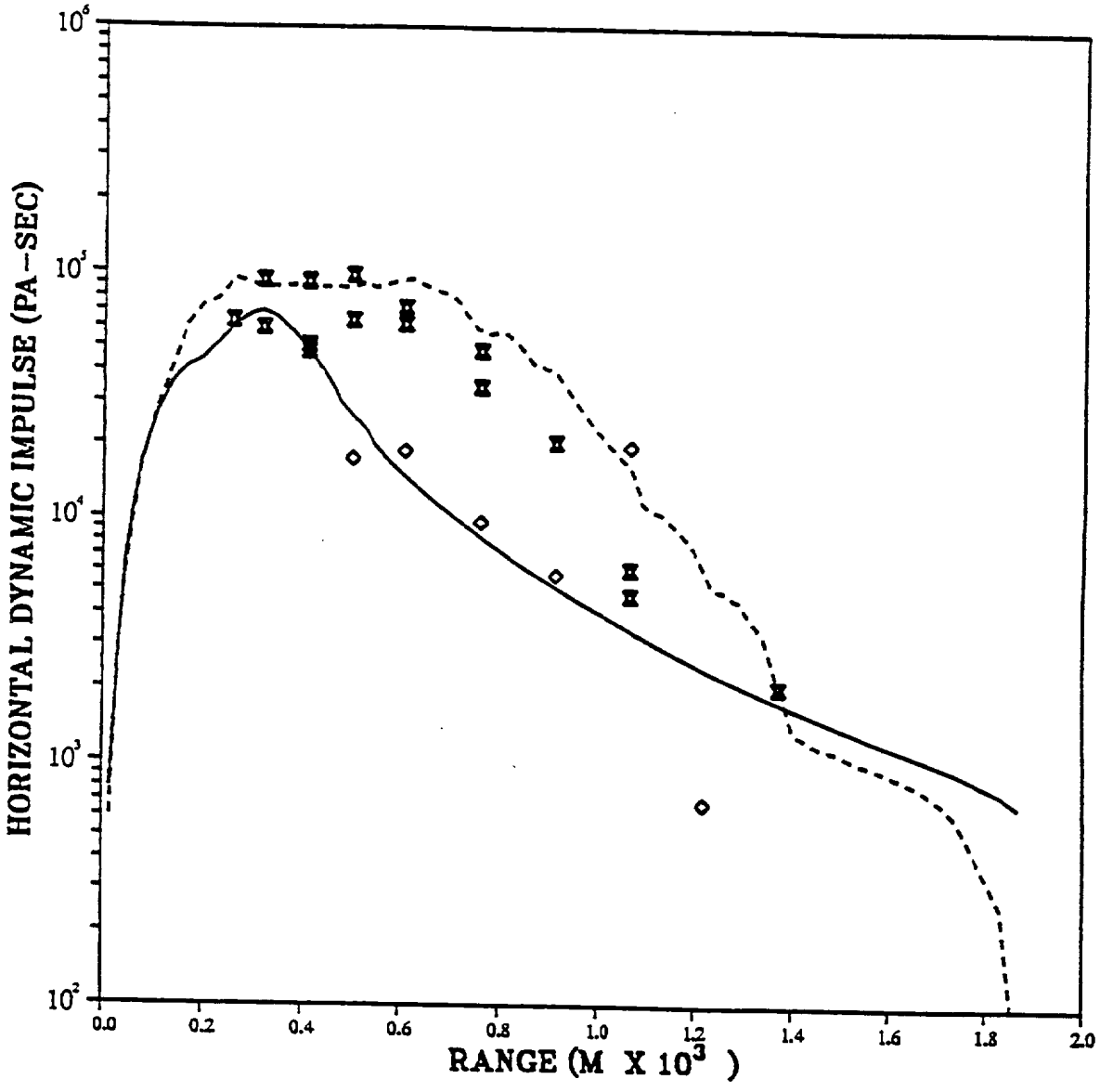

IDEAL - 0.914 M (3FT)
GRASSLAND - 0.914 M (3FT)
DATA - 0.914 M (3FT)
DATA - 0.914 M (3FT) (QUESTIONABLE RECORD)

PRISCILLA GRASSLAND
HORIZONTAL DYNAMIC PRESSURE PEAKS
3.048 M (10FT) ABOVE SURFACE

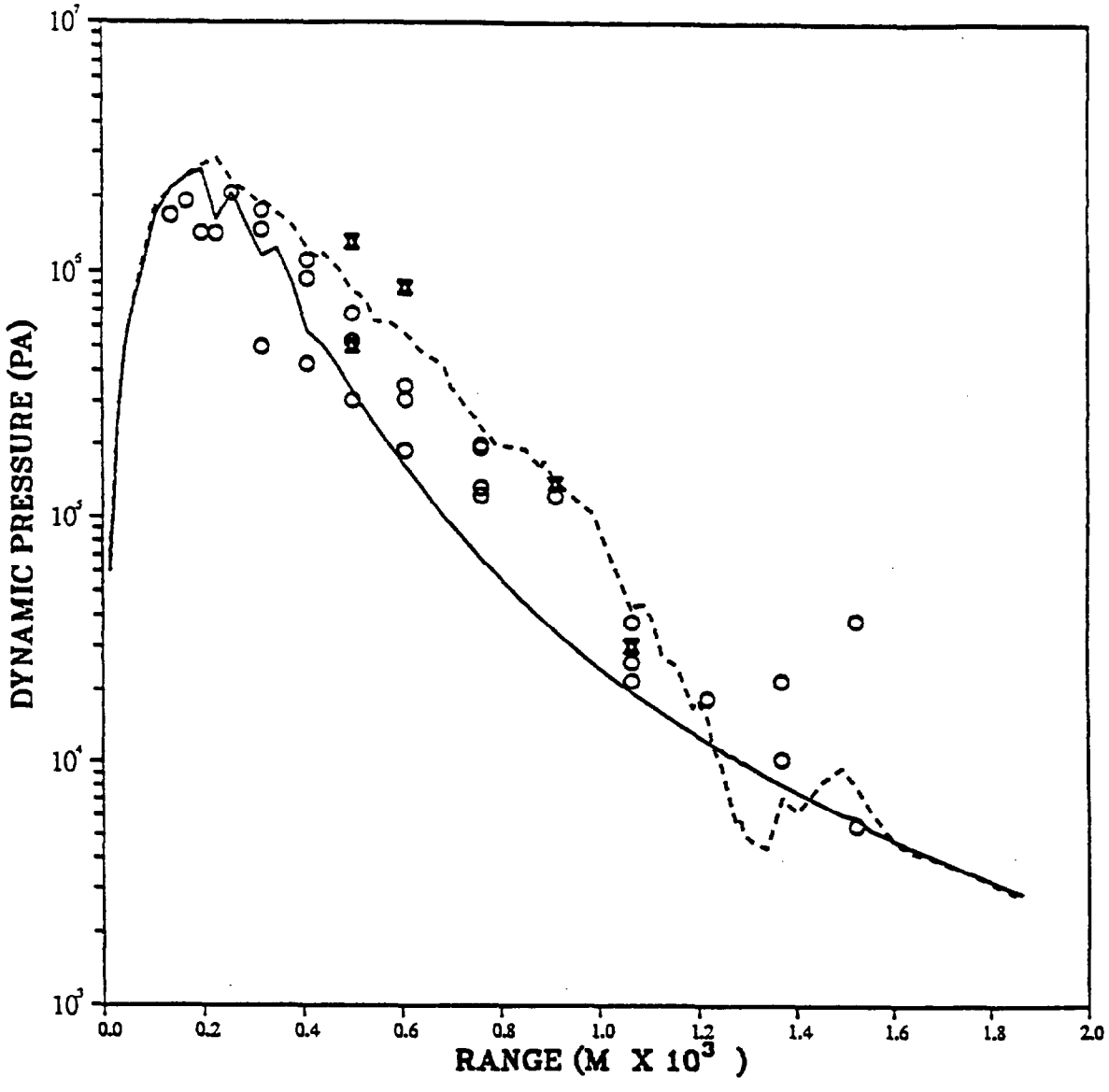

IDEAL 3.048 M (10FT)
GRASSLAND - 3.048 M (10FT)
DATA 0.914 M (3FT)
DATA 3.048 M (10FT)

PRISCILLA GRASSLAND
HORIZONTAL DYNAMIC PRESSURE IMPULSE
AT 3.048 M (10FT) ABOVE SURFACE

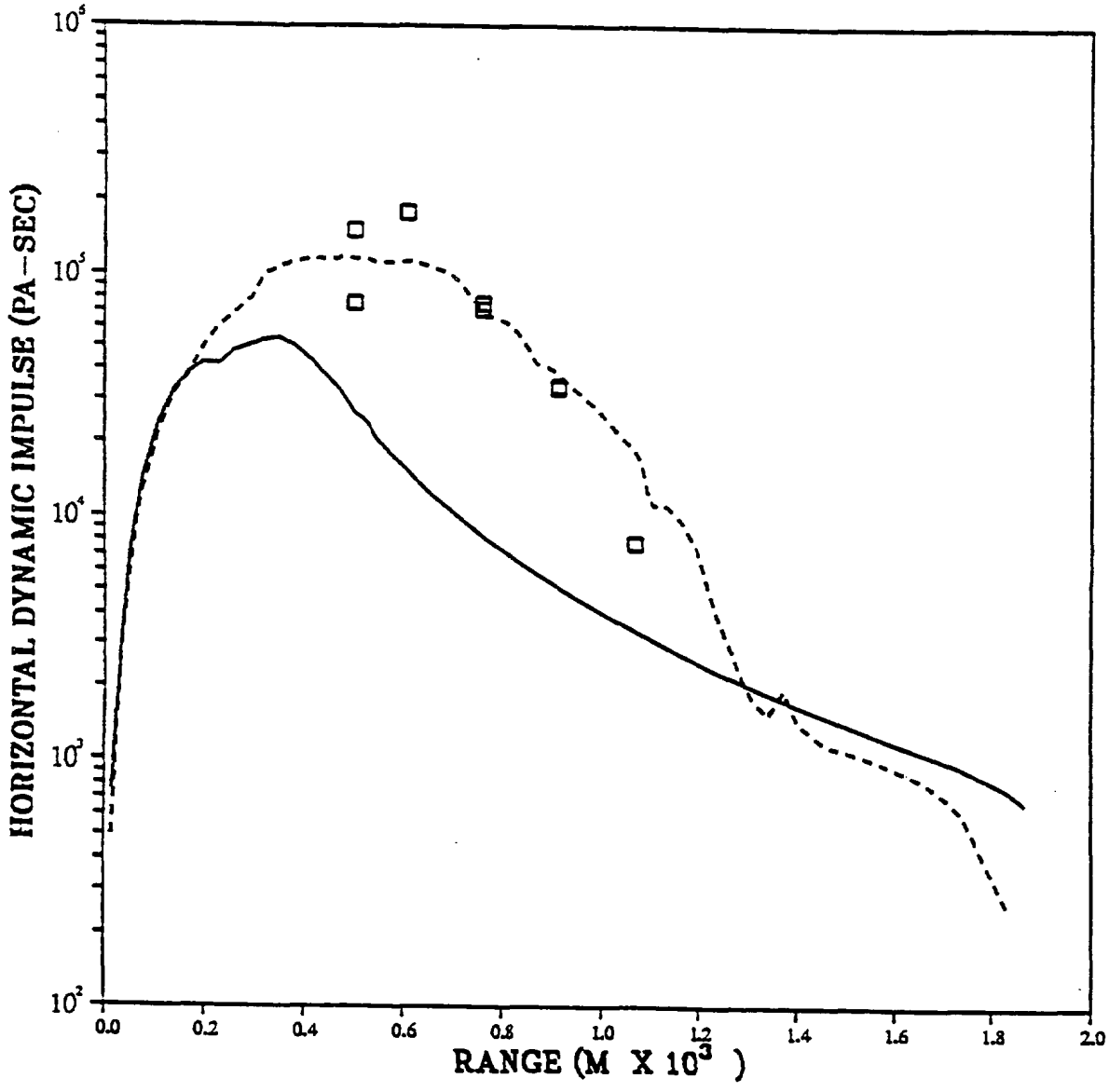

IDEAL - 3.048 M (10FT)
GRASSLAND - 3.048 M (10FT)
GAGE DATA - 3.048 M (10FT)

APPENDIX B
WAVEFORM COMPARISONS

This Appendix contains waveform comparisons of overpressure, dynamic pressure, and their impulses. Each plot contains the ideal waveform, the calculated precursor waveform, and at least one measured waveform at the corresponding distance. Arrival time of the measured waveform has been shifted to agree with the precursor calculation.

More information is available. The dust density as a function of time has been calculated and saved. It is possible to determine the calculated air and dust dynamic pressures independently. Any desired dust registry coefficient or a functional form of the dust registry coefficient may be used. Mach number of the flow as a function of time is also available at any of the station positions. Full descriptions of the turbulence environment are also available at each station, including the turbulent energy and the rate of turbulence dissipation.

PRISCILLA
CALCULATION - DATA COMPARISONS
OVERPRESSURE AT 107 METERS (350FT)

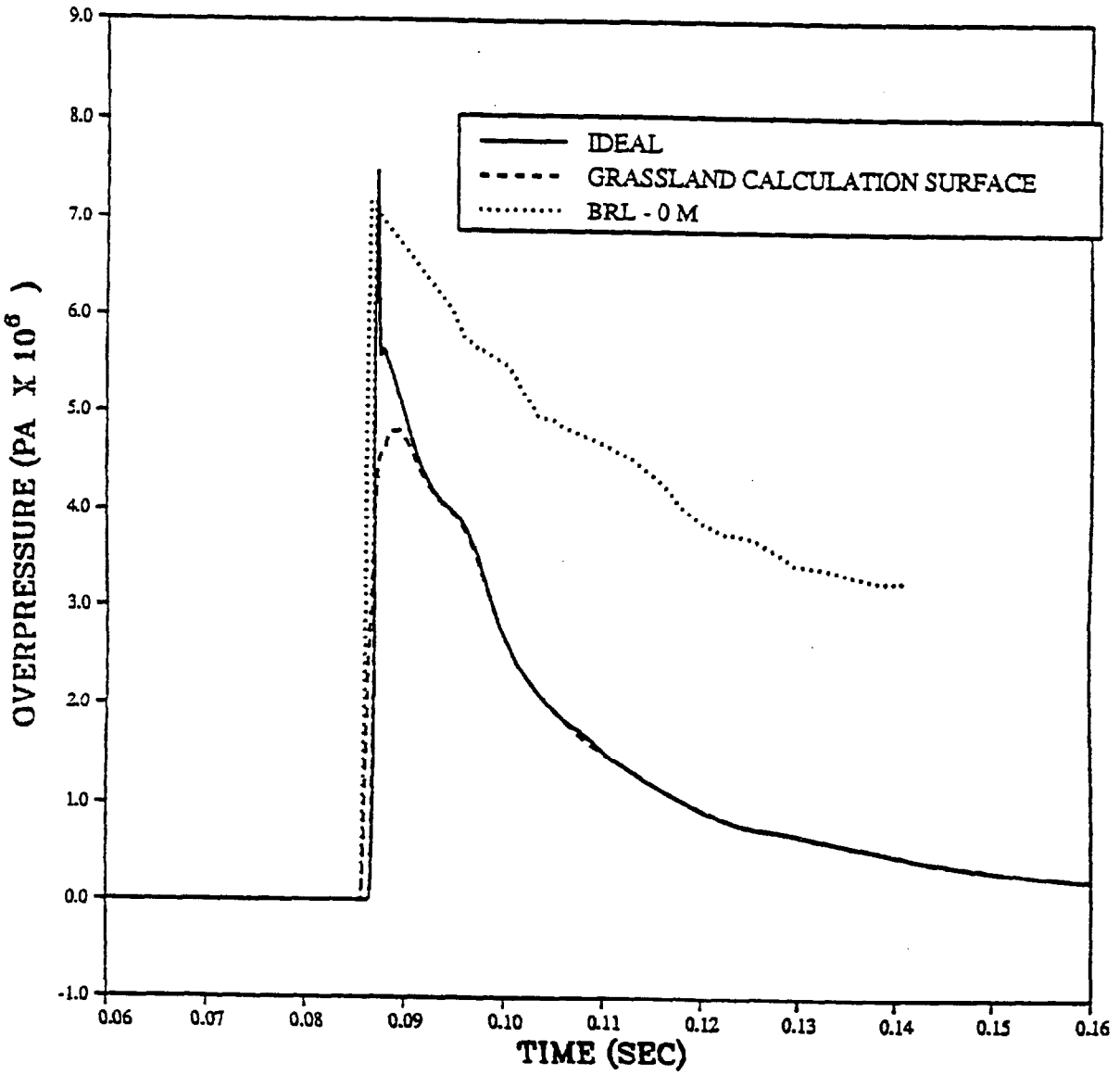

PRISCILLA
CALCULATION - DATA COMPARISONS
OVERPRESSURE IMPULSE AT 107 METERS (350FT)

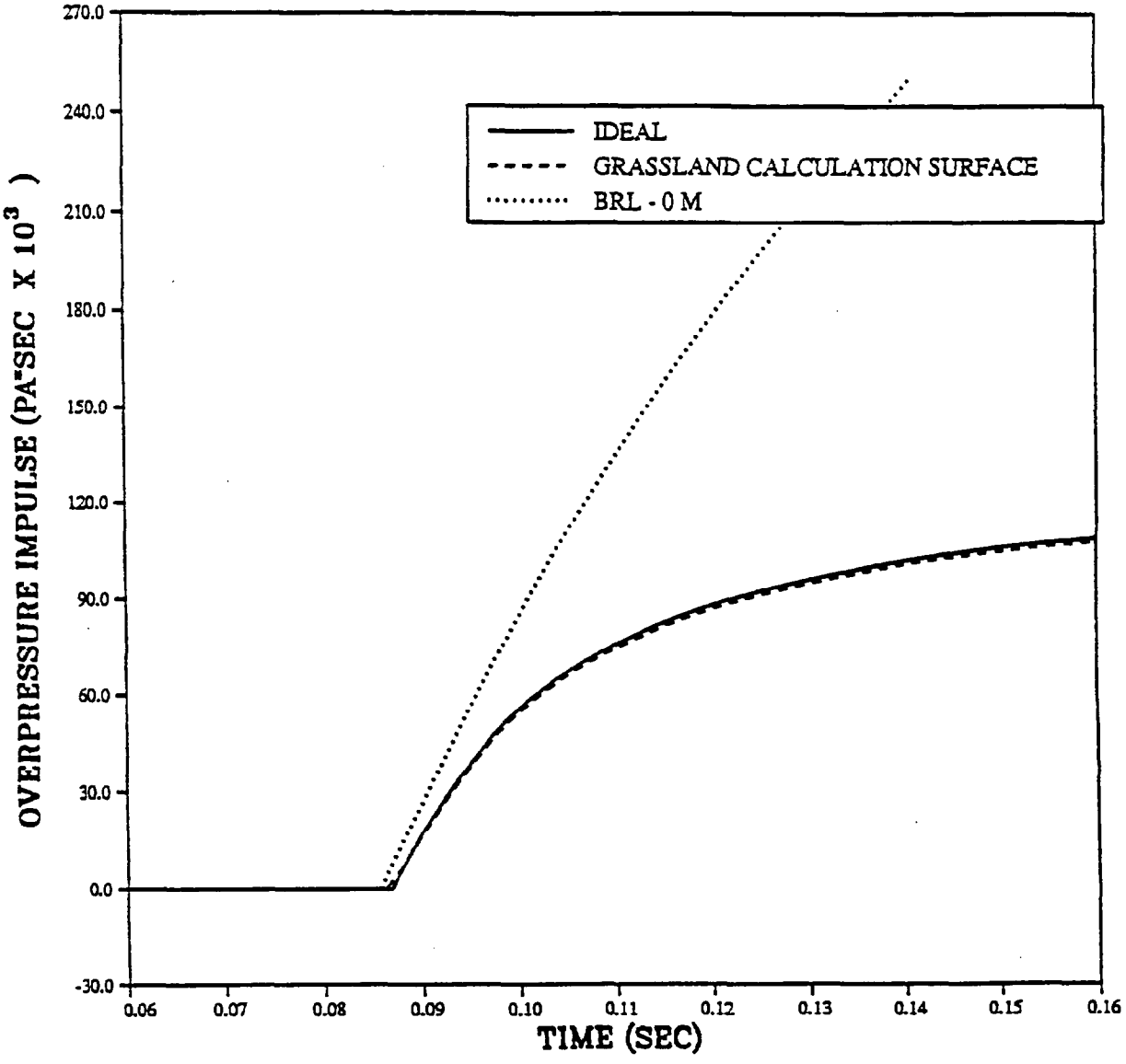

PRISCILLA
CALCULATION - DATA COMPARISONS
OVERPRESSURE AT 137 METERS (450FT)

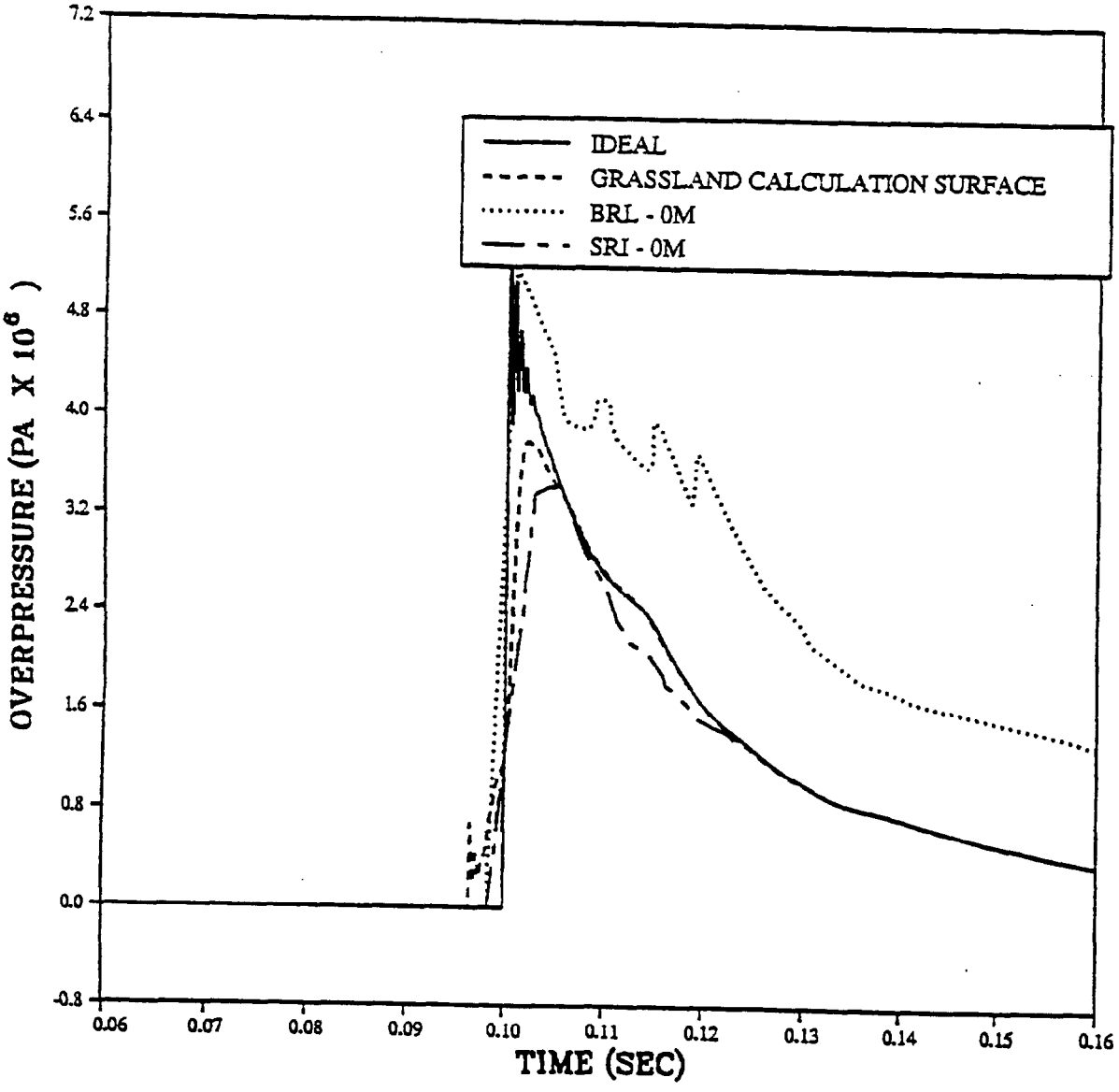

PRISCILLA
CALCULATION - DATA COMPARISONS
OVERPRESSURE IMPULSE AT 137 METERS (450FT)

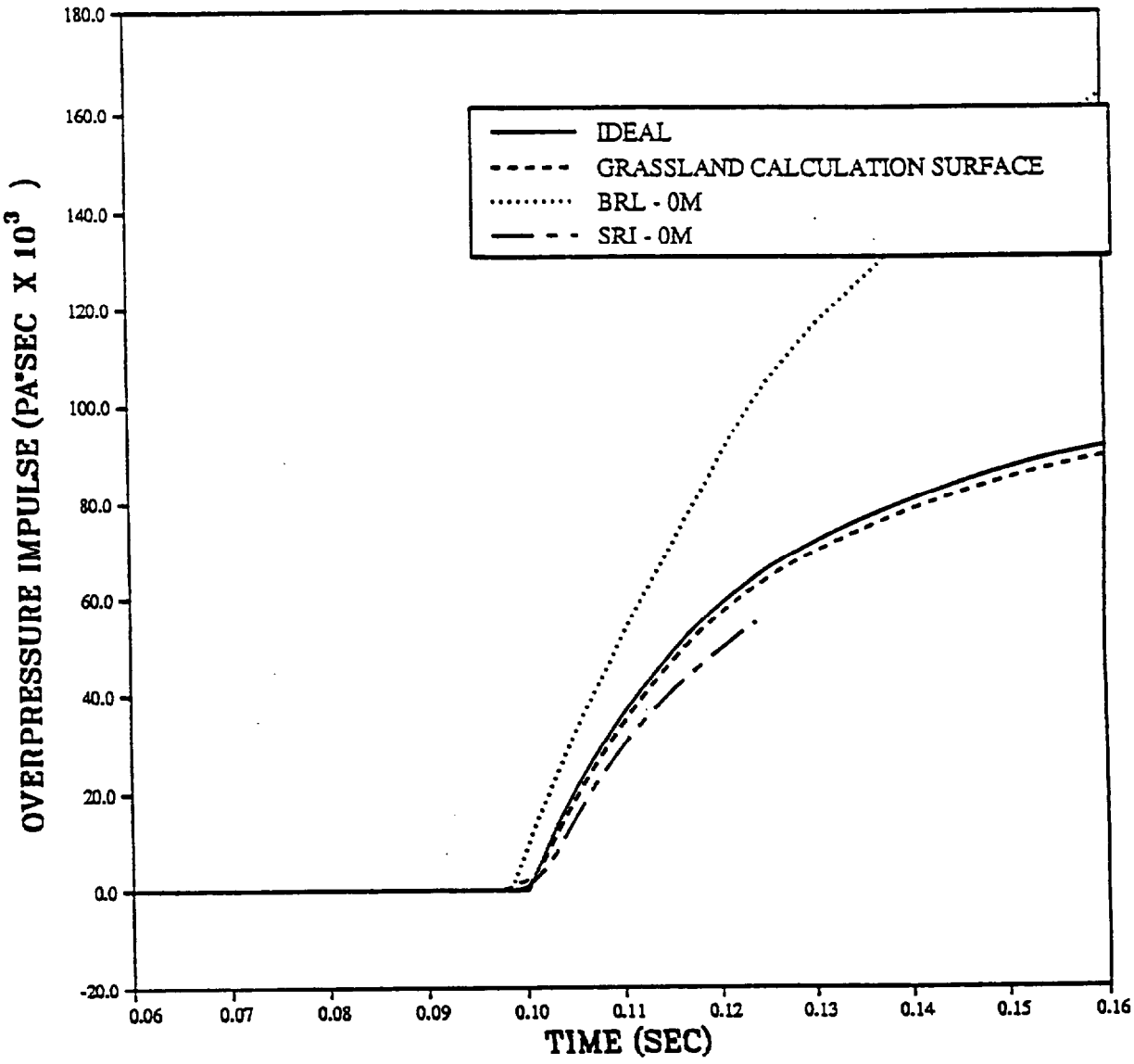

PRISCILLA
CALCULATION - DATA COMPARISONS
OVERPRESSURE AT 168 METERS (550FT)

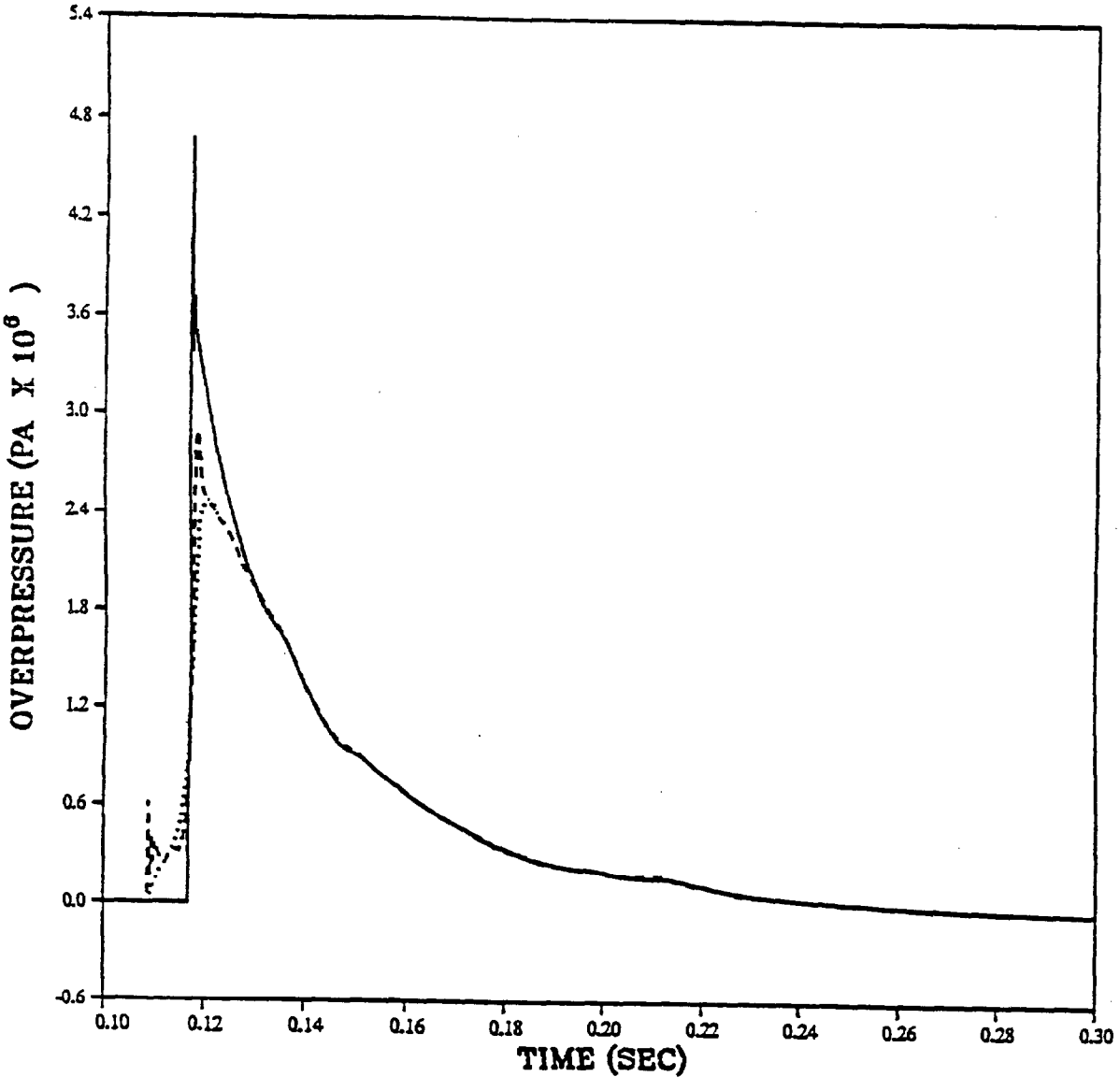

PRISCILLA
CALCULATION - DATA COMPARISONS
OVERPRESSURE IMPULSE AT 168 METERS (550FT)

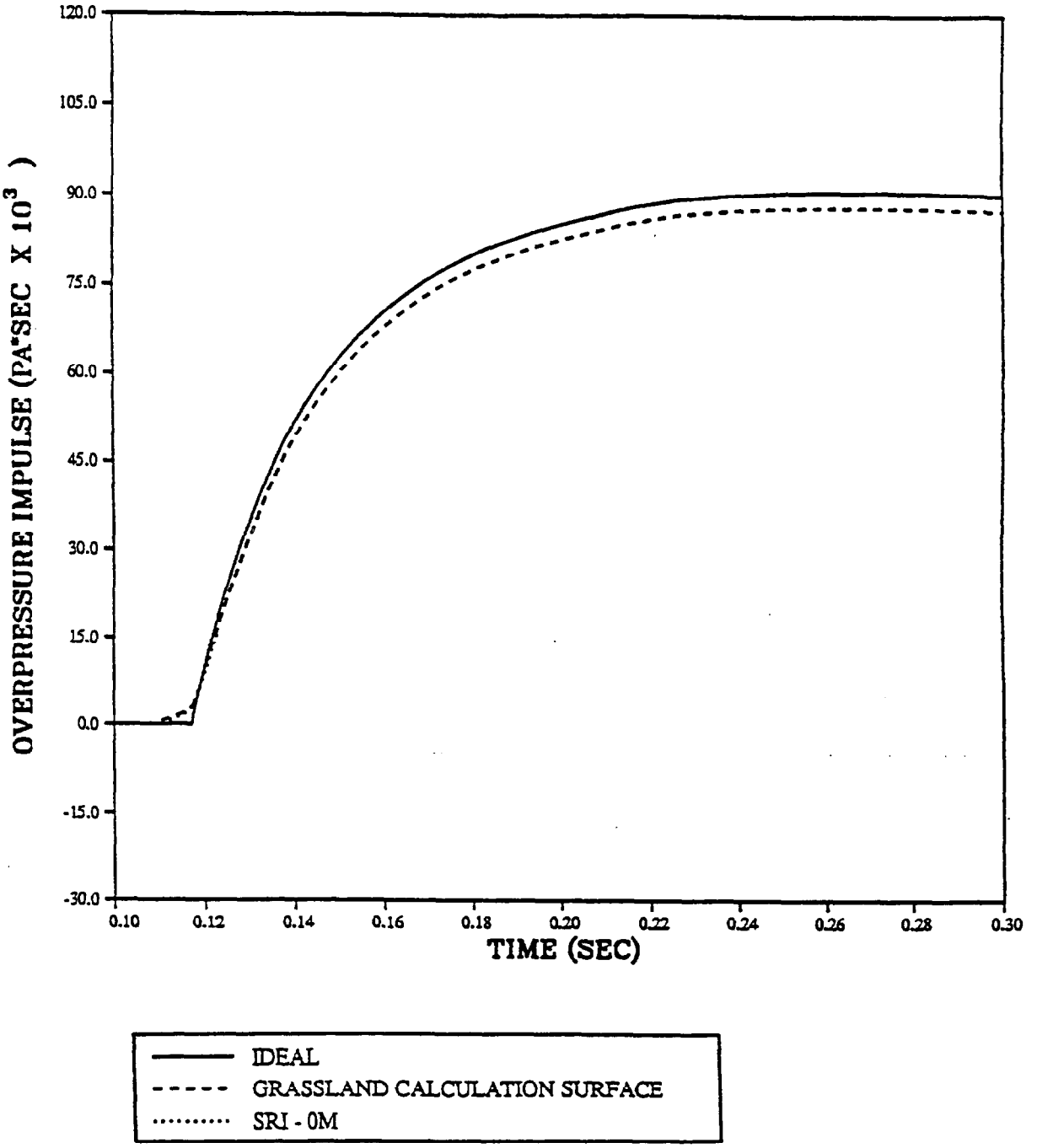

PRISCILLA
CALCULATION - DATA COMPARISONS
OVERPRESSURE AT 198 METERS (650 FEET)

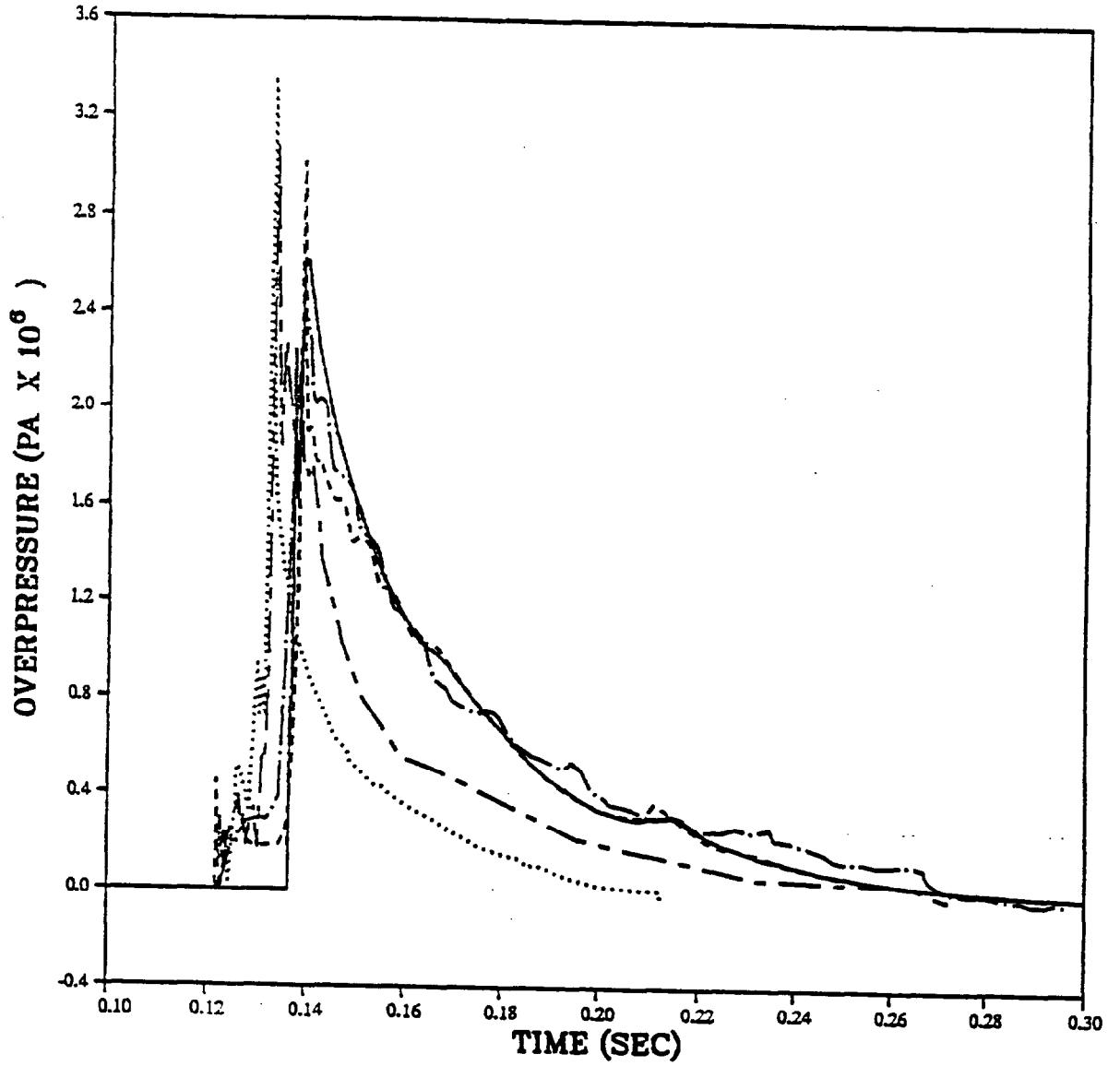

IDEAL
GRASSLAND CALCULATION SURFACE
BRL - 0 M
BRL - 0 M
SRI - 0 M

PRISCILLA
CALCULATION - DATA COMPARISONS
OVERPRESSURE IMPULSE AT 198 METERS (650 FEET)

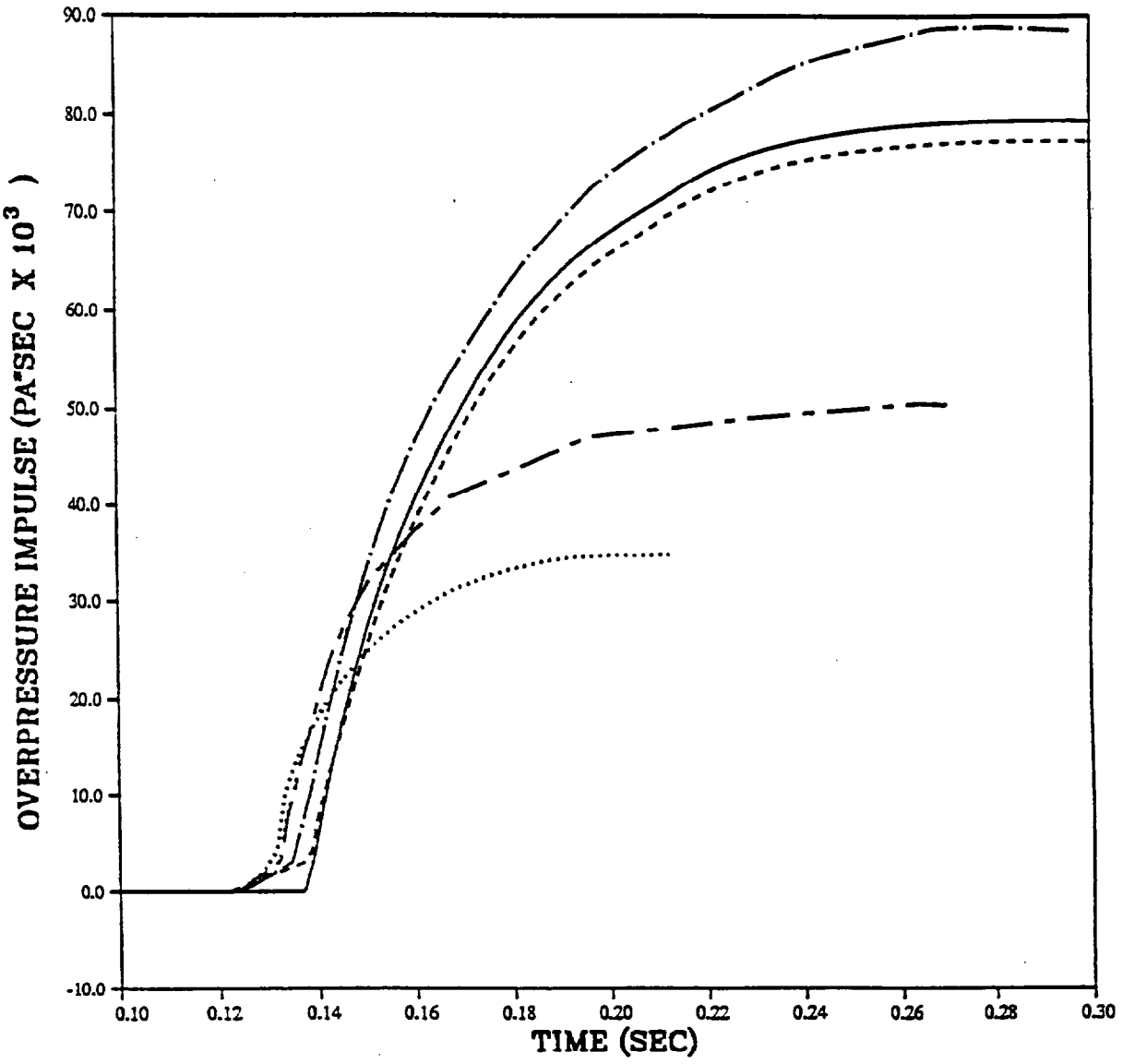

IDEAL
GRASSLAND CALCULATION SURFACE
BRL - 0 M
BRL - 0 M
SRI - 0 M

PRISCILLA
CALCULATION - DATA COMPARISONS
OVERPRESSURE AT 229 METERS (750 FEET)

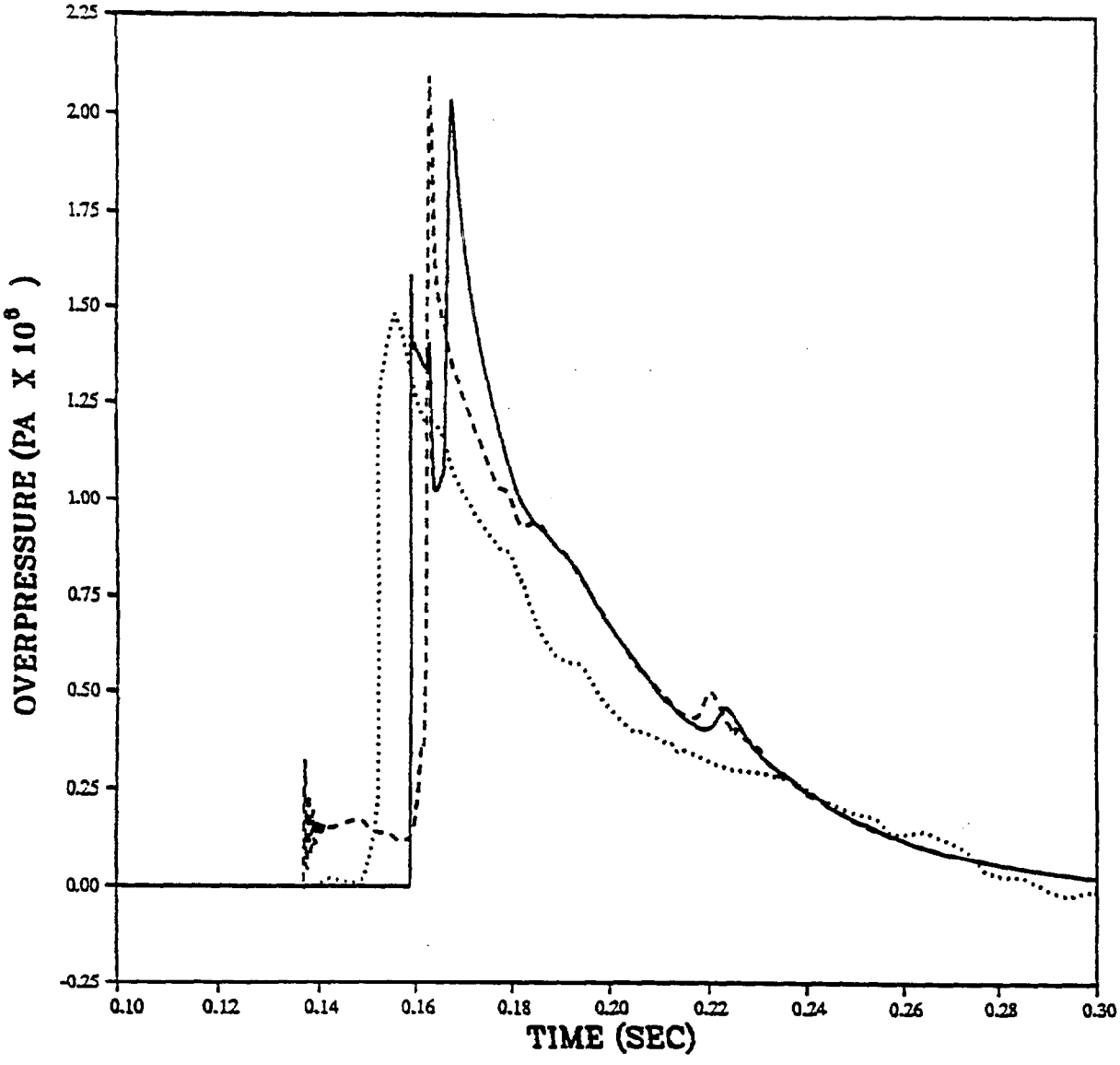

PRISCILLA
CALCULATION - DATA COMPARISONS
OVERPRESSURE IMPULSE AT 229 METERS (750 FEET)

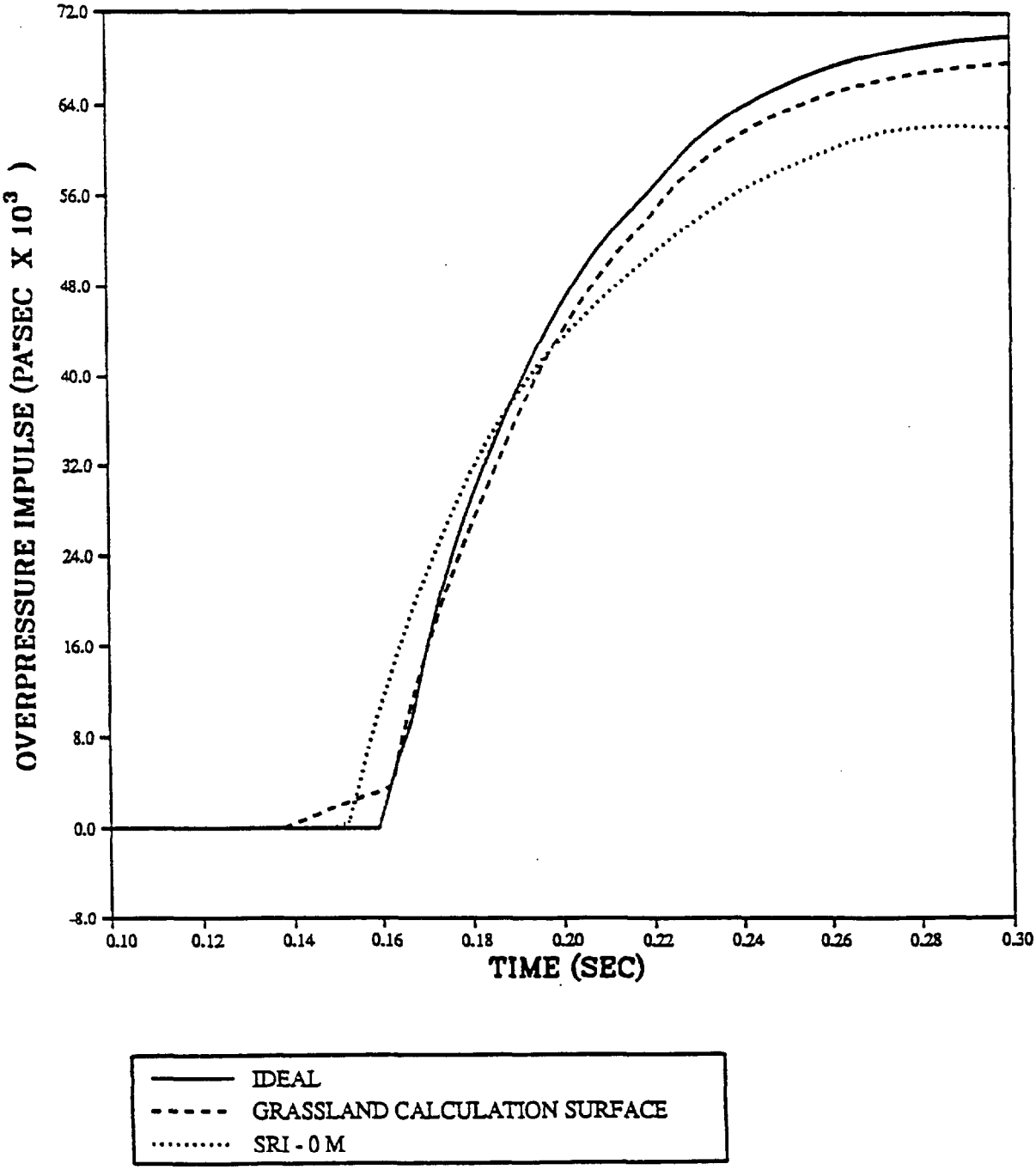

PRISCILLA
CALCULATION - DATA COMPARISONS
OVERPRESSURE AT 850 FEET (260 M)

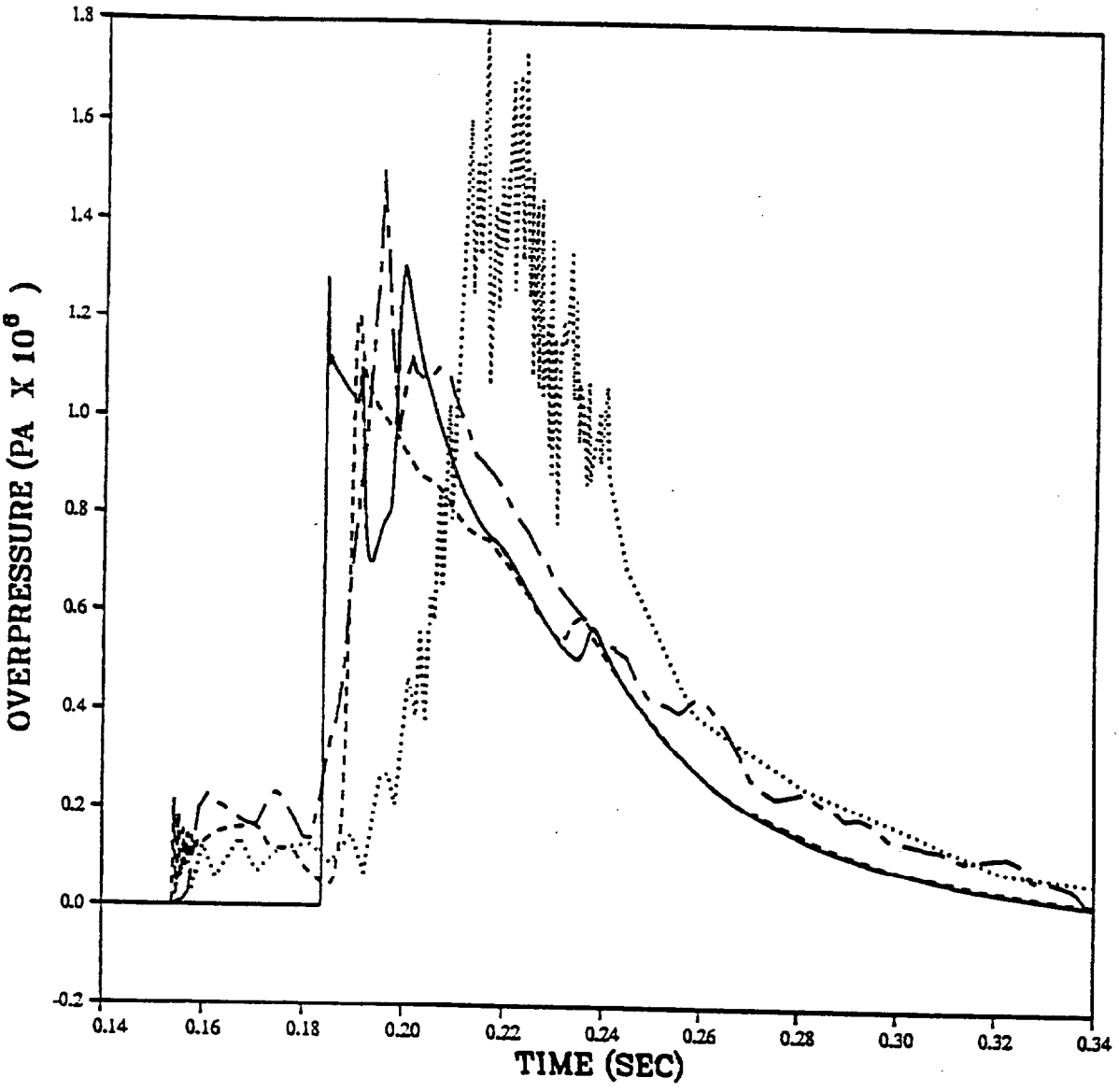

IDEAL
GRASSLAND CALCULATION SURFACE
BRL - 0 M
SRI - 0 M

PRISCILLA
CALCULATION - DATA COMPARISONS
OVERPRESSURE IMPULSE AT 850 FEET (260 M)

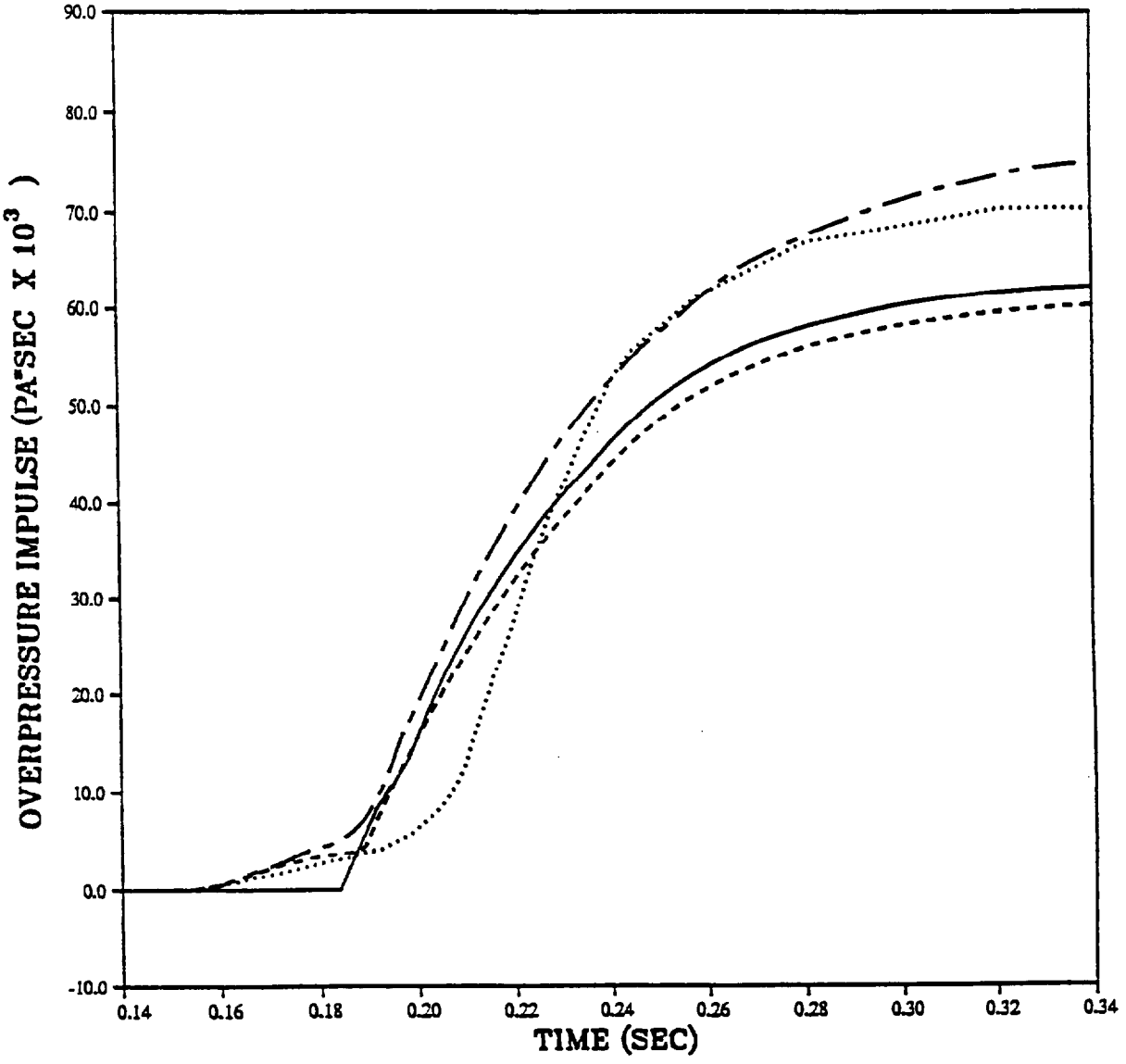

IDEAL
GRASSLAND CALCULATION SURFACE
BRL - 0 M
SRI - 0 M

PRISCILLA
CALCULATION - DATA COMPARISONS
OVERPRESSURE AT 320 METERS (1050 FEET)

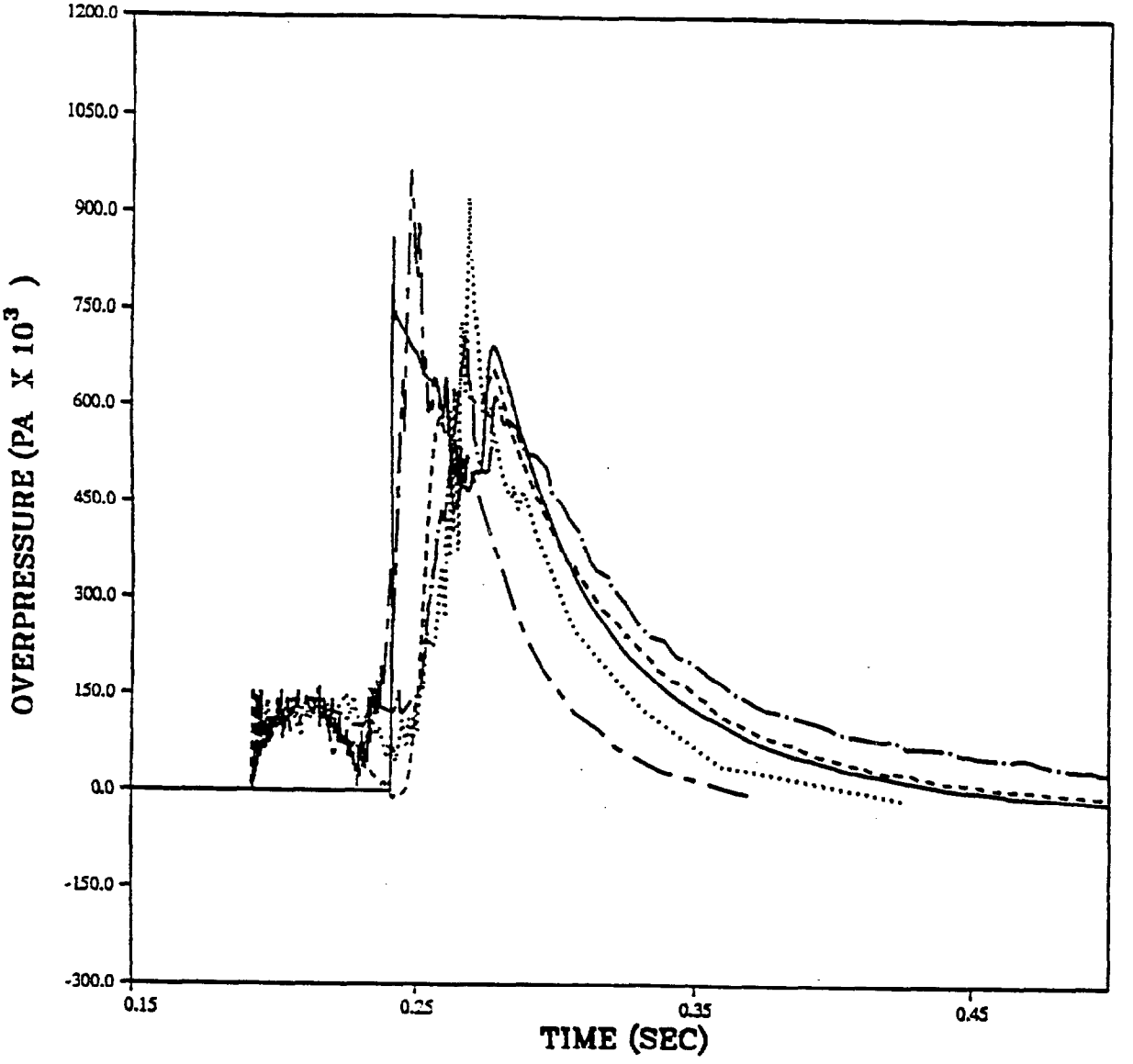

IDEAL
GRASSLAND CALCULATION SURFACE
BRL - 0 M
BRL - 0 M
SRI - 0 M

PRISCILLA
CALCULATION - DATA COMPARISONS
OVERPRESSURE IMPULSE AT 320 METERS (1050 FEET)

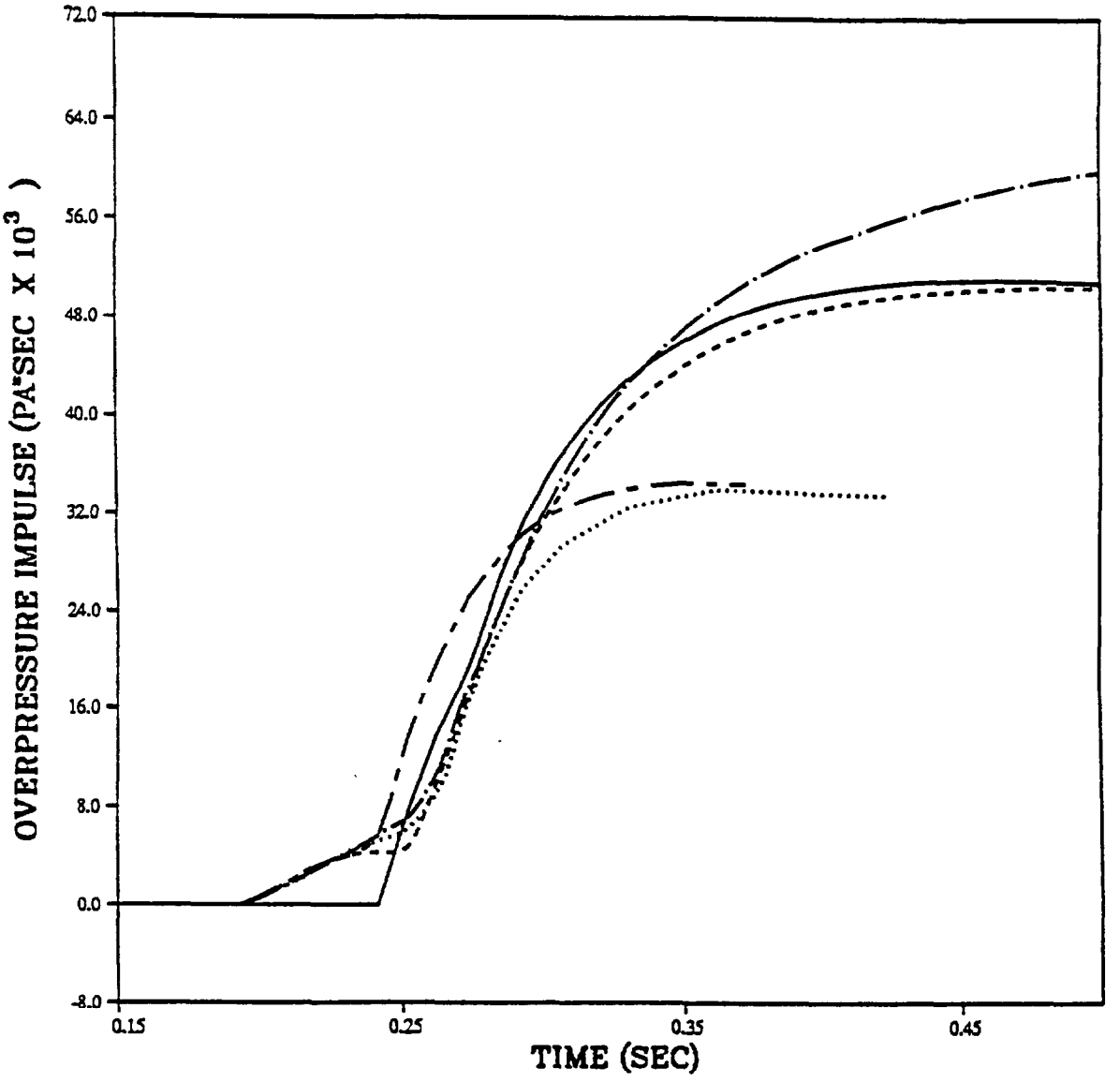

IDEAL
GRASSLAND CALCULATION SURFACE
BRL - 0 M
BRL - 0 M
SRI - 0 M

PRISCILLA
CALCULATION - DATA COMPARISONS
OVERPRESSURE AT 410 METERS (1350 FEET)

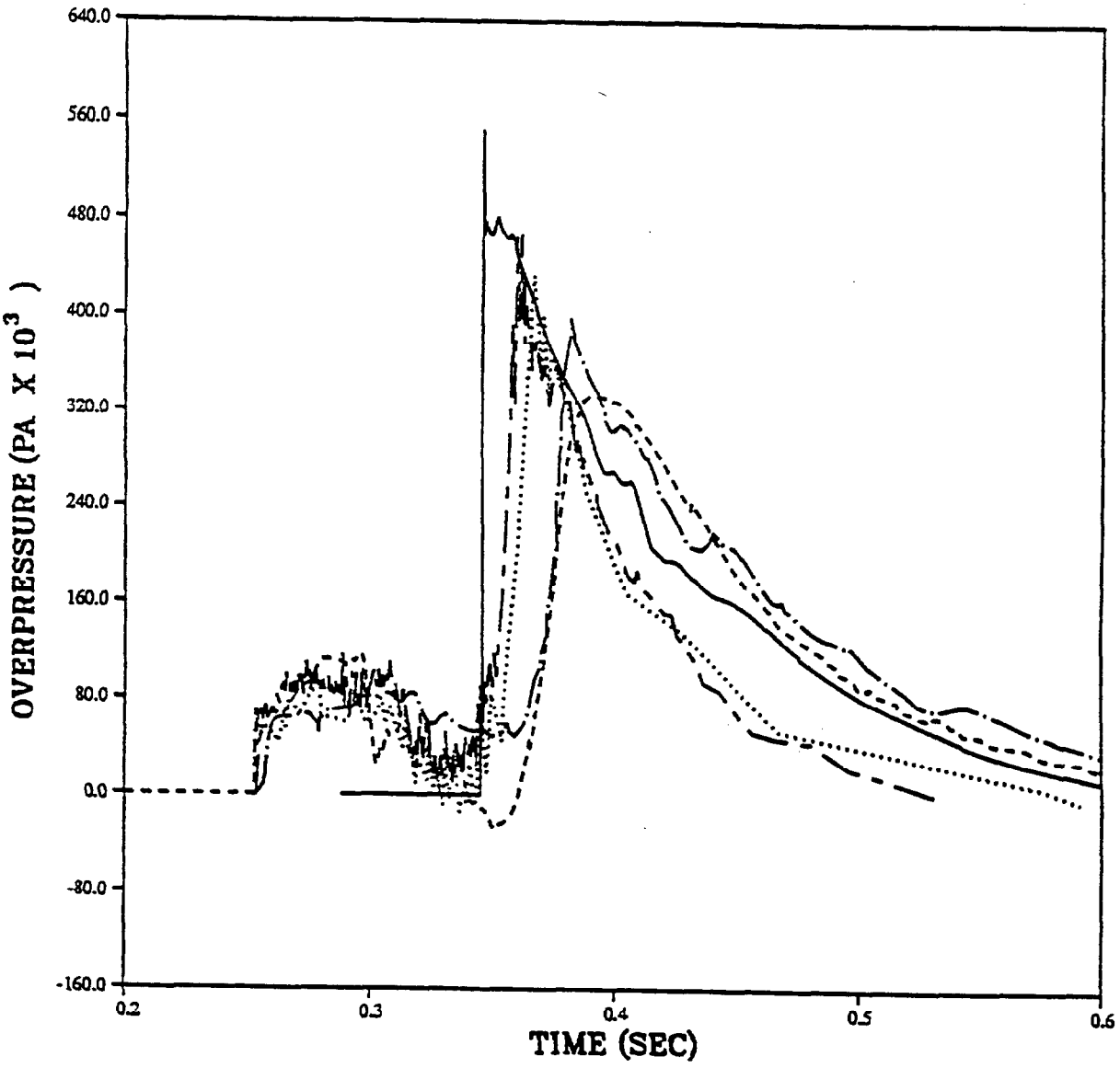

IDEAL
GRASSLAND CALCULATION SURFACE
BRL - 0 M
BRL - 0 M
SRI - 0 M

PRISCILLA
CALCULATION - DATA COMPARISONS
OVERPRESSURE IMPULSE AT 410 METERS (1350 FEET)

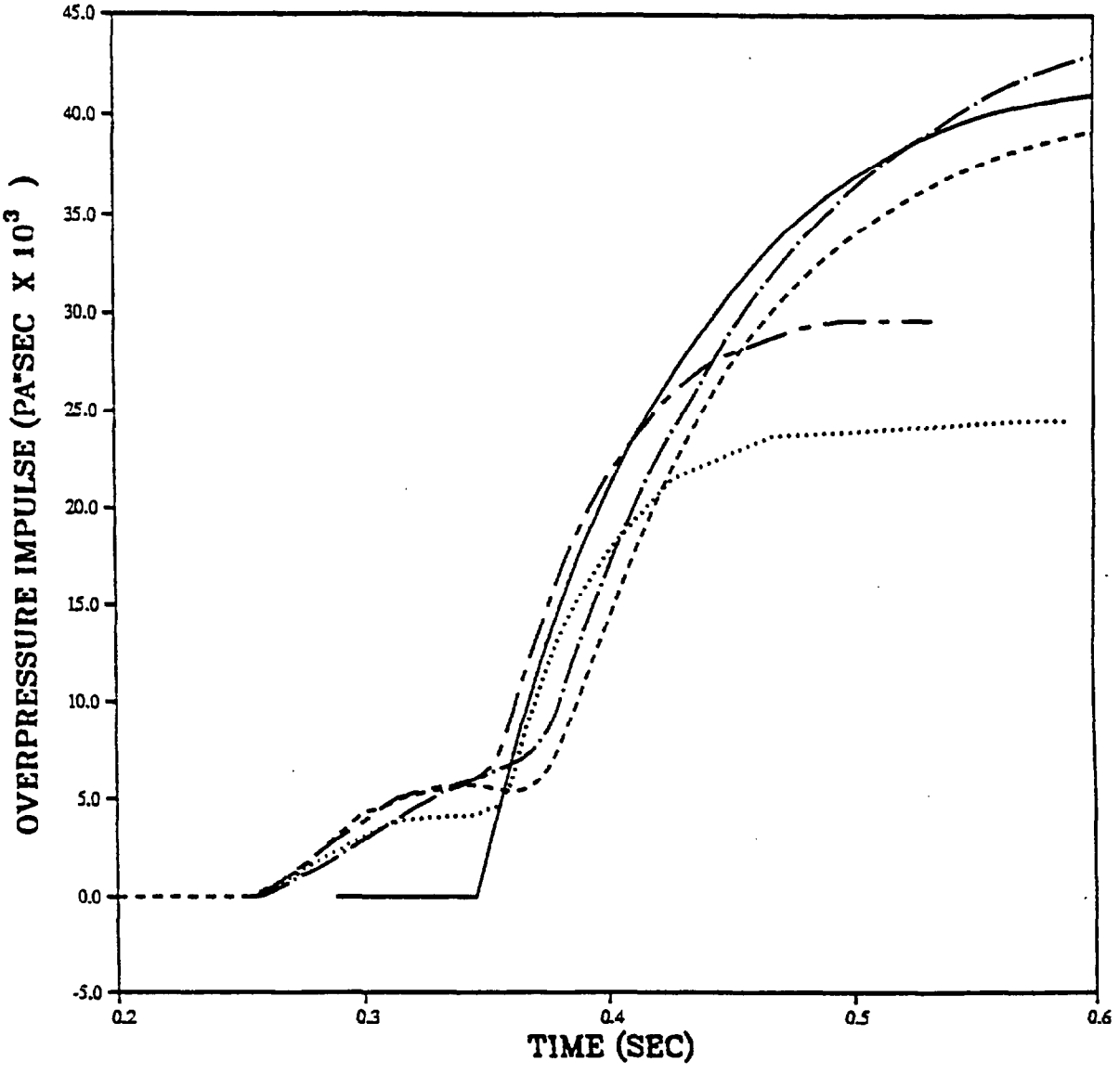

IDEAL
GRASSLAND CALCULATION SURFACE
BRL - 0 M
BRL - 0 M
SRI - 0 M

PRISCILLA
CALCULATION - DATA COMPARISONS
OVERPRESSURE AT 503 METERS (1650 FEET)

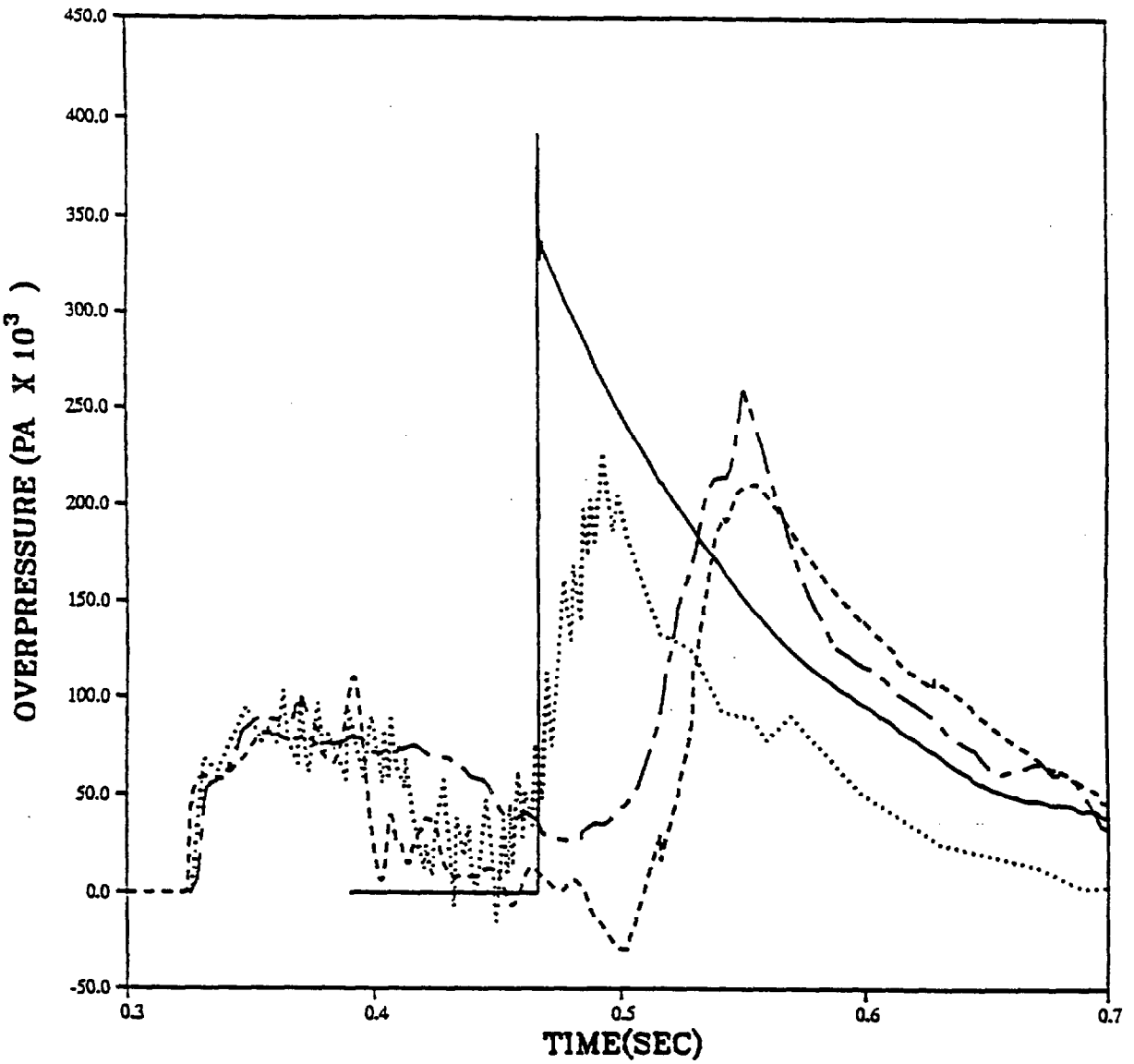

IDEAL
GRASSLAND CALCULATION SURFACE
BRL - 0 M
SRI - 0 M

PRISCILLA
CALCULATION - DATA COMPARISONS
OVERPRESSURE IMPULSE AT 503 METERS (1650 FEET)

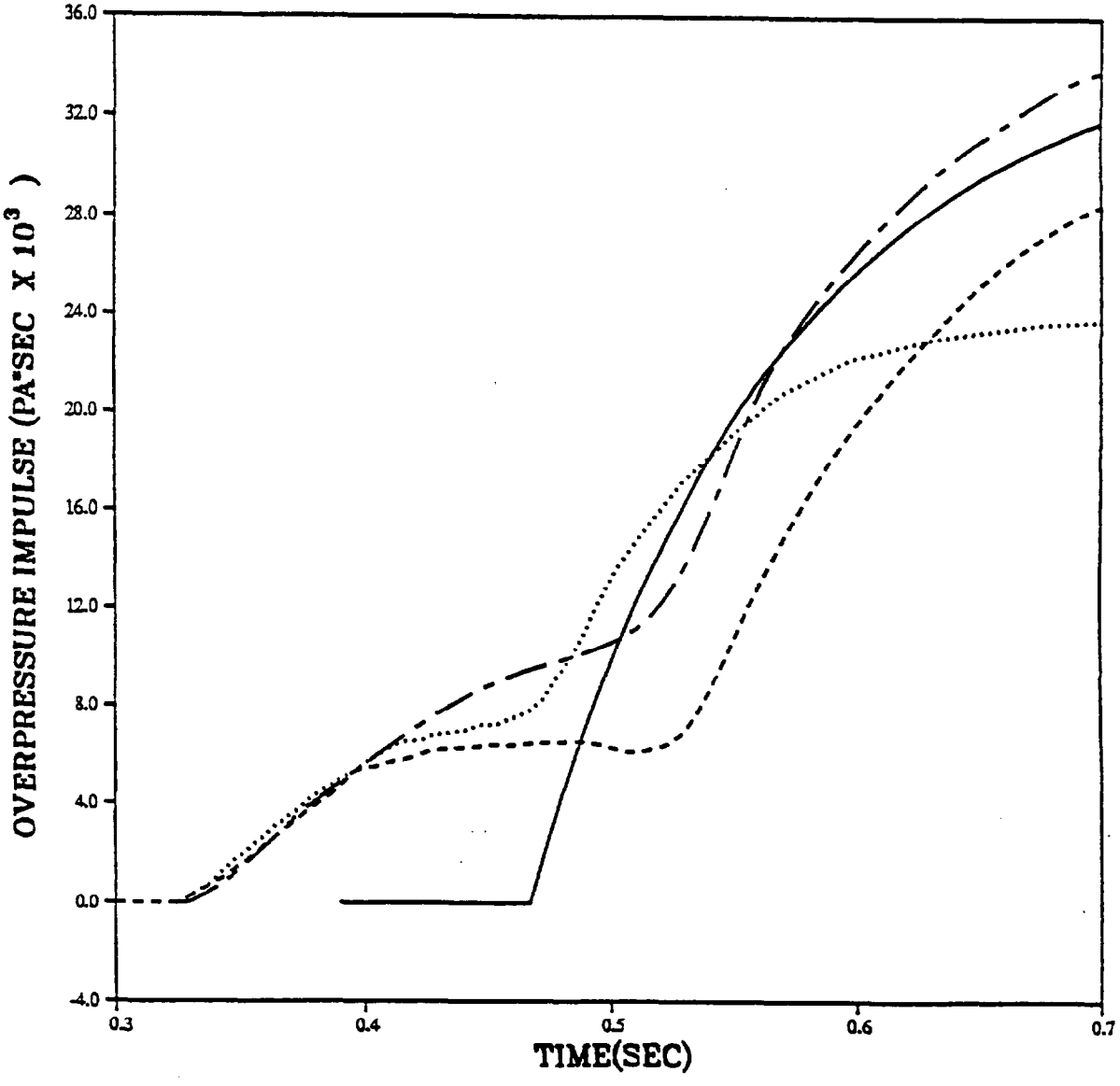

PRISCILLA
CALCULATION - DATA COMPARISONS
OVERPRESSURE AT 610 METERS (2000 FEET)

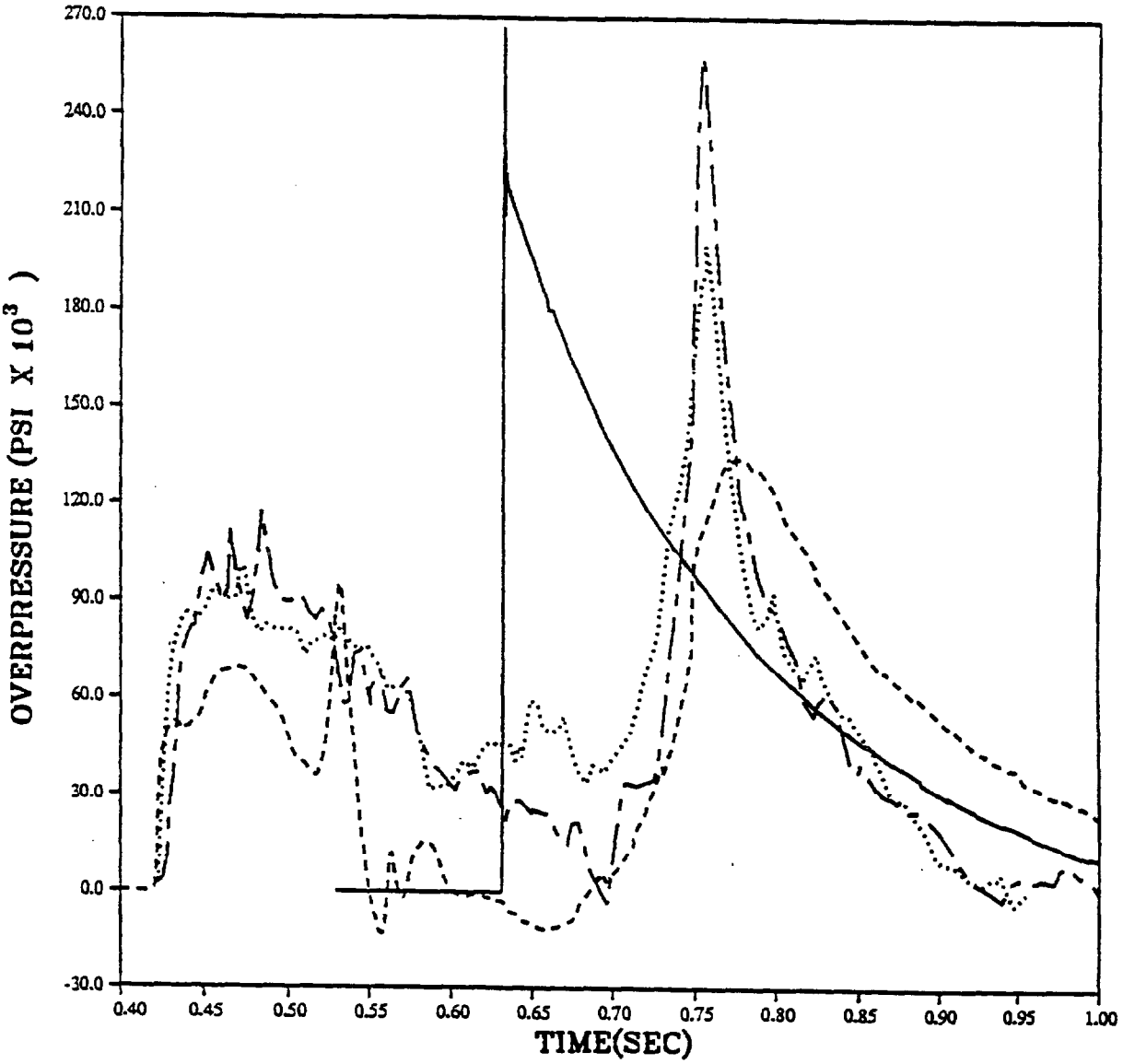

PRISCILLA
CALCULATION - DATA COMPARISONS
OVERPRESSURE IMPULSE AT 610 METERS (2000 FEET)

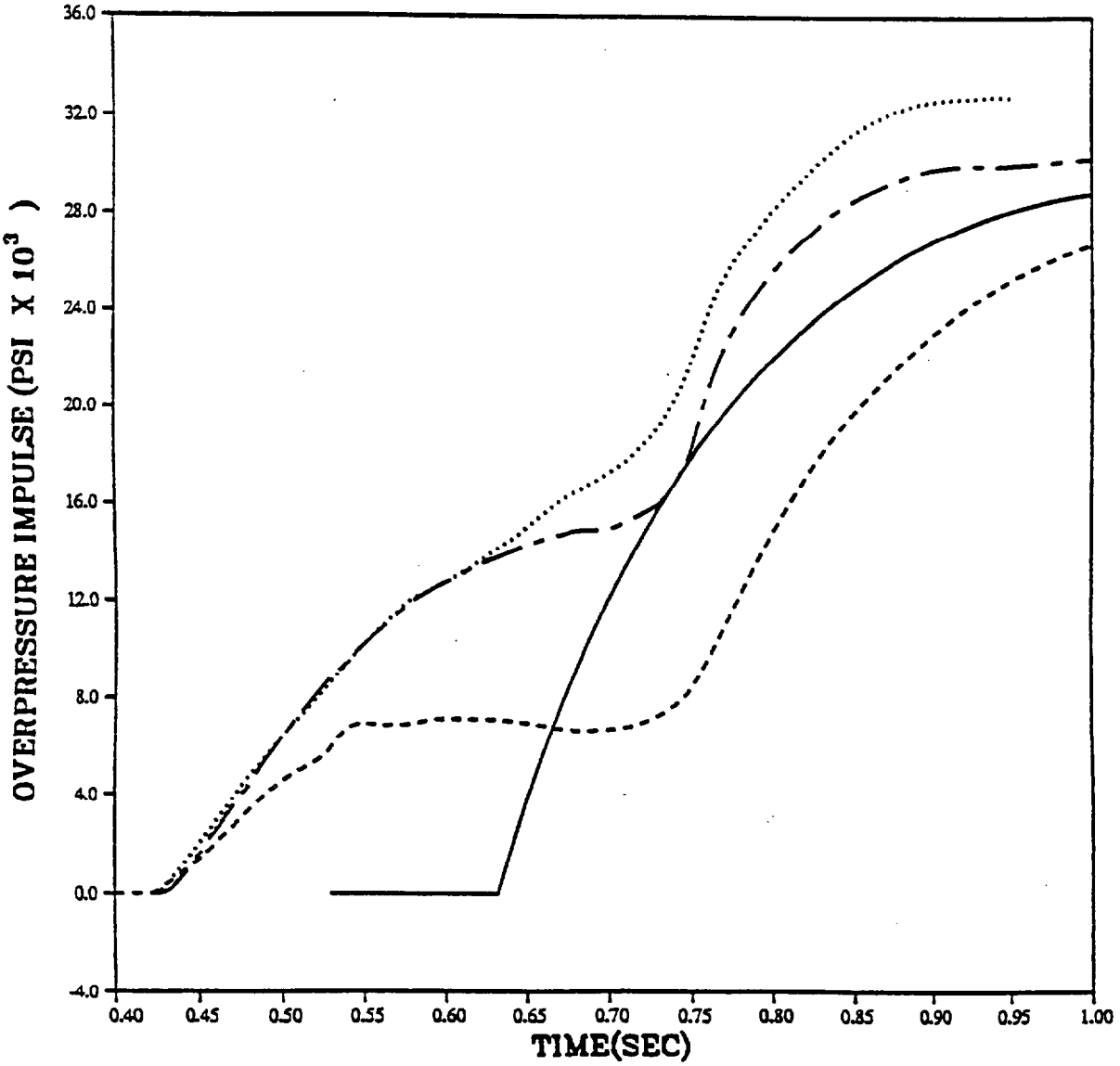

PRISCILLA
CALCULATION - DATA COMPARISONS
OVERPRESSURE AT 686 METERS (2250 FEET)

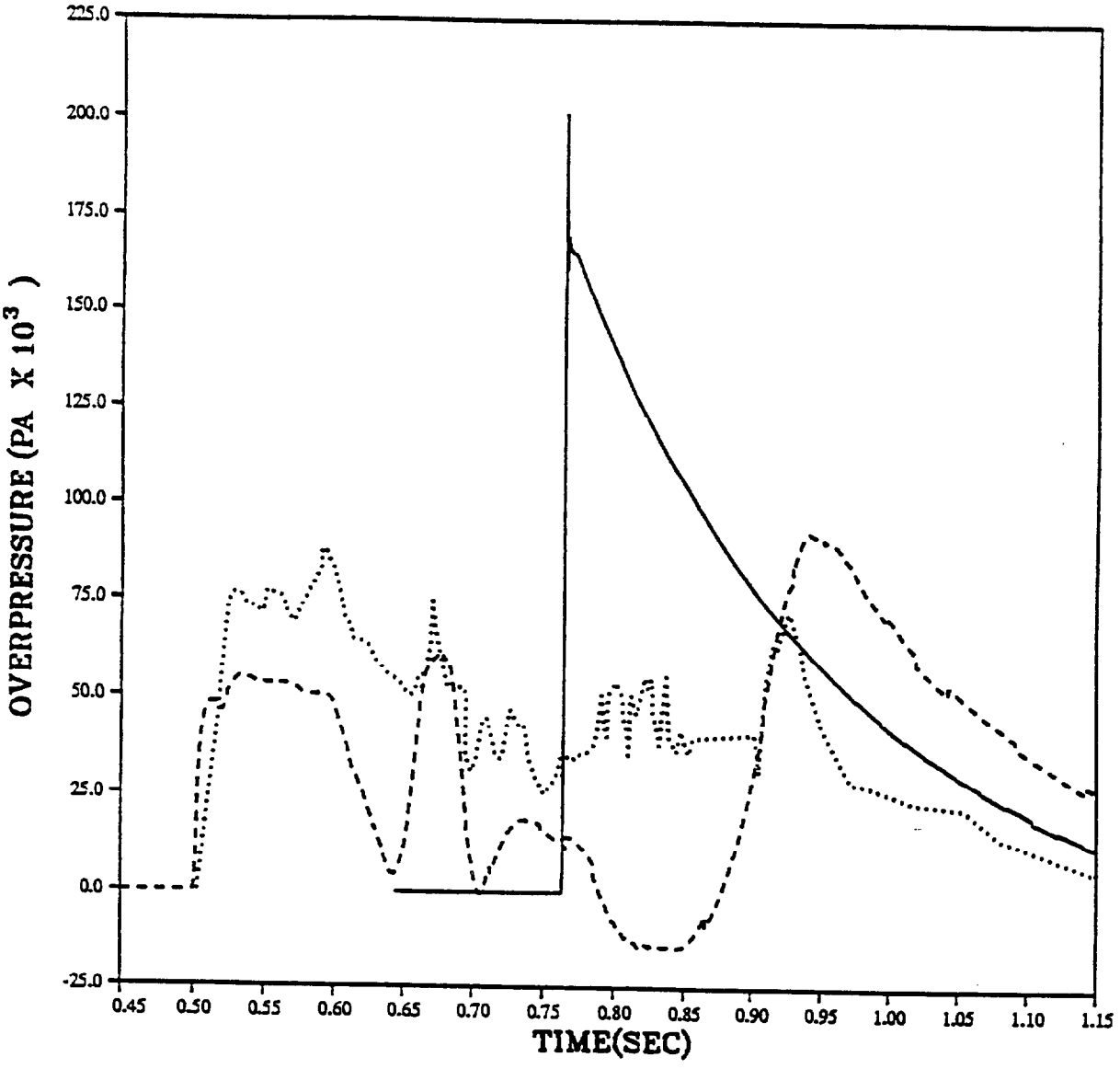

PRISCILLA
CALCULATION - DATA COMPARISONS
OVERPRESSURE IMPULSE AT 686 METERS (2250 FEET)

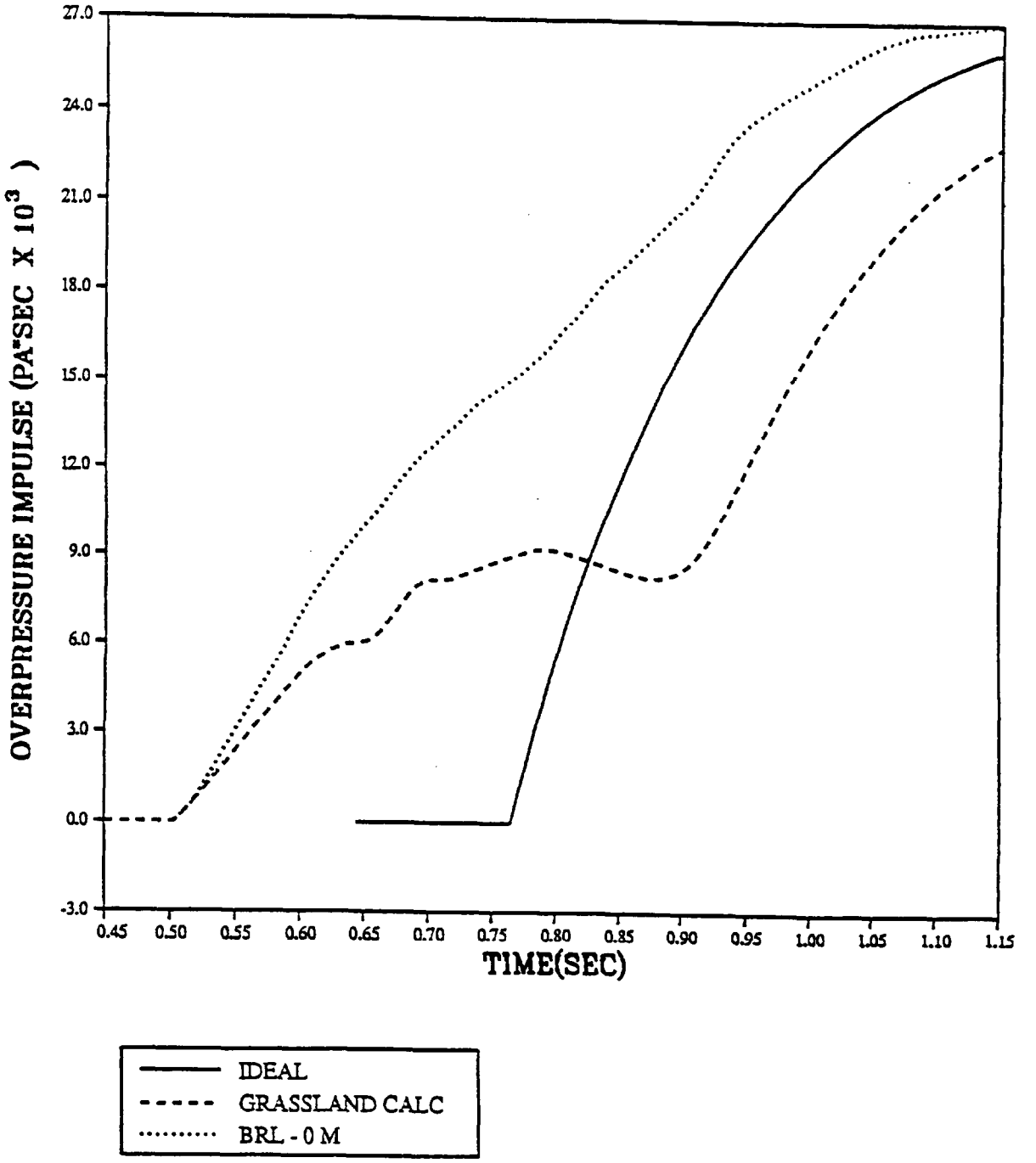

PRISCILLA
CALCULATION - DATA COMPARISONS
OVERPRESSURE AT 762 METERS (2500 FEET)

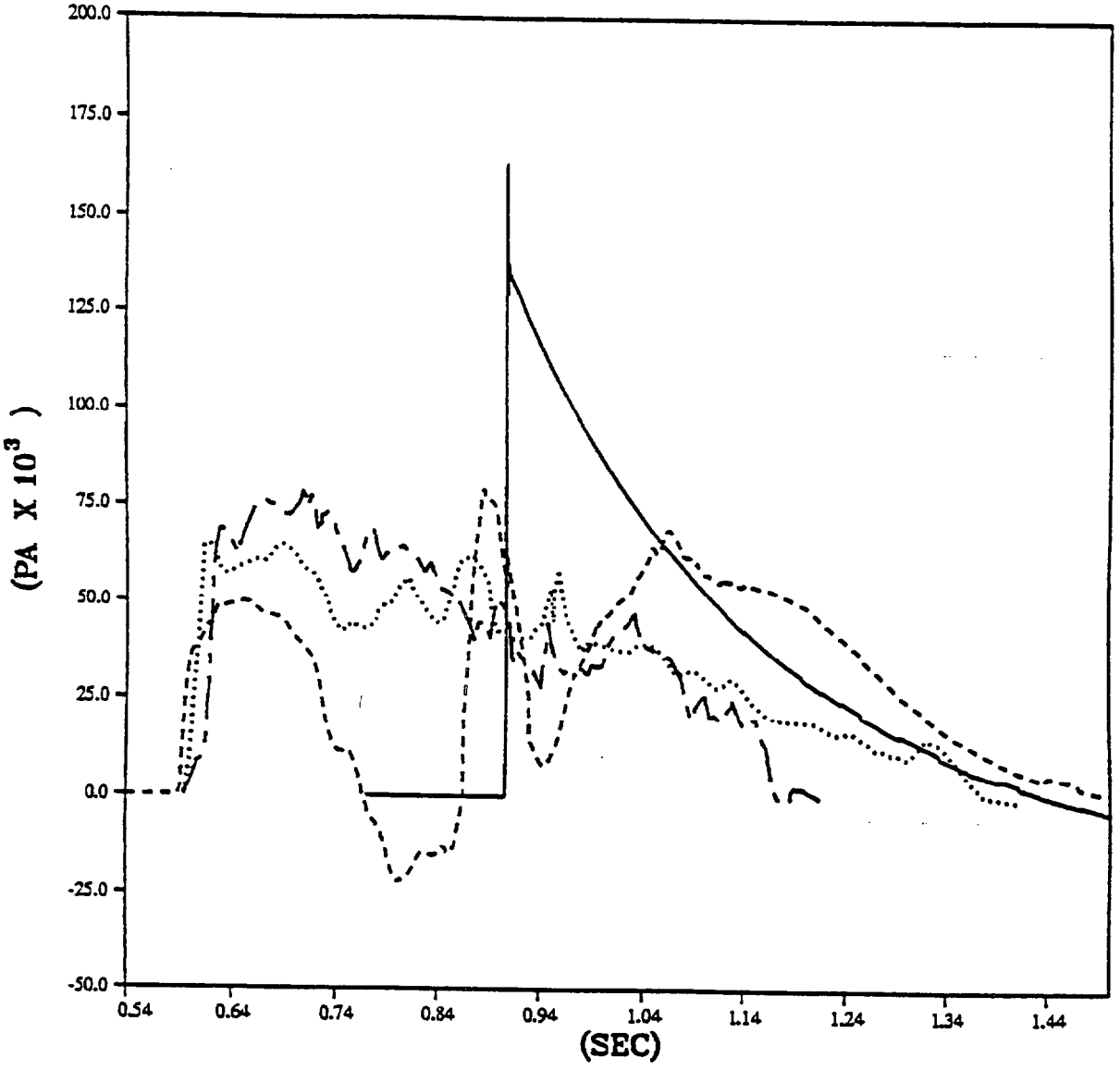

PRISCILLA
CALCULATION - DATA COMPARISONS
OVERPRESSURE IMPULSE AT 762 METERS (2500 FEET)

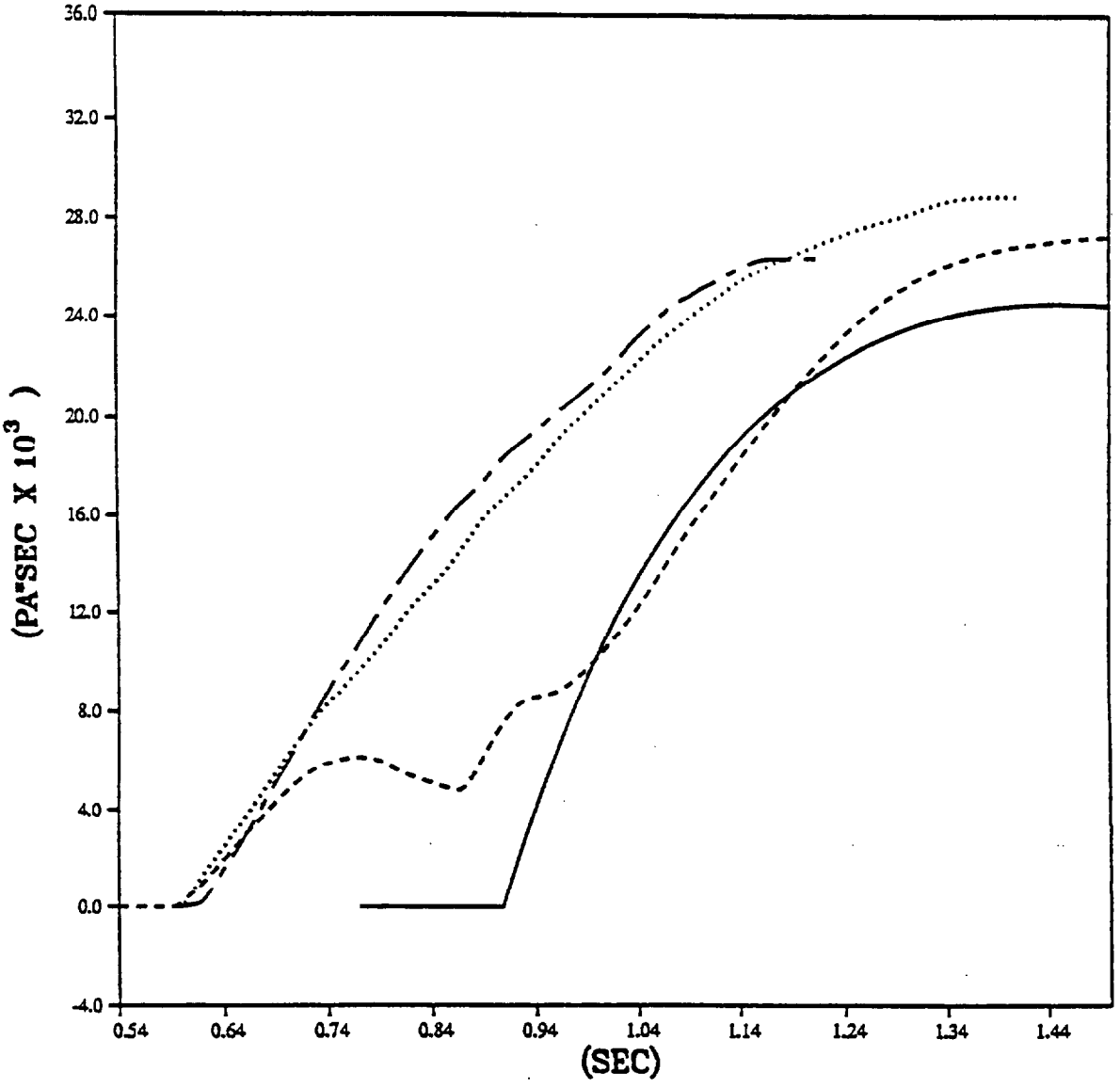

PRISCILLA
CALCULATION - DATA COMPARISONS
OVERPRESSURE AT 762 METERS (2500 FEET)

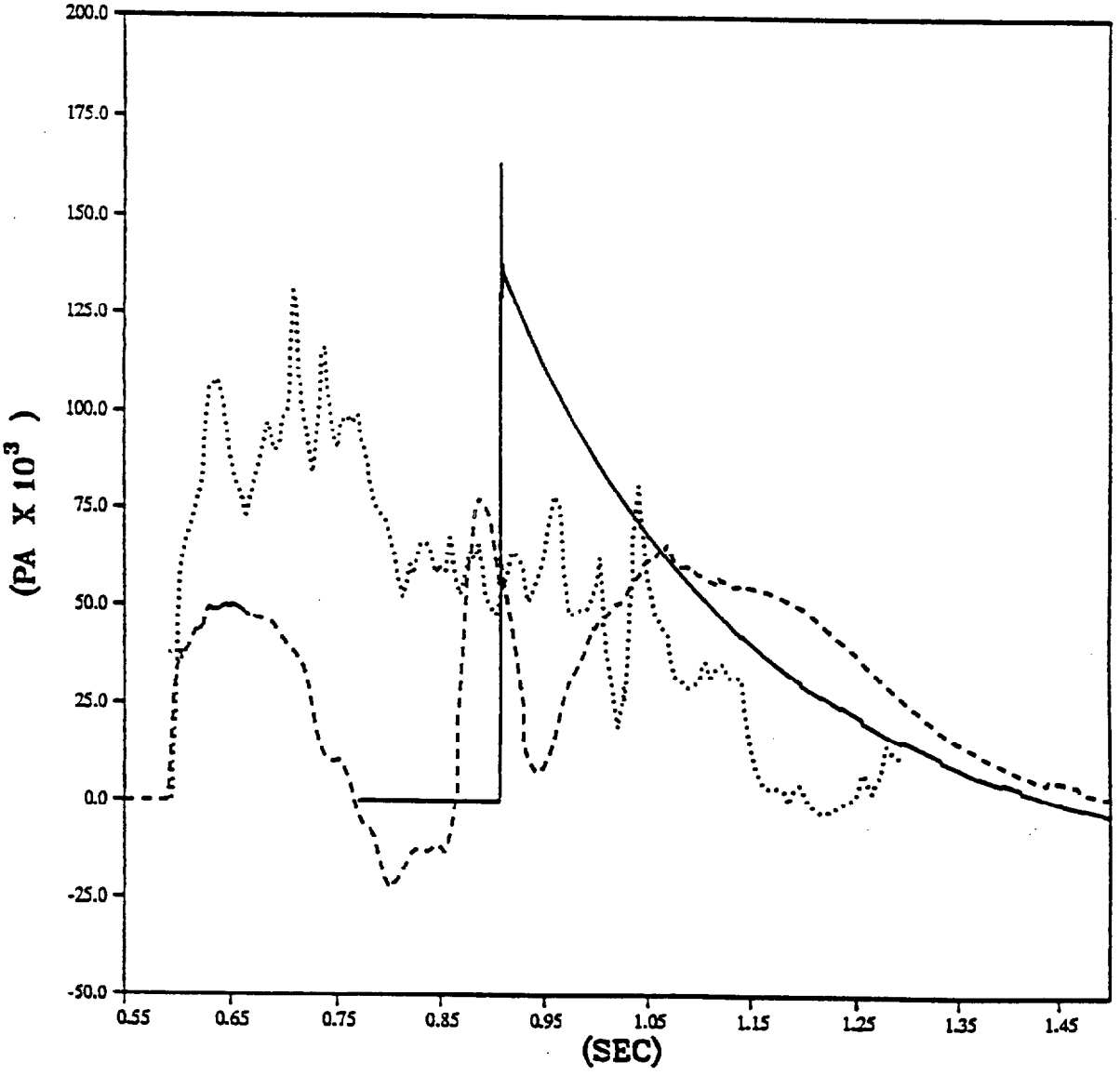

PRISCILLA
CALCULATION - DATA COMPARISONS
OVERPRESSURE IMPULSE AT 762 METERS (2500 FEET)

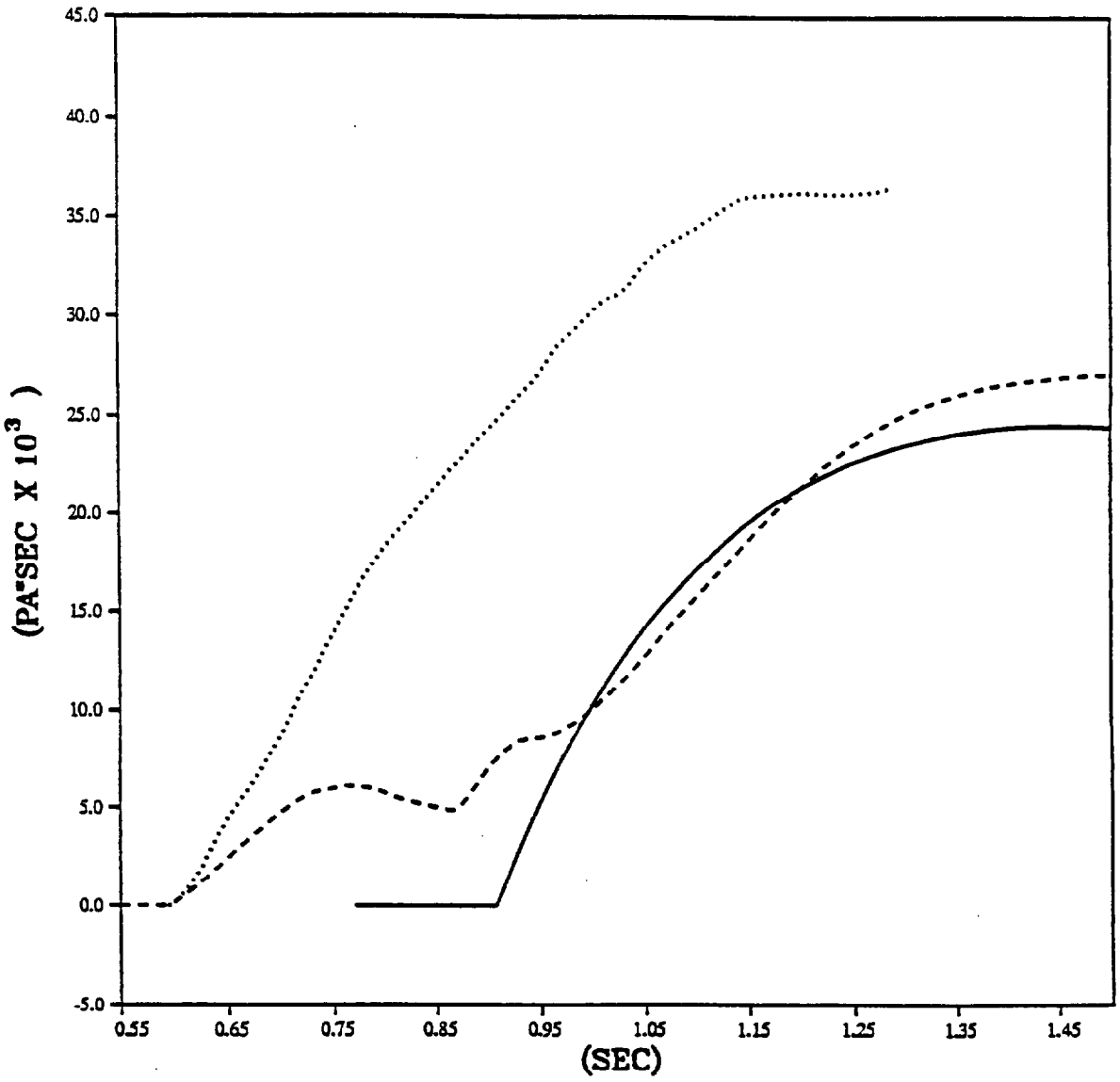

PRISCILLA
CALCULATION - DATA COMPARISONS
OVERPRESSURE AT 762 METERS (2500 FEET)

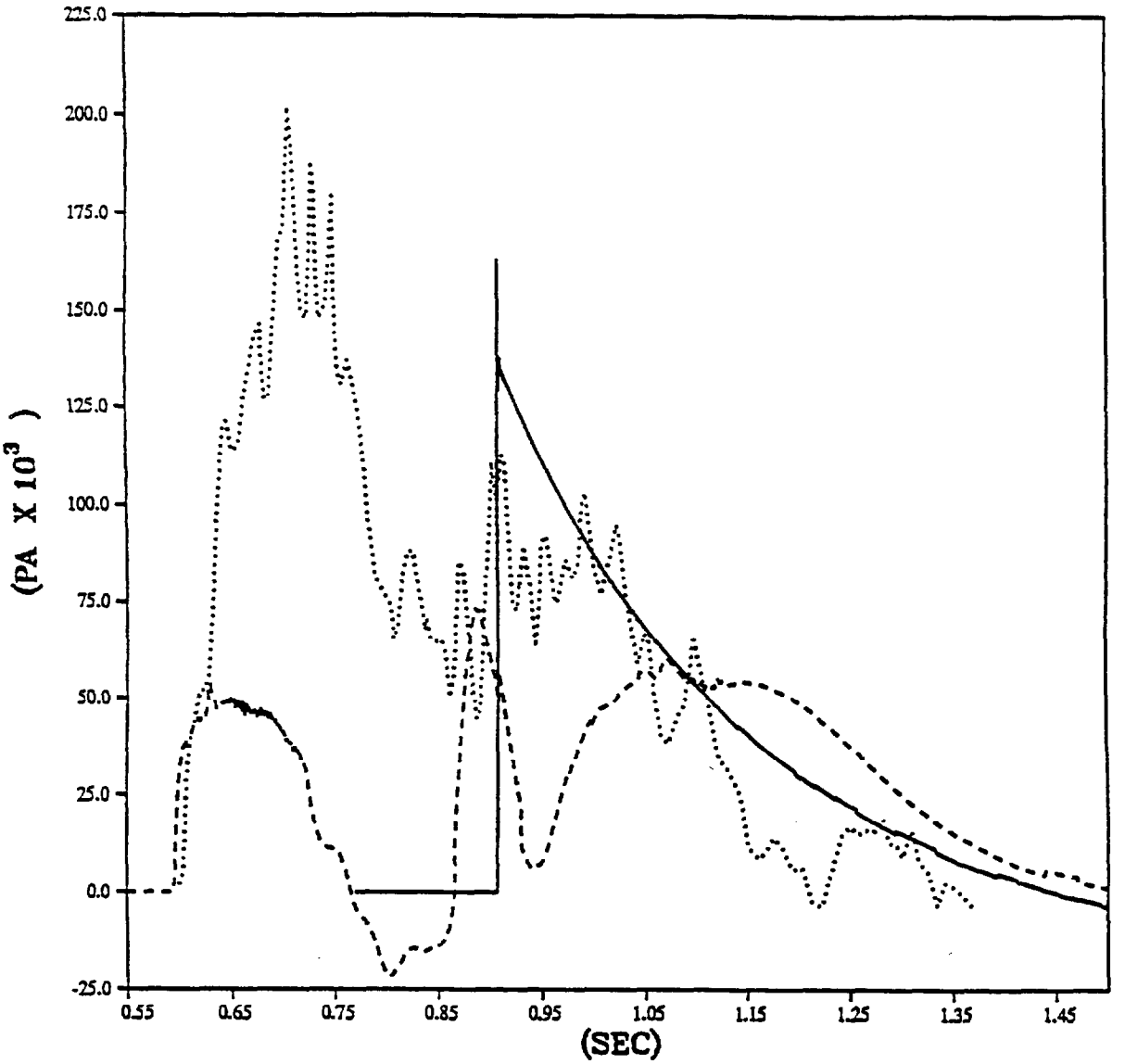

IDEAL - 3.05 M (10 FT)
GRASSLAND CALC - 3.05 M (10 FT)
SRI - 3.05 M (10 FT)

PRISCILLA
CALCULATION - DATA COMPARISONS
OVERPRESSURE IMPULSE AT 762 METERS (2500 FEET)

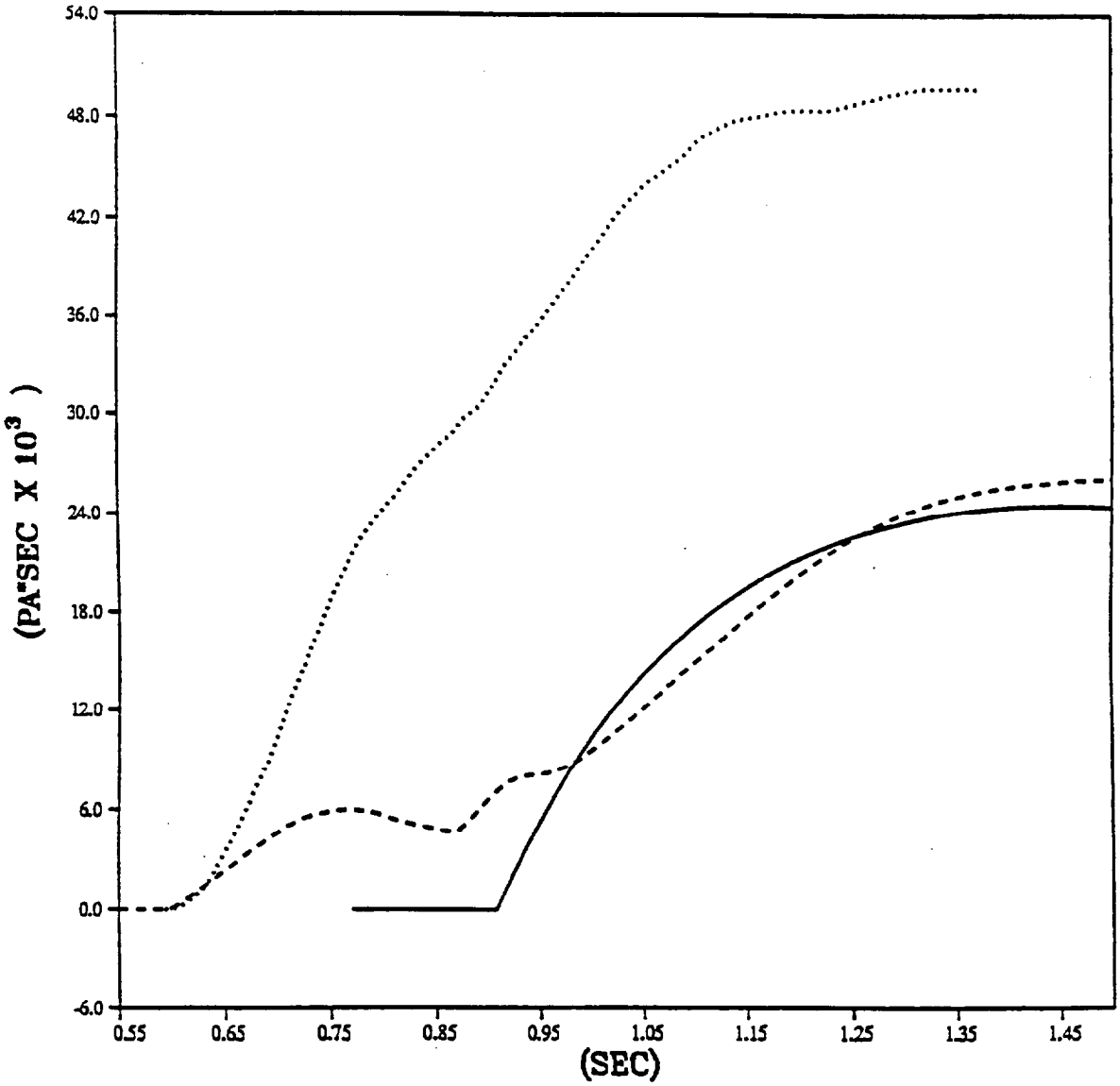

IDEAL - 3.05 M (10 FT)
GRASSLAND CALC - 3.05 M (10 FT)
SRI - 3.05 M (10 FT)

PRISCILLA
CALCULATION - DATA COMPARISONS
OVERPRESSURE AT 762 METERS (2500 FEET)

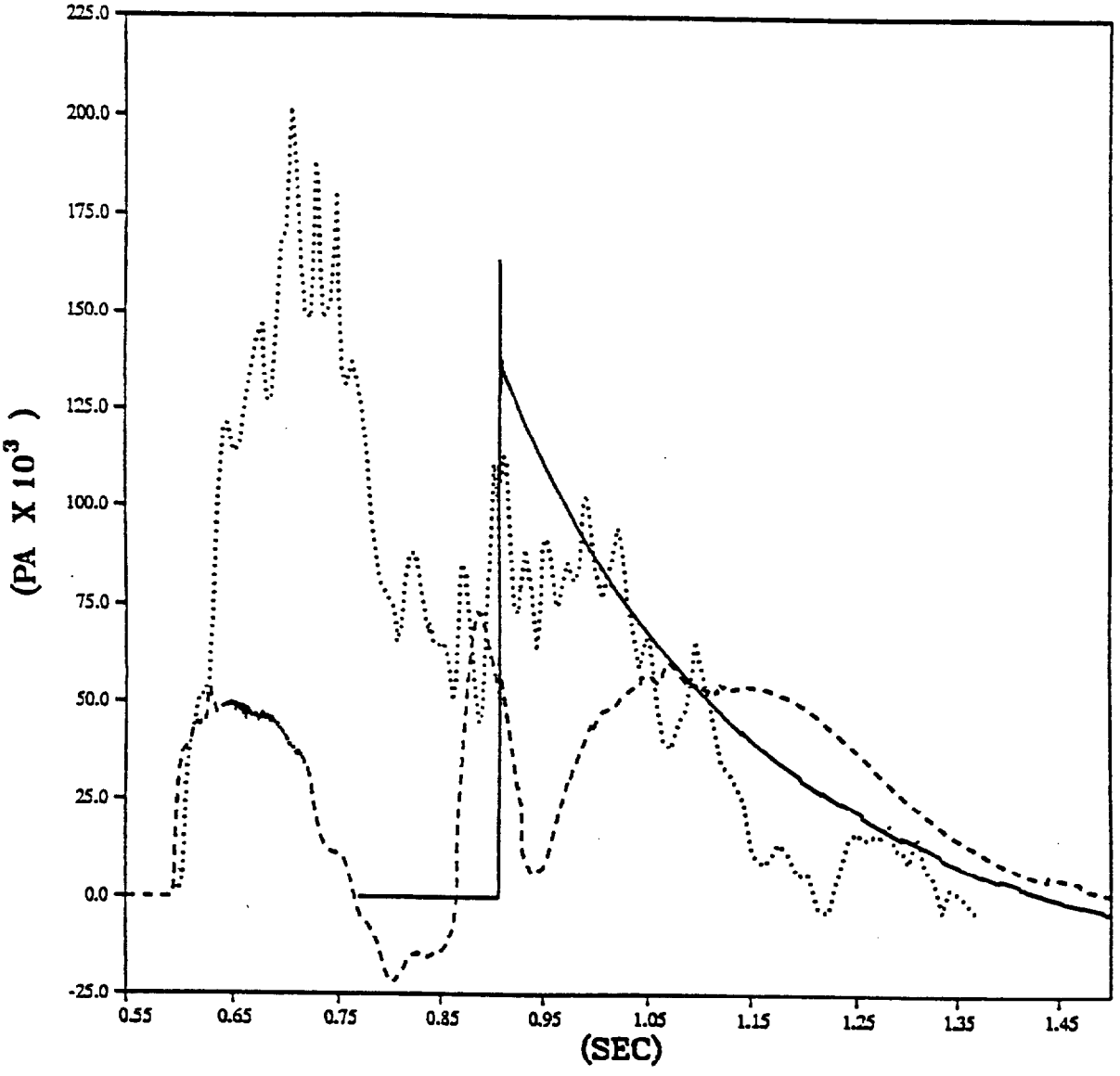

IDEAL - 3.05 M (10 FT)
GRASSLAND CALC - 3.05 M (10 FT)
SRI - 3.05 M (10 FT)

PRISCILLA
CALCULATION - DATA COMPARISONS
OVERPRESSURE AT 914 METERS (3000 FEET)

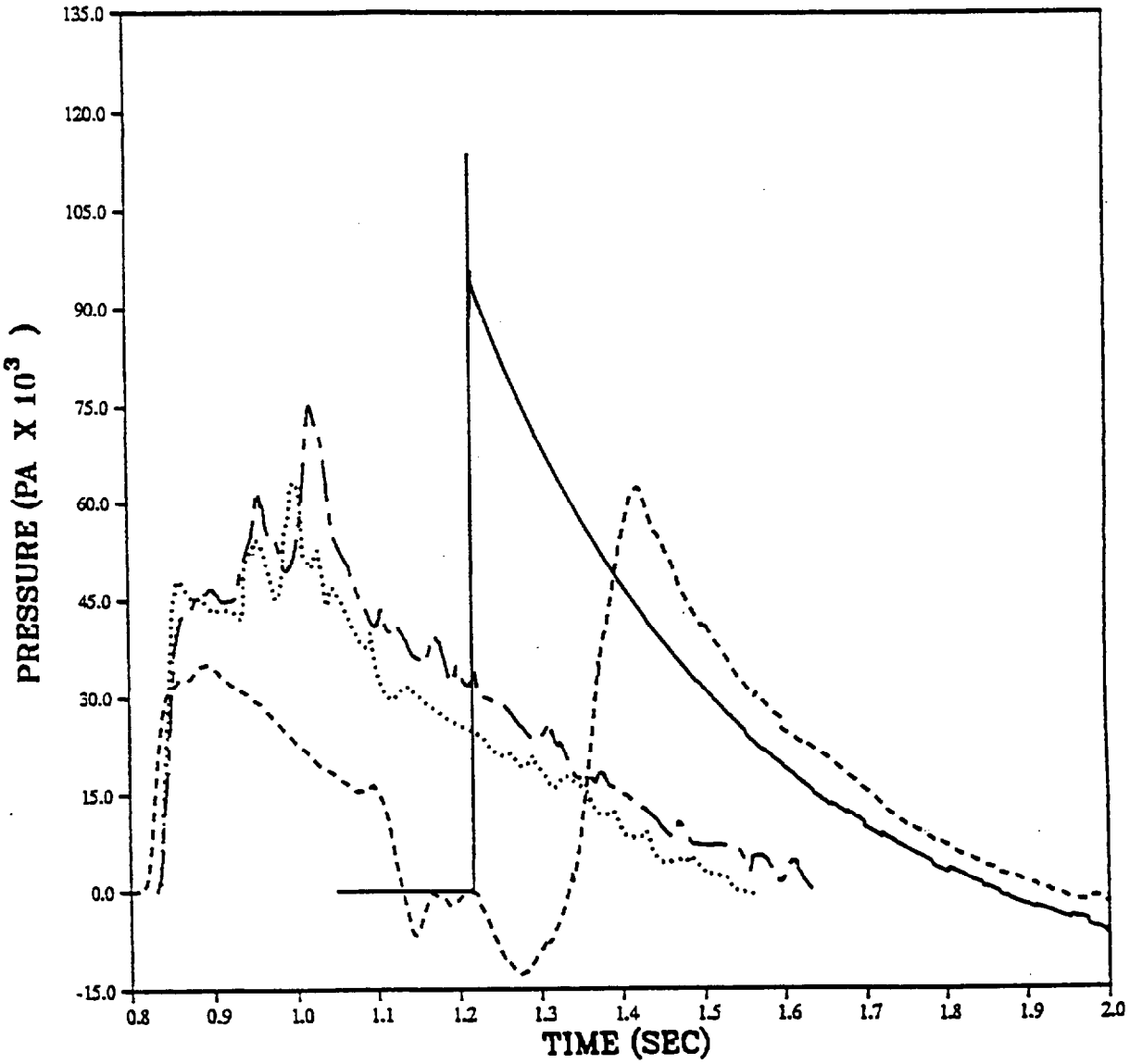

IDEAL 0 M
GRASSLAND CALC 0M
BRL 0M
SRI 0M

PRISCILLA
CALCULATION - DATA COMPARISONS
OVERPRESSURE IMPULSE AT 914 METERS (3000 FEET)

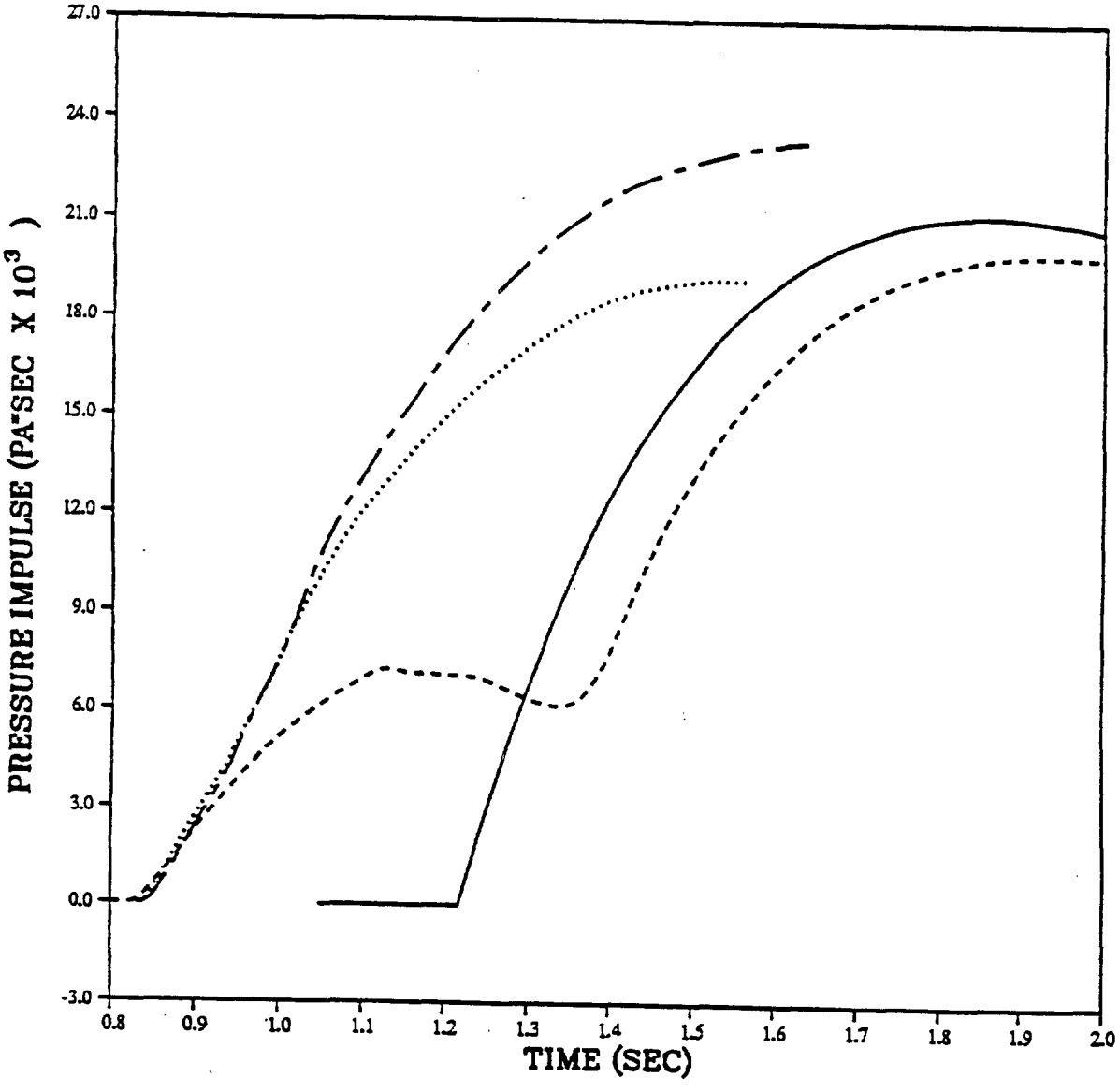

IDEAL 0 M
GRASSLAND CALC 0M
BRL 0M
SRI 0M

PRISCILLA
CALCULATION - DATA COMPARISONS
OVERPRESSURE AT 914 METERS (3000 FEET)

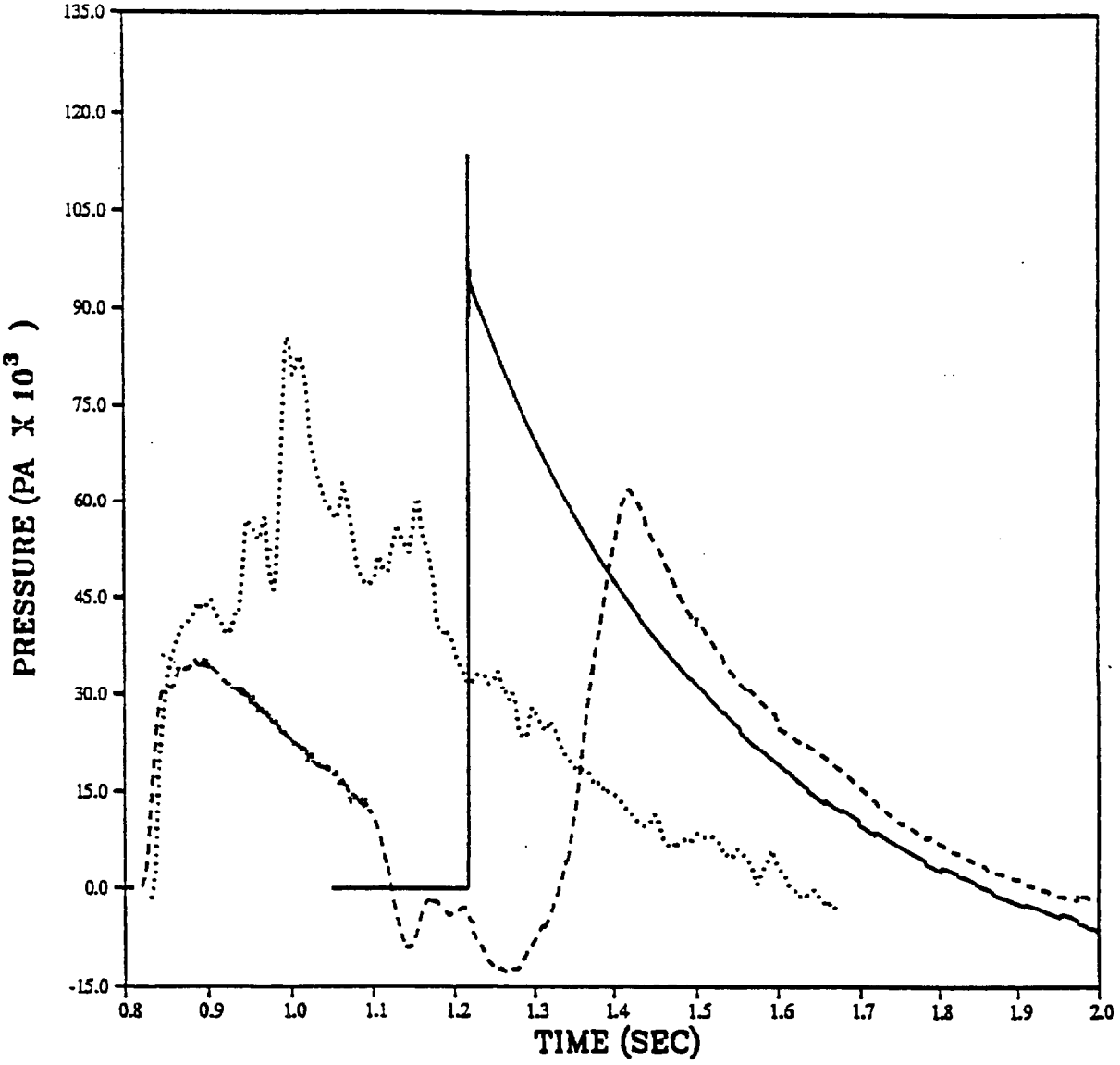

PRISCILLA
CALCULATION - DATA COMPARISONS
OVERPRESSURE IMPULSE AT 914 METERS (3000 FEET)

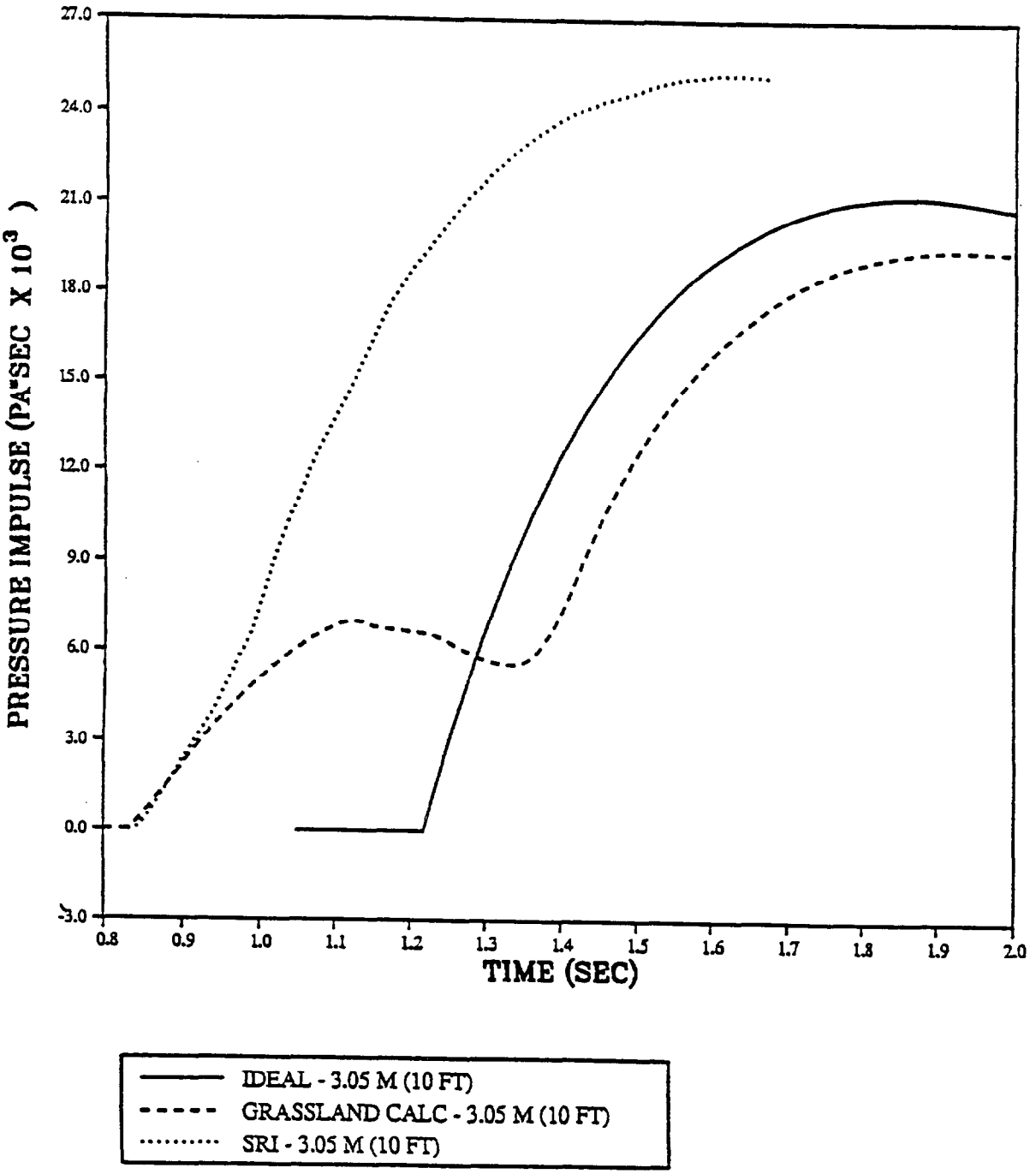

PRISCILLA
CALCULATION - DATA COMPARISONS
OVERPRESSURE AT 1067 METERS (3500 FEET)

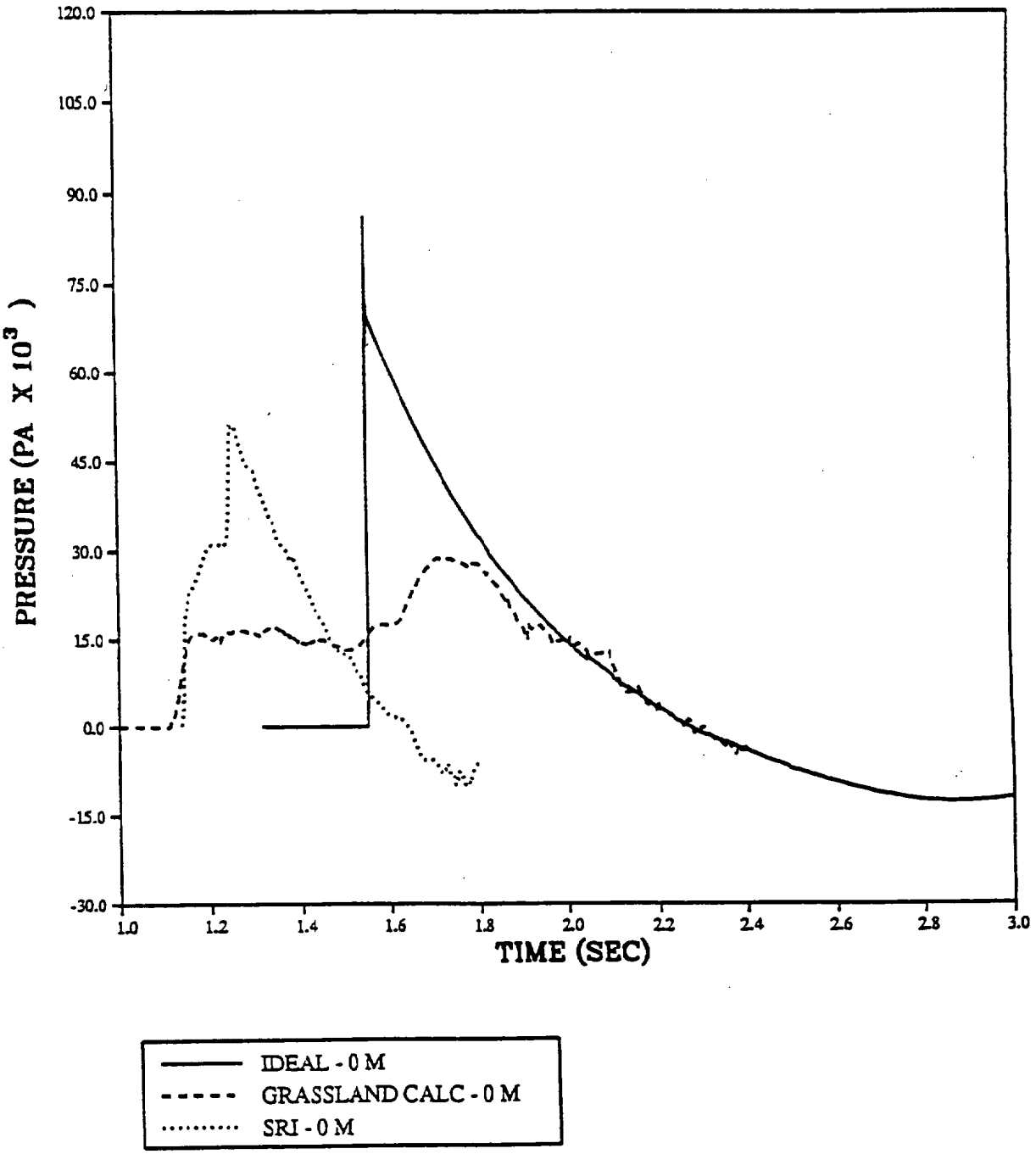

PRISCILLA
CALCULATION - DATA COMPARISONS
OVERPRESSURE IMPULSE AT 1067 METERS (3500 FEET)

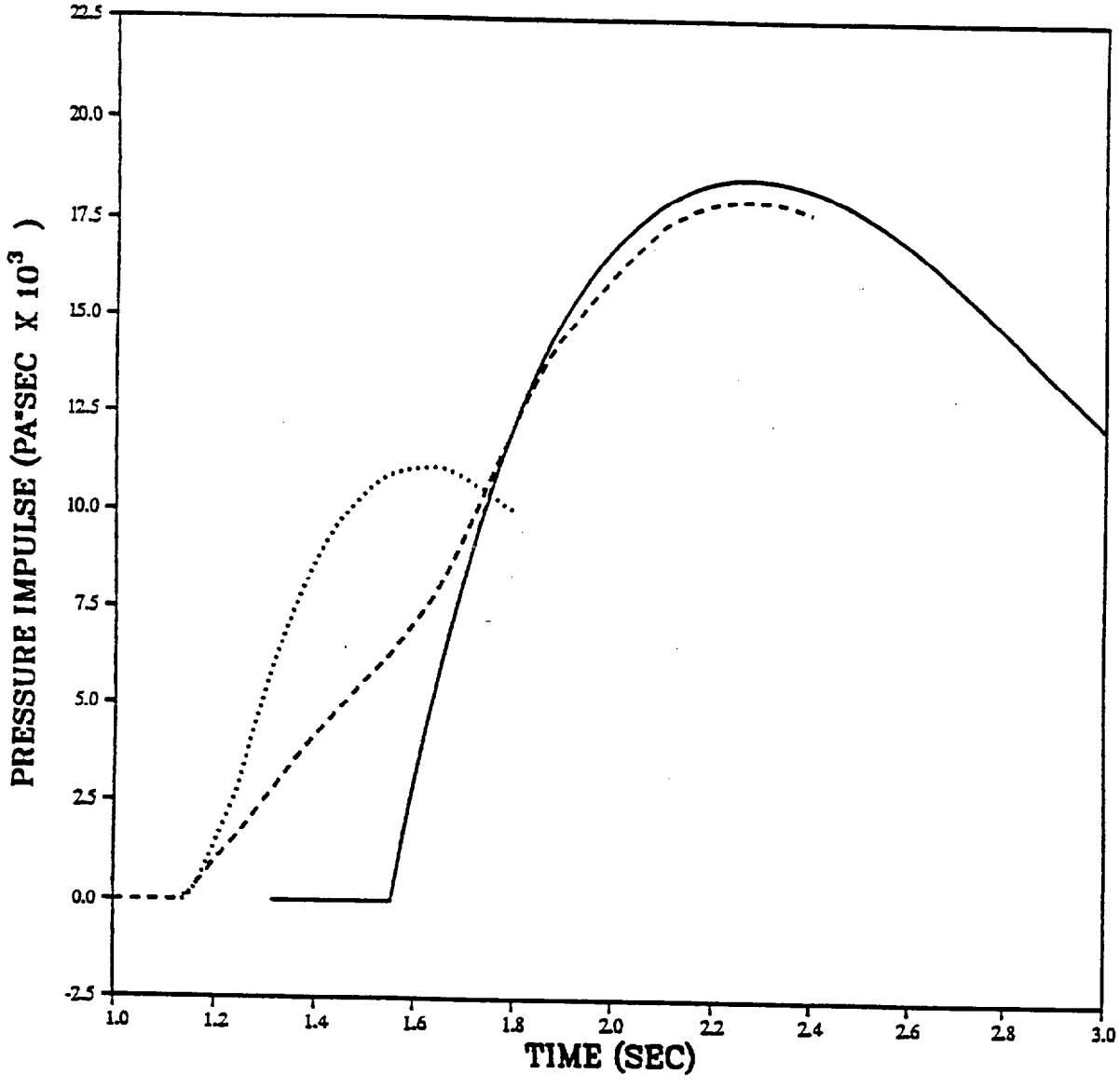

IDEAL - 0 M
GRASSLAND CALC - 0 M
SRI - 0 M

PRISCILLA
CALCULATION - DATA COMPARISONS
OVERPRESSURE AT 1067 METERS (3500 FEET)

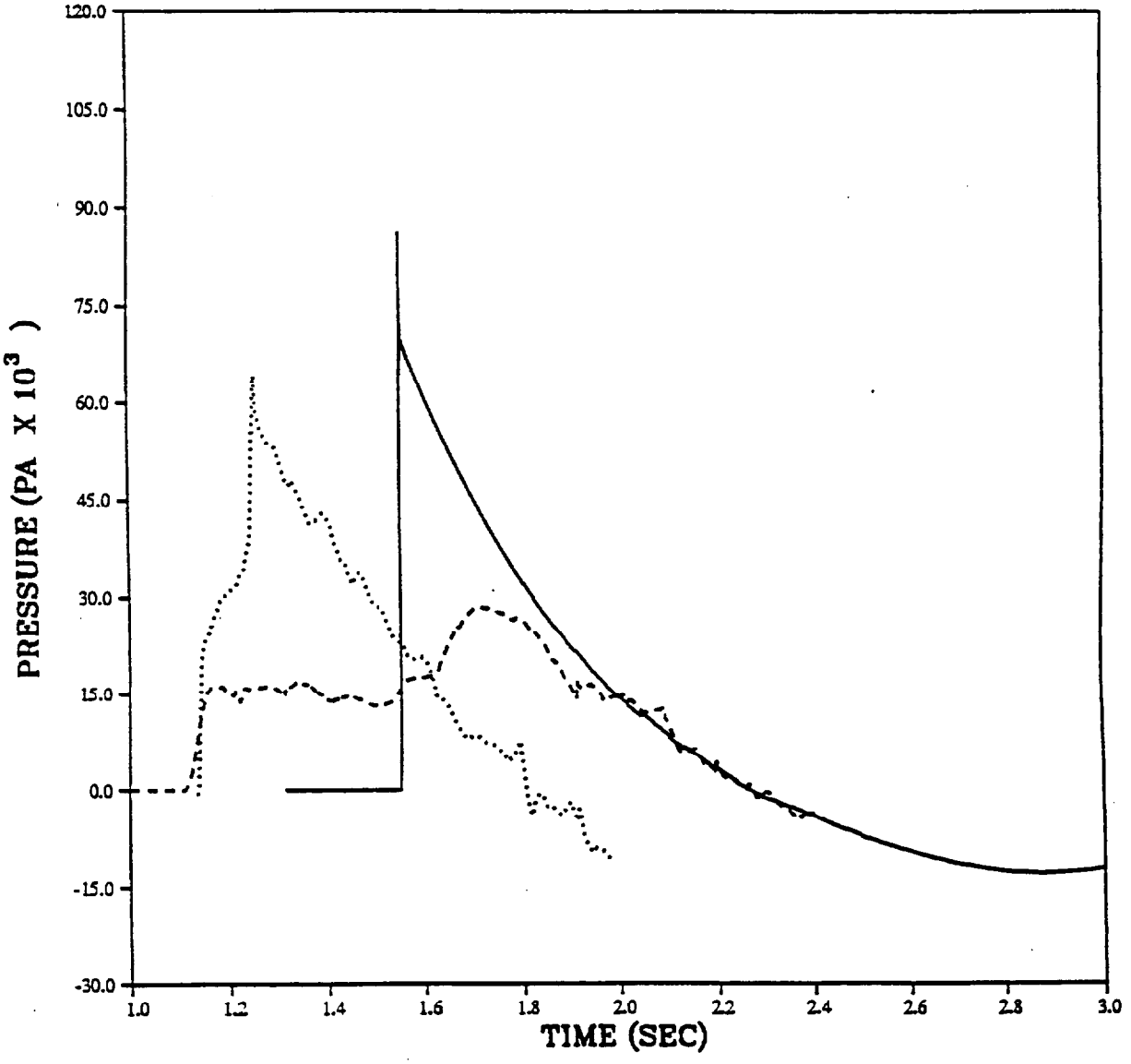

PRISCILLA
CALCULATION - DATA COMPARISONS
OVERPRESSURE IMPULSE AT 1067 METERS (3500 FEET)

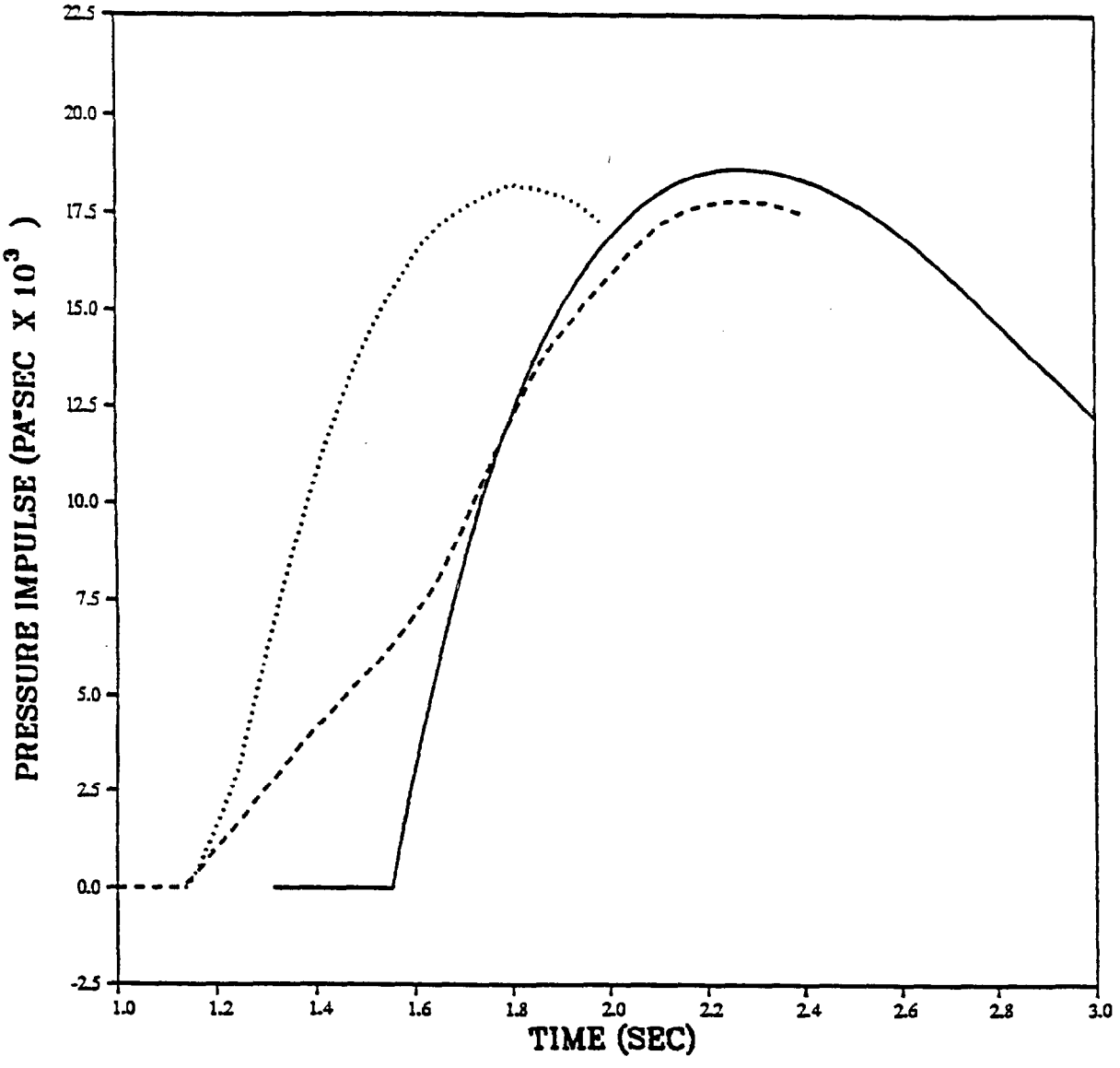

PRISCILLA
CALCULATION - DATA COMPARISONS
OVERPRESSURE AT 1219 METERS (4000 FEET)

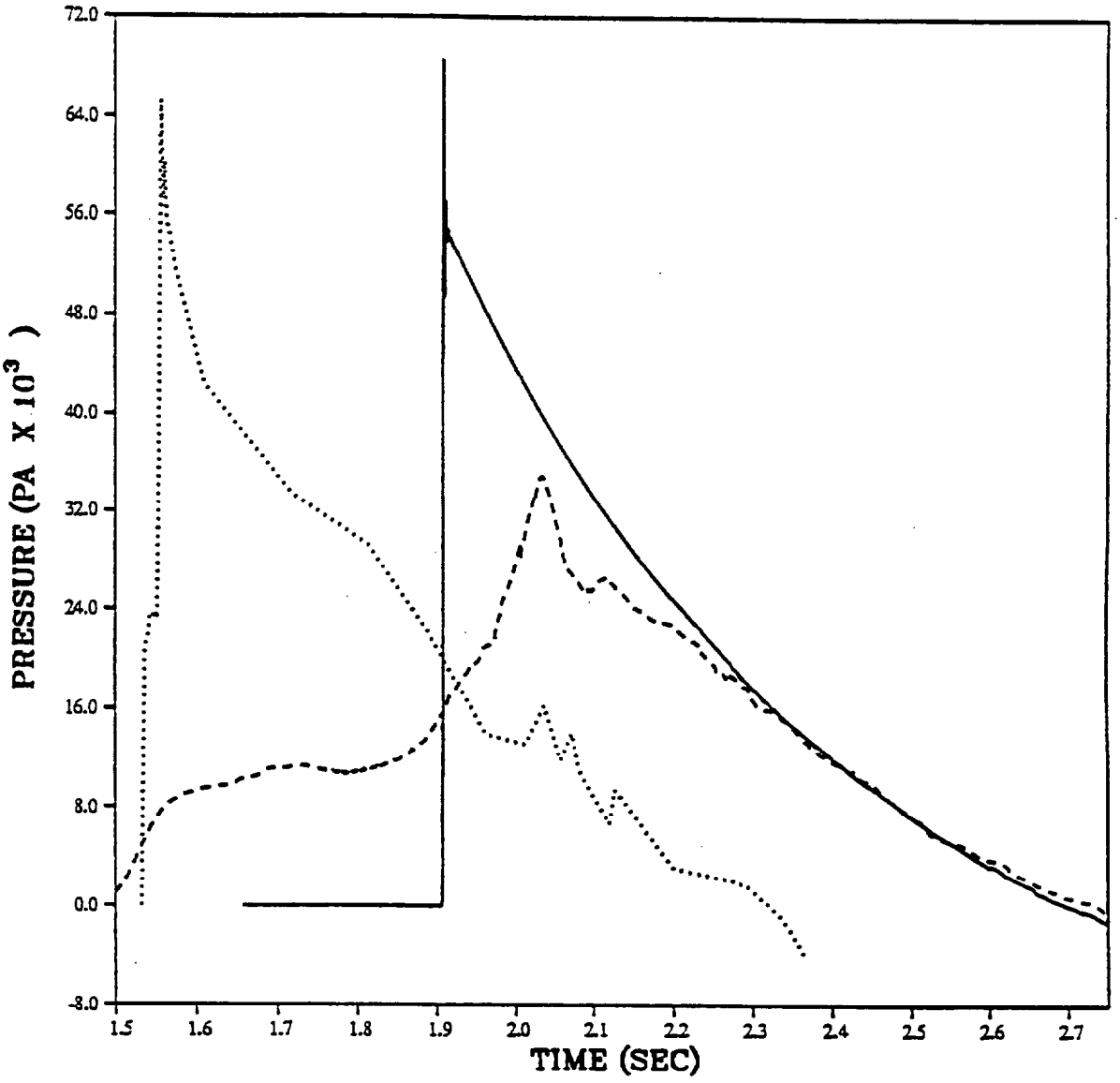

IDEAL 0 M
GRASSLAND CALC 0 M
BRL 0 M

PRISCILLA
CALCULATION - DATA COMPARISONS
OVERPRESSURE IMPULSE AT 1219 METERS (4000 FEET)

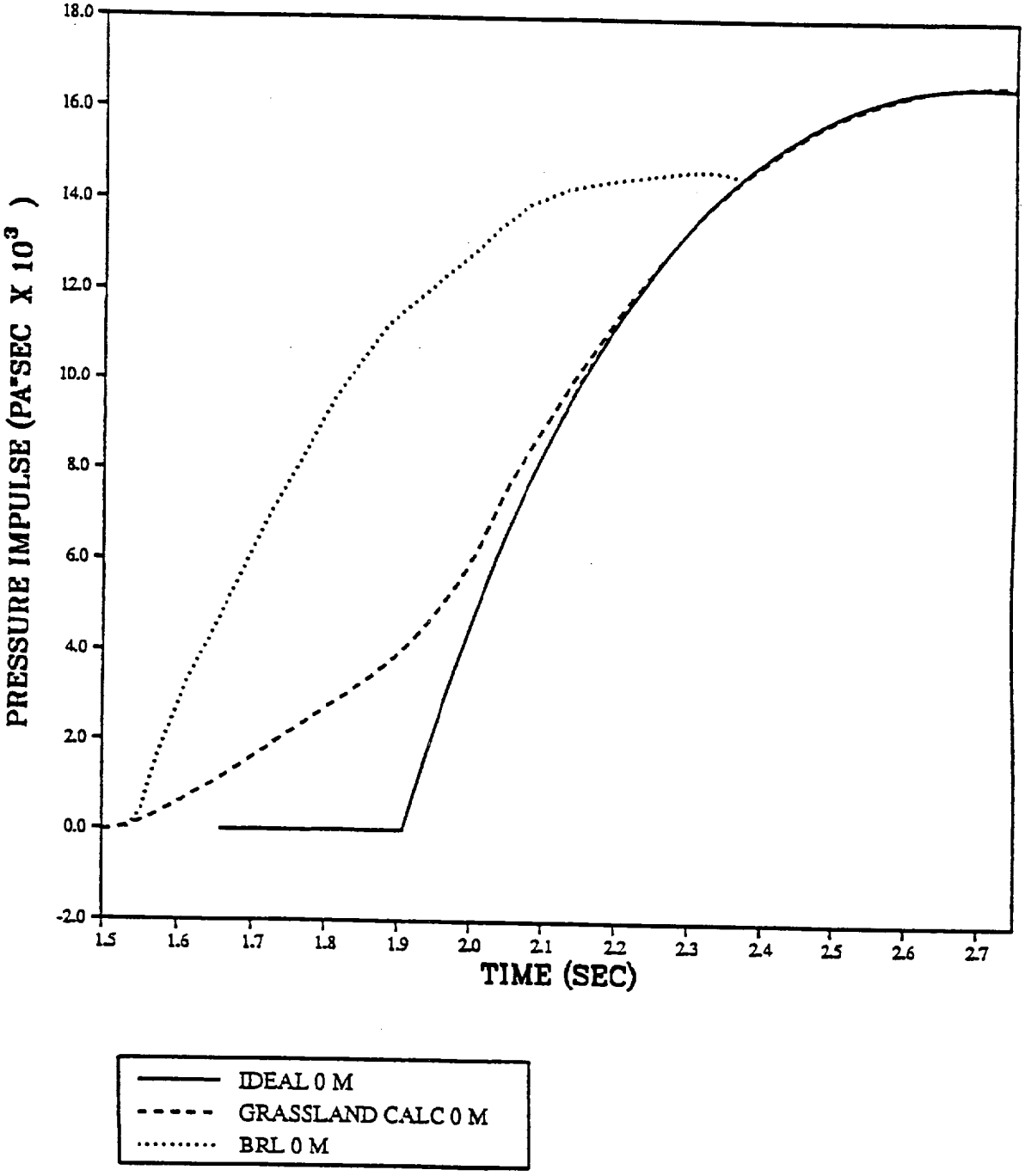

PRISCILLA
CALCULATION - DATA COMPARISONS
OVERPRESSURE AT 1524 METERS (5000 FEET)

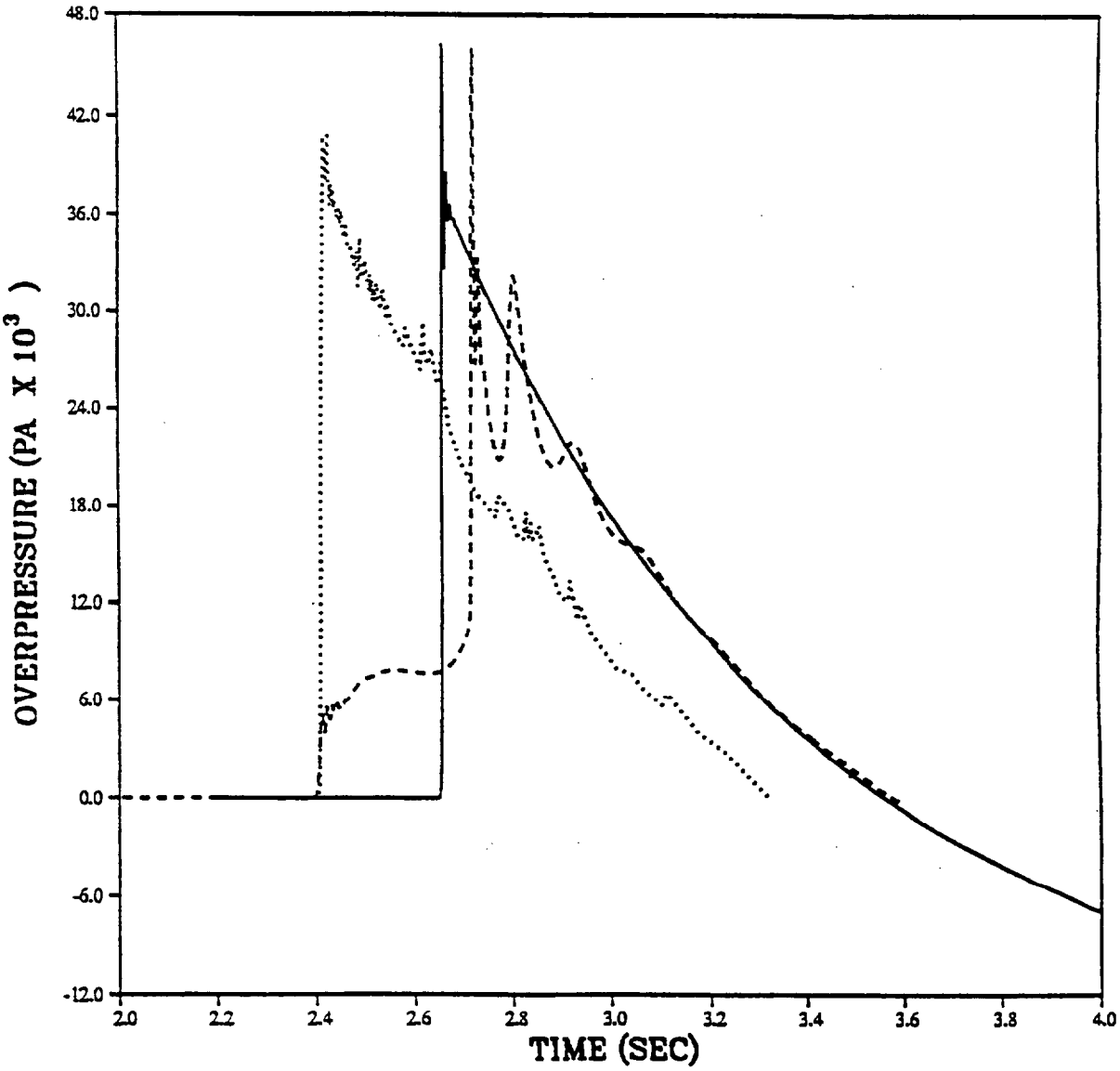

PRISCILLA
CALCULATION - DATA COMPARISONS
OVERPRESSURE IMPULSE AT 1524 METERS (5000 FEET)

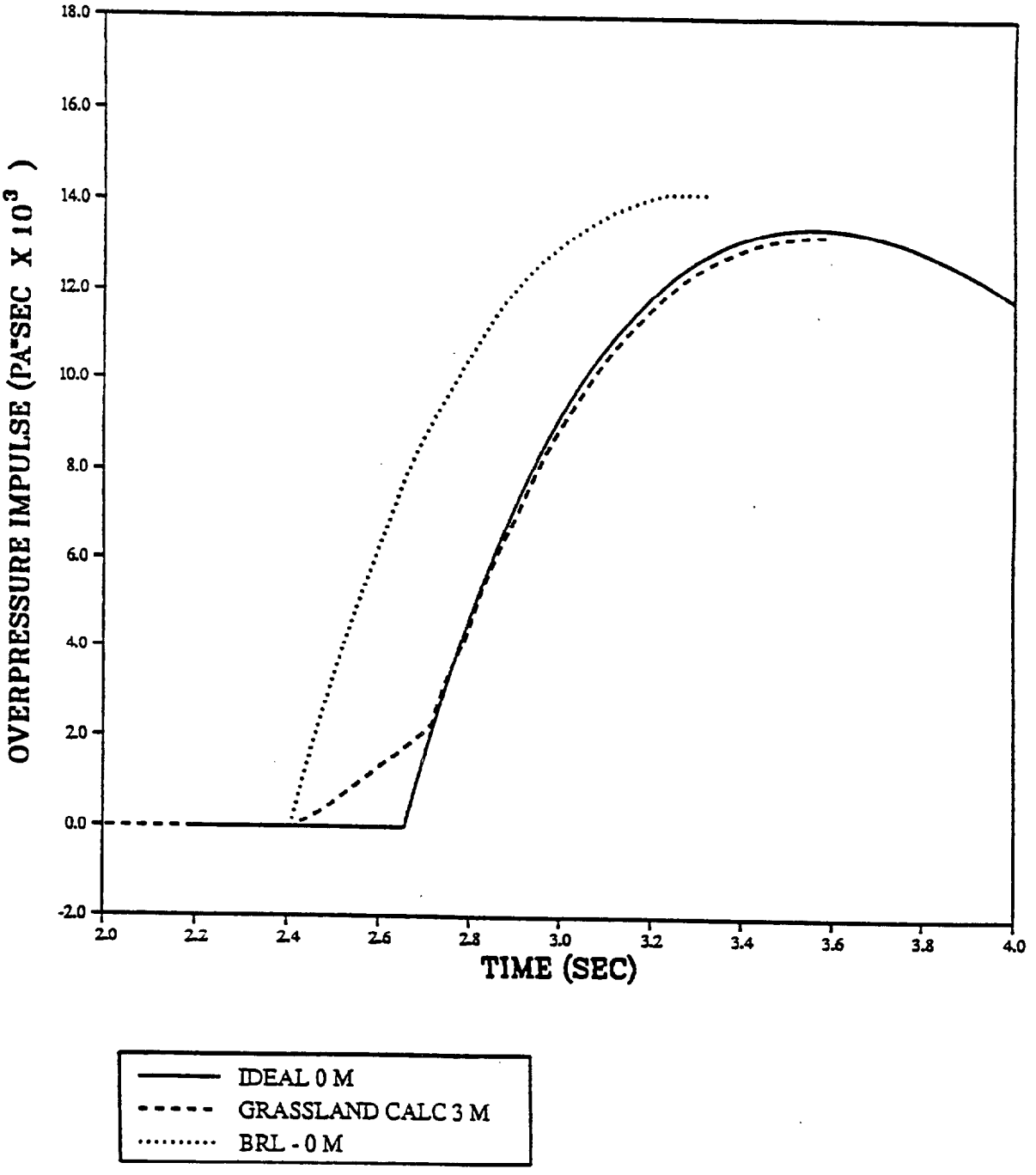

PRISCILLA
CALCULATION - DATA COMPARISONS
DYNAMIC PRESSURE AT 137 METERS (450 FEET)

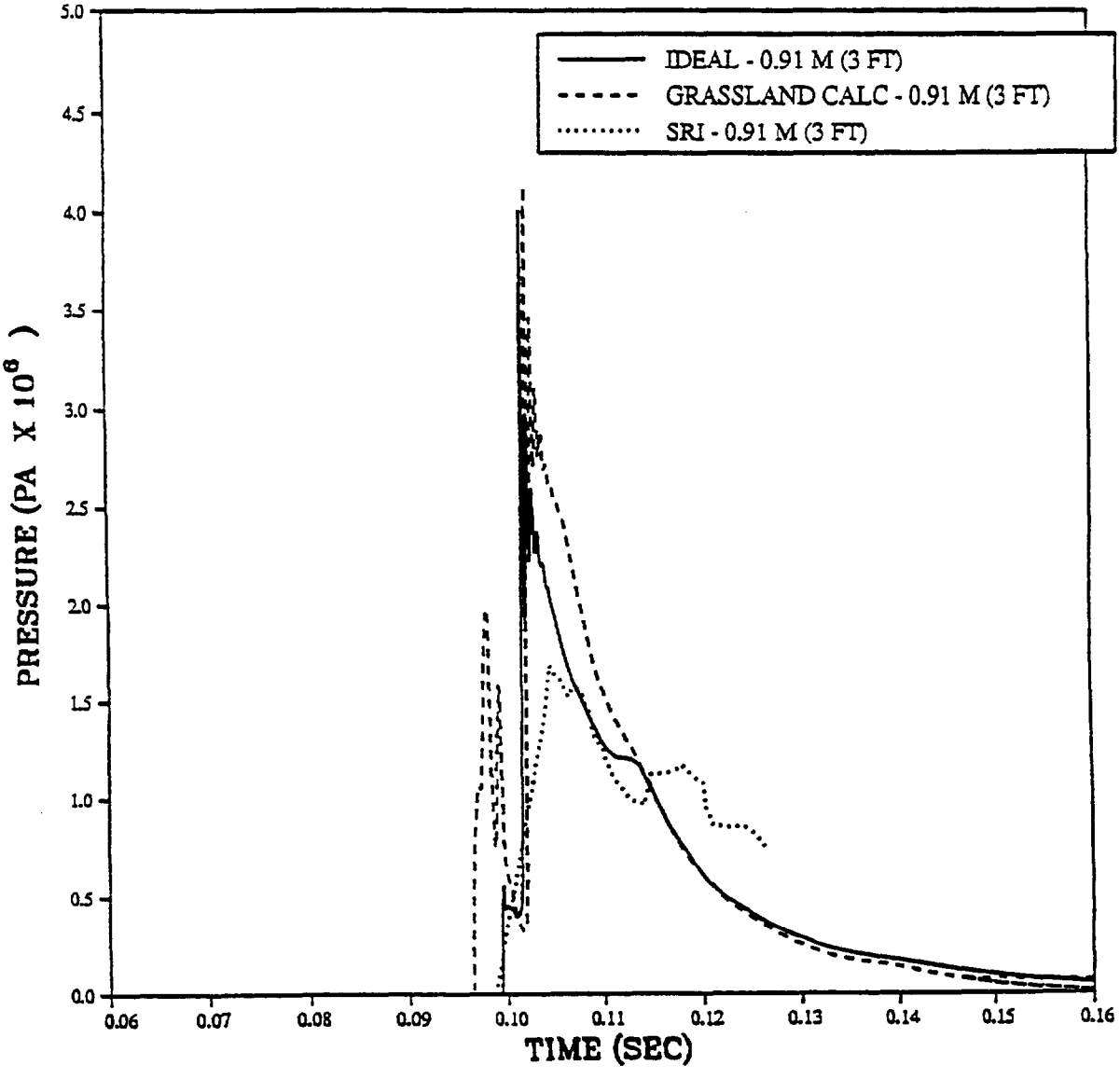

PRISCILLA
CALCULATION - DATA COMPARISONS
DYNAMIC PRESSURE IMPULSE AT 137 METERS (450 FEET)

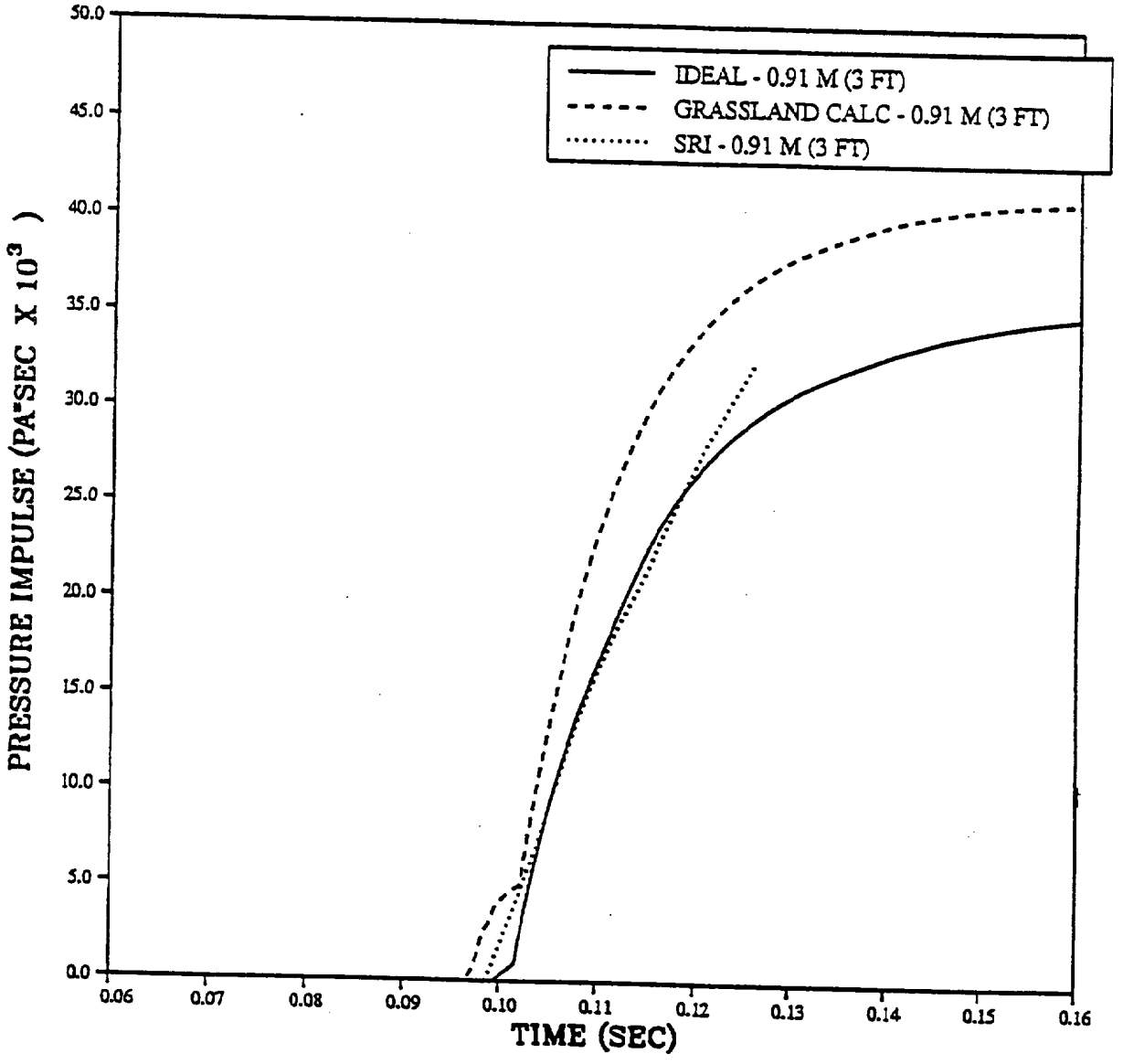

PRISCILLA
CALCULATION - DATA COMPARISONS
DYNAMIC PRESSURE AT 167 METERS (550 FEET)

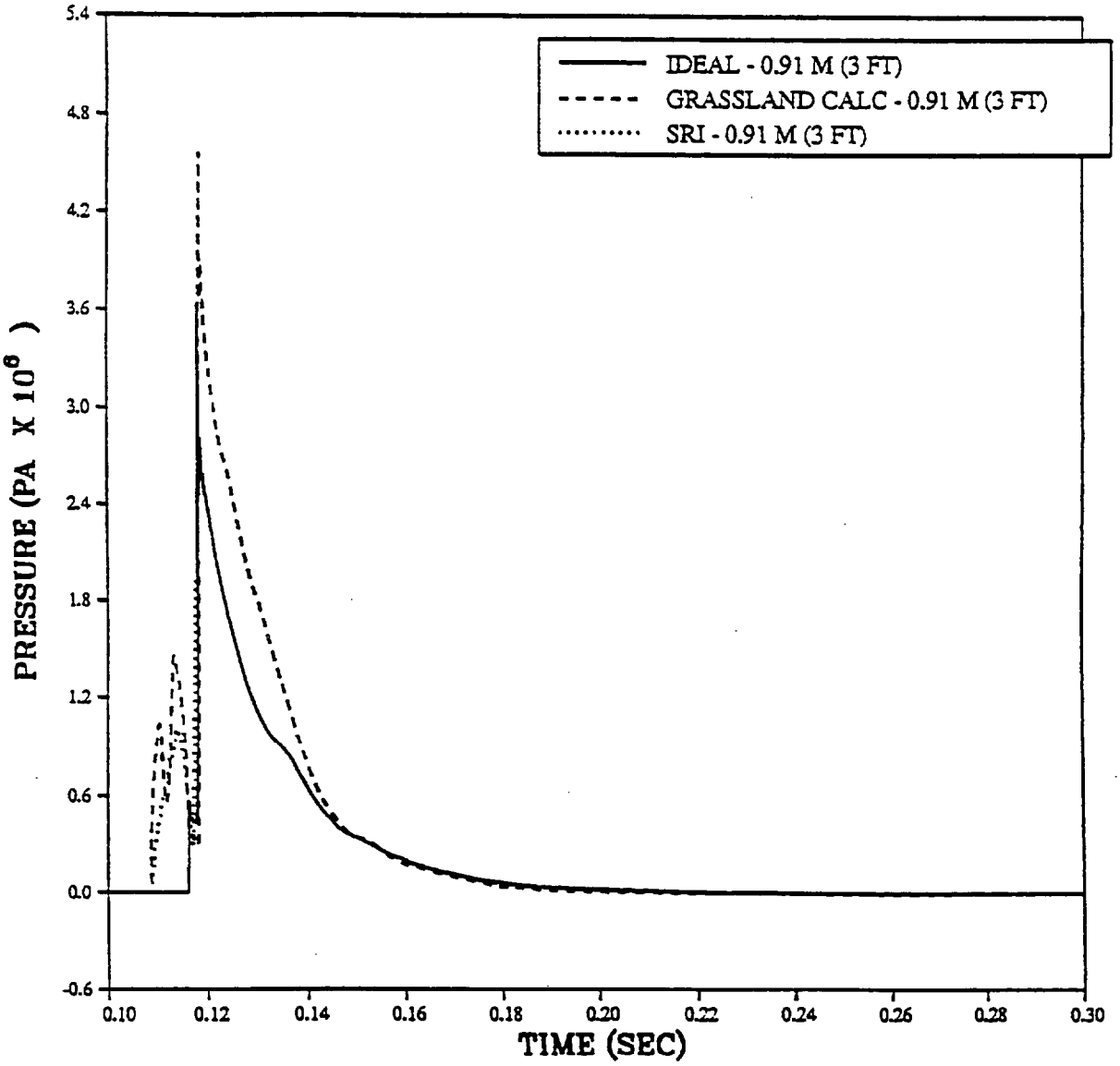

PRISCILLA
CALCULATION - DATA COMPARISONS
DYNAMIC PRESSURE IMPULSE AT 167 METERS (550 FEET)

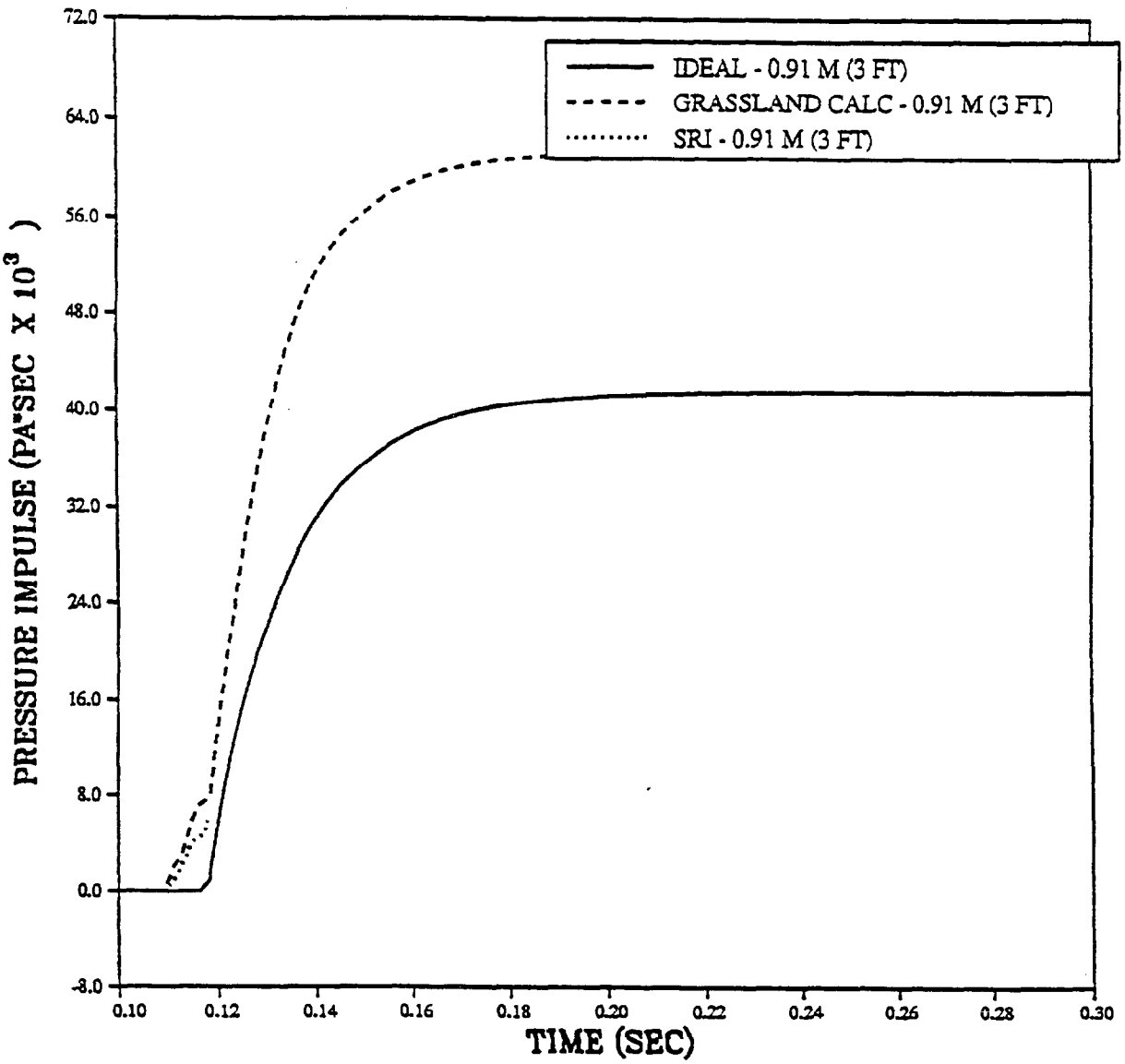

PRISCILLA
CALCULATION - DATA COMPARISONS
DYNAMIC PRESSURE AT 198 METERS (650 FEET)

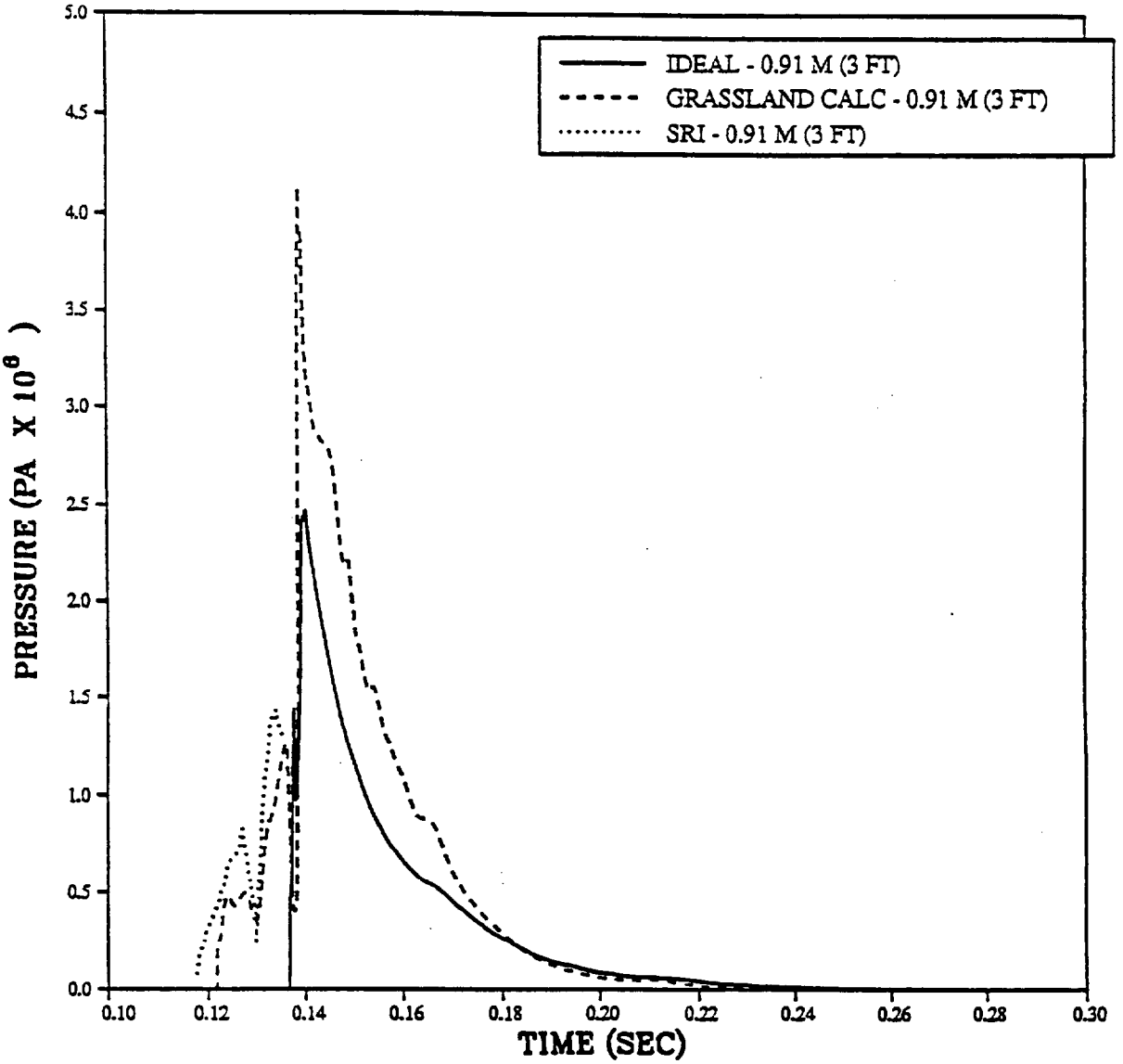

PRISCILLA
CALCULATION - DATA COMPARISONS
DYNAMIC PRESSURE IMPULSE AT 198 METERS (650 FEET)

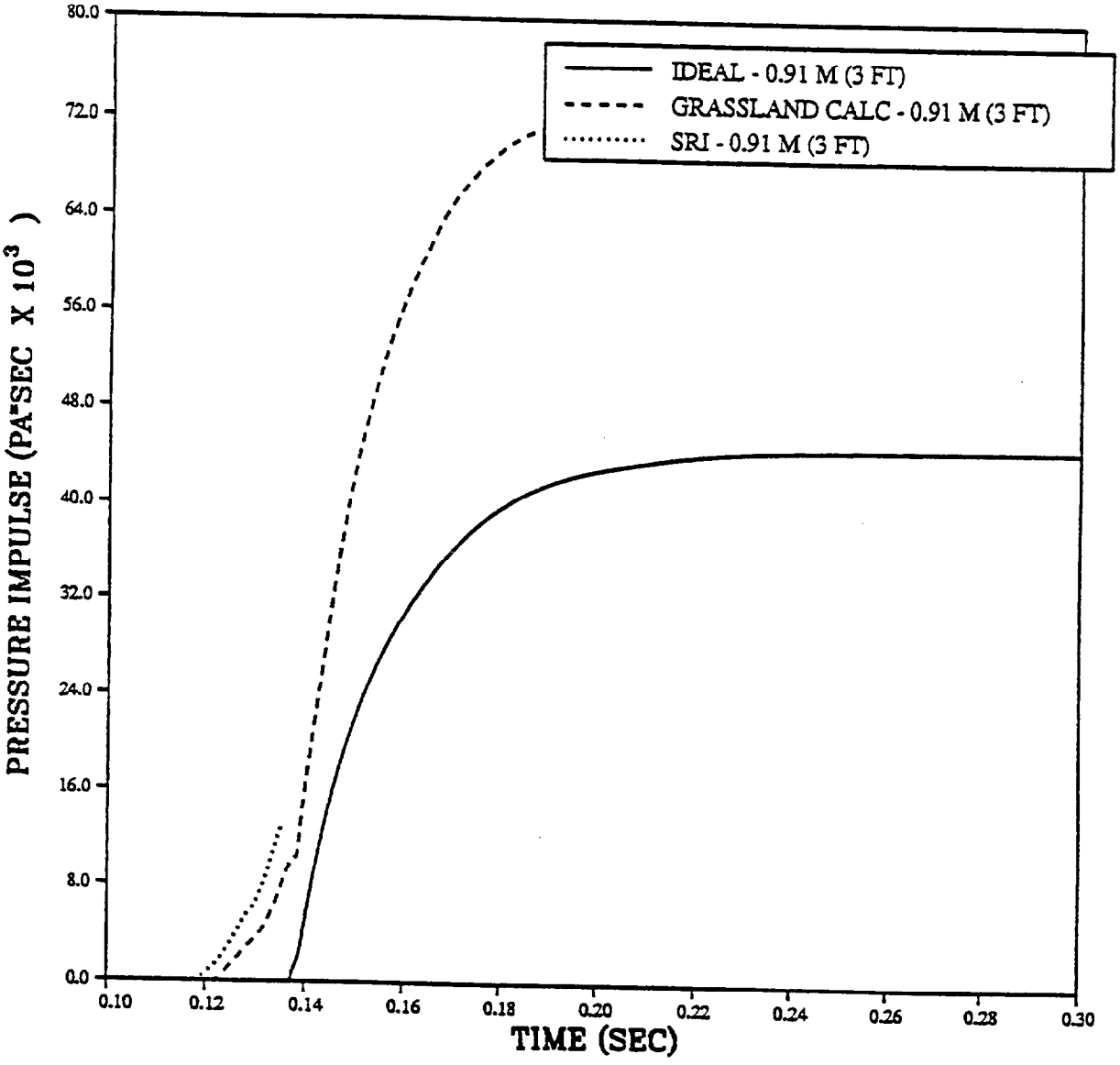

PRISCILLA
CALCULATION - DATA COMPARISONS
DYNAMIC PRESSURE AT 228 METERS (750 FEET)

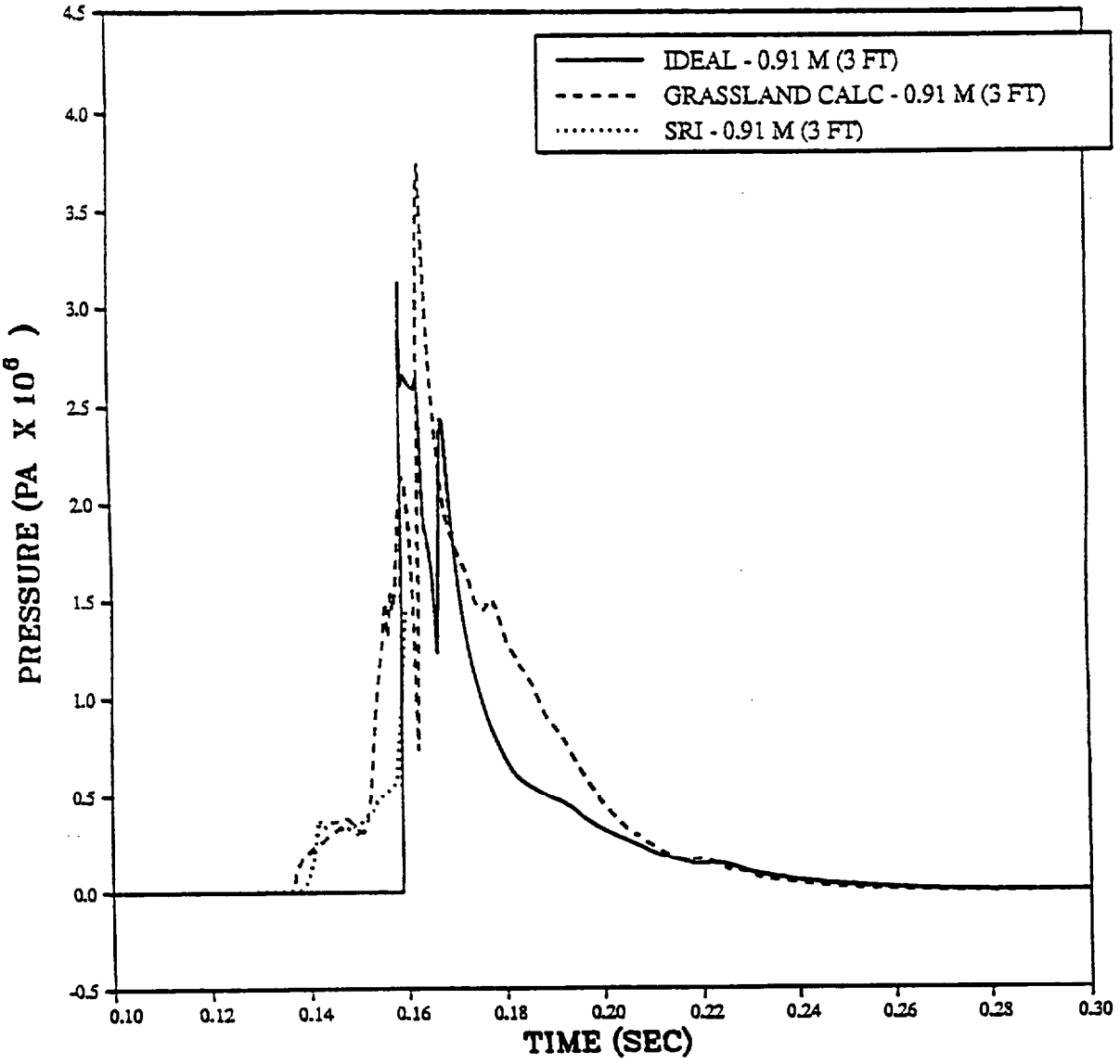

PRISCILLA
CALCULATION - DATA COMPARISONS
DYNAMIC PRESSURE IMPULSE AT 228 METERS (750 FEET)

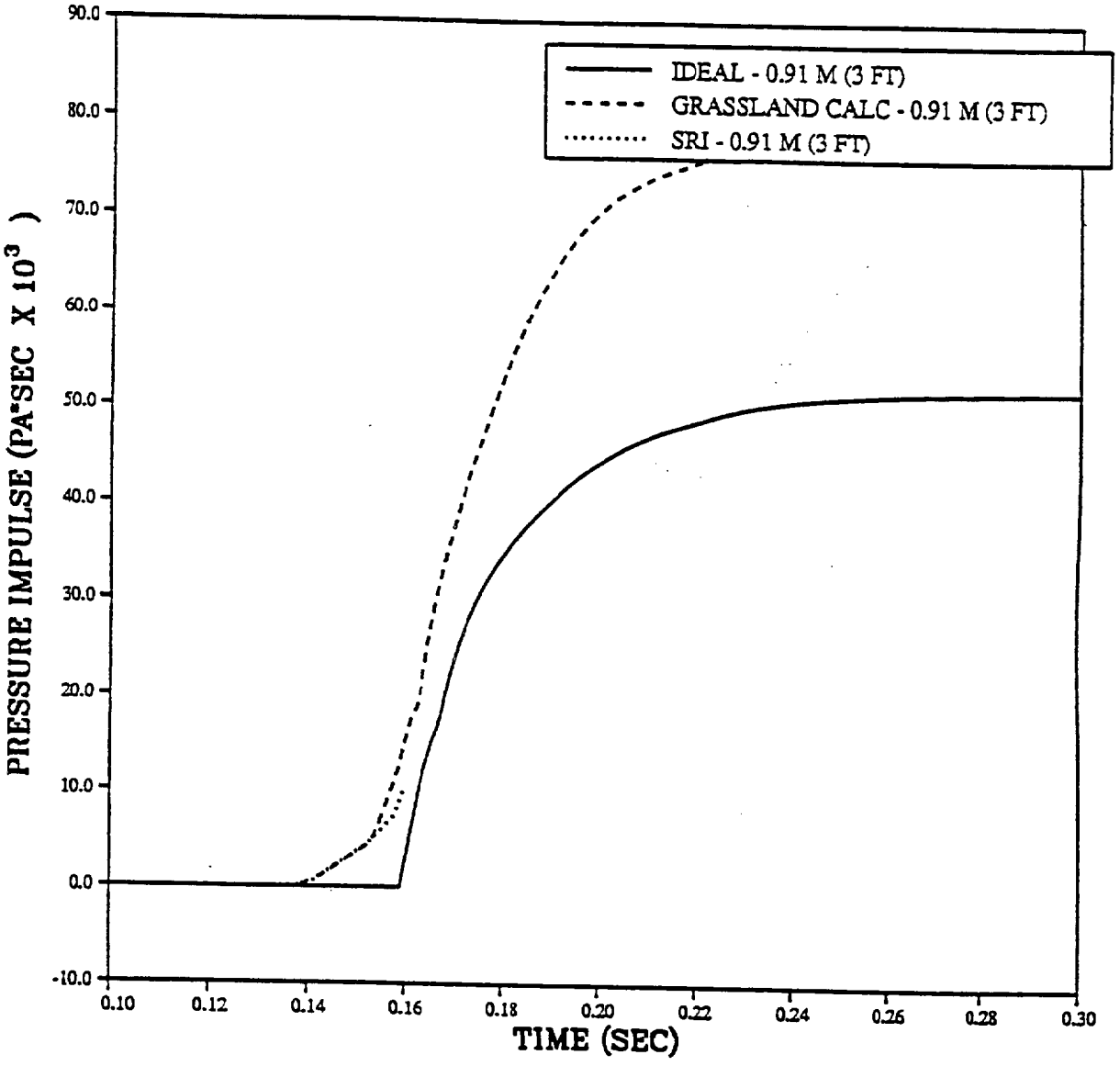

PRISCILLA
CALCULATION - DATA COMPARISONS
DYNAMIC PRESSURE AT 260 METERS (850 FEET)

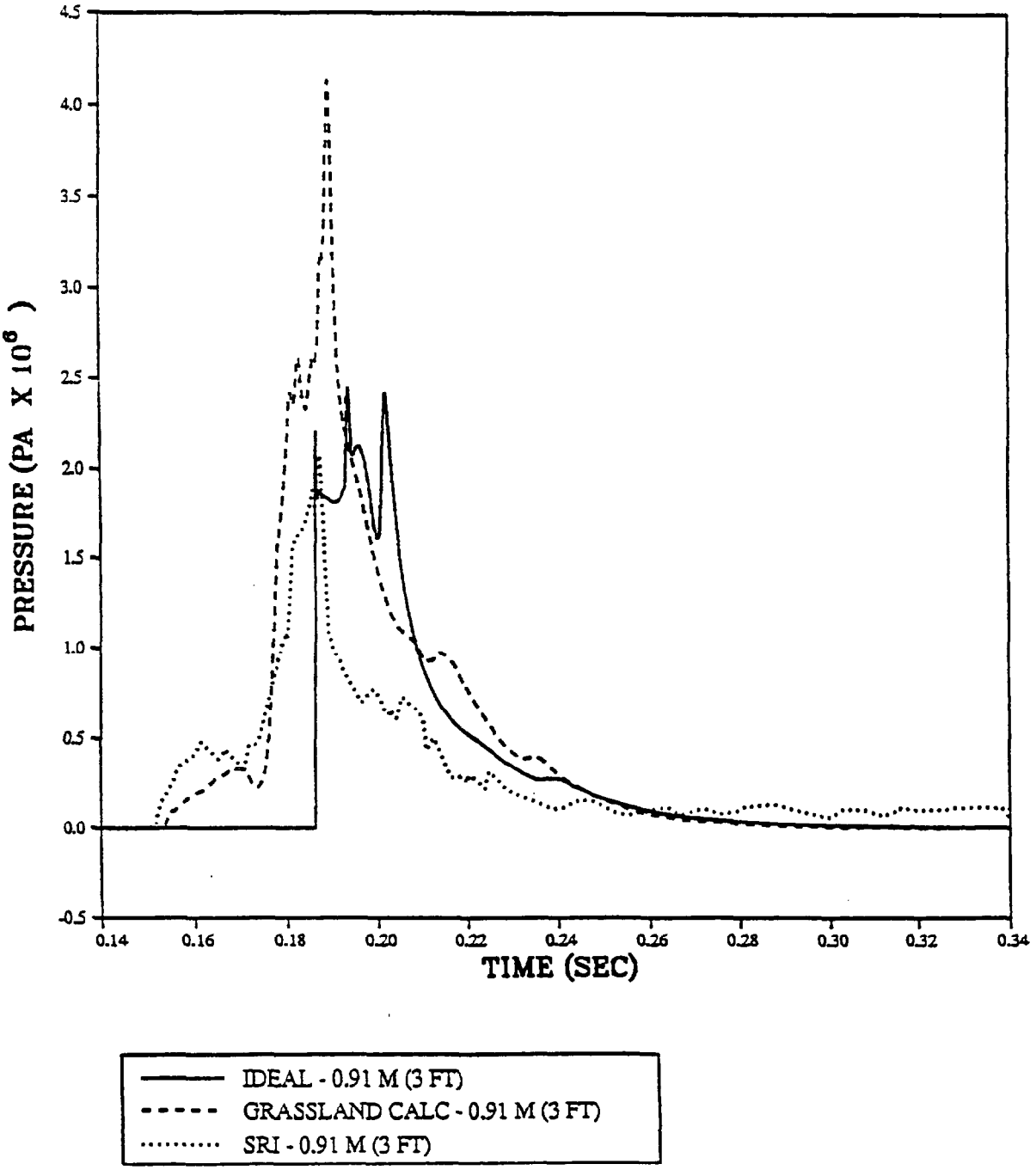

PRISCILLA
CALCULATION - DATA COMPARISONS
DYNAMIC PRESSURE IMPULSE AT 260 METERS (850 FEET)

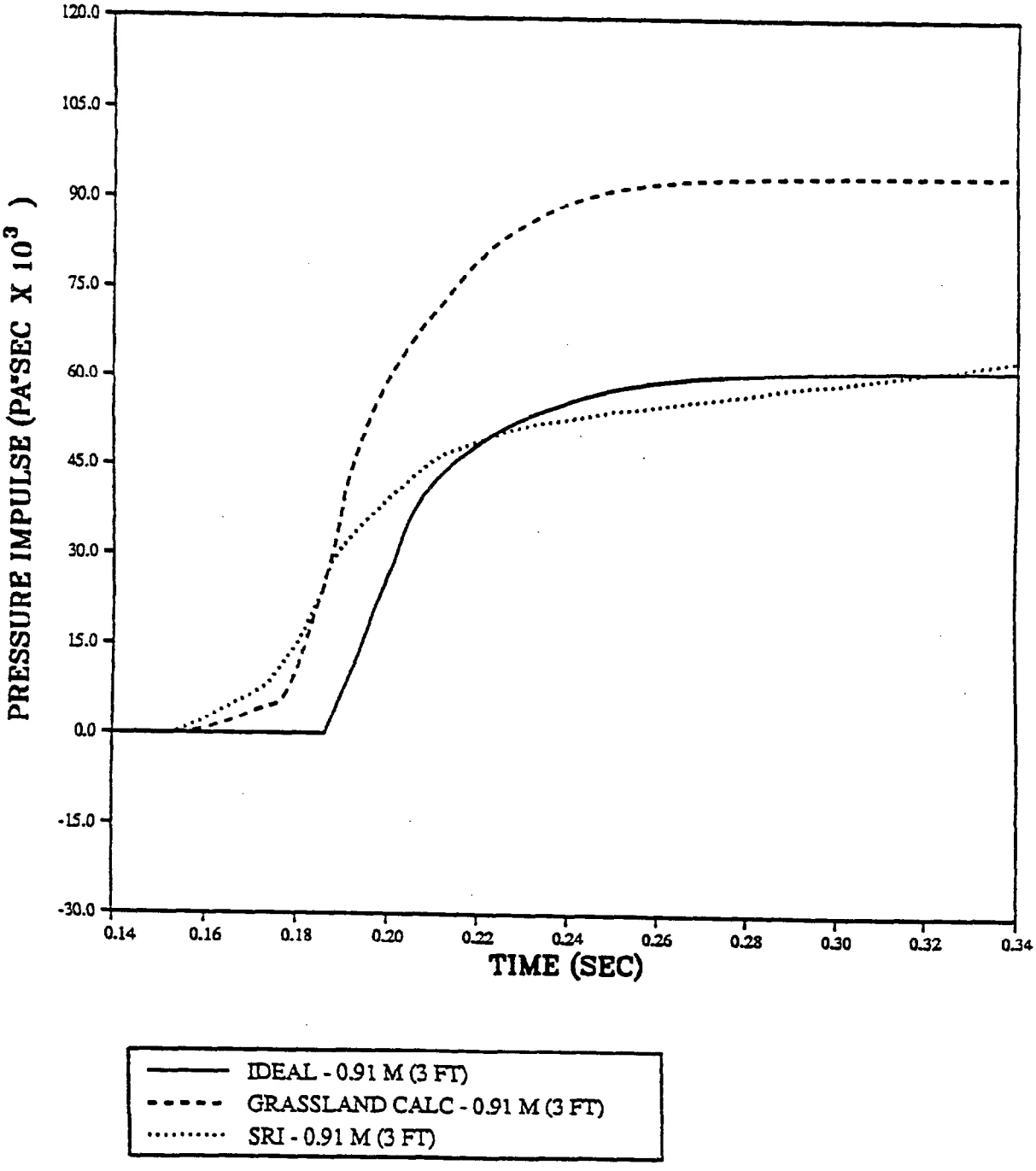

PRISCILLA
CALCULATION - DATA COMPARISONS
DYNAMIC PRESSURE AT 320 METERS (1050 FEET)

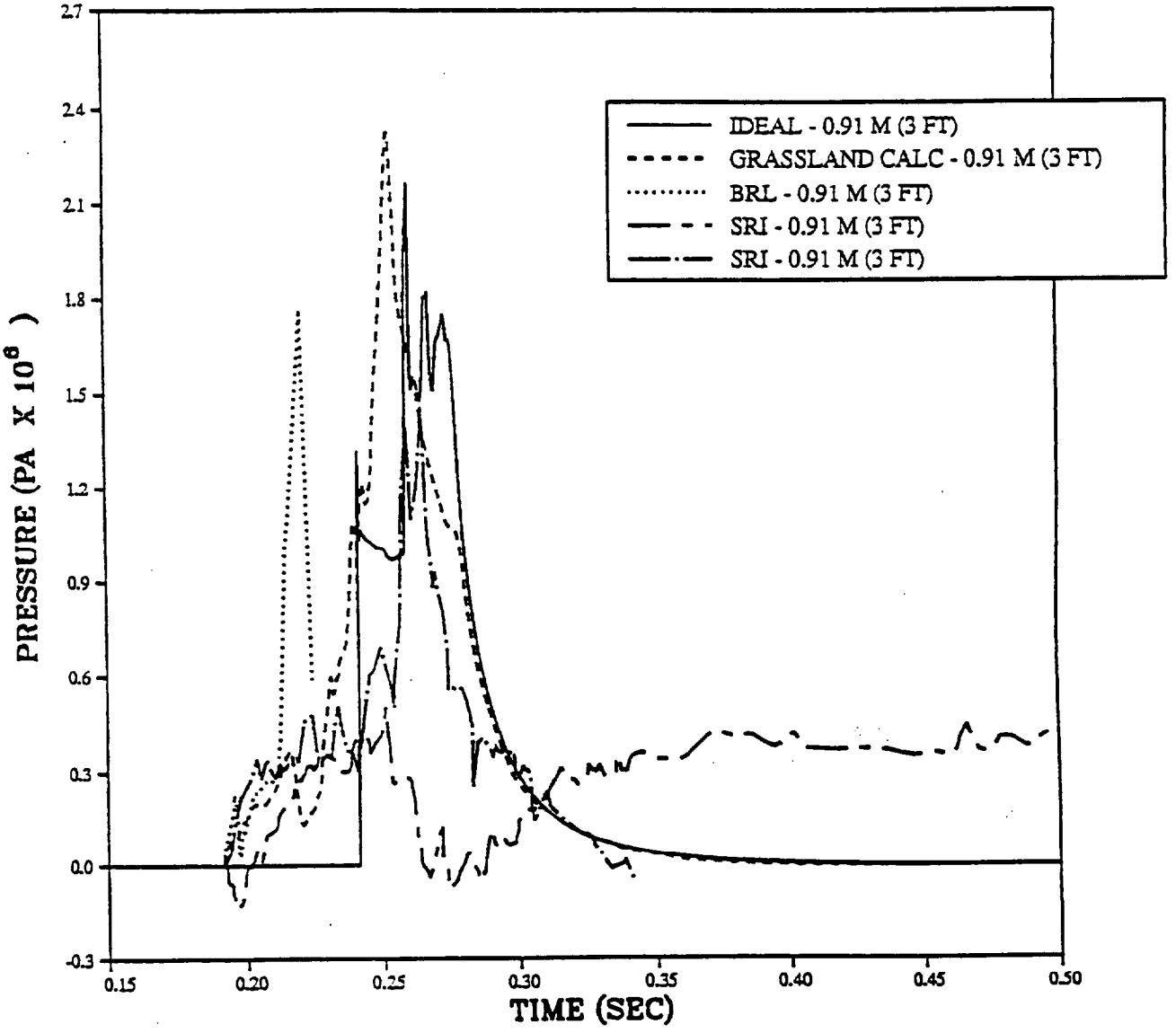

PRISCILLA
CALCULATION - DATA COMPARISONS
DYNAMIC PRESSURE AT 410 METERS (1350 FEET)

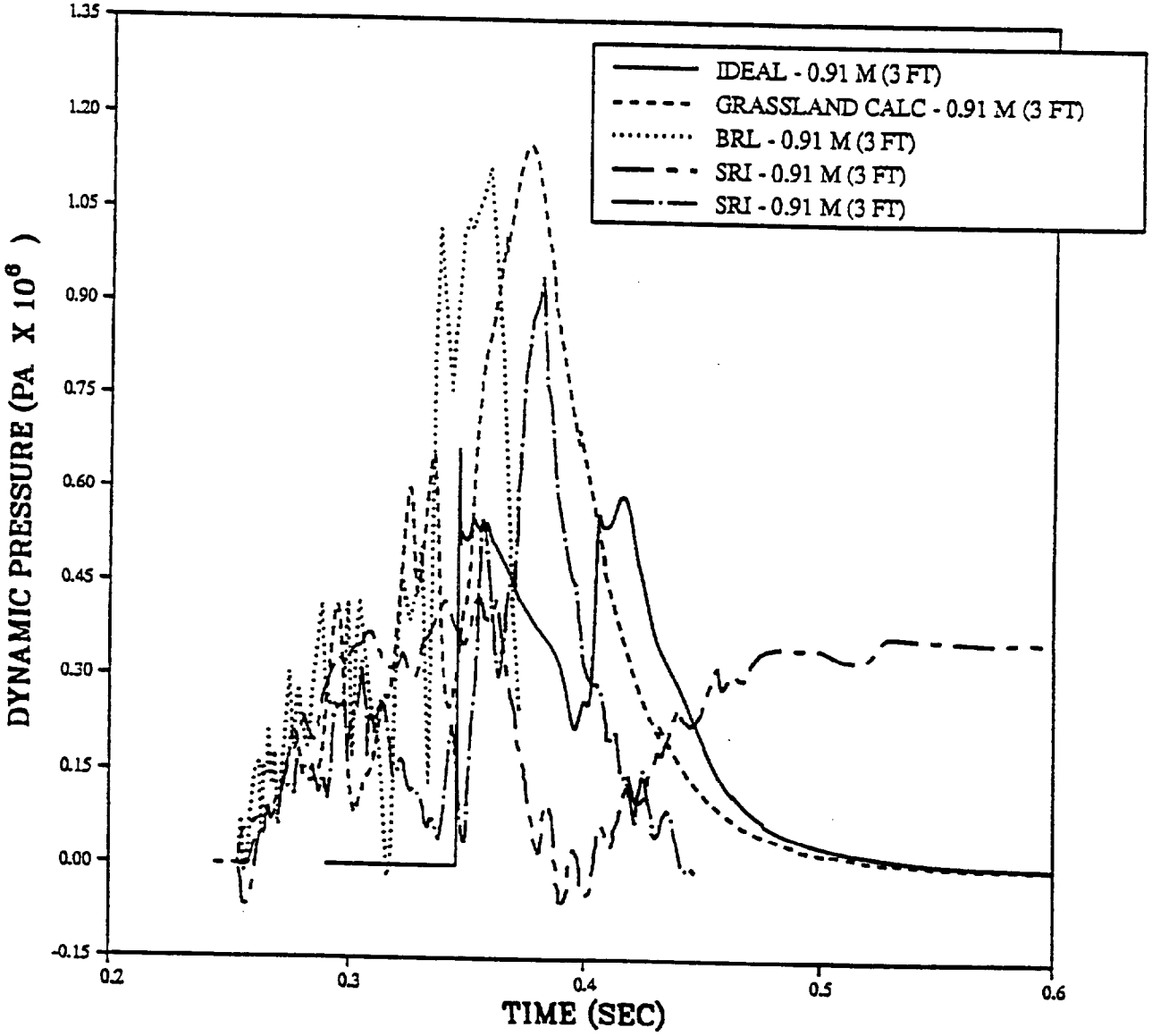

PRISCILLA
CALCULATION - DATA COMPARISONS
DYNAMIC PRESSURE IMPULSE AT 410 METERS (1350 FEET)

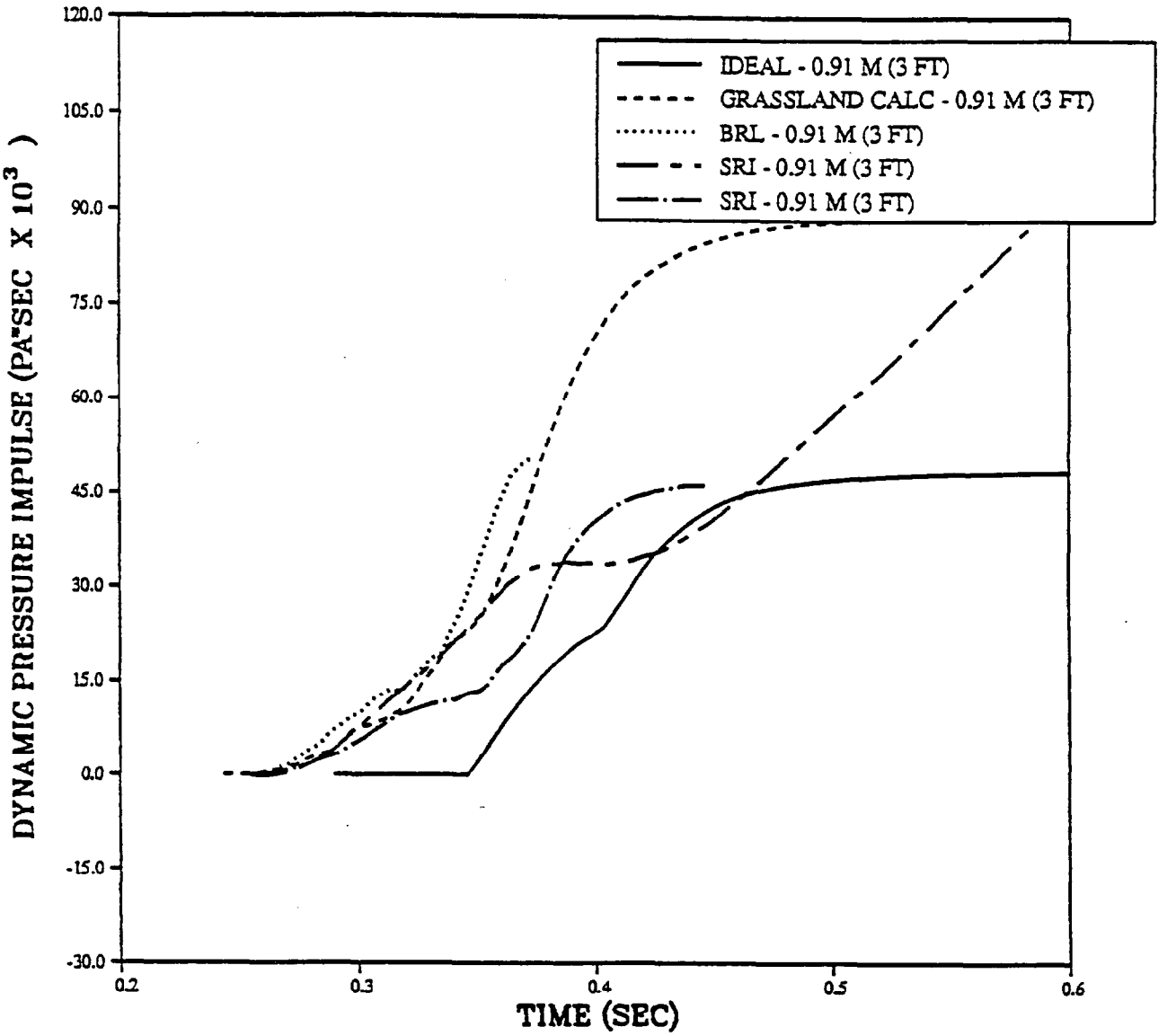

PRISCILLA
CALCULATION - DATA COMPARISONS
DYNAMIC PRESSURE AT 503 METERS (1650 FEET)

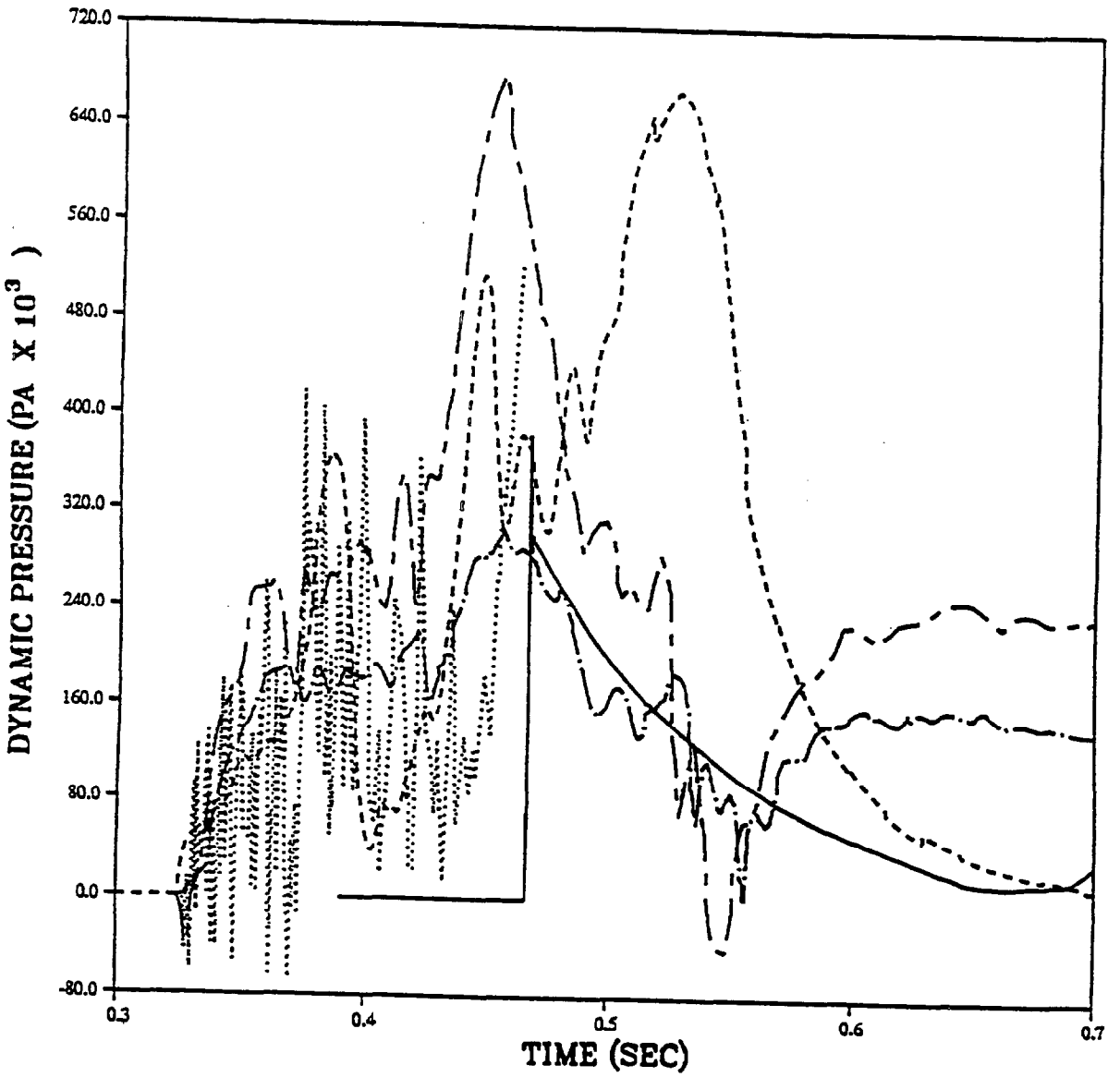

IDEAL 0.91 M (3 FT)
GRASSLAND CALC - 0.91 M (3 FT)
BRL - 0.91 M (3 FT)
SRI - 0.91 M (3 FT)
SRI - 0.91 M (3 FT)

PRISCILLA
CALCULATION - DATA COMPARISONS
DYNAMIC PRESSURE IMPULSE AT 503 METERS (1650 FEET)

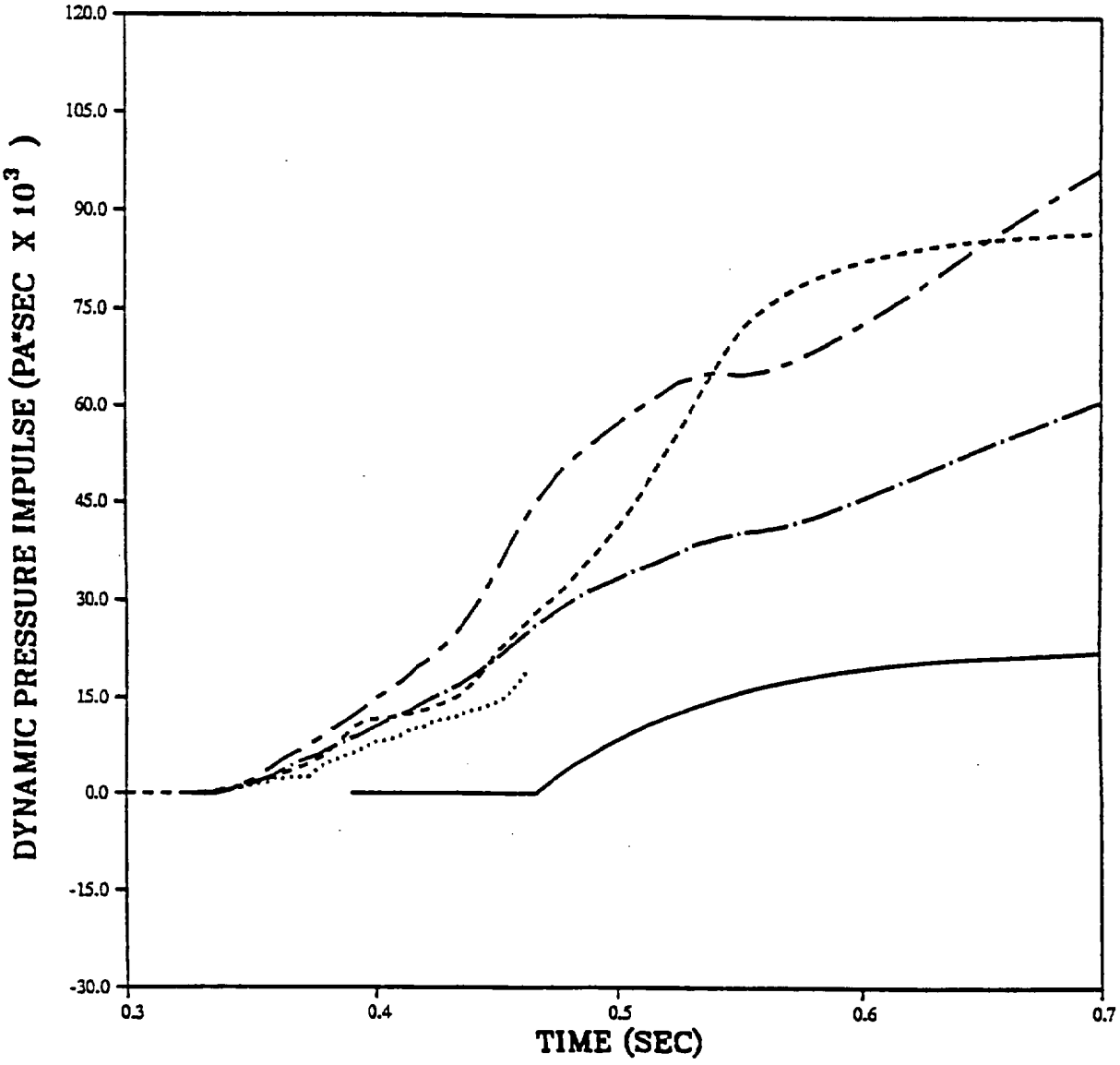

IDEAL 0.91 M (3 FT)
GRASSLAND CALC - 0.91 M (3 FT)
BRL - 0.91 M (3 FT)
SRI - 0.91 M (3 FT)
SRI - 0.91 M (3 FT)

PRISCILLA
CALCULATION - DATA COMPARISONS
DYNAMIC PRESSURE AT 503 METERS (1650 FEET)

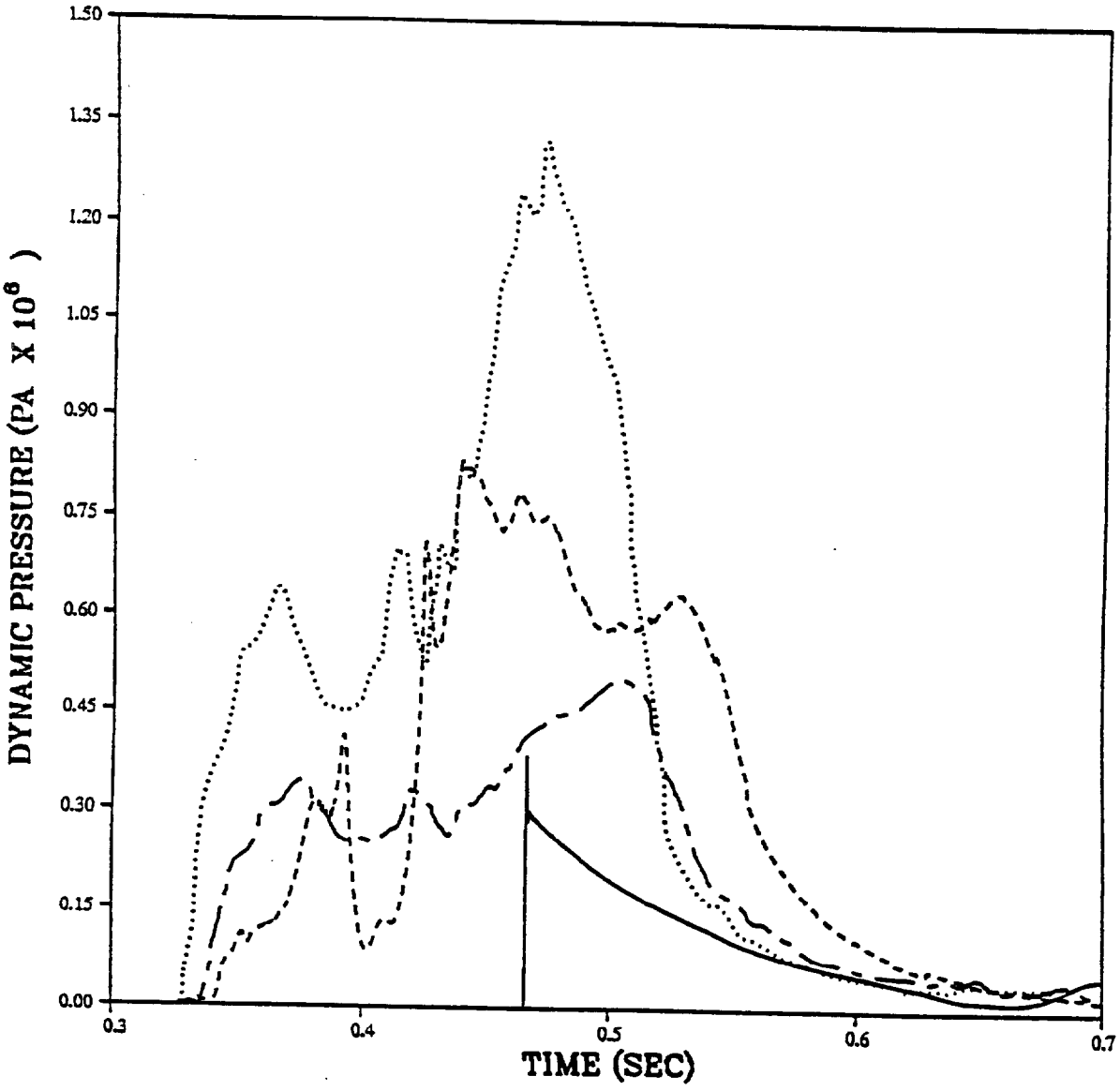

IDEAL - 3.05 M (10 FT)
GRASSLAND CALC - 3.05 M (10 FT)
BRL - 3.05 M (10 FT)
SRI - 3.05 M (10 FT)

PRISCILLA
CALCULATION - DATA COMPARISONS
DYNAMIC PRESSURE IMPULSE AT 503 METERS (1650 FEET)

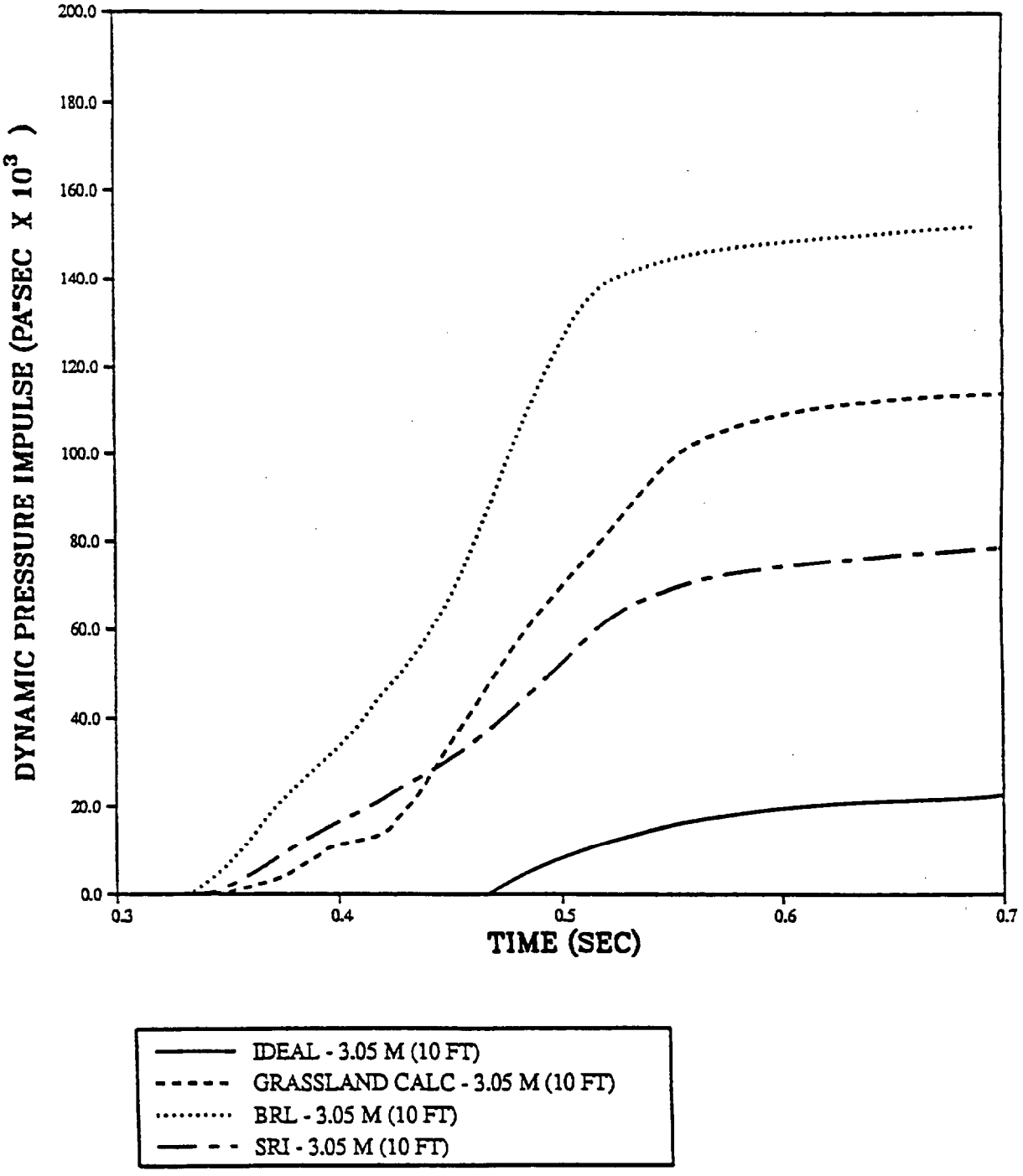

PRISCILLA
CALCULATION - DATA COMPARISONS
DYNAMIC PRESSURE AT 607 METERS (2000 FEET)

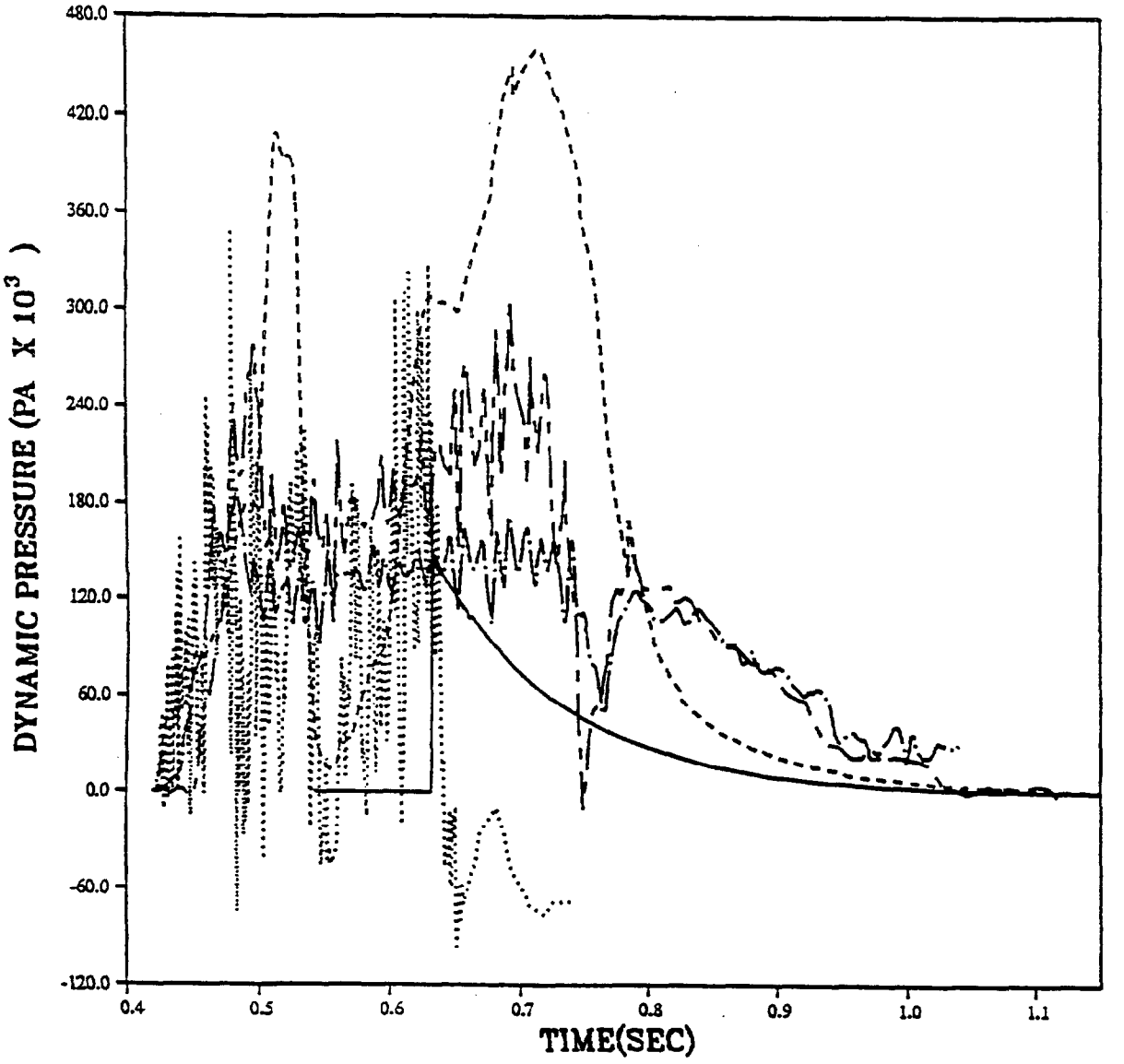

IDEAL - 0.91 M (3 FT)
GRASSLAND CALC - 0.91 M (3 FT)
BRL - 0.91 M (3 FT)
SRI - 0.91 M (3 FT)
SRI - 0.91 M (3 FT)

PRISCILLA
CALCULATION - DATA COMPARISONS
DYNAMIC PRESSURE IMPULSE AT 607 METERS (2000 FEET)

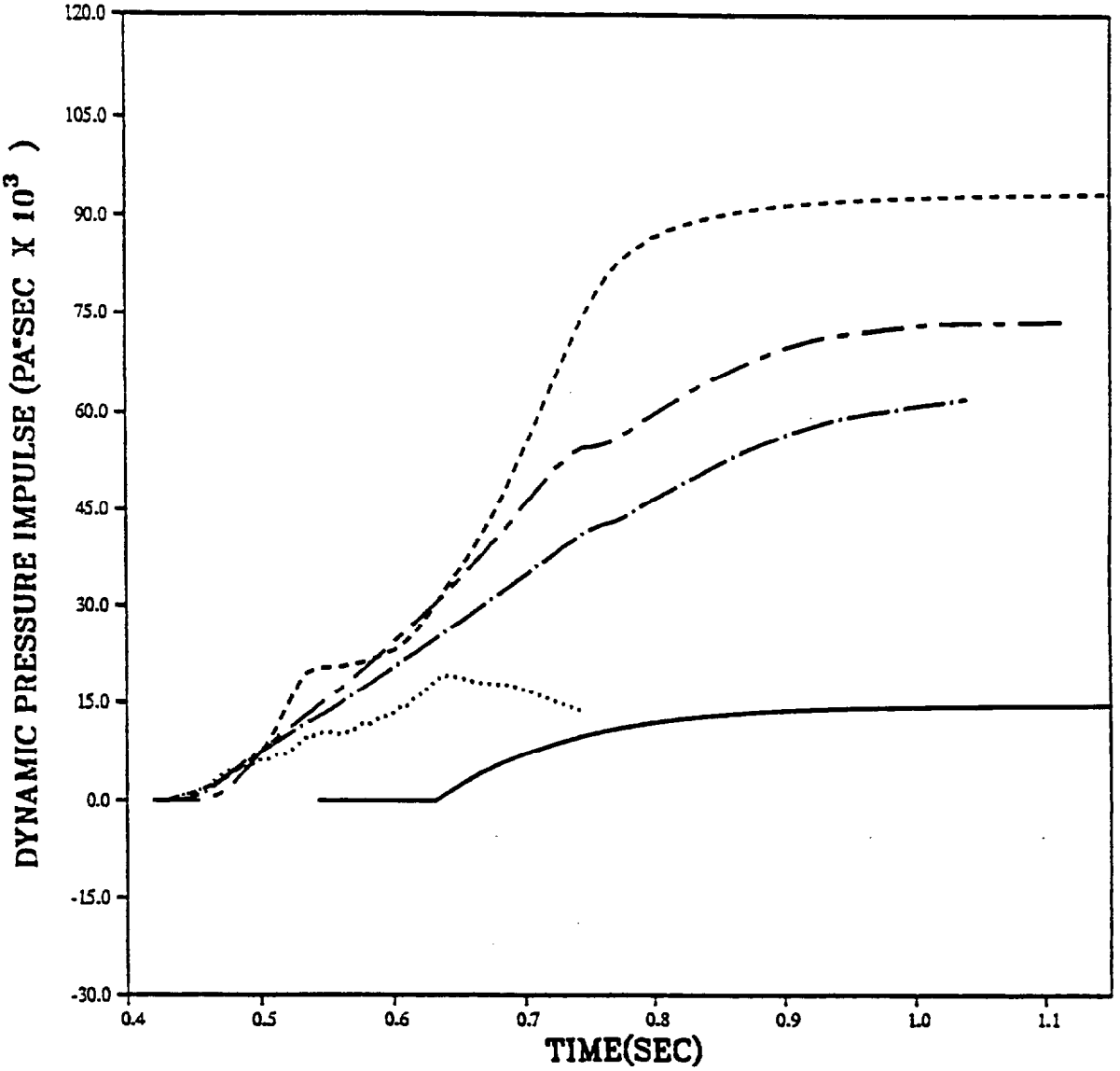

IDEAL - 0.91 M (3 FT)
GRASSLAND CALC - 0.91 M (3 FT)
BRL - 0.91 M (3 FT)
SRI - 0.91 M (3 FT)
SRI - 0.91 M (3 FT)

PRISCILLA
CALCULATION - DATA COMPARISONS
DYNAMIC PRESSURE AT 607 METERS (2000 FEET)

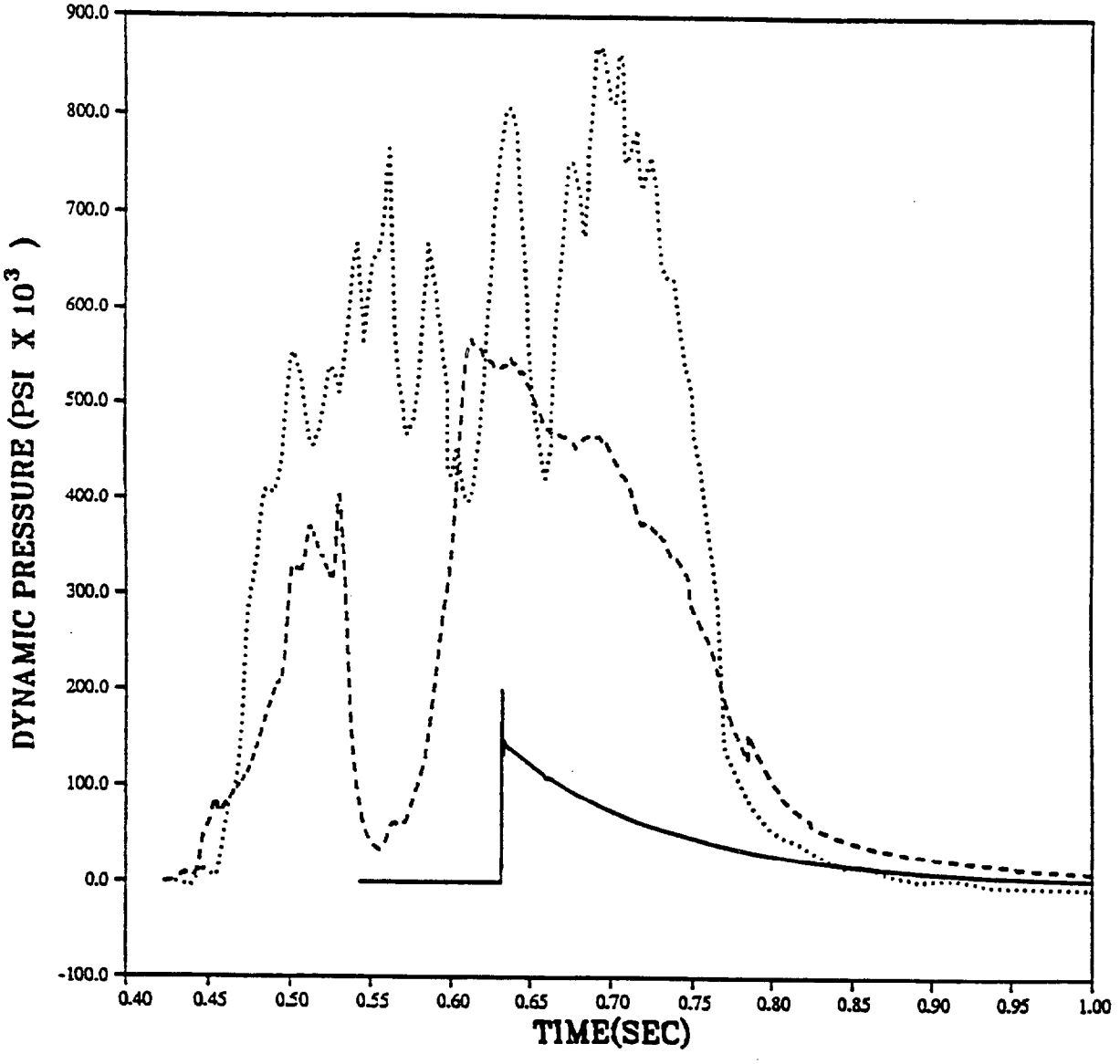

IDEAL - 3.05 M (10 FT)
GRASSLAND CALC - 3.05 M (10 FT)
SRI - 3.05 M (10 FT)

PRISCILLA
CALCULATION - DATA COMPARISONS
DYNAMIC PRESSURE IMPULSE AT 607 METERS (2000 FEET)

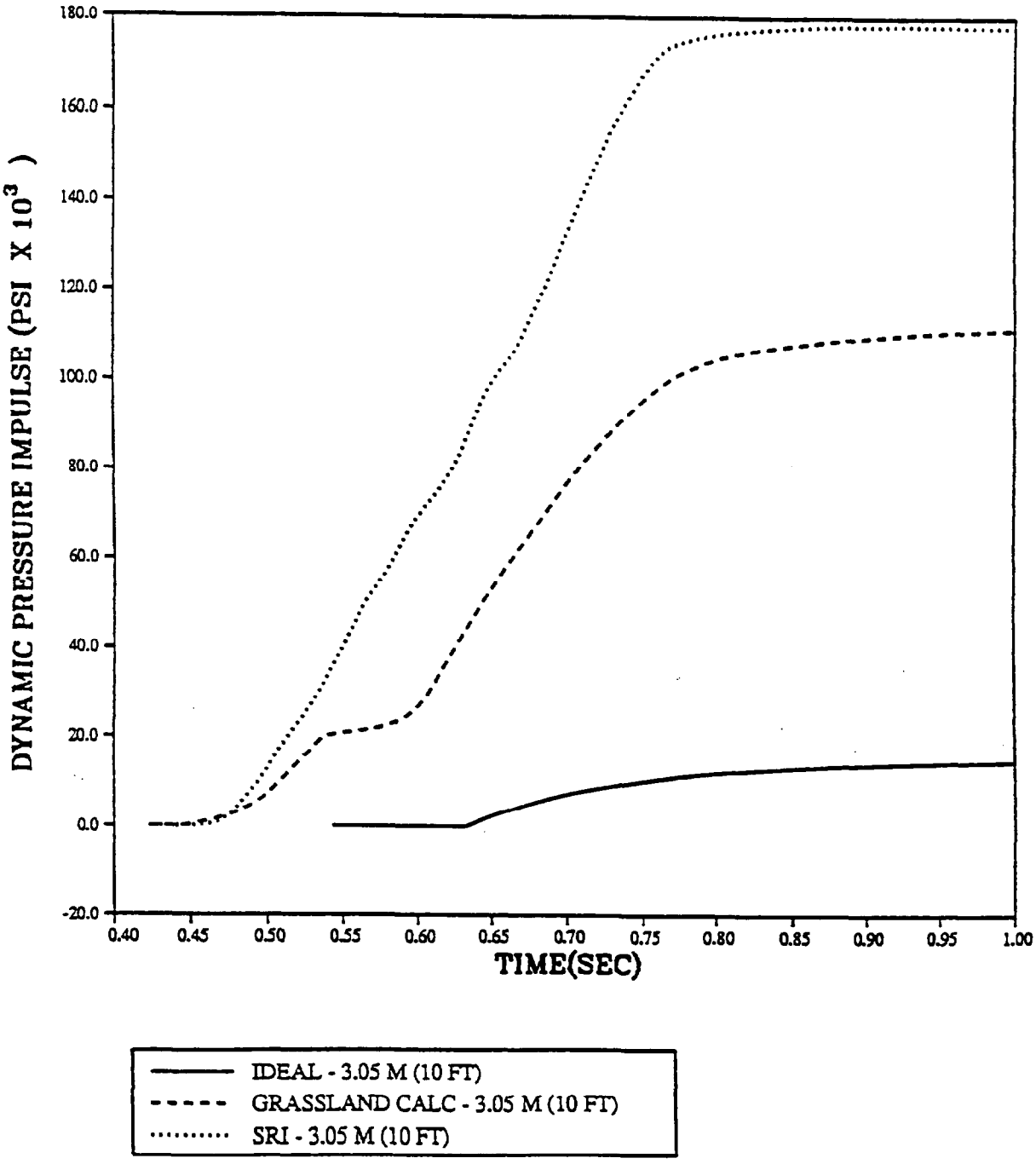

PRISCILLA
CALCULATION - DATA COMPARISONS
DYNAMIC PRESSURE AT 762 M (2500 FEET)

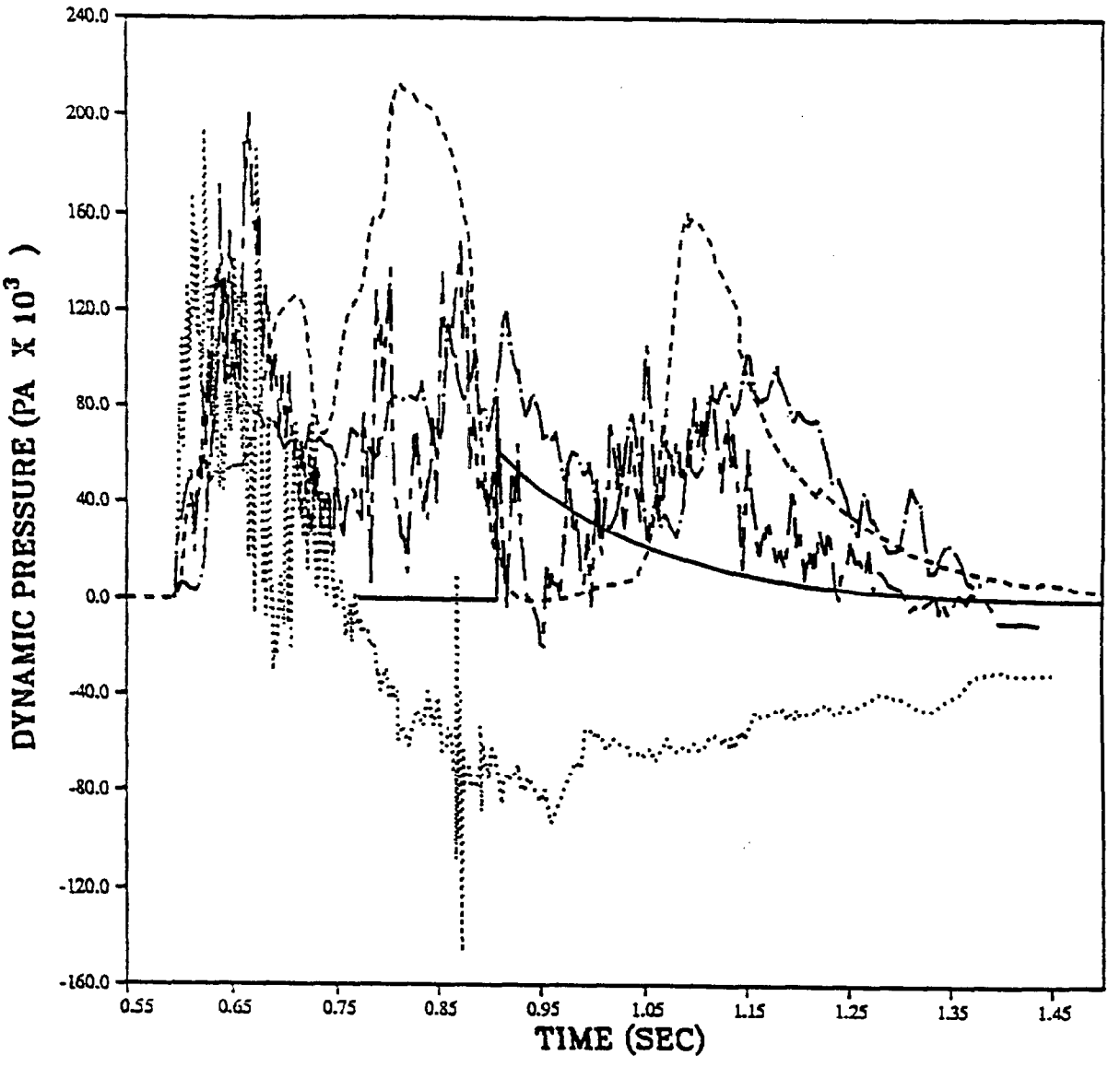

IDEAL - 0.91 M (3 FT)
GRASSLAND CALC 0.91 M (3 FT)
BRL - 0.91 M (3 FT)
BRL - 0.91 M (3 FT)
SRI - 0.91 M (3 FT)

PRISCILLA
CALCULATION - DATA COMPARISONS
DYNAMIC PRESSURE IMPULSE AT 762 M (2500 FEET)

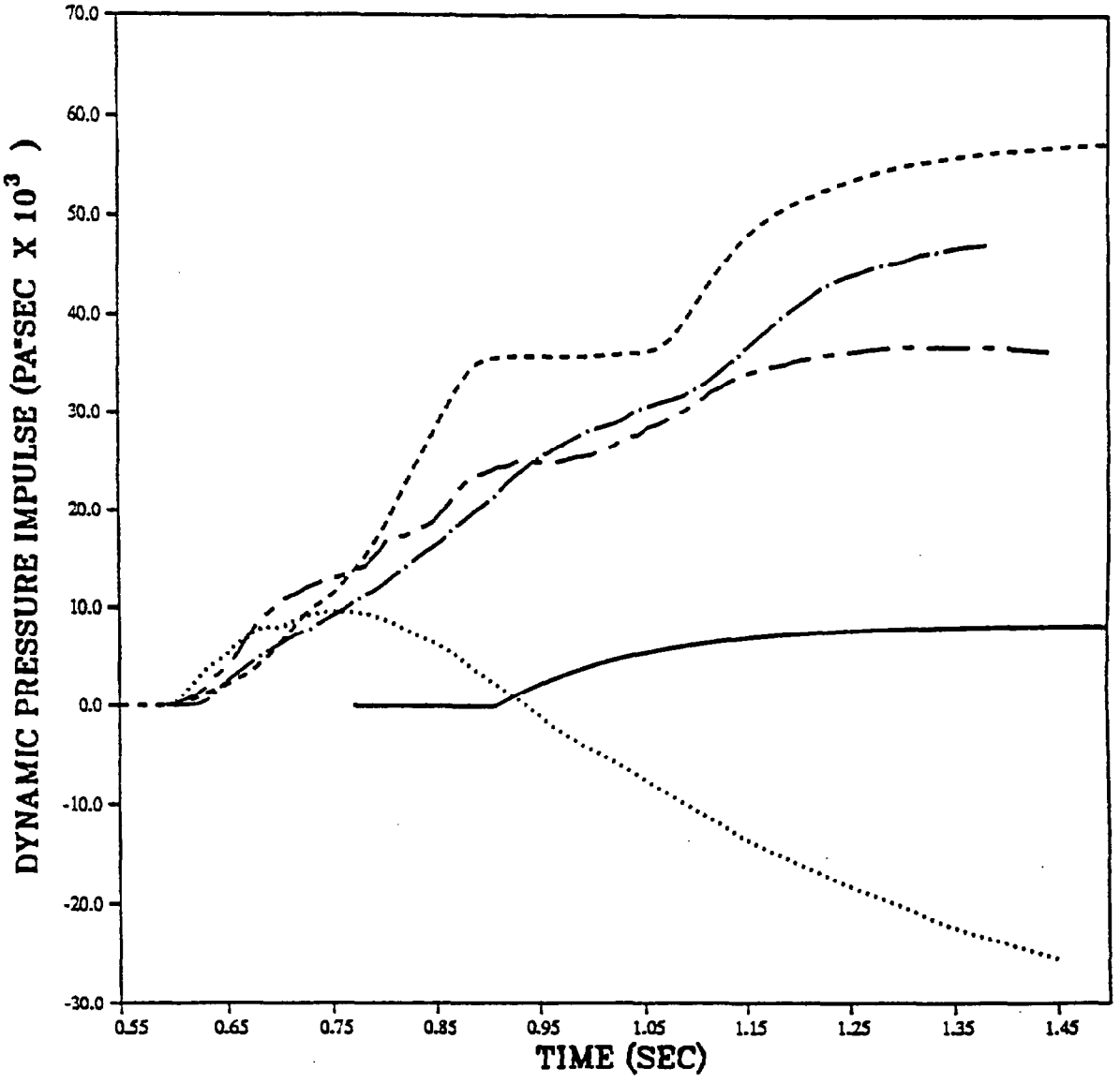

IDEAL - 0.91 M (3 FT)
GRASSLAND CALC 0.91 M (3 FT)
BRL - 0.91 M (3 FT)
BRL - 0.91 M (3 FT)
SRI - 0.91 M (3 FT)

PRISCILLA
CALCULATION - DATA COMPARISONS
DYNAMIC PRESSURE IMPULSE AT 762 METERS (2500 FEET)

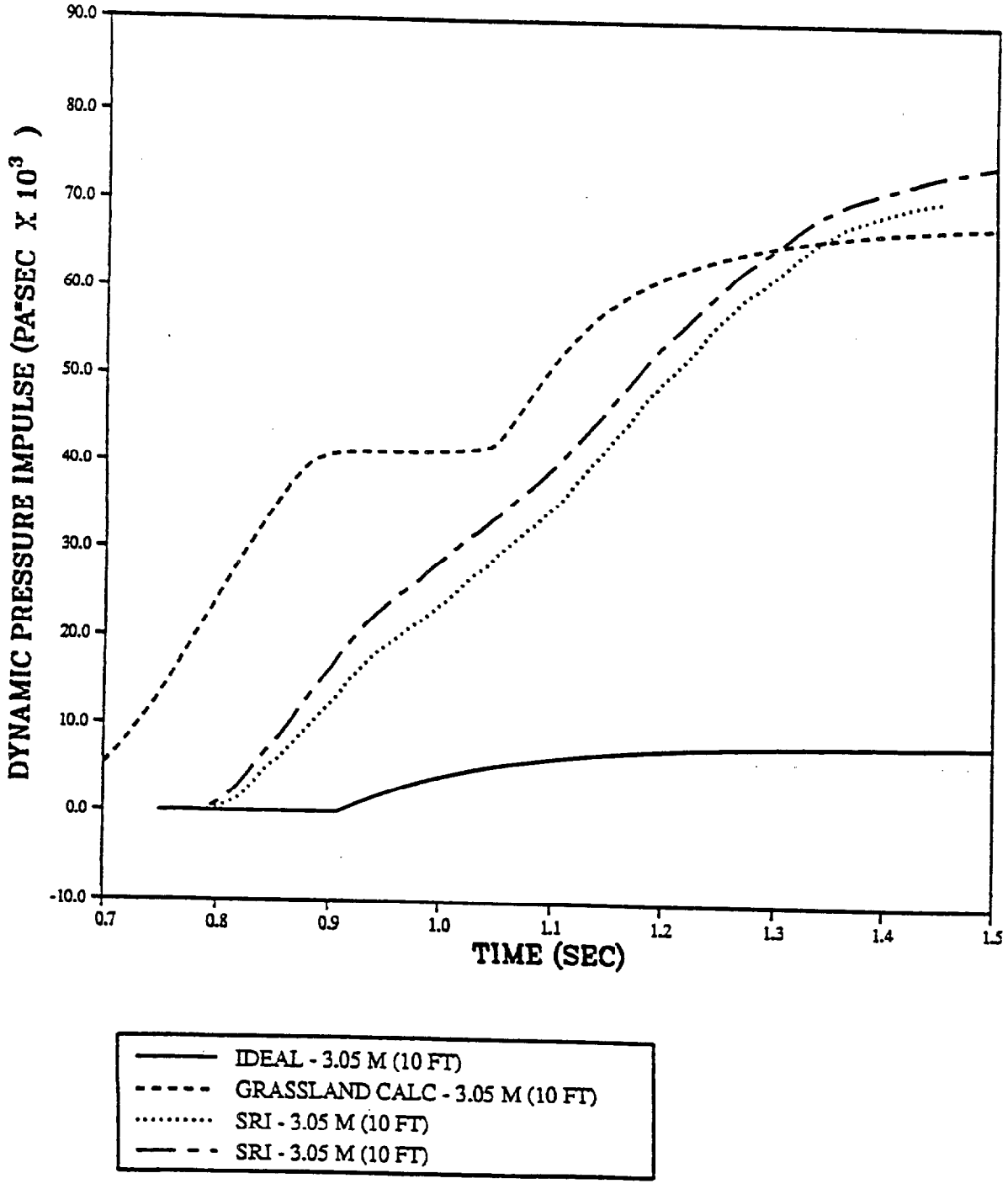

PRISCILLA
CALCULATION - DATA COMPARISONS
DYNAMIC PRESSURE AT 914 METERS (3000 FEET)

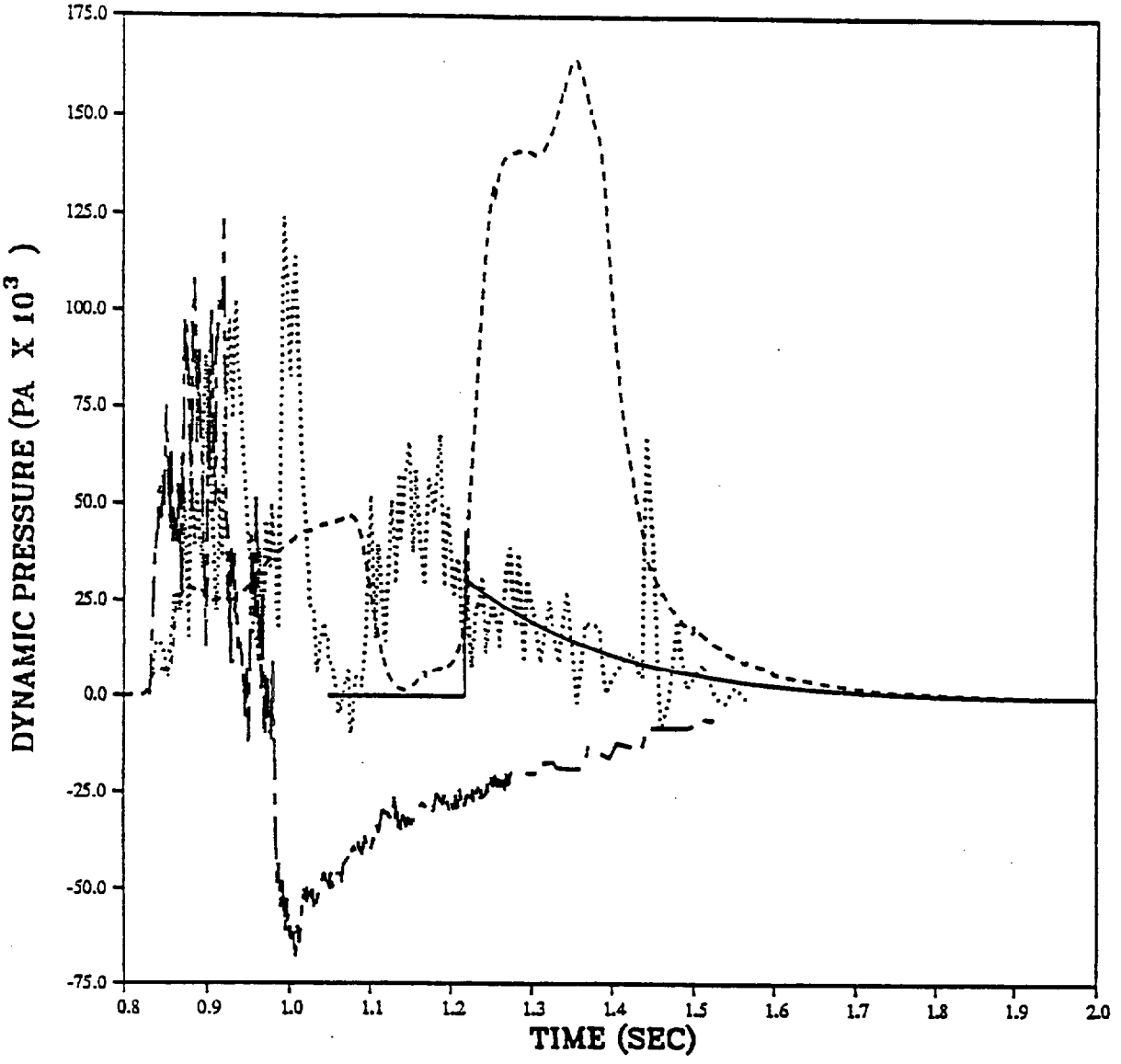

IDEAL - 0.91 M (3 FT)
GRASSLAND CALC - 0.91 M (3 FT)
BRL - 0.91 M (3 FT)
BRL - 0.91 M (3 FT)

PRISCILLA
CALCULATION - DATA COMPARISONS
DYNAMIC PRESSURE IMPULSE AT 914 METERS (3000 FEET)

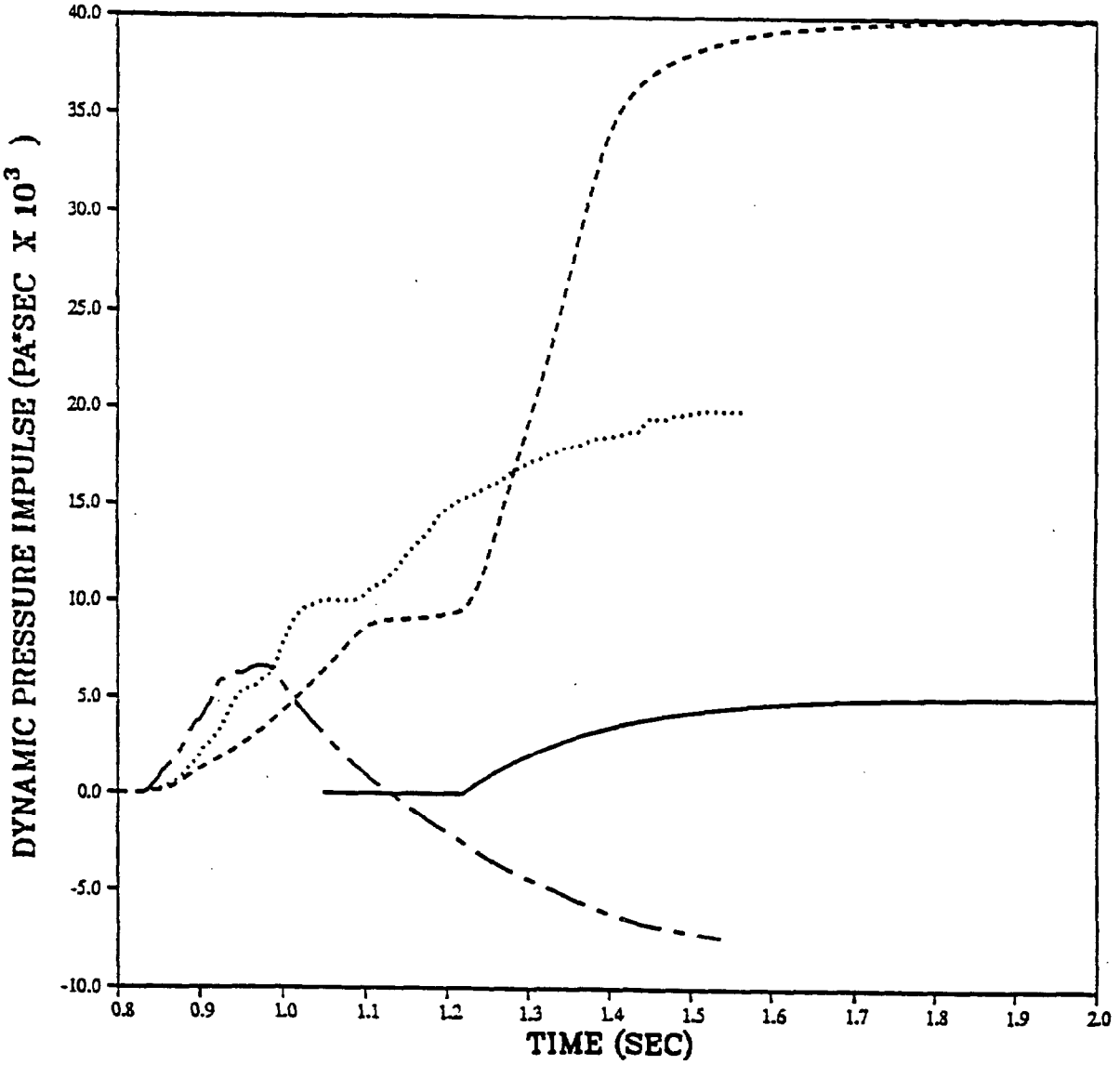

PRISCILLA
CALCULATION - DATA COMPARISONS
DYNAMIC PRESSURE AT 914 METERS (3000 FEET)

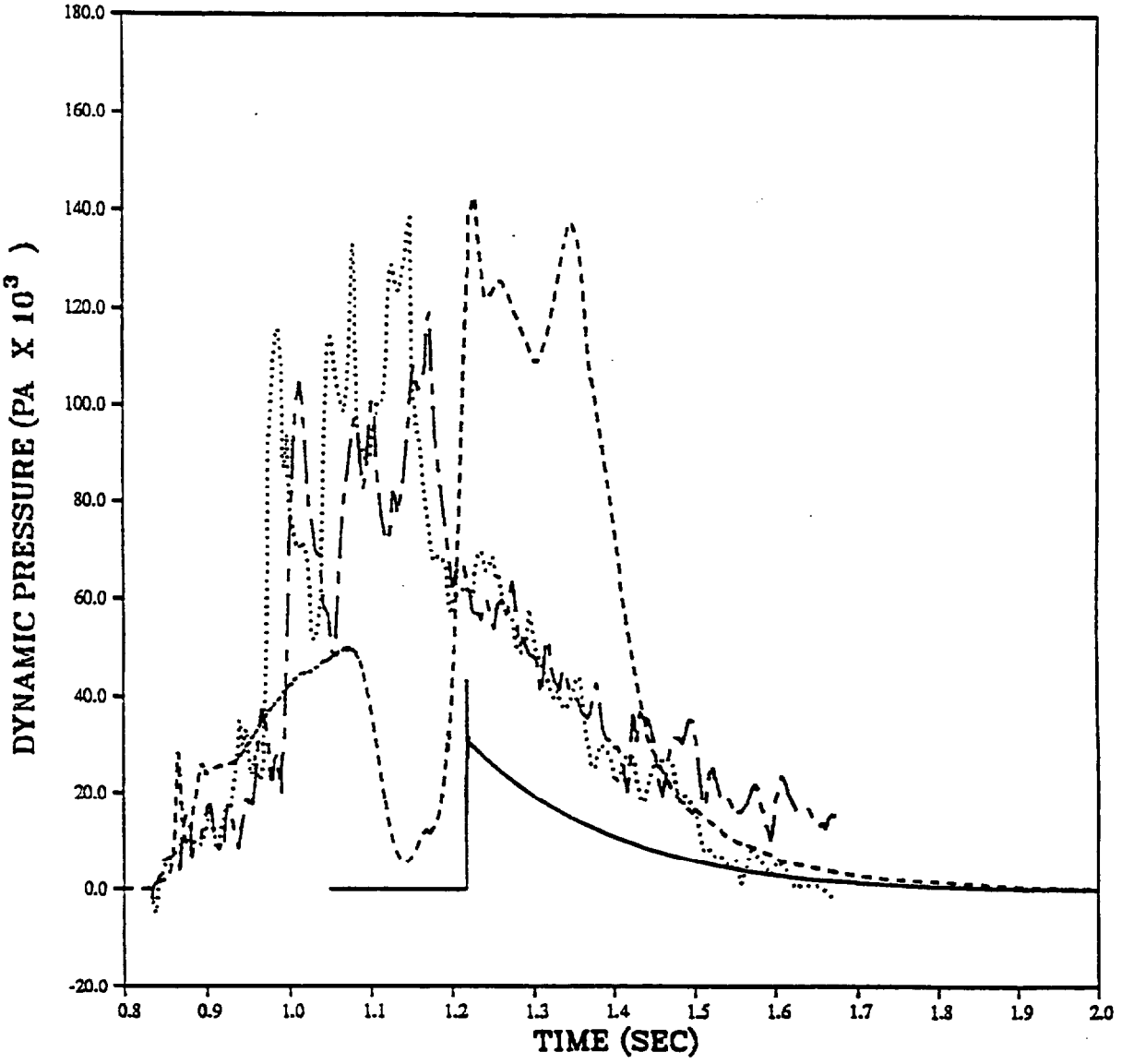

IDEAL - 3.05 M (10 FT)
GRASSLAND CALC - 3.05 M (10 FT)
SRI - 3.05 M (10 FT)
SRI - 3.05 M (10 FT)

PRISCILLA
CALCULATION - DATA COMPARISONS
DYNAMIC PRESSURE IMPULSE AT 914 METERS (3000 FEET)

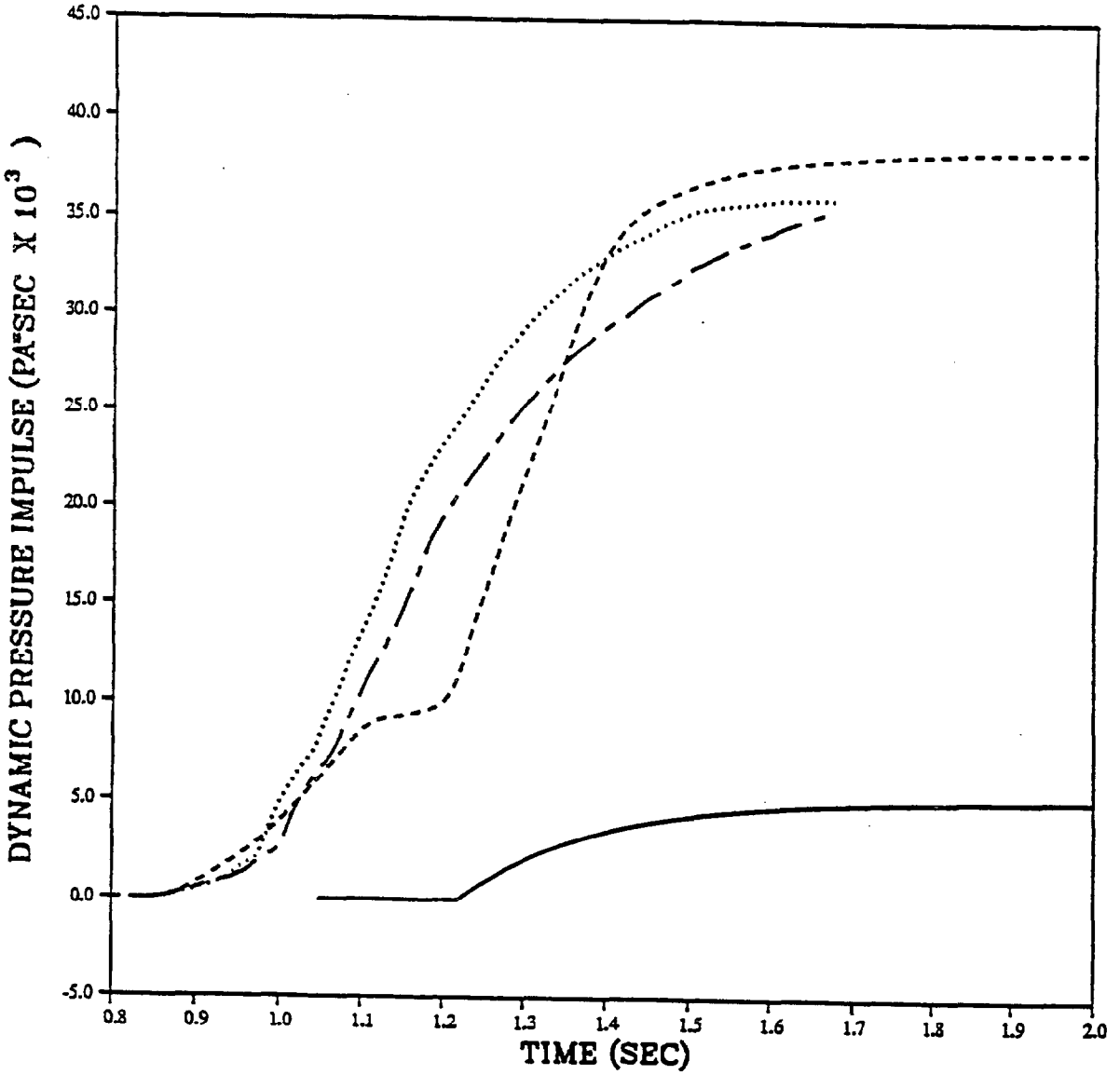

IDEAL - 3.05 M (10 FT)
GRASSLAND CALC - 3.05 M (10 FT)
SRI - 3.05 M (10 FT)
SRI - 3.05 M (10 FT)

PRISCILLA
CALCULATION - DATA COMPARISONS
DYNAMIC PRESSURE IMPULSE AT 914 METERS (3000 FEET)

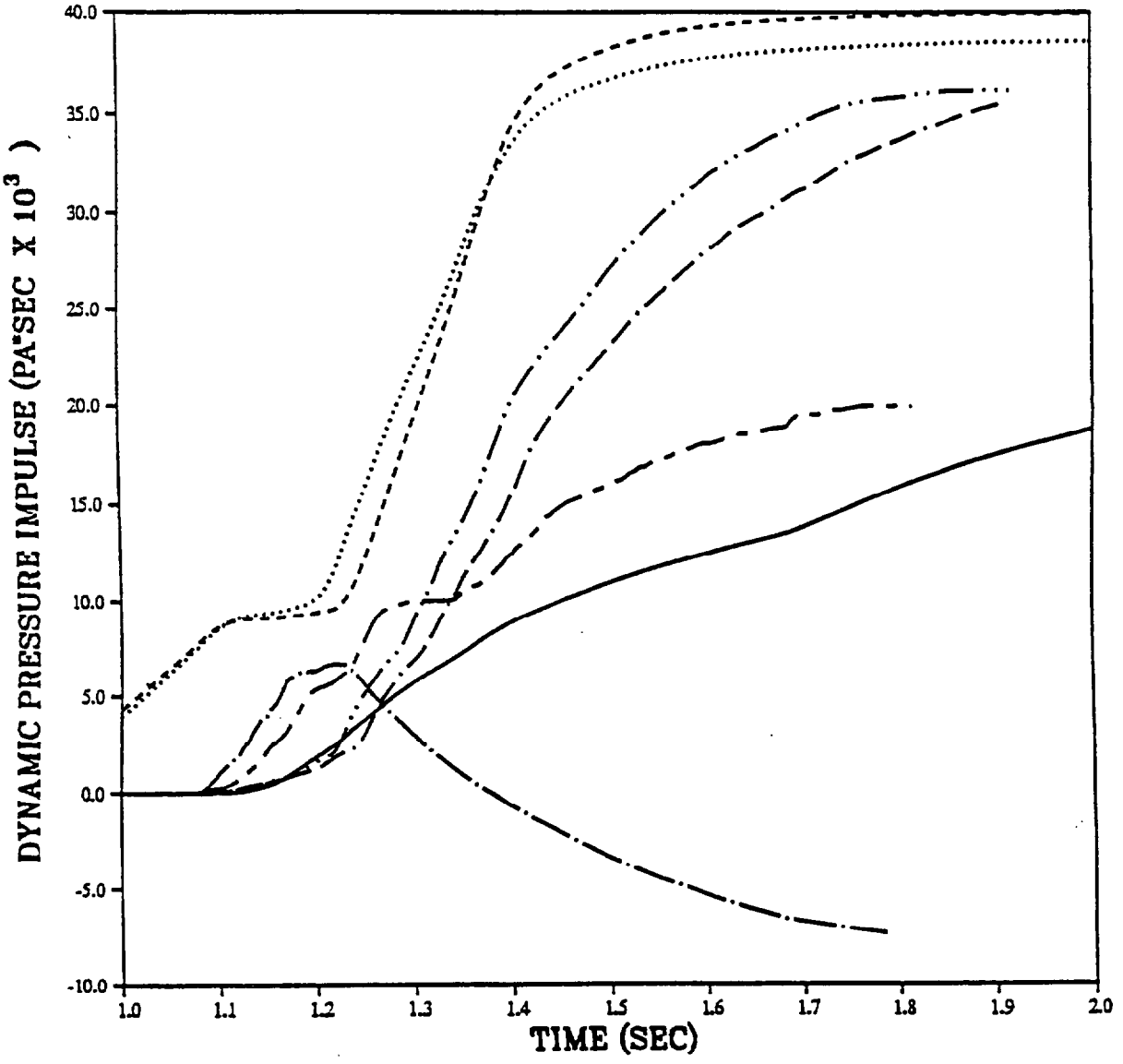

GRASSLAND CALC - 0.91 M (3 FT)
GRASSLAND CALC - 0.91 M (3 FT)
GRASSLAND CALC - 3.05 M (10 FT)
BRL - 0.91 M (3 FT)
BRL - 0.91 M (3 FT)
SRI - 3.05 M (10 FT)
SRI - 3.05 M (10 FT)

PRISCILLA
CALCULATION - DATA COMPARISONS
DYNAMIC PRESSURE AT 1067 METERS (3500 FEET)

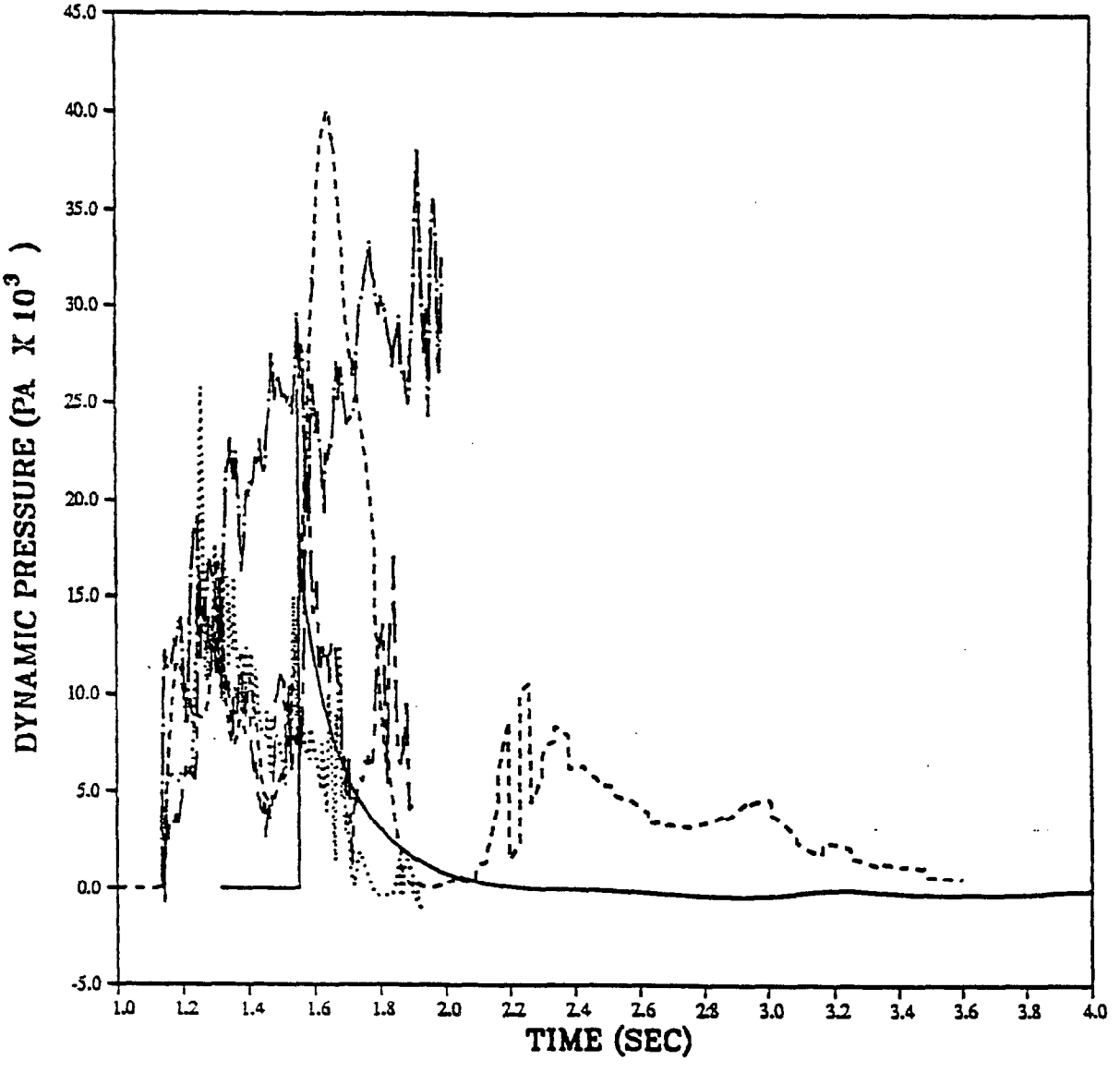

IDEAL - 0.91 M (3 FT)
GRASSLAND CALC - 0.91 M (3 FT)
BRL - 0.91 M (3 FT)
SRI - 0.91 M (3 FT)
SRI - 0.91 M (3 FT)

PRISCILLA
CALCULATION - DATA COMPARISONS
DYNAMIC PRESSURE IMPULSE AT 1067 METERS (3500 FEET)

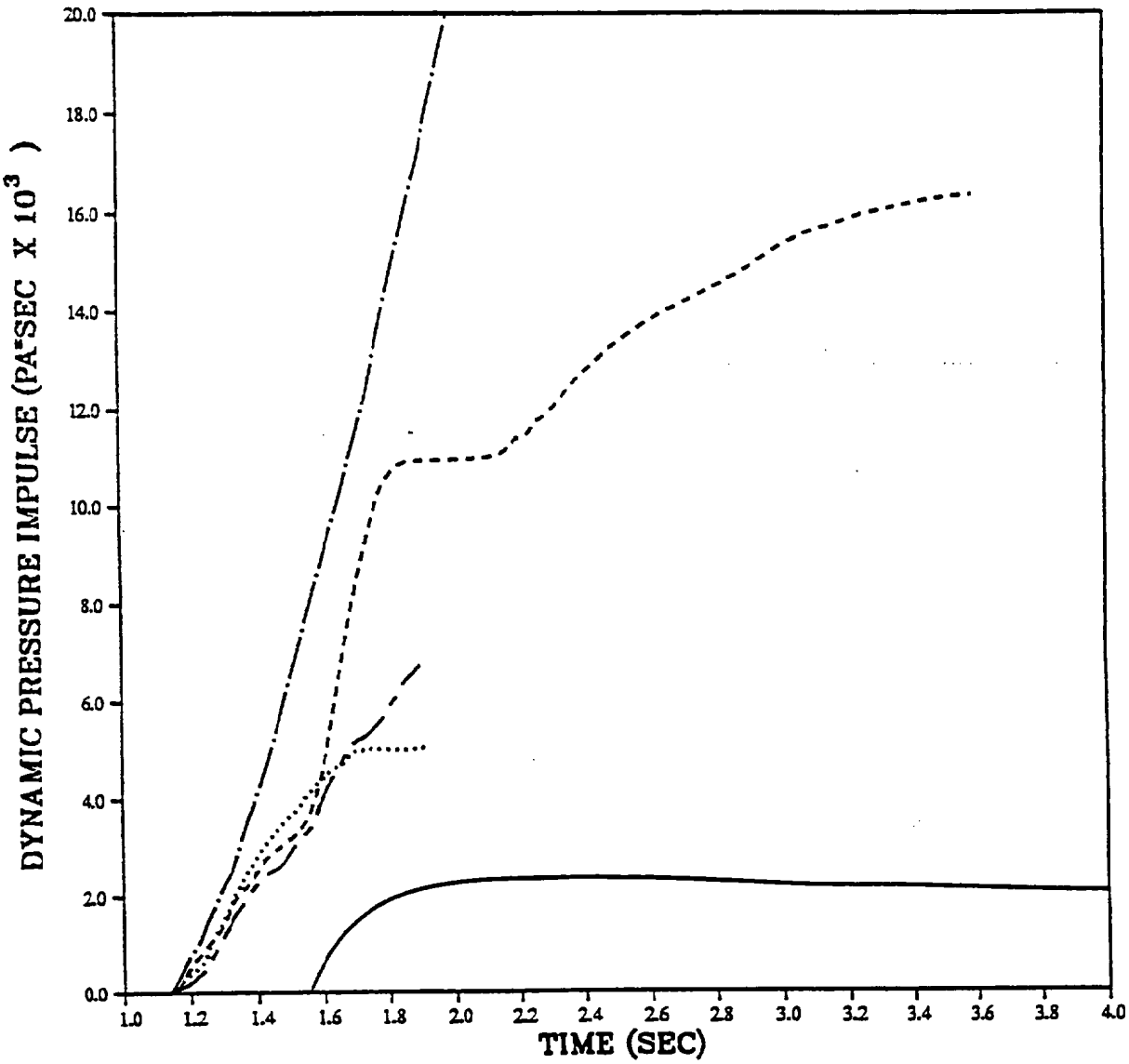

IDEAL - 0.91 M (3 FT)
GRASSLAND CALC - 0.91 M (3 FT)
BRL - 0.91 M (3 FT)
SRI - 0.91 M (3 FT)
SRI - 0.91 M (3 FT)

PRISCILLA
CALCULATION - DATA COMPARISONS
DYNAMIC PRESSURE AT 1067 METERS (3500 FEET)

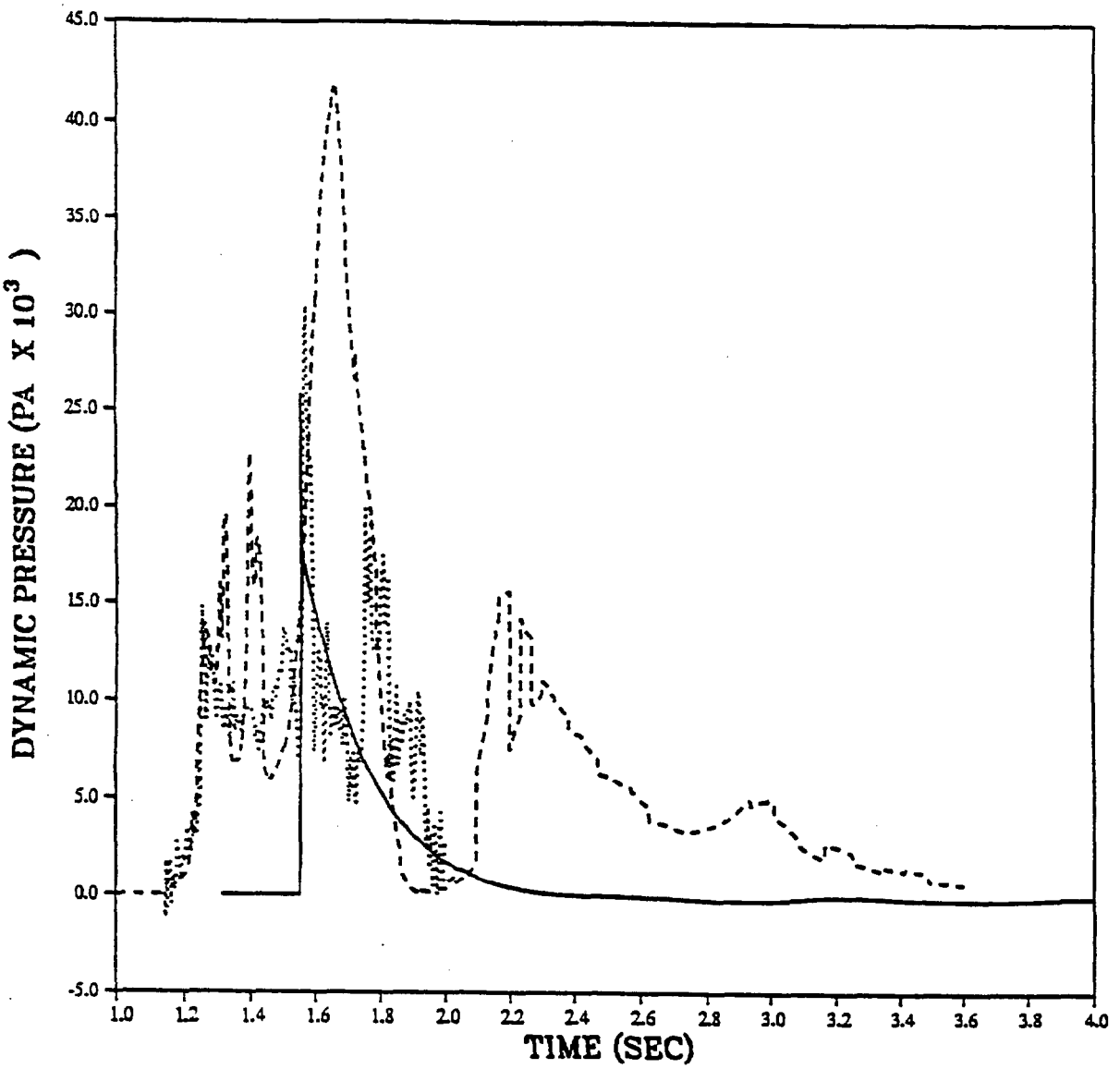

IDEAL - 3.05 M (10 FT)
GRASSLAND CALC - 3.05 M (10 FT)
SRI - 3.05 M (10 FT)

PRISCILLA
CALCULATION - DATA COMPARISONS
DYNAMIC PRESSURE IMPULSE AT 1067 METERS (3500 FEET)

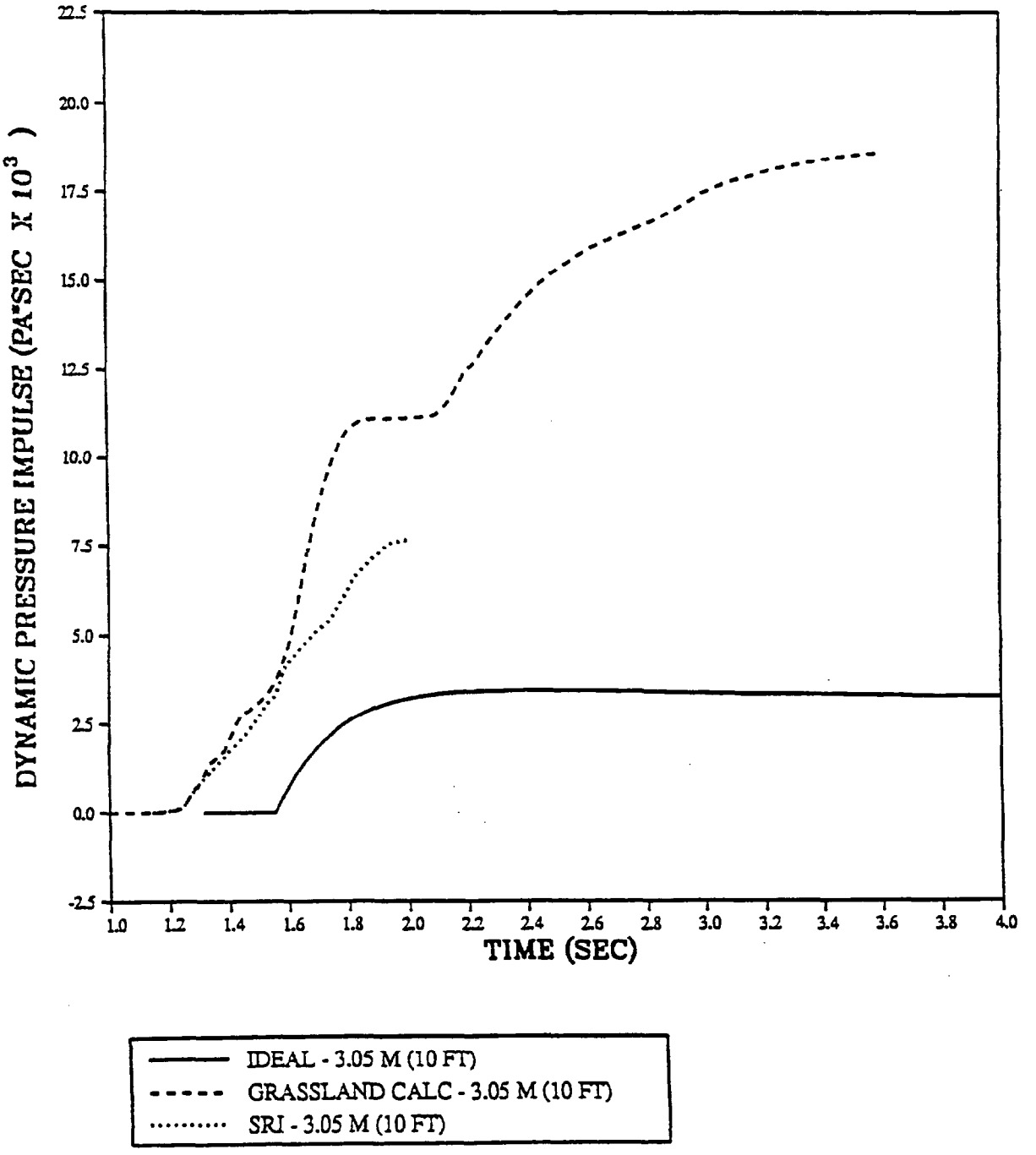

PRISCILLA
CALCULATION - DATA COMPARISONS
DYNAMIC PRESSURE AT 1219 METERS (4000 FEET)

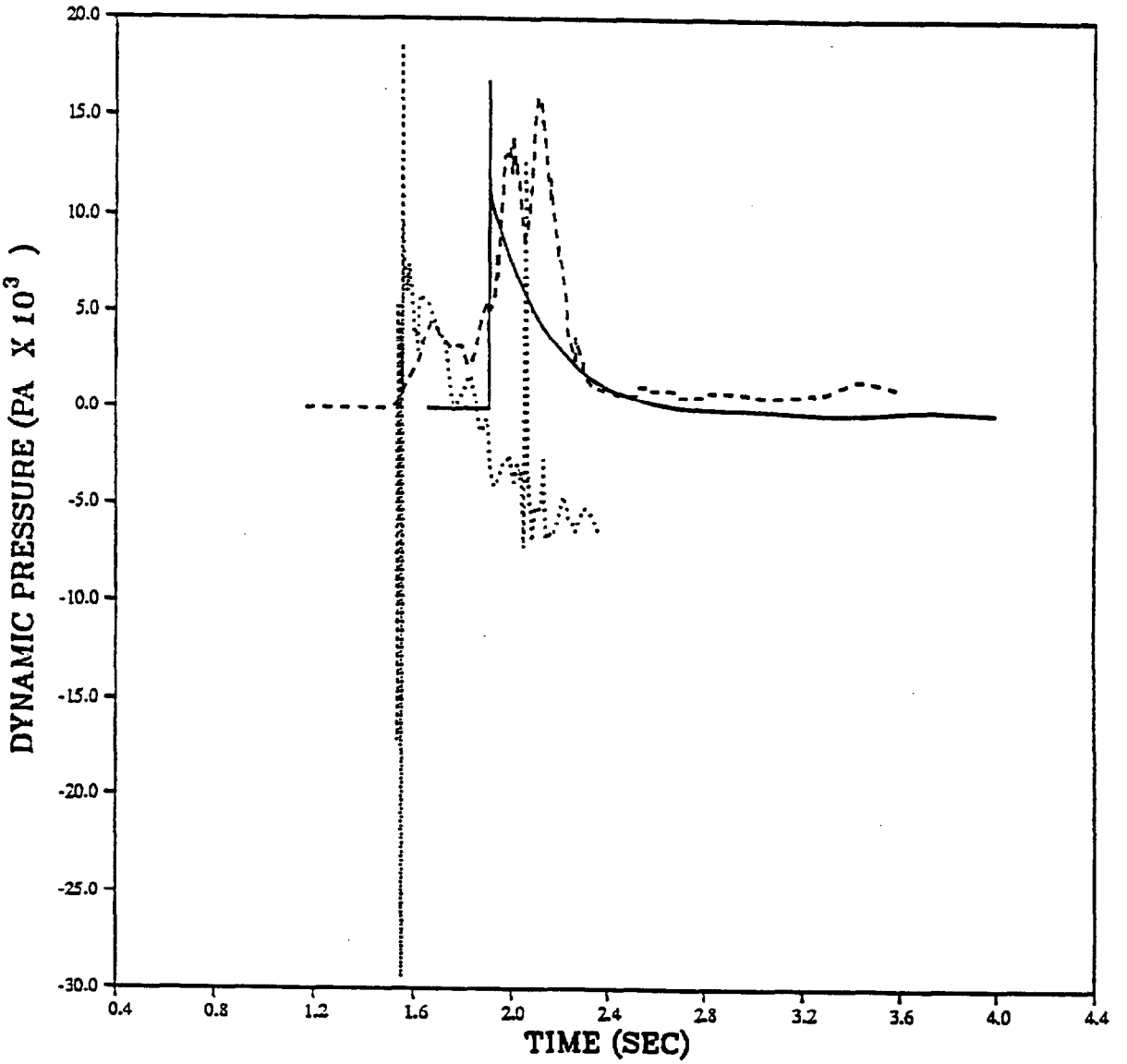

IDEAL - 0.91 M (3 FT)
GRASSLAND CALC - 0.91 M (3 FT)
BRL - 0.91 M (3 FT)

PRISCILLA
CALCULATION - DATA COMPARISONS
DYNAMIC PRESSURE IMPULSE AT 1219 METERS (4000 FEET)

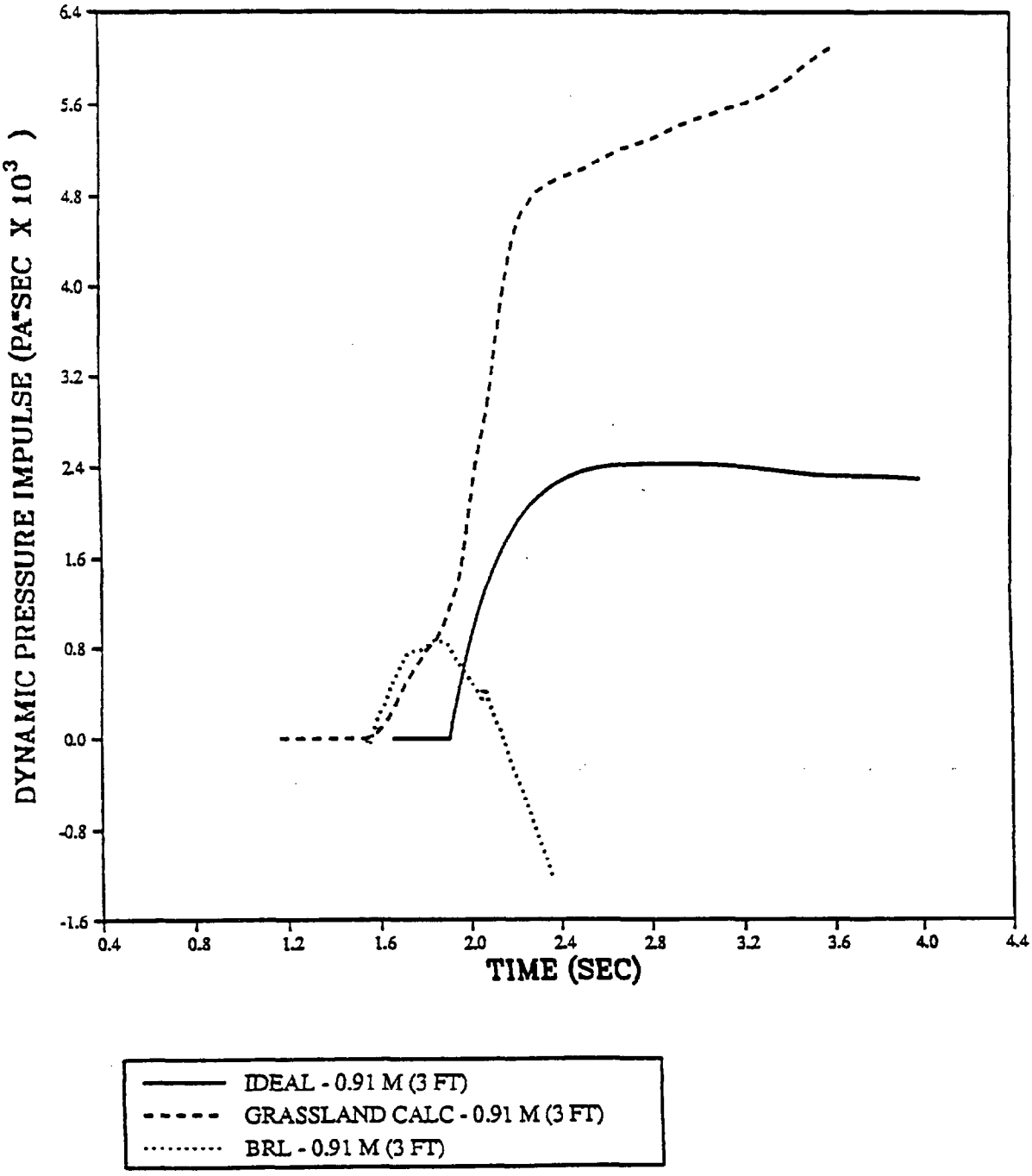

PRISCILLA
CALCULATION - DATA COMPARISONS
DYNAMIC PRESSURE AT 1372 METERS (4500 FEET)

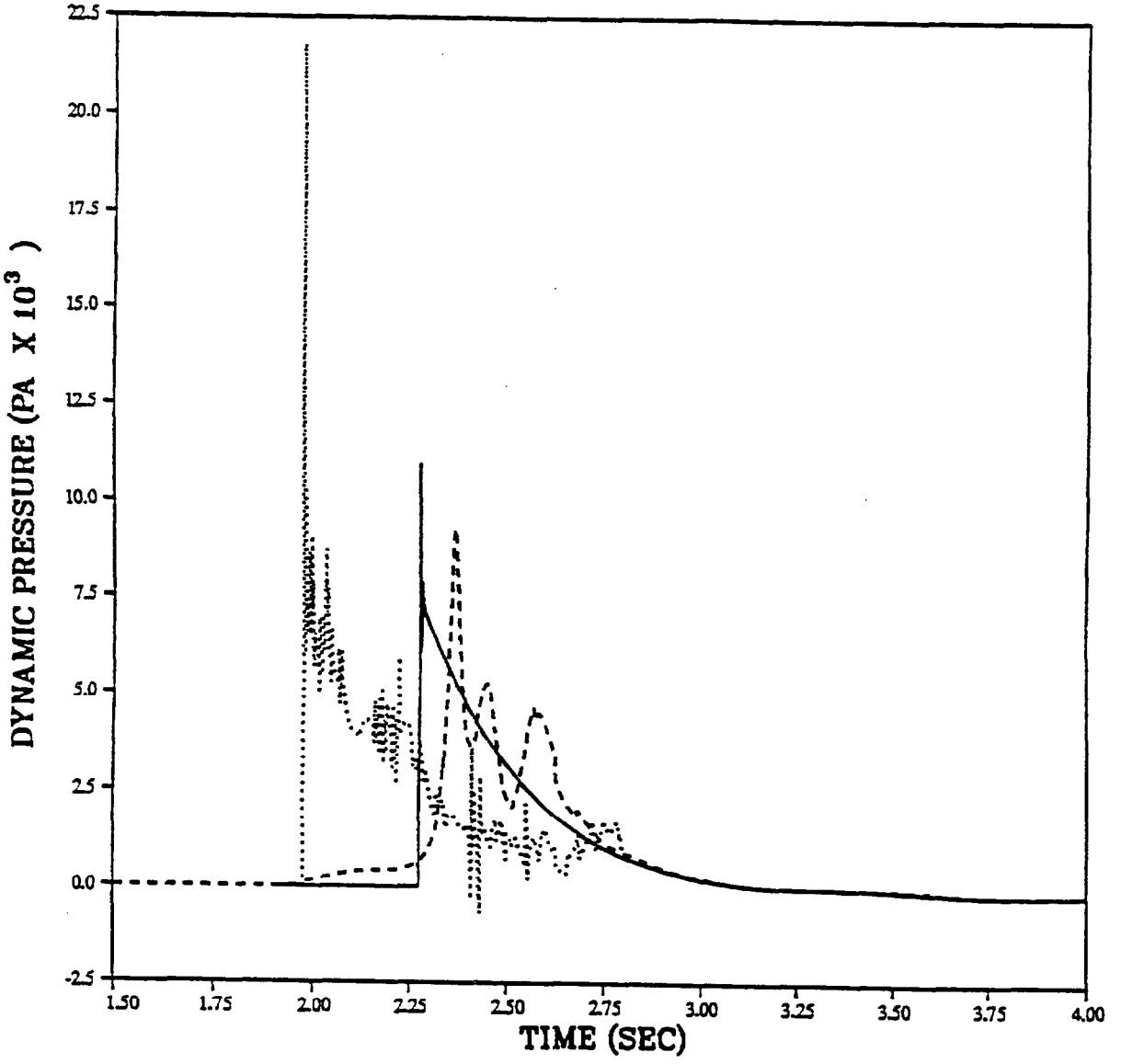

IDEAL - 0.91 M (3 FT)
GRASSLAND CALC - 0.91 M (3 FT)
BRL - 0.91 M (3 FT)

PRISCILLA
CALCULATION - DATA COMPARISONS
DYNAMIC PRESSURE IMPULSE AT 1372 METERS (4500 FEET)

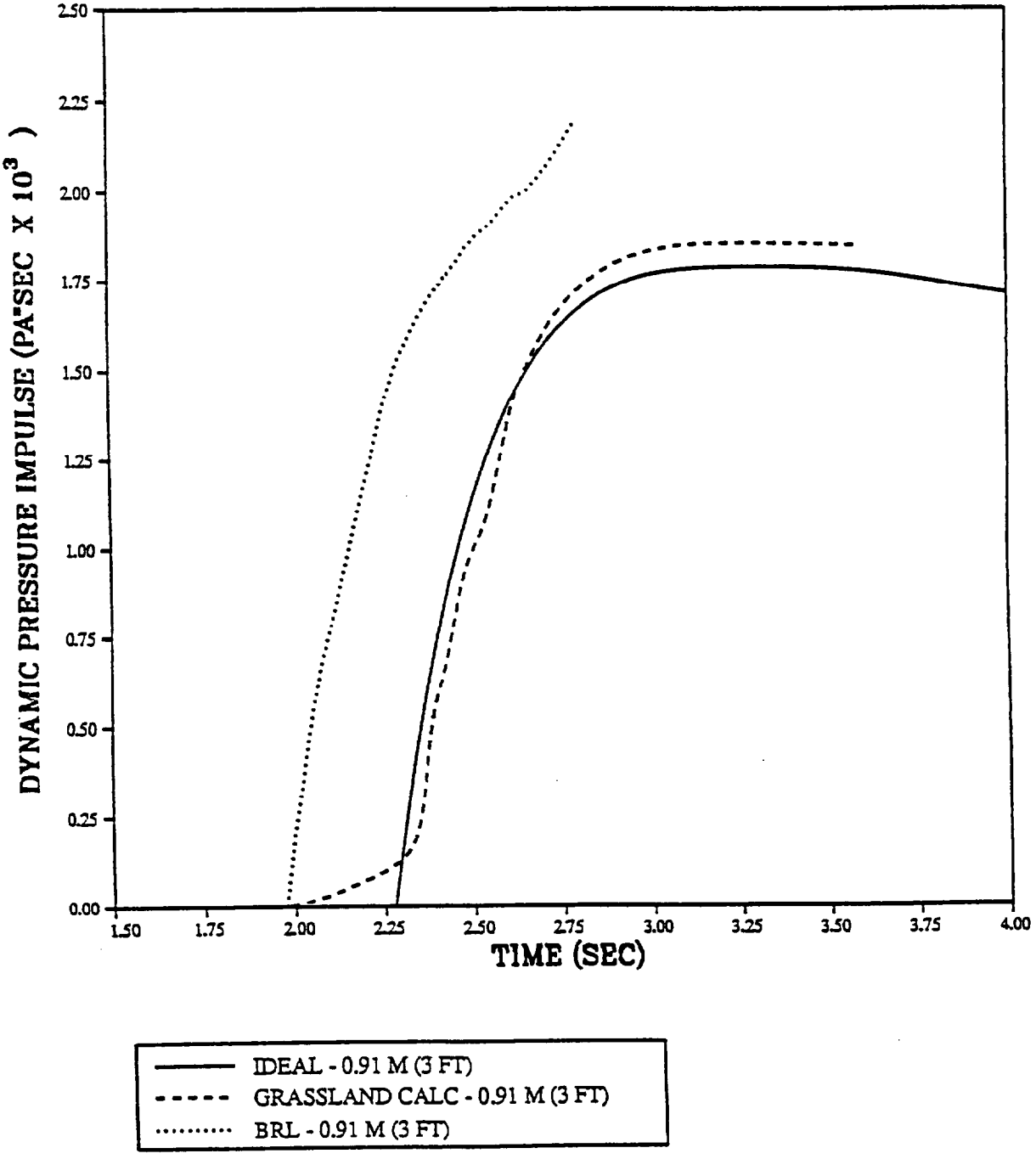

PRISCILLA
CALCULATION - DATA COMPARISONS
DYNAMIC PRESSURE AT 1524 METERS (5000 FEET)

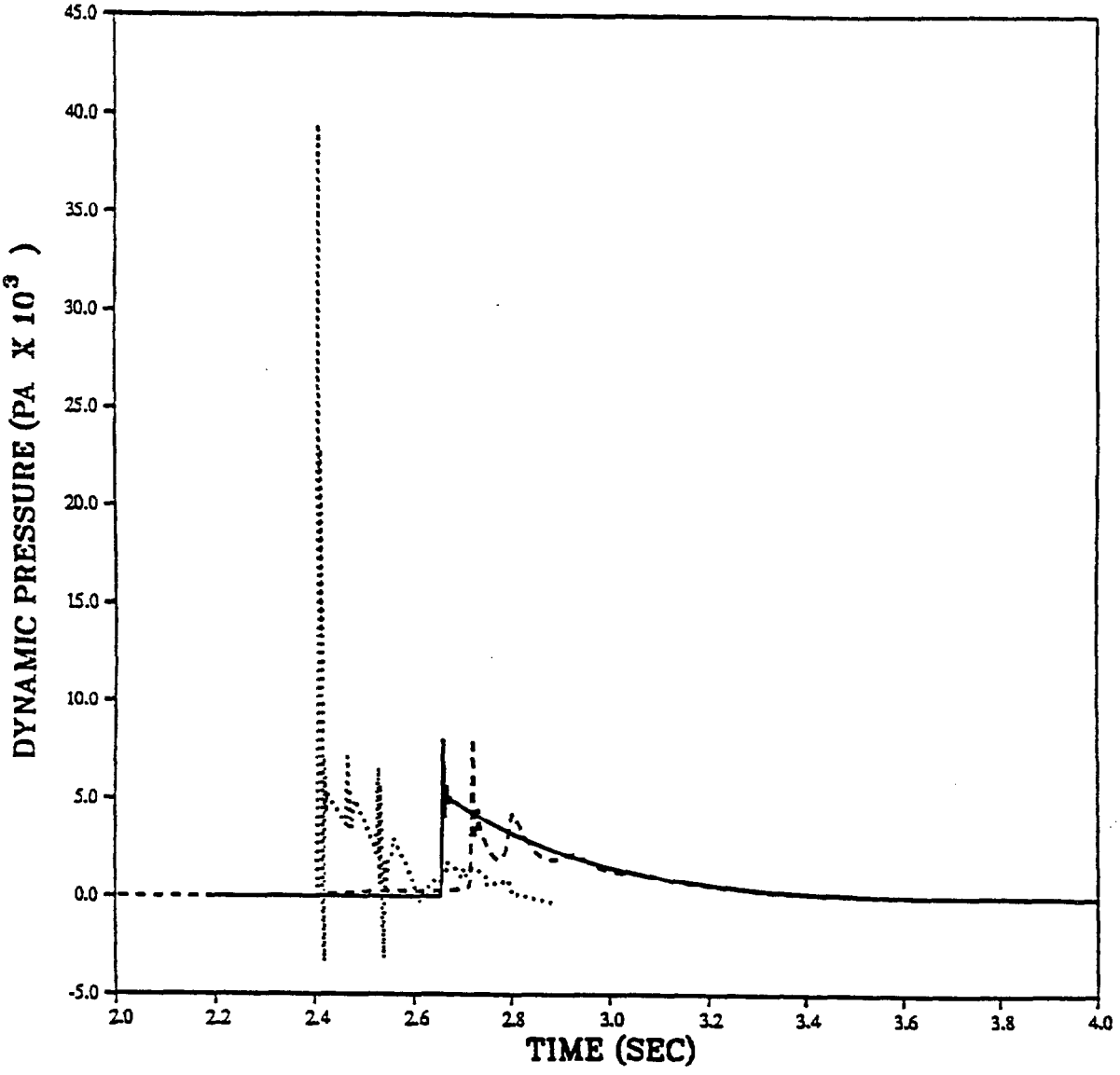

PRISCILLA
CALCULATION - DATA COMPARISONS
DYNAMIC PRESSURE IMPULSE AT 1524 METERS (5000 FEET)

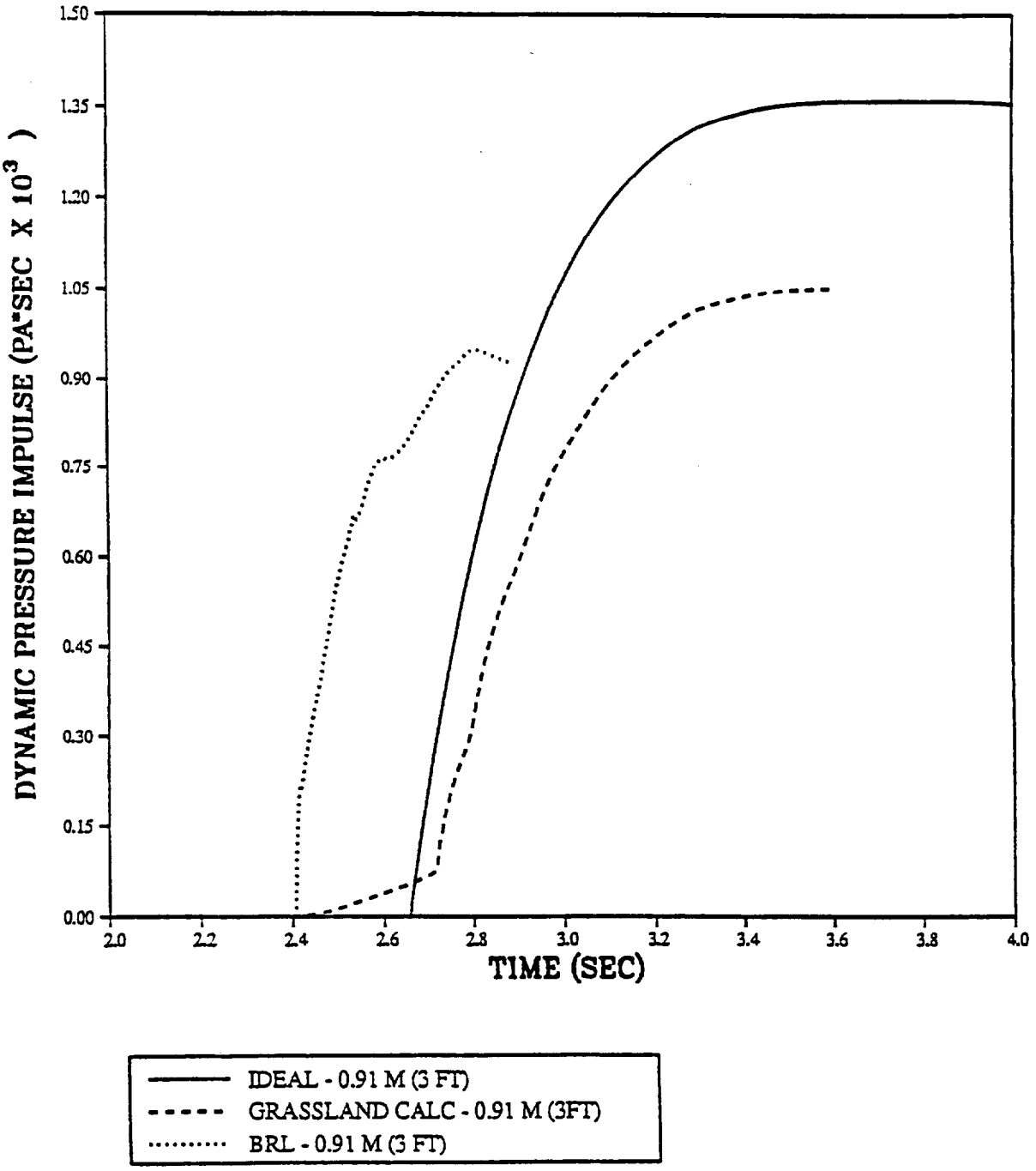

INTENTIONALLY LEFT BLANK.

APPENDIX C
HYDRODYNAMIC PARAMETERS AS A FUNCTION OF HEIGHT FOR SELECTED GROUND RANGES

This Appendix contains plots of important hydrodynamic parameters as a function of height above the surface at several ground ranges. The ground ranges were selected on the basis of predicted ideal overpressure levels. Results of calculated ideal and precursor parameters are displayed on each plot.

PRISCILLA
ARRIVAL TIME AT 640 METERS (2100 FEET)
VERTICAL PROFILE (30 PSI OVERPRESSURE LEVEL).

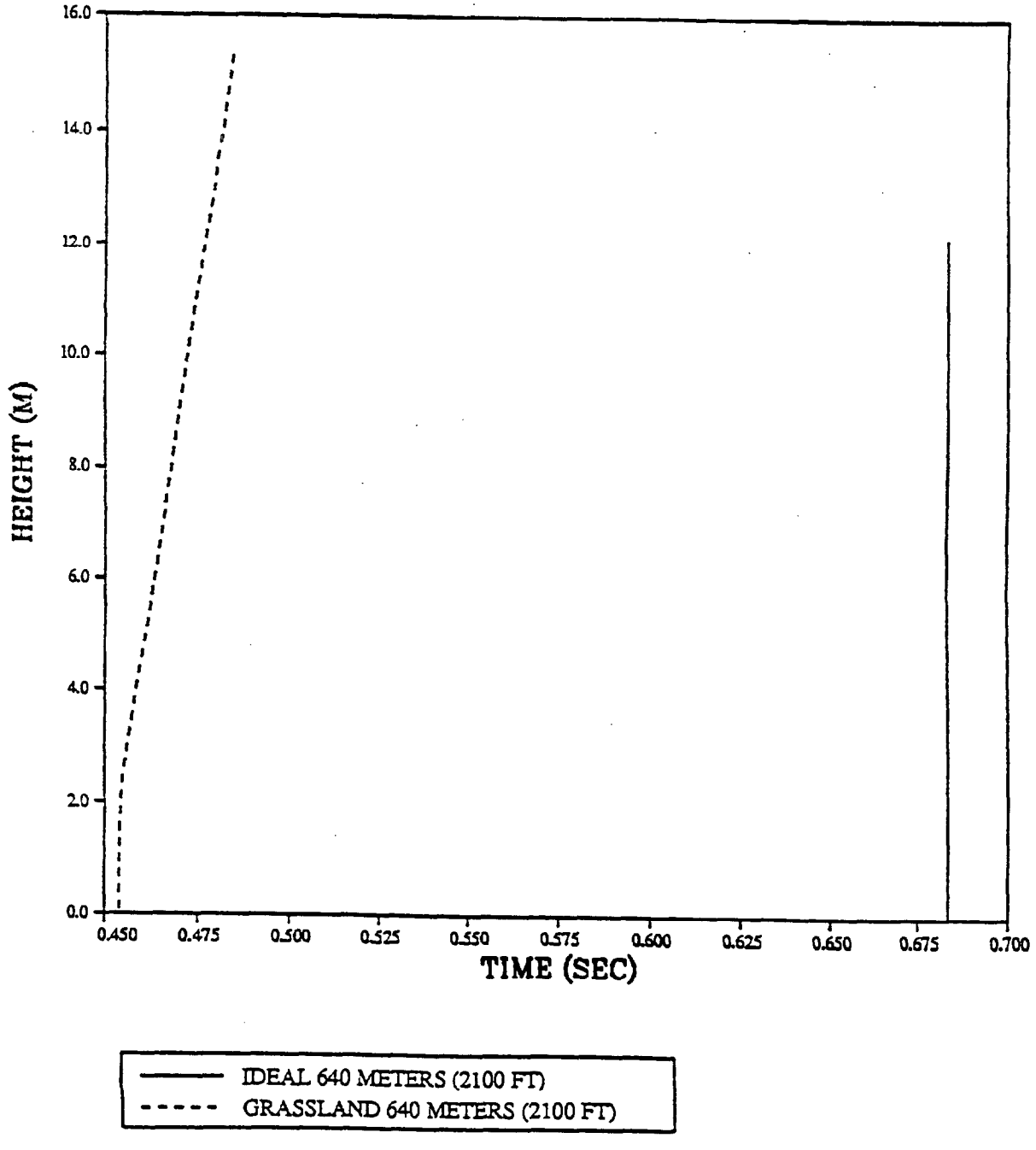

PRISCILLA
ARRIVAL TIME AT 701 METERS (2300 FEET)
VERTICAL PROFILE (25 PSI OVERPRESSURE LEVEL).

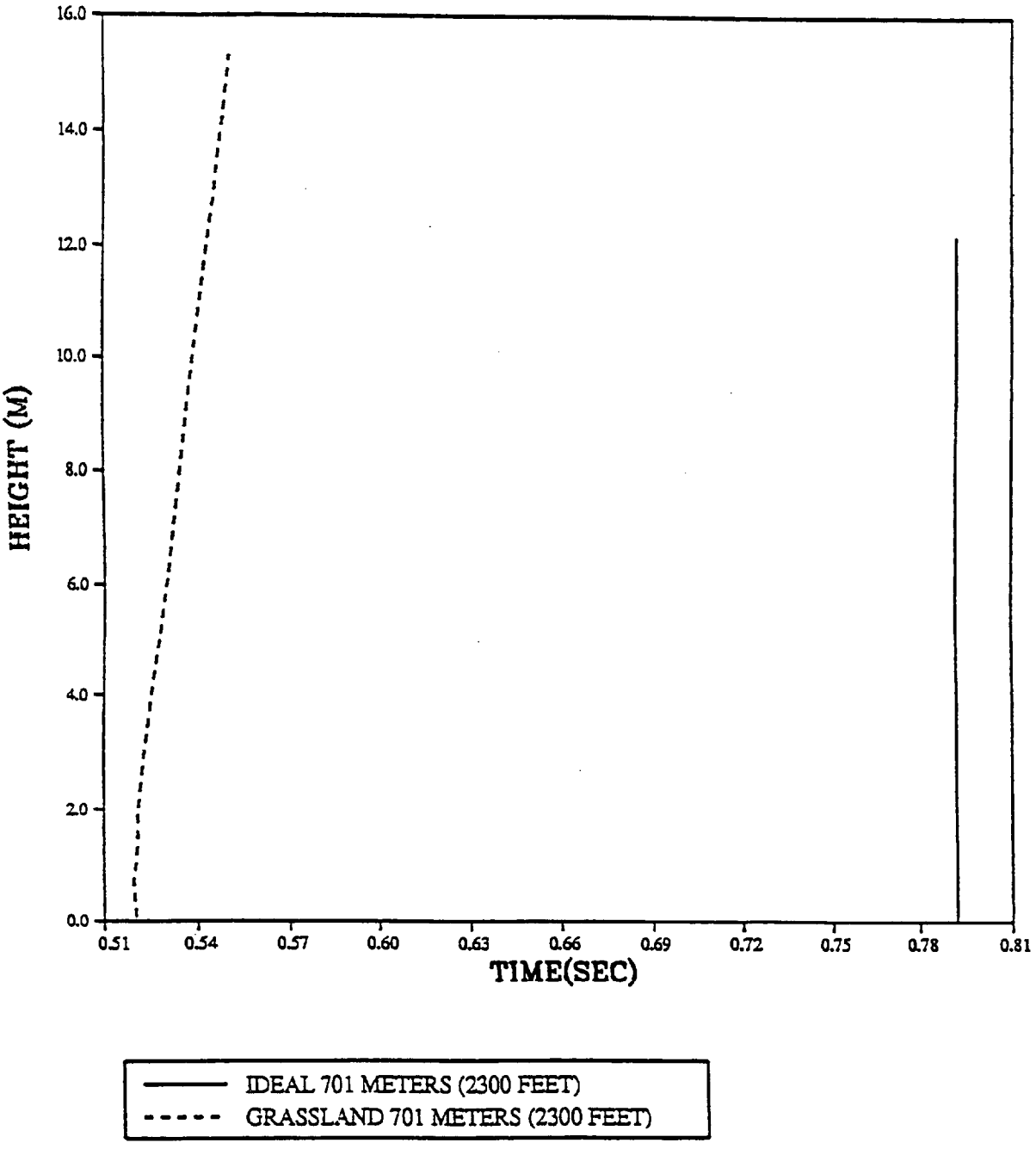

PRISCILLA
ARRIVAL TIME AT 701 METERS (2300 FEET)
VERTICAL PROFILE (25 PSI OVERPRESSURE LEVEL).

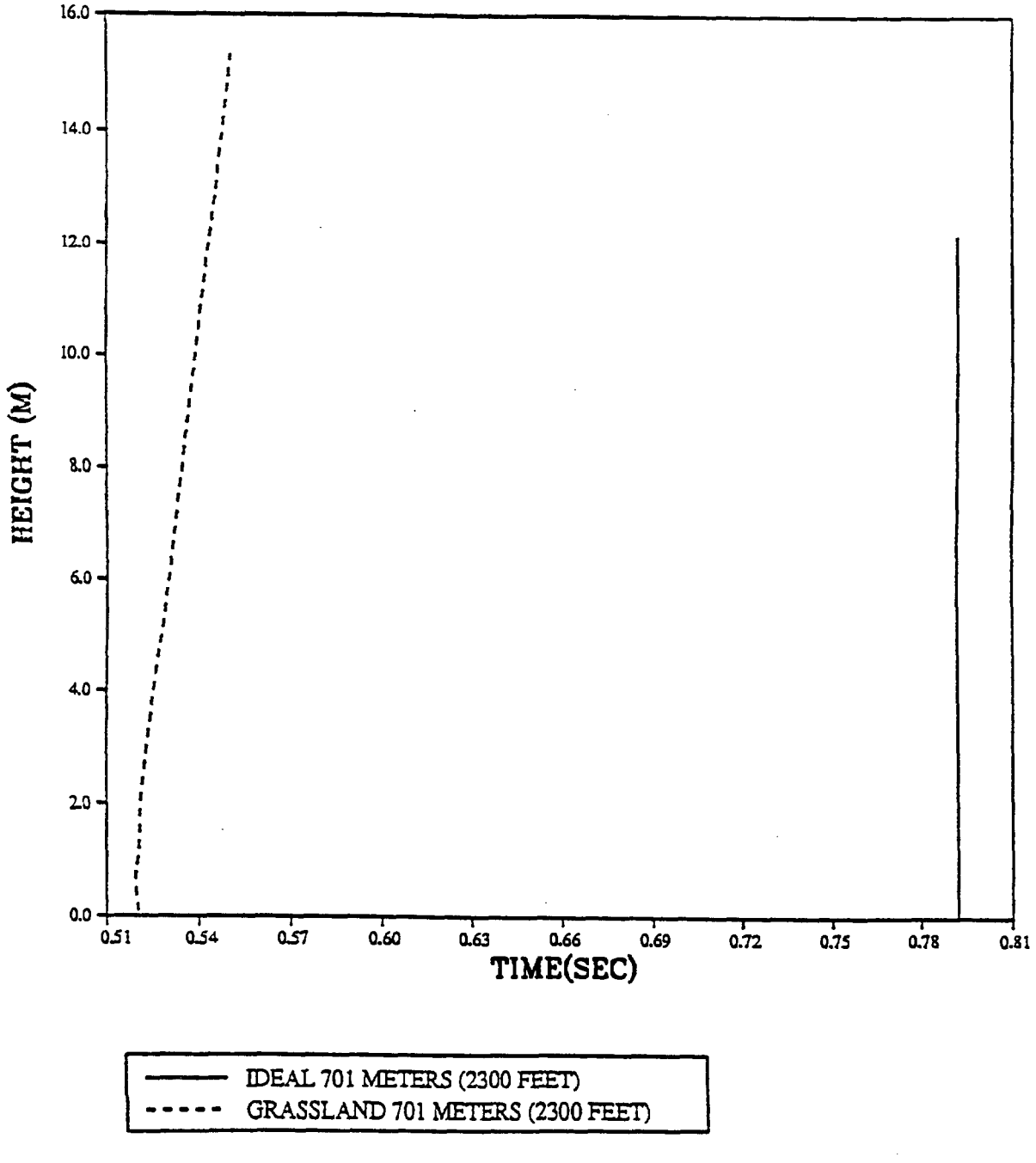

PRISCILLA
ARRIVAL TIME AT 777 METERS (2550 FEET)
VERTICAL PROFILE (20 PSI OVERPRESSSURE LEVEL)

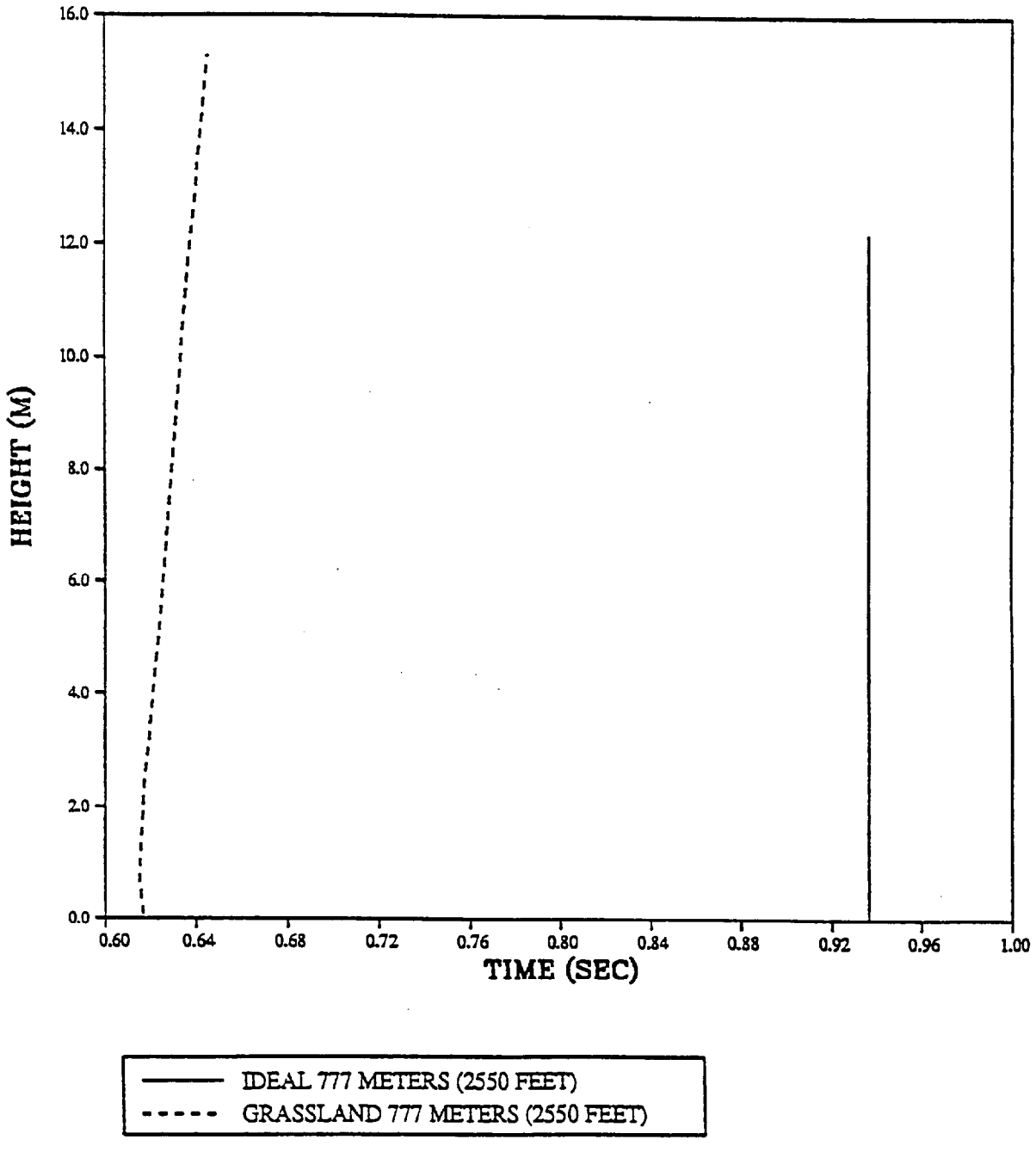

PRISCILLA
ARRIVAL TIME 899 METERS (2950 FT)
VERTICAL PROFILE (15 PSI OVERPRESSURE LEVEL)

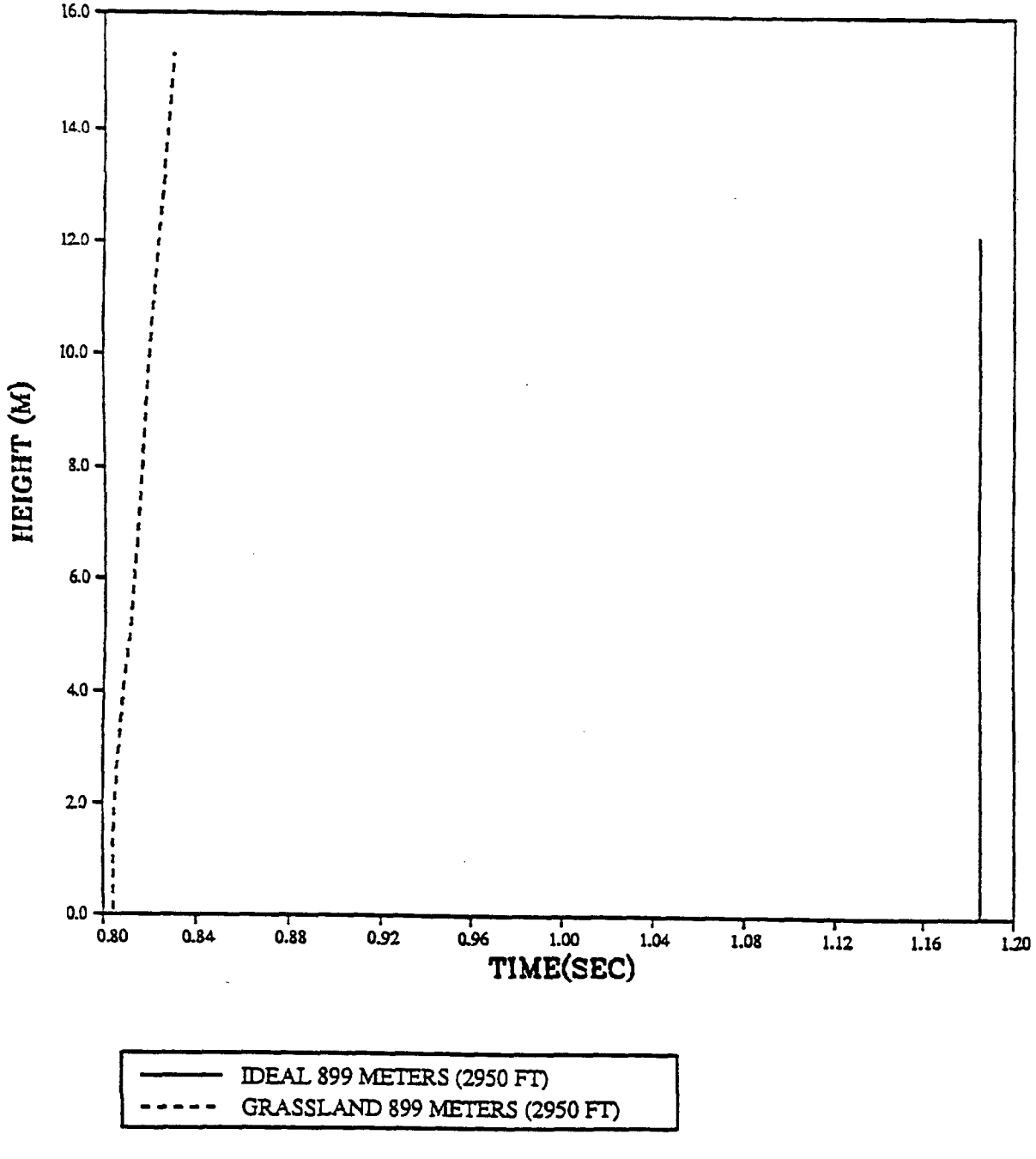

PRISCILLA
ARRIVAL TIME AT 990 METERS (3250 FT)
VERTICAL PROFILE (12 PSI OVERPRESSURE LEVEL).

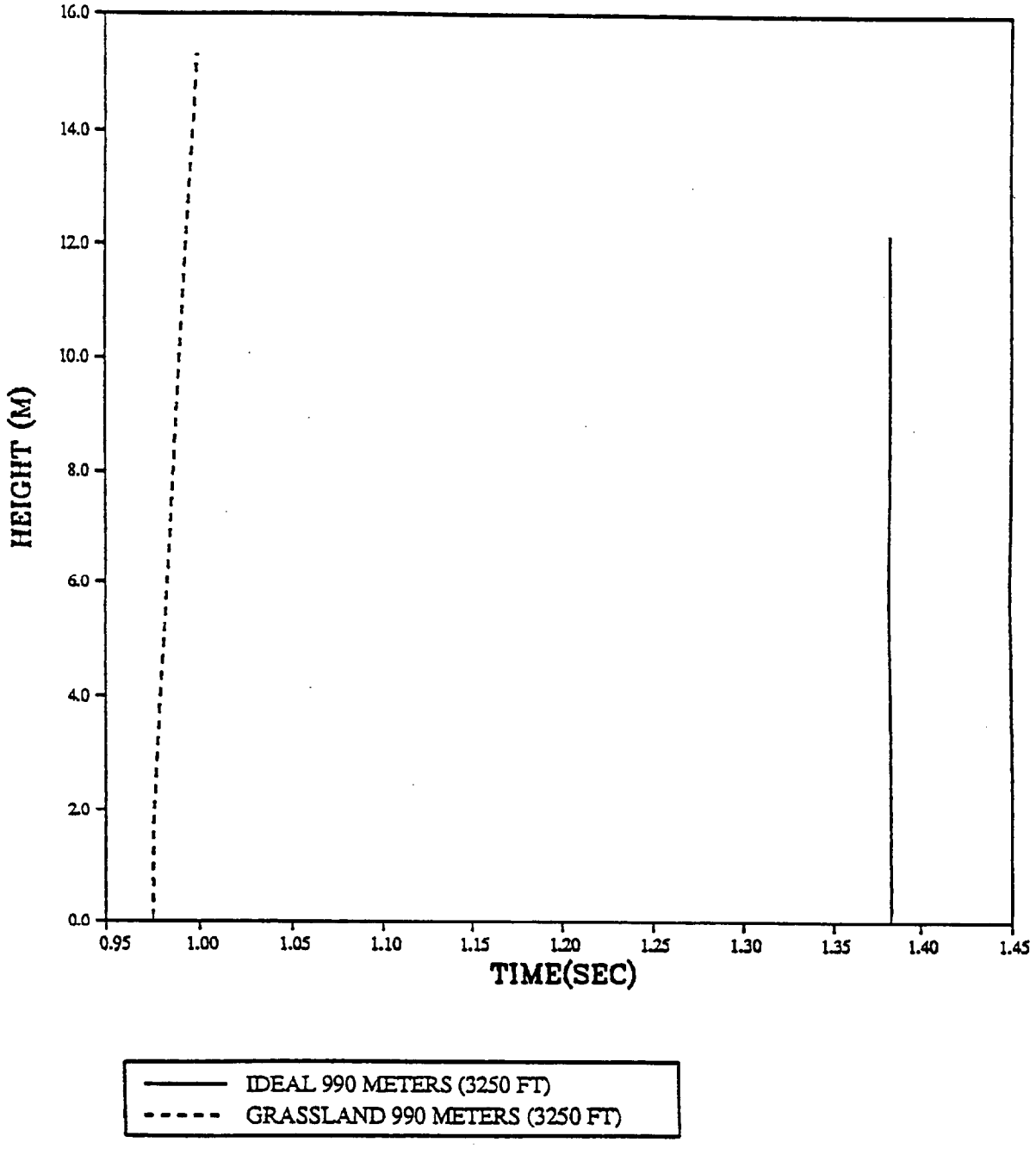

PRISCILLA
ARRIVAL TIME AT 1113 METERS (3650 FT)
VERTICAL PROFILE AT (10 PSI OVERPRESSURE LEVEL)

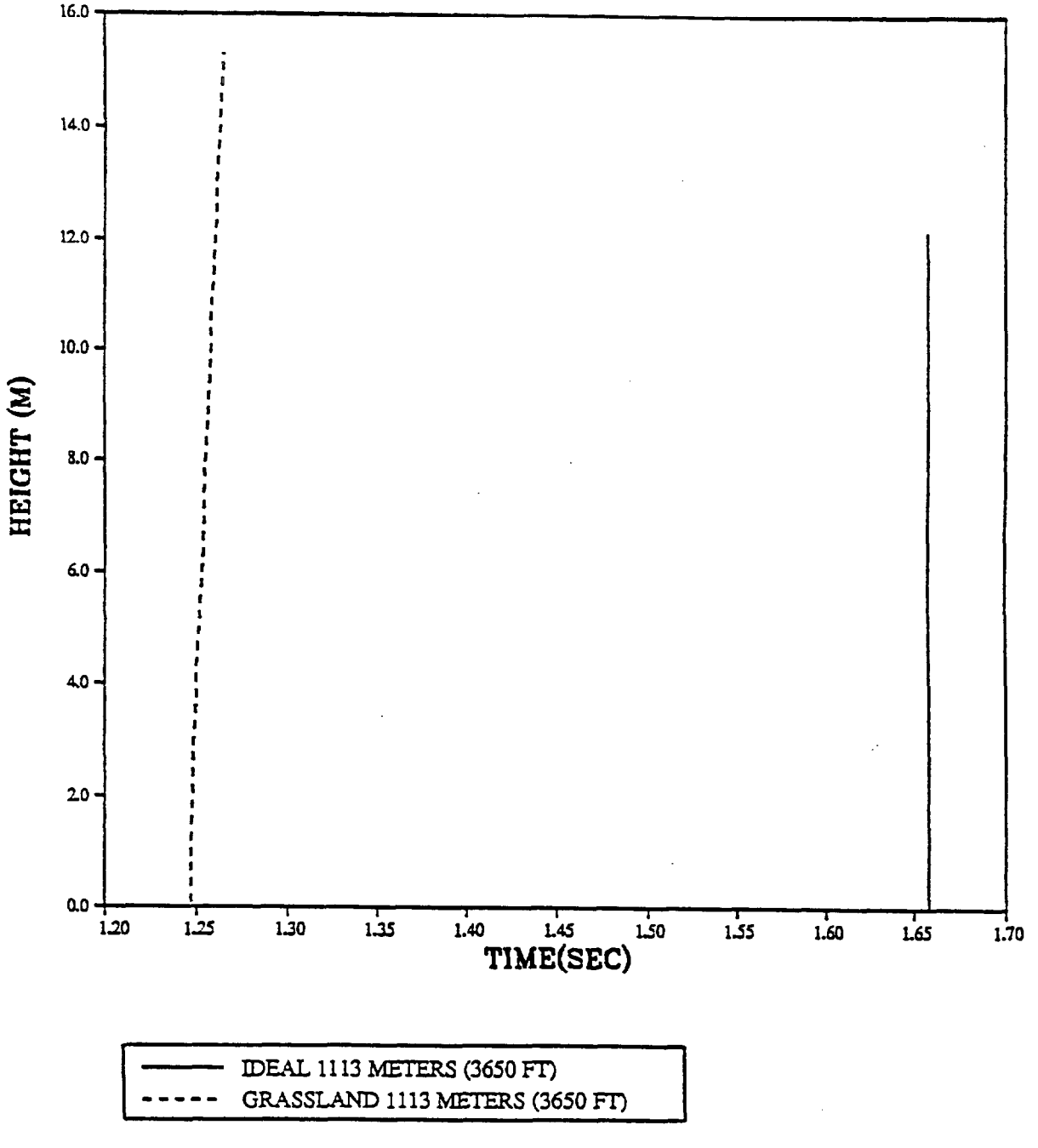

PRISCILLA
ARRIVAL TIME AT 1250 METERS (4100 FT)
VERTICAL PROFILE (8 PSI OVERPRESSURE LEVEL)

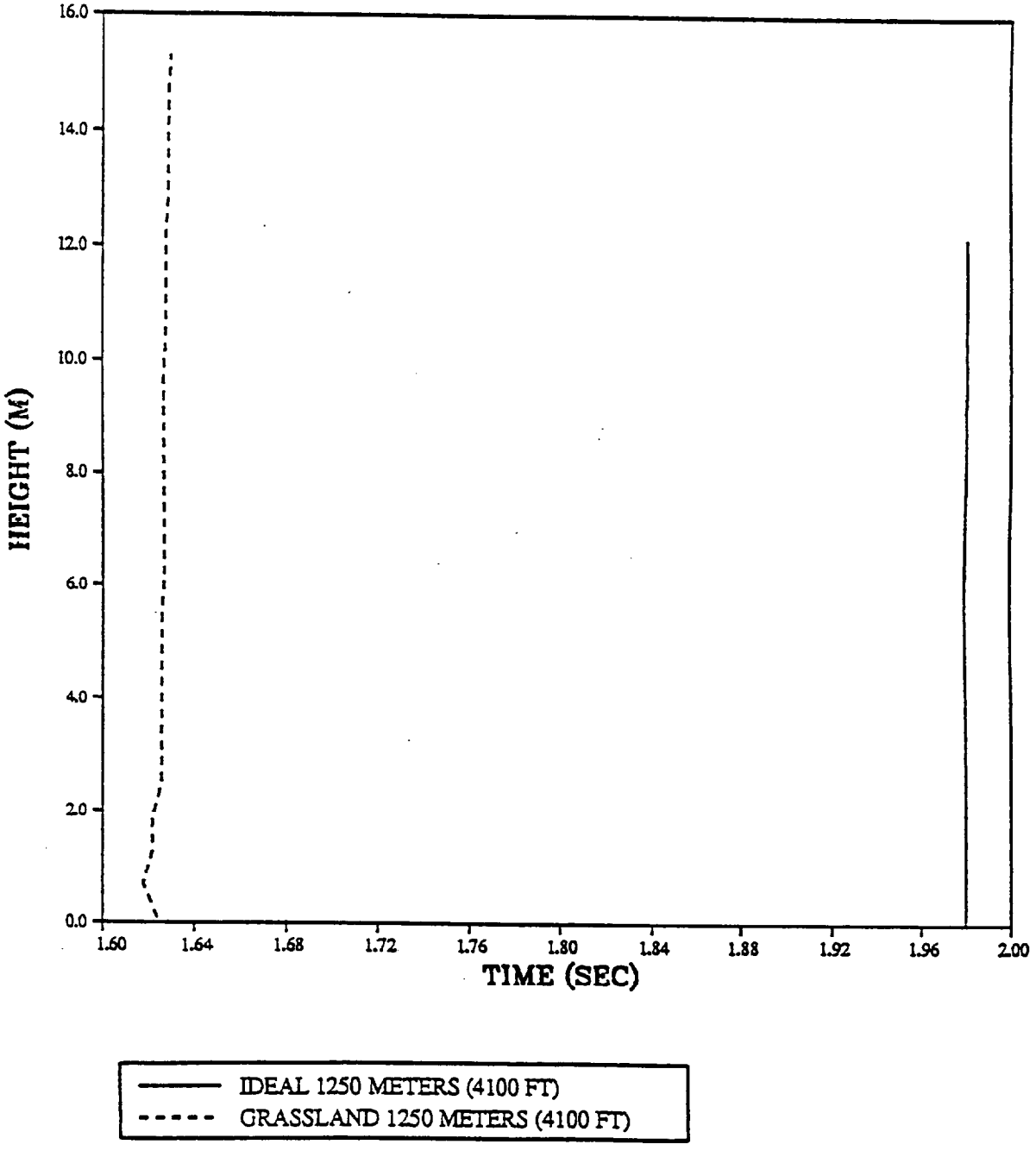

PRISCILLA
ARRIVAL TIME AT 1494 METERS (4900 FT)
VERTICAL PROFILE (6 PSI OVERPRESSURE LEVEL)

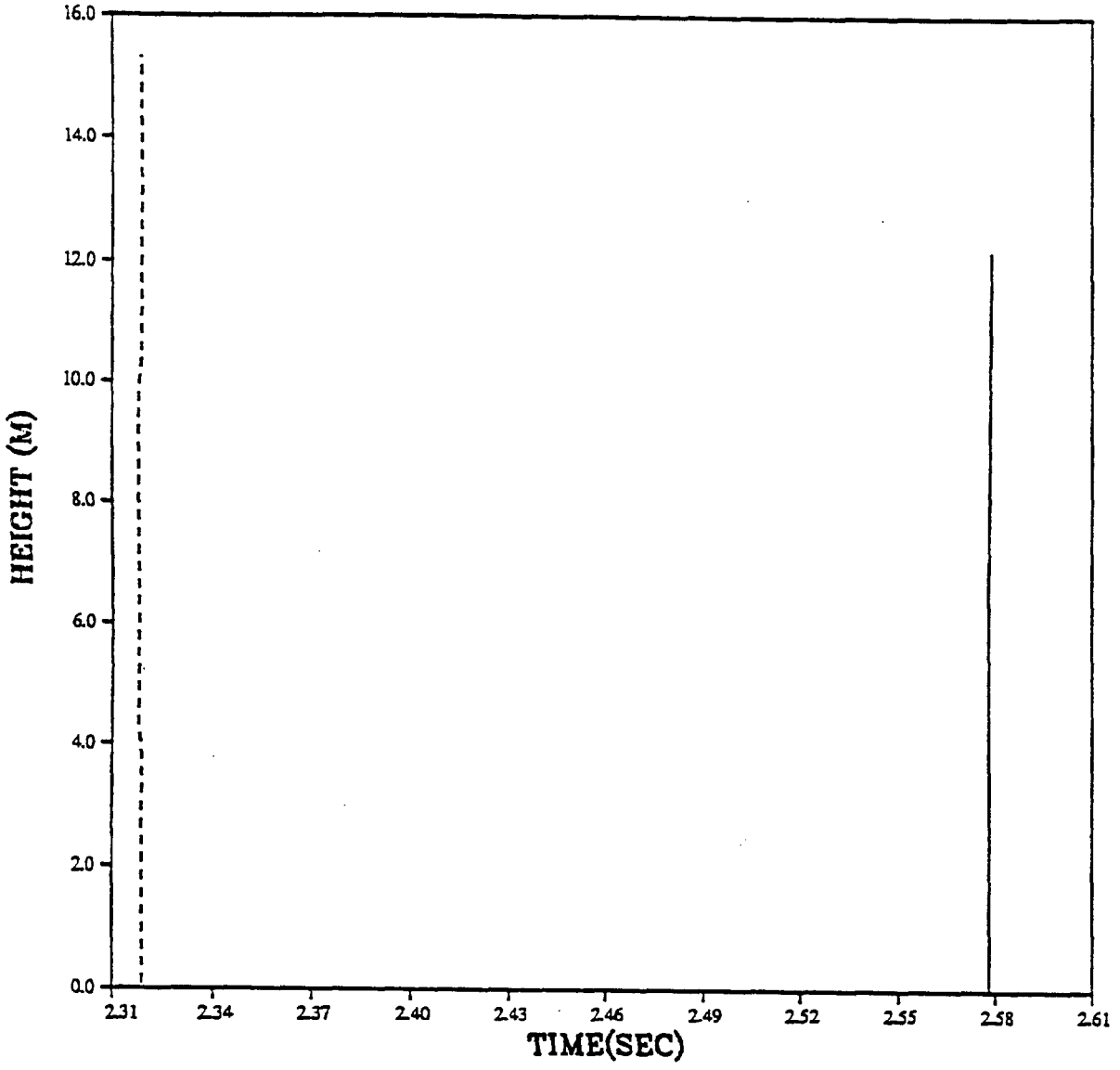

PRISCILLA
ARRIVAL TIME AT 1630 METERS (5350 FT)
VERTICAL PROFILE (5 PSI OVERPRESSURE LEVEL)

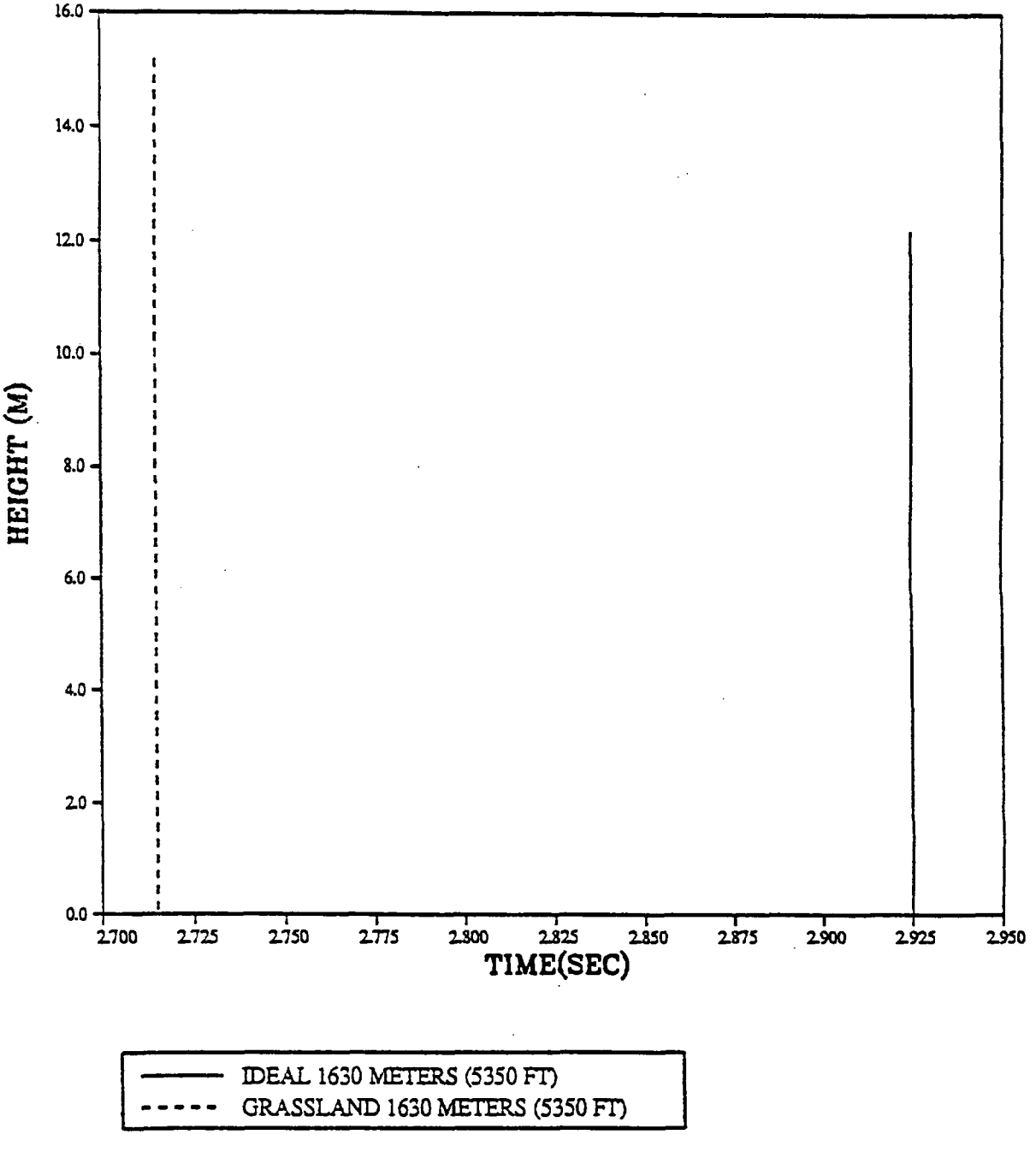

PRISCILLA
OVERPRESSURE AT 640 METERS (2100 FEET)
VERTICAL PROFILE (30 PSI OVERPRESSURE LEVEL).

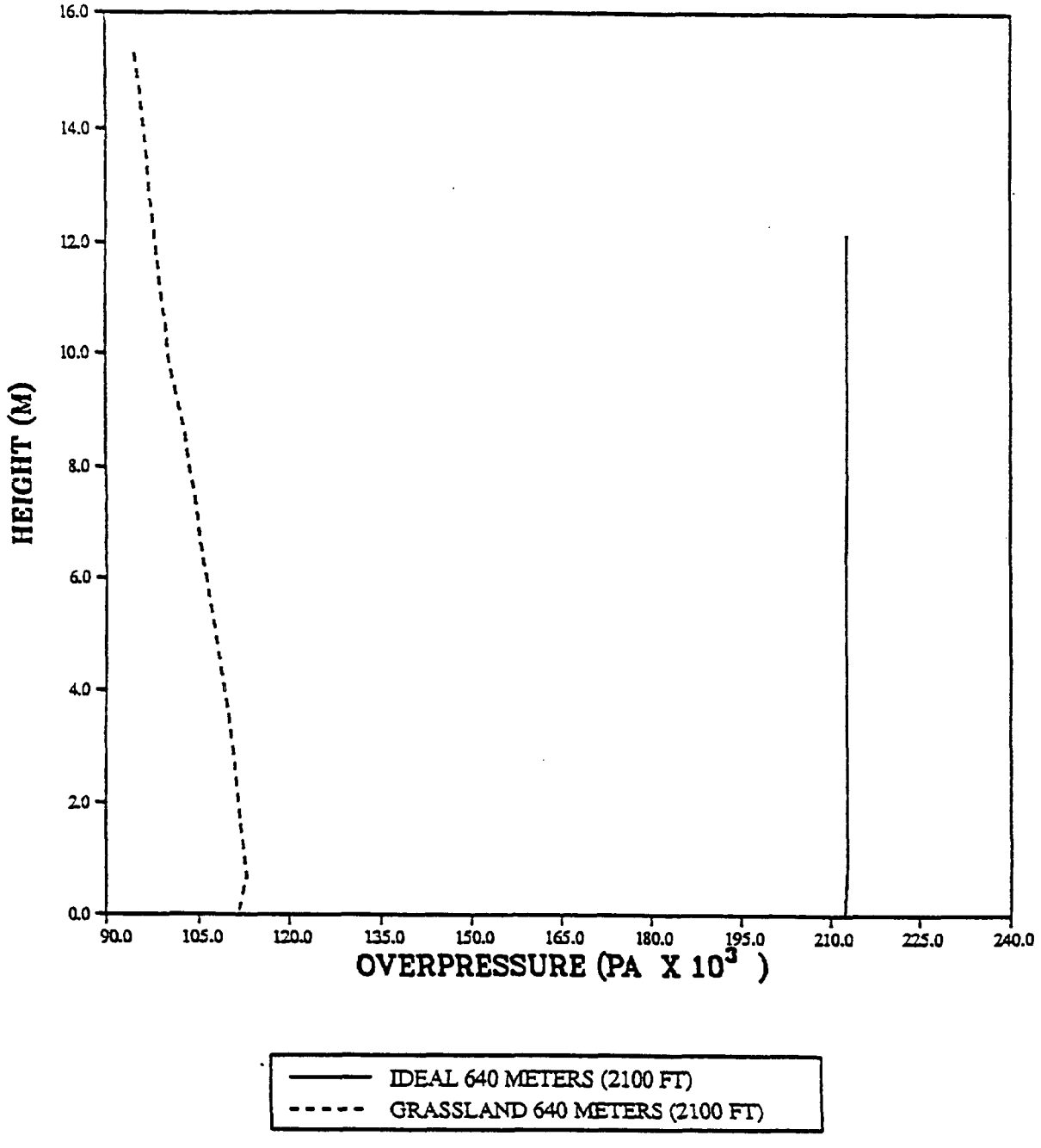

PRISCILLA
OVERPRESSURE AT 701 METERS (2300 FEET)
VERTICAL PROFILE (25 PSI OVERPRESSURE LEVEL)

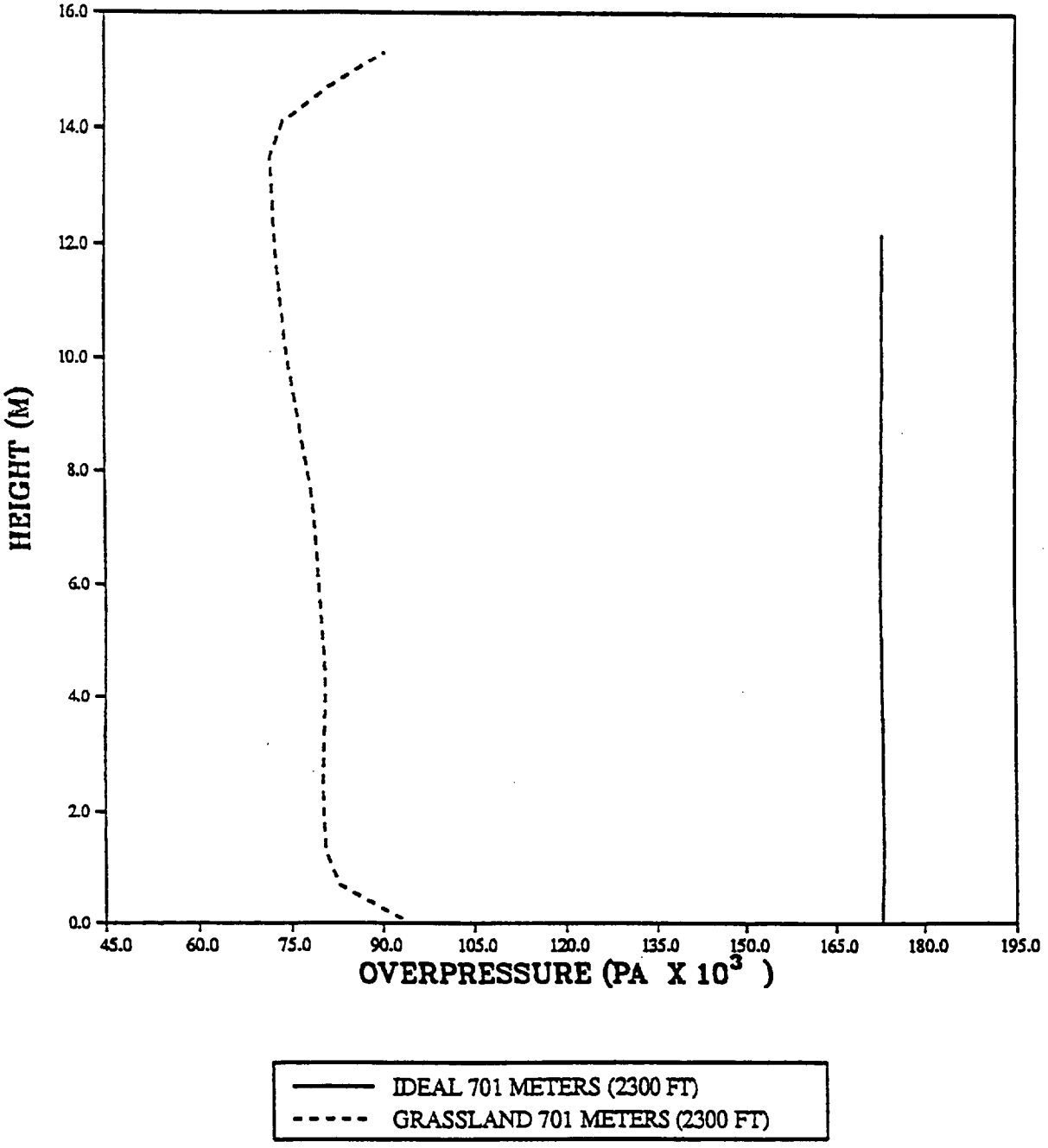

PRISCILLA
OVERPRESSURE AT 777 METERS (2550 FEET)
VERTICAL PROFILE (20 PSI OVERPRESSURE LEVEL)

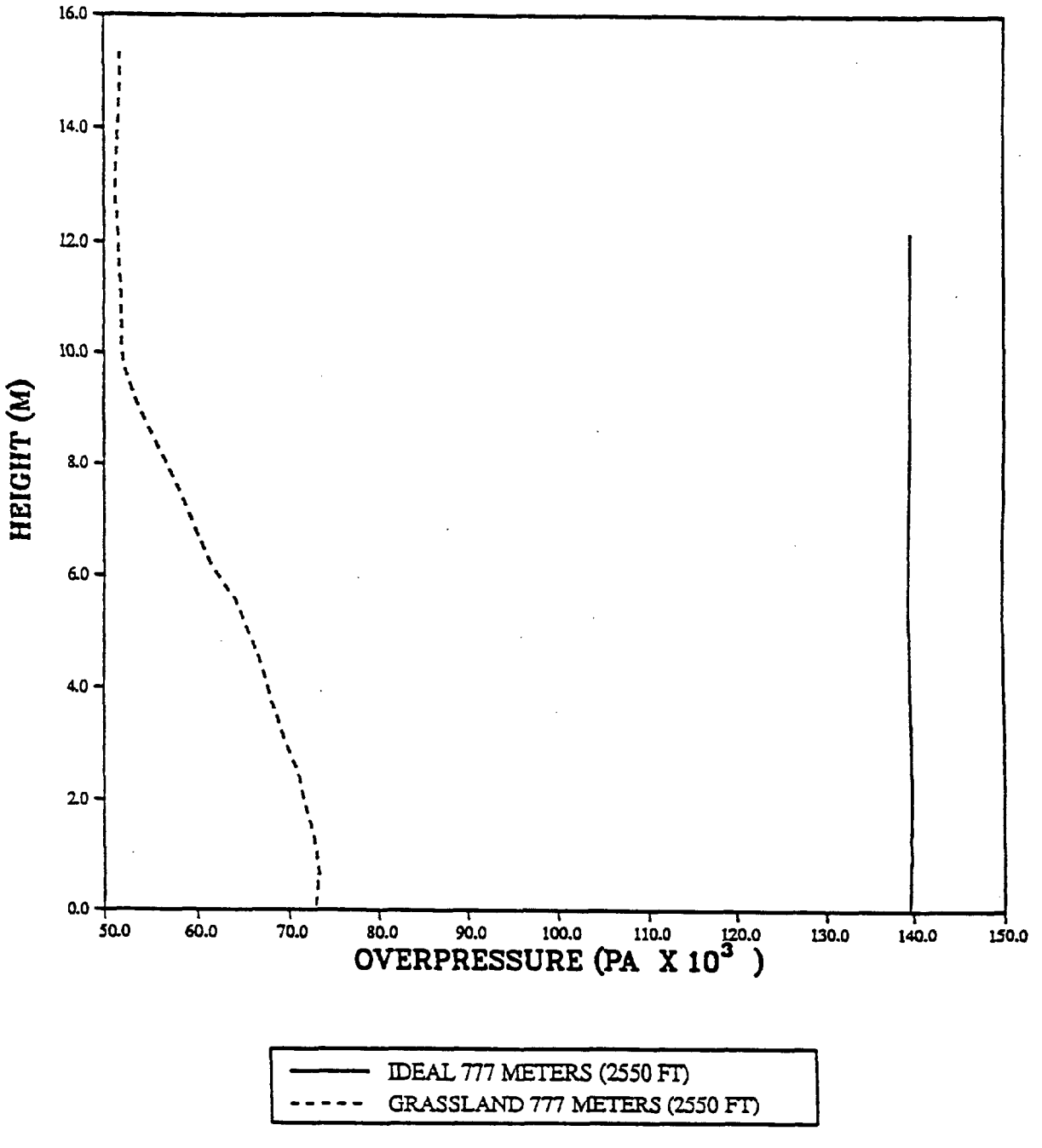

PRISCILLA
OVERPRESSURE AT 899 METERS (2950 FEET)
VERTICAL PROFILE (15 PSI OVERPRESSURE LEVEL)

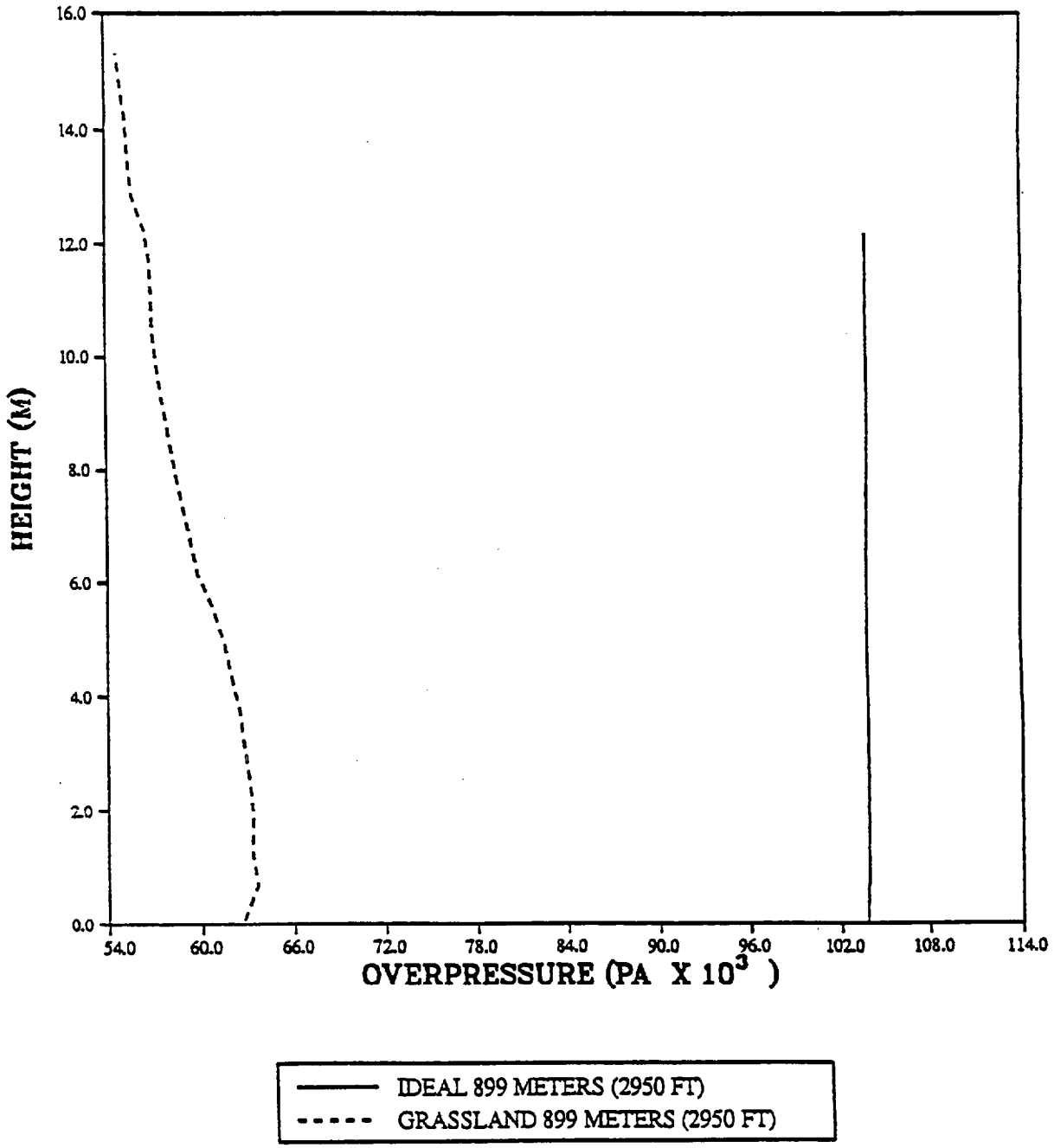

PRISCILLA
OVERPRESSURE AT 990 METERS (3250 FEET)
VERTICAL PROFILE (12 PSI OVERPRESSURE LEVEL)

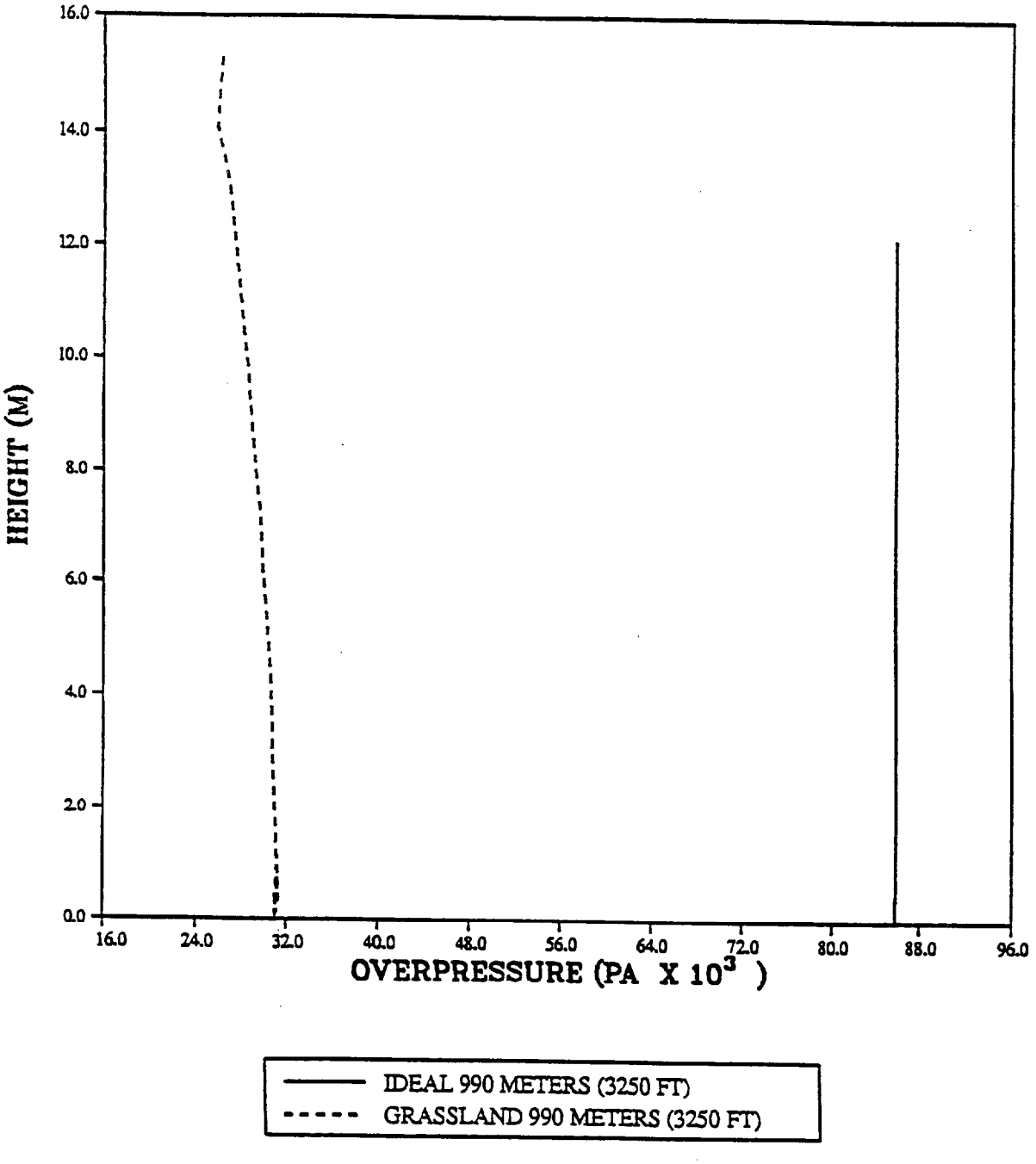

PRISCILLA
OVERPRESSURE AT 1113 METERS (3650 FEET)
VERTICAL PROFILE (10 PSI OVERPRESSURE LEVEL)

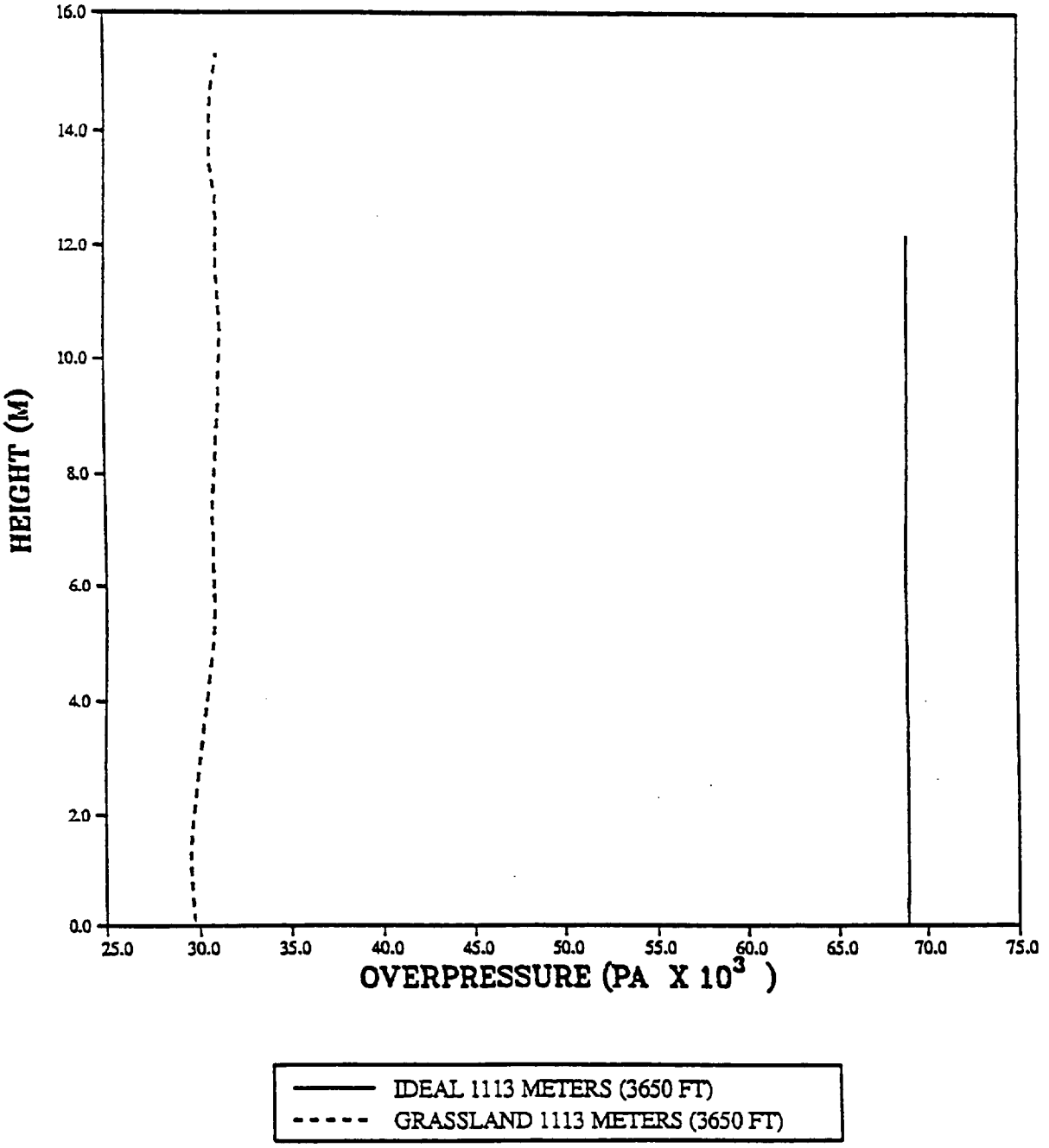

PRISCILLA
OVERPRESSURE AT 1250 METERS (4100 FEET)
VERTICAL PROFILE (8 PSI OVERPRESSURE LEVEL)

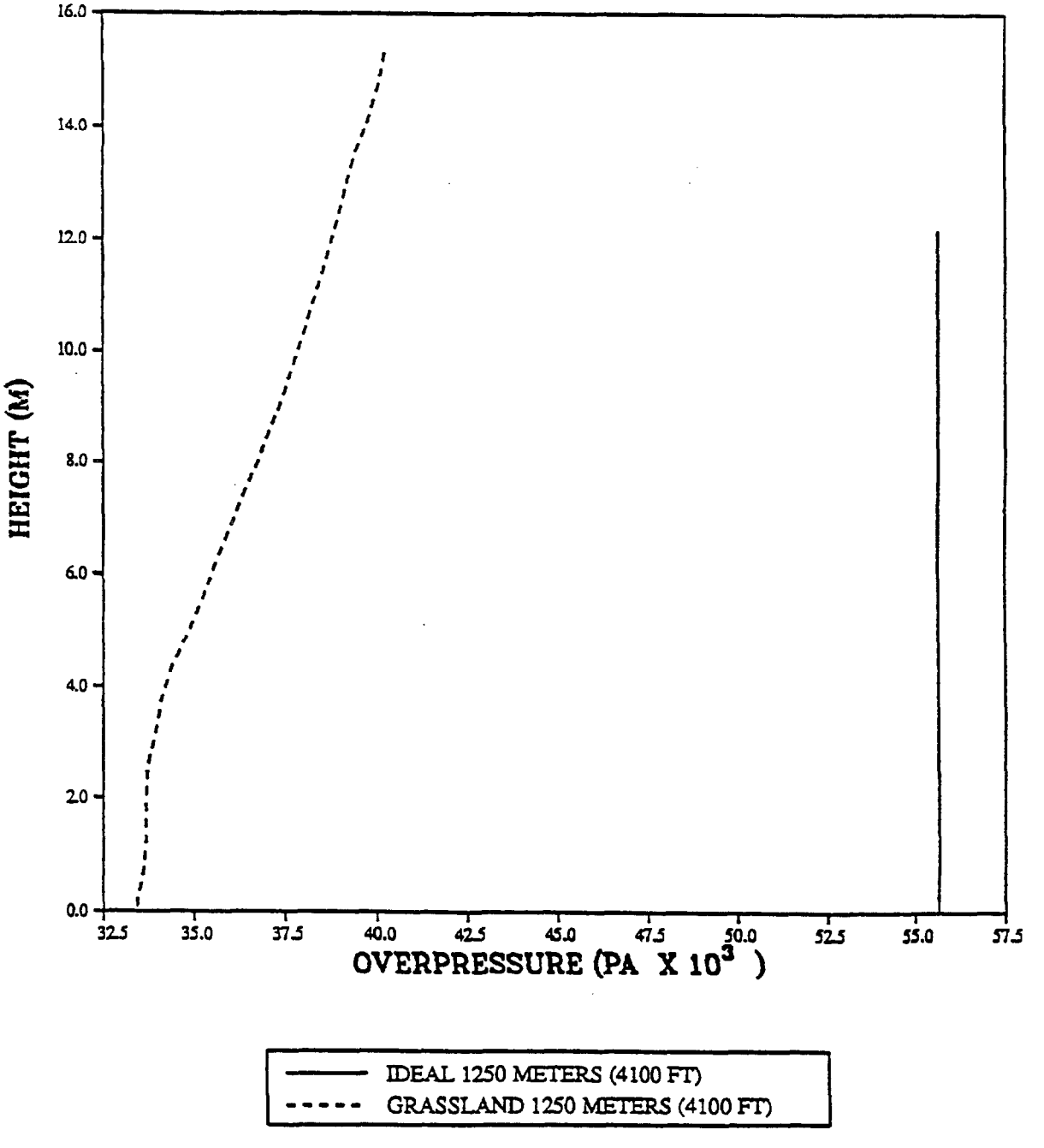

PRISCILLA
OVERPRESSURE AT 1494 METERS (4900 FEET)
VERTICAL PROFILE (6 PSI OVERPRESSURE LEVEL)

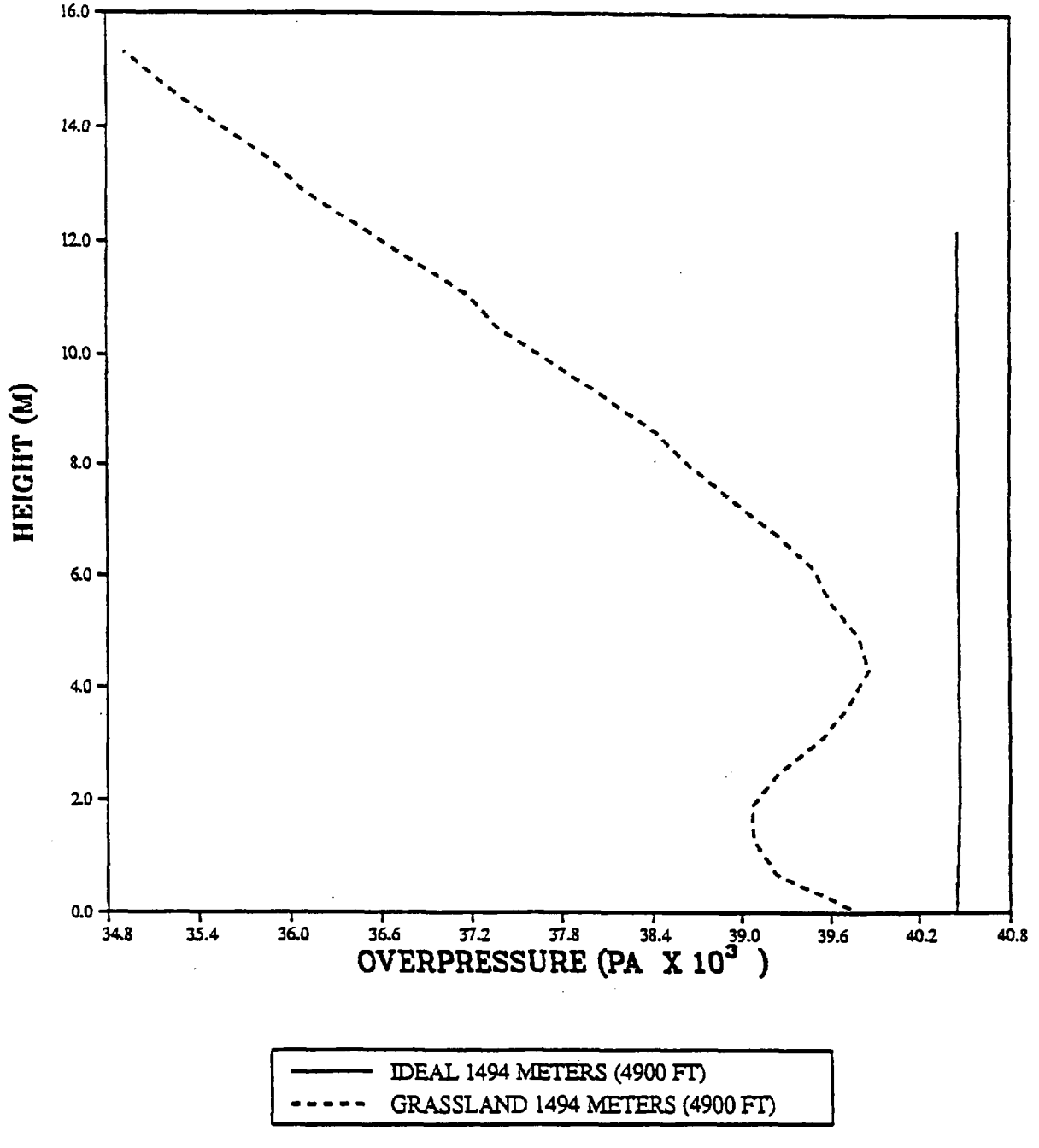

PRISCILLA
OVERPRESSURE AT 1630 METERS (5350 FEET)
VERTICAL PROFILE (5 PSI OVERPRESSURE LEVEL)

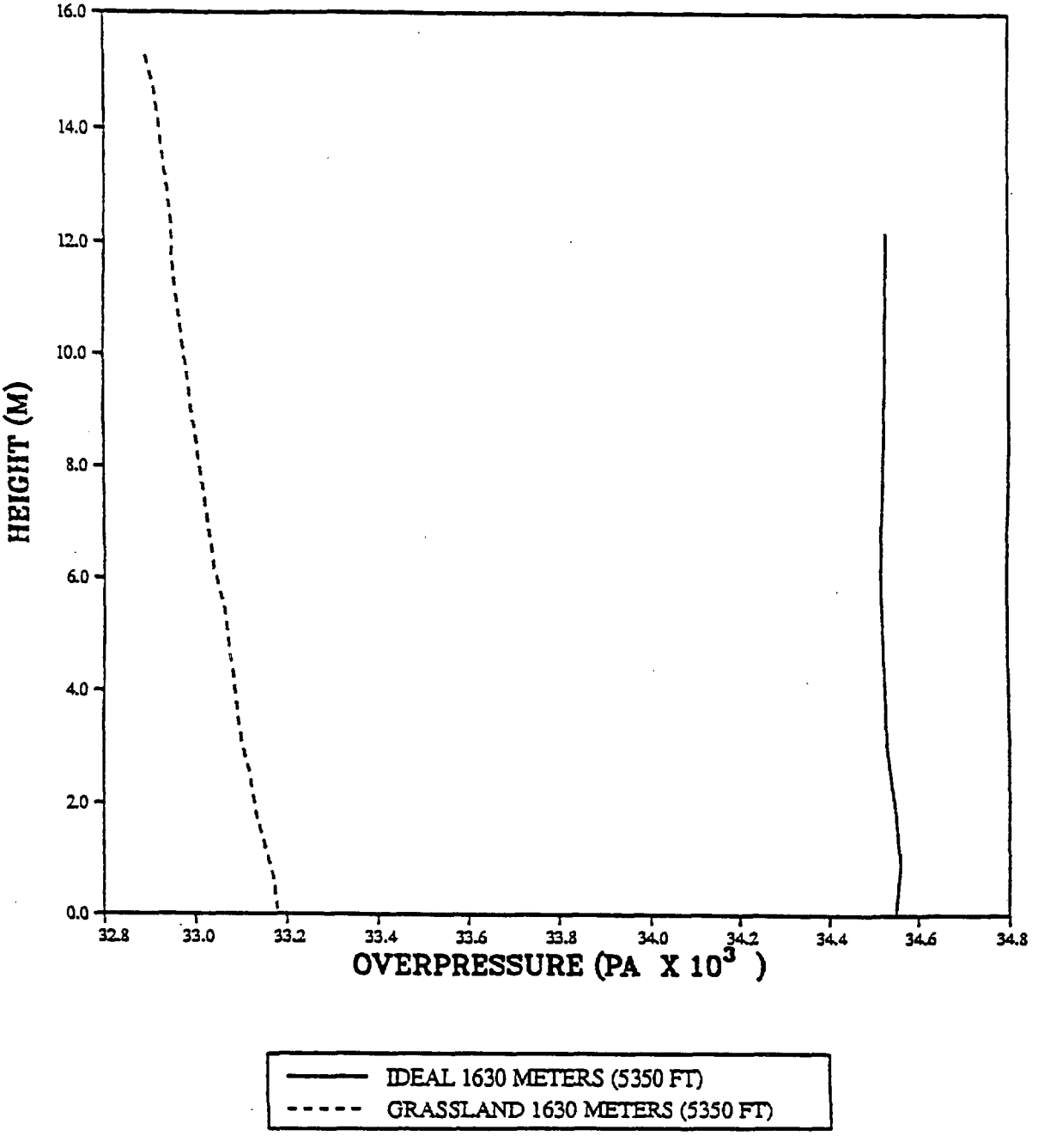

PRISCILLA
OVERPRESSURE IMPULSE AT 640 METERS (2100 FEET)
VERTICAL PROFILE (30 PSI OVERPRESSURE LEVEL)

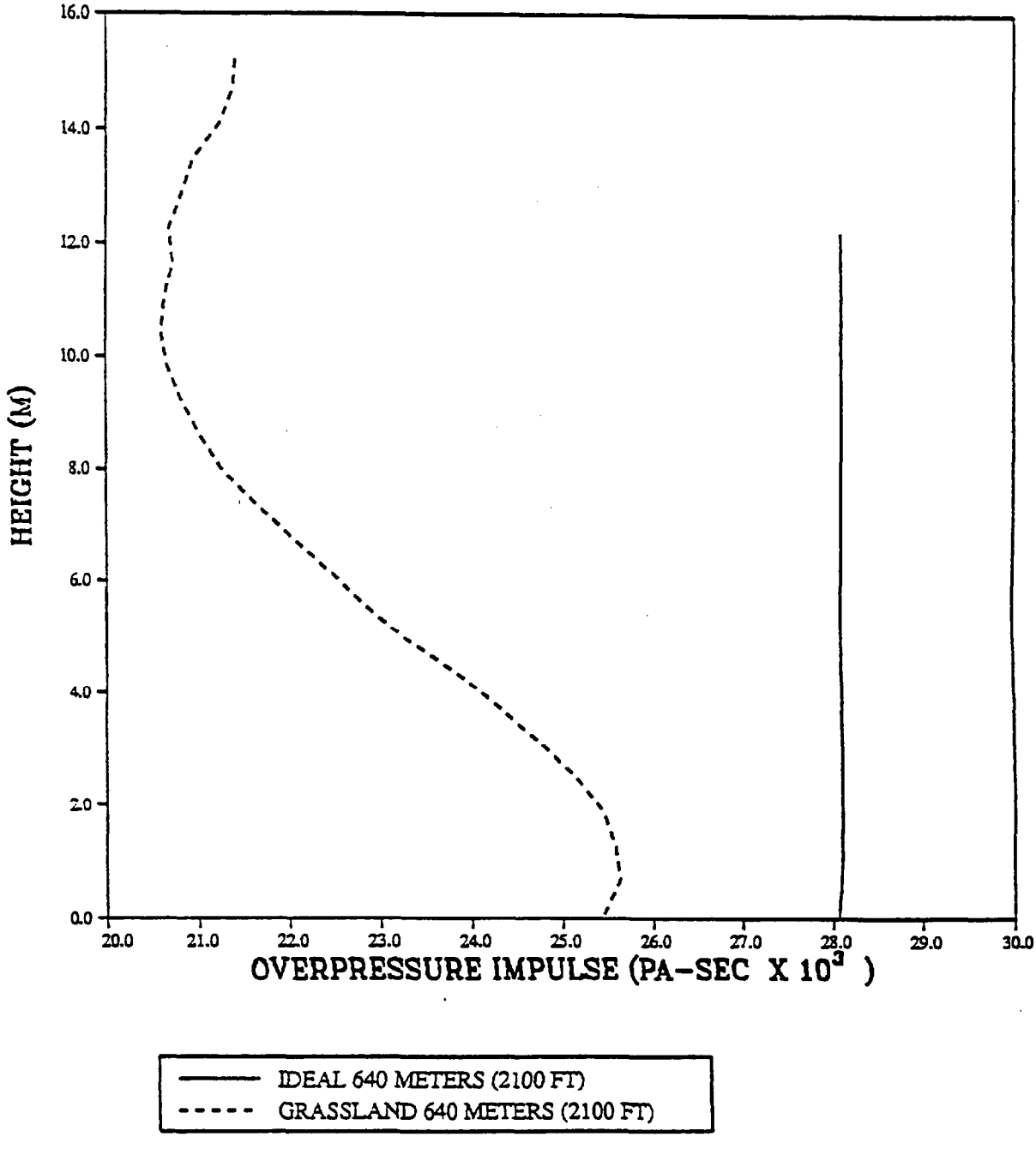

PRISCILLA
OVERPRESSURE IMPULSE AT 2300 FEET
VERTICAL PROFILE (25 PSI OVERPRESSURE LEVEL)

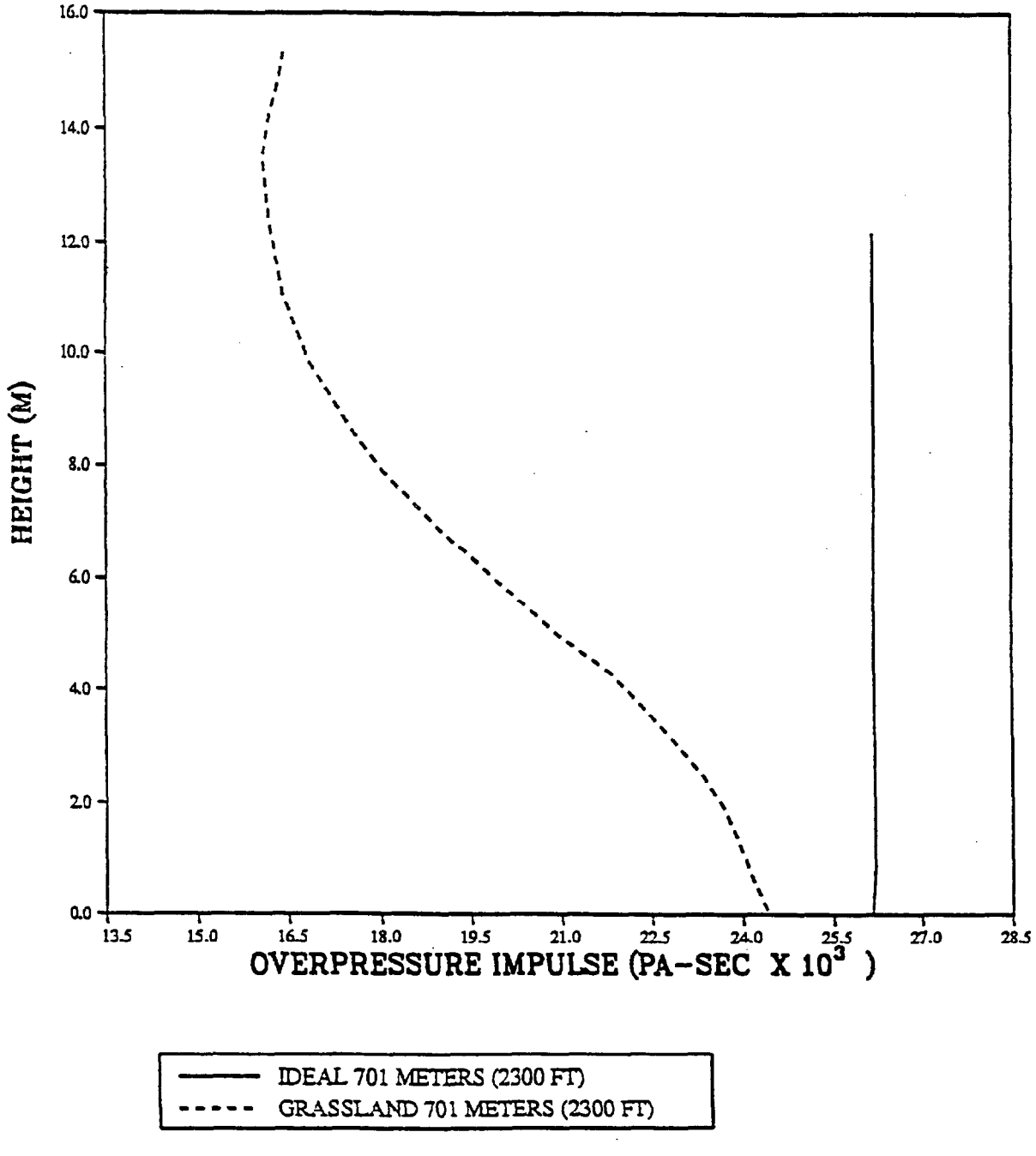

PRISCILLA
OVERPRESSURE IMPULSE AT 777 METERS (2550 FEET)
VERTICAL PROFILE (20 PSI OVERPRESSURE LEVEL)

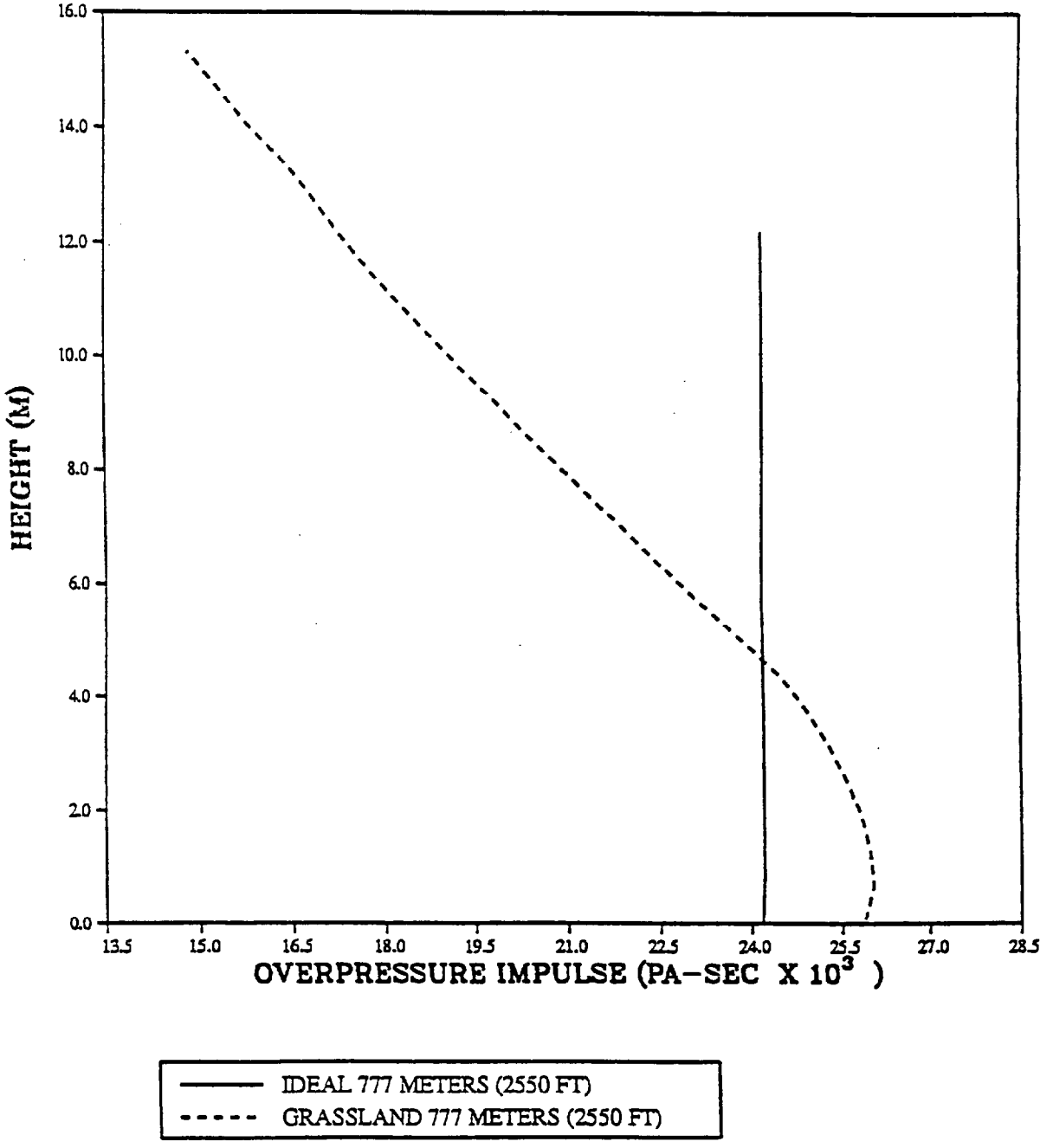

PRISCILLA
OVERPRESSURE IMPULSE AT 899 METERS (2950 FEET)
VERTICAL PROFILE (15 PSI OVERPRESSURE LEVEL)

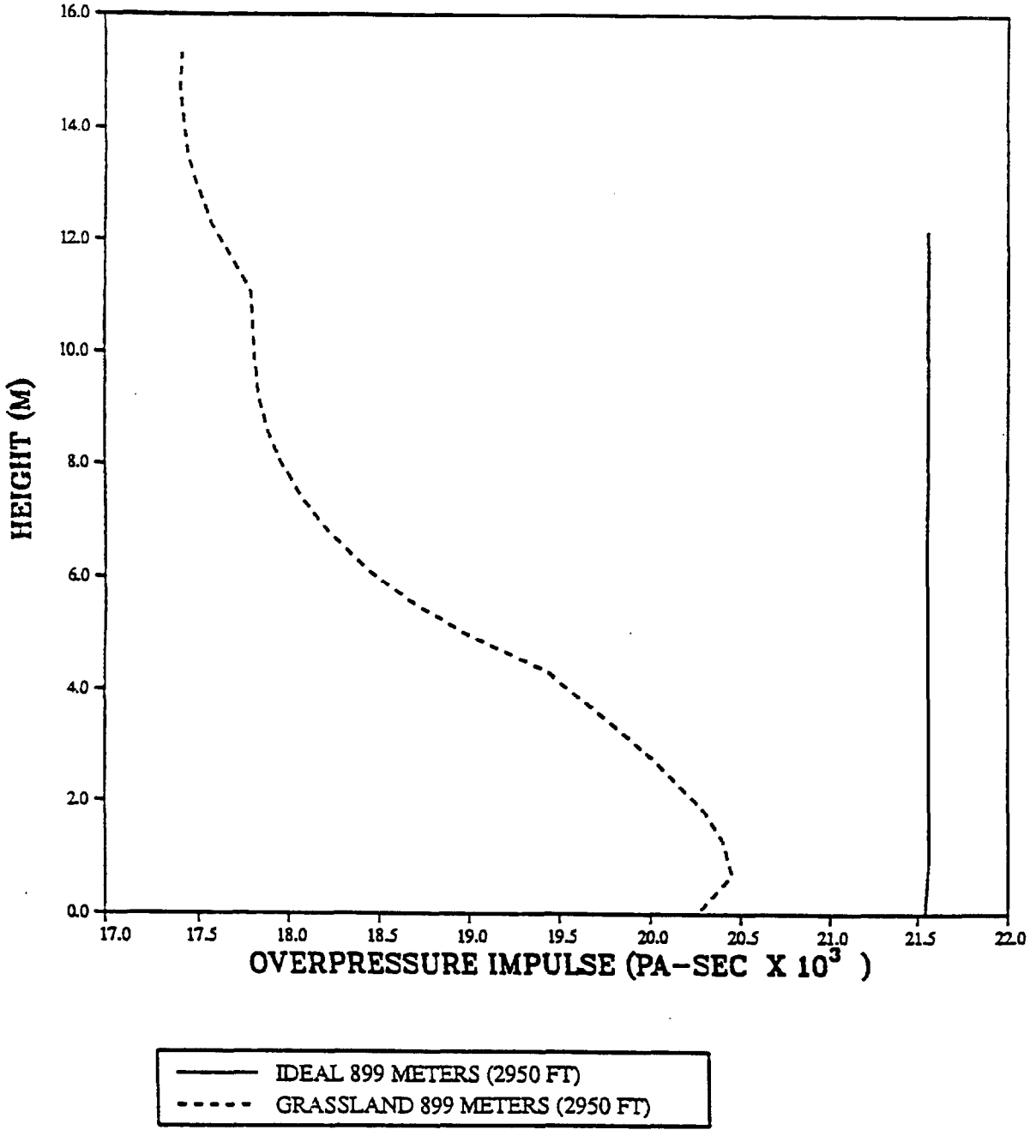

PRISCILLA
OVERPRESSURE IMPULSE AT 990 METERS (3250 FEET)
VERTICAL PROFILE (12 PSI OVERPRESSURE LEVEL)

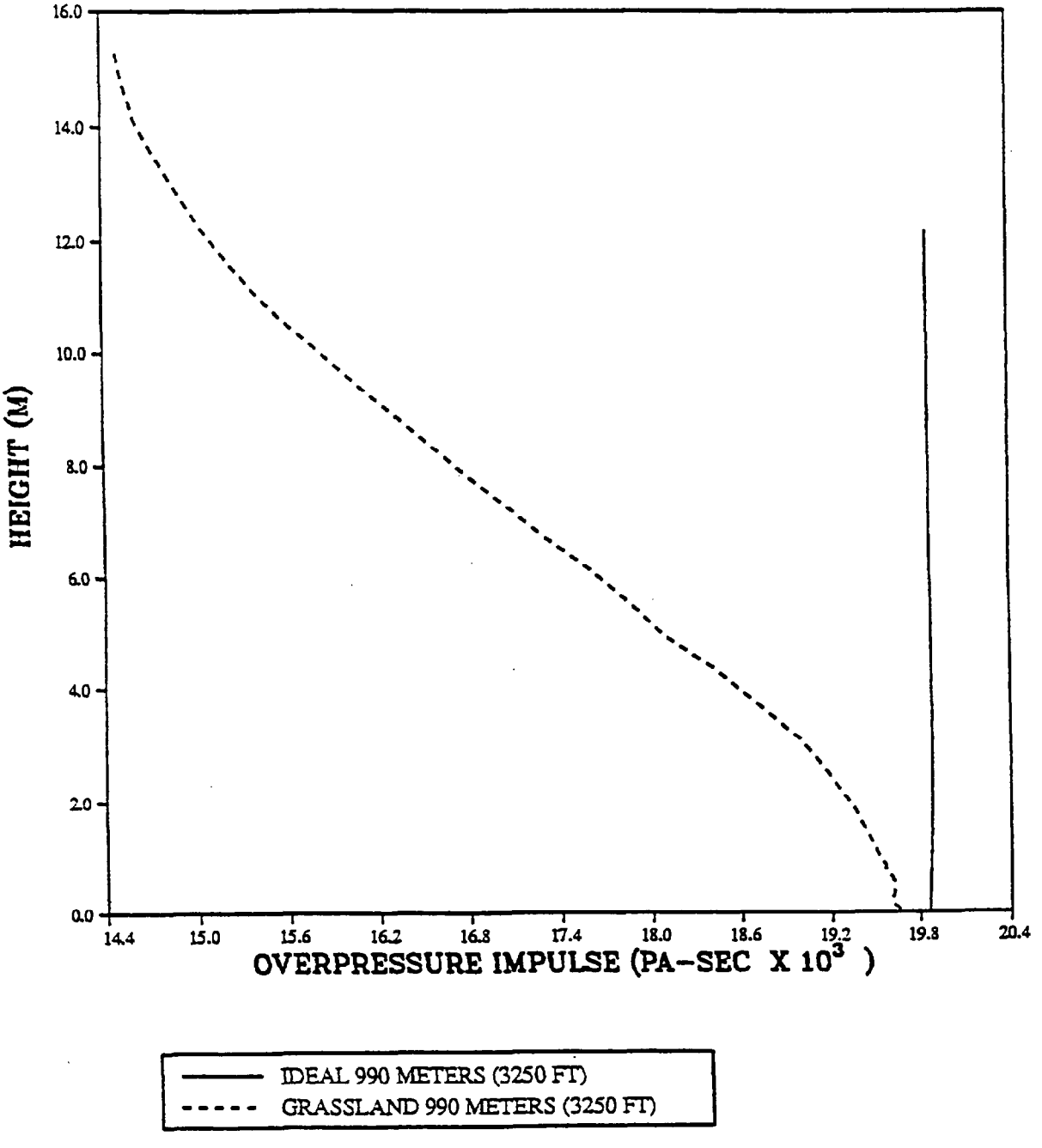

PRISCILLA
OVERPRESSURE IMPULSE AT 1113 (3650 FEET)
VERTICAL PROFILE (10 PSI OVERPRESSURE LEVEL).

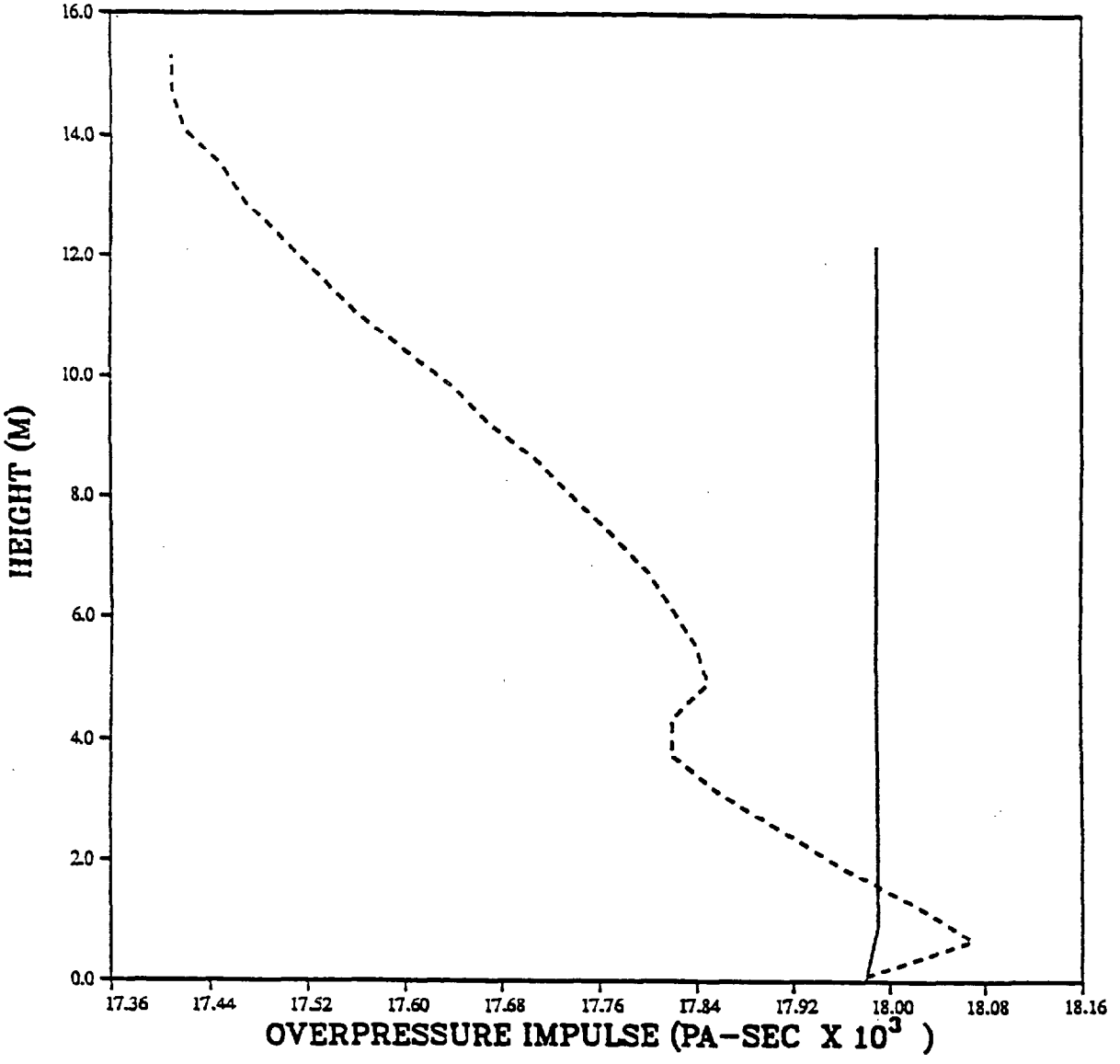

PRISCILLA
OVERPRESSURE IMPULSE AT 1250 METERS (4100 FEET)
VERTICAL PROFILE (8 PSI OVERPRESSURE LEVEL)

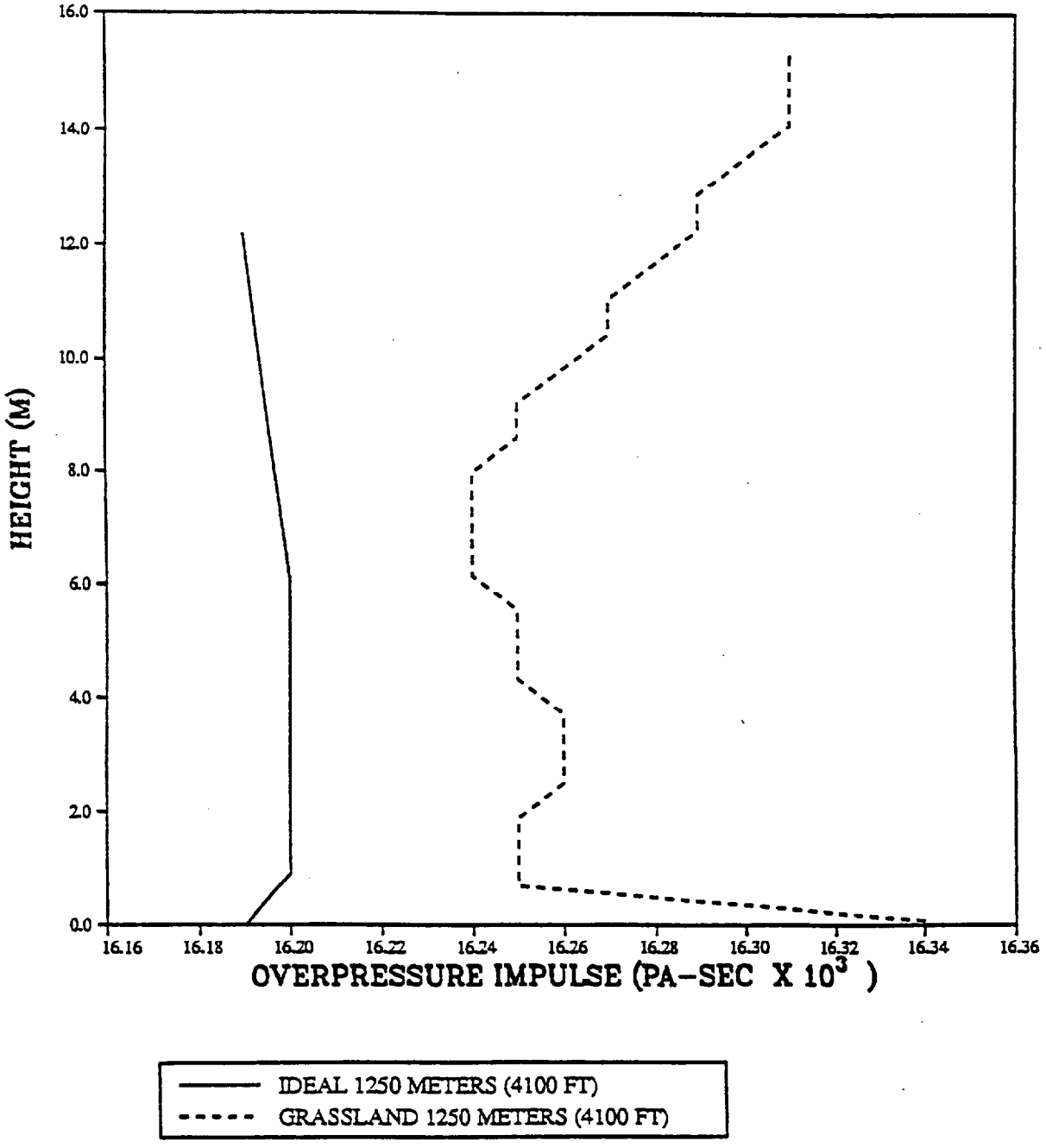

PRISCILLA
OVERPRESSURE IMPULSE AT 1494 METERS (4900 FEET)
VERTICAL PROFILE (6 PSI OVERPRESSURE LEVEL)

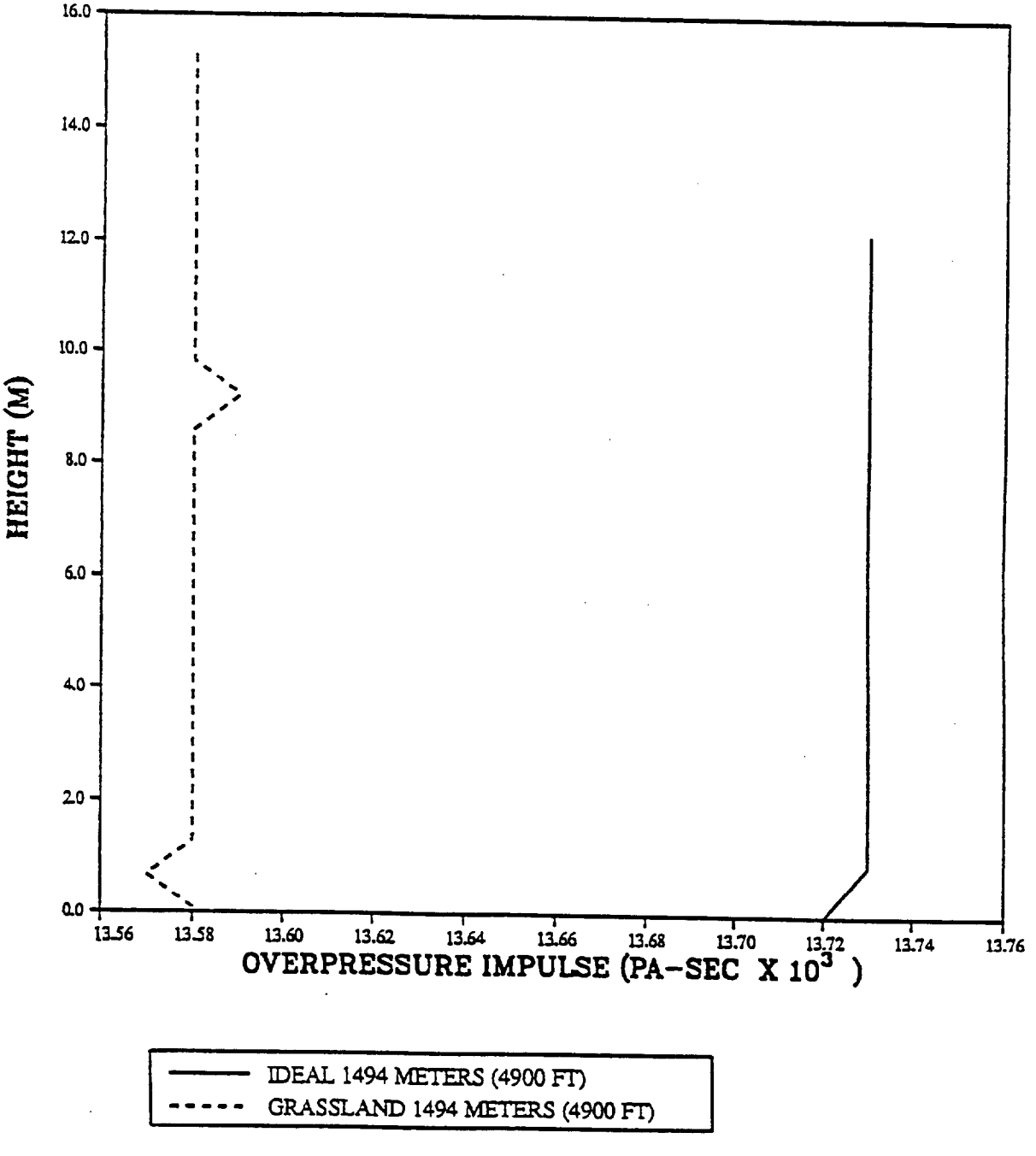

PRISCILLA
OVERPRESSURE IMPULSE AT 1630 METERS (5350 FEET)
VERTICAL PROFILE (5 PSI OVERPRESSURE LEVEL)

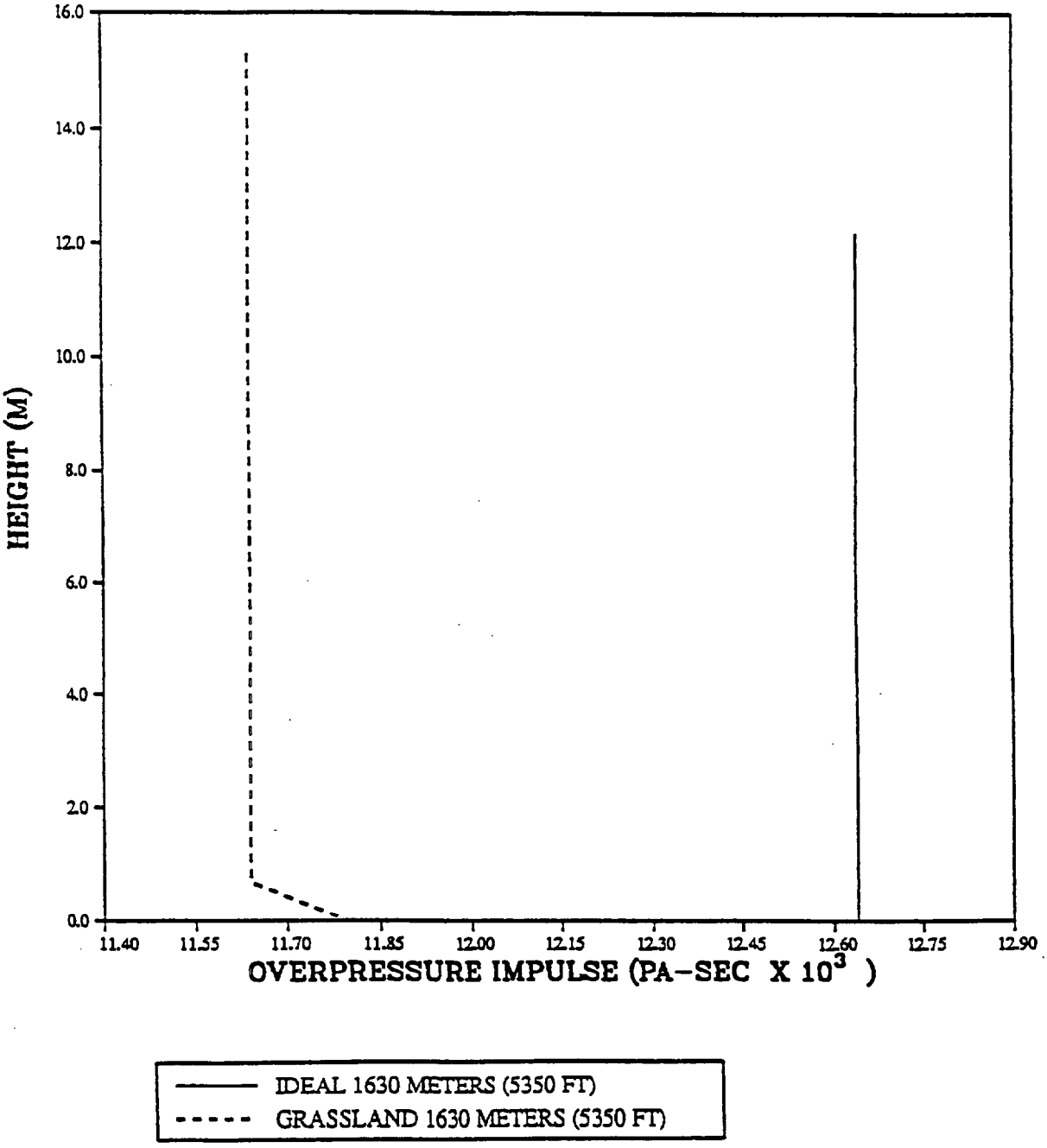

PRISCILLA
HORIZONTAL DYNAMIC PRESSURE PEAKS
VERTICAL PROFILE (30 PSI OVERPRESSURE LEVEL)

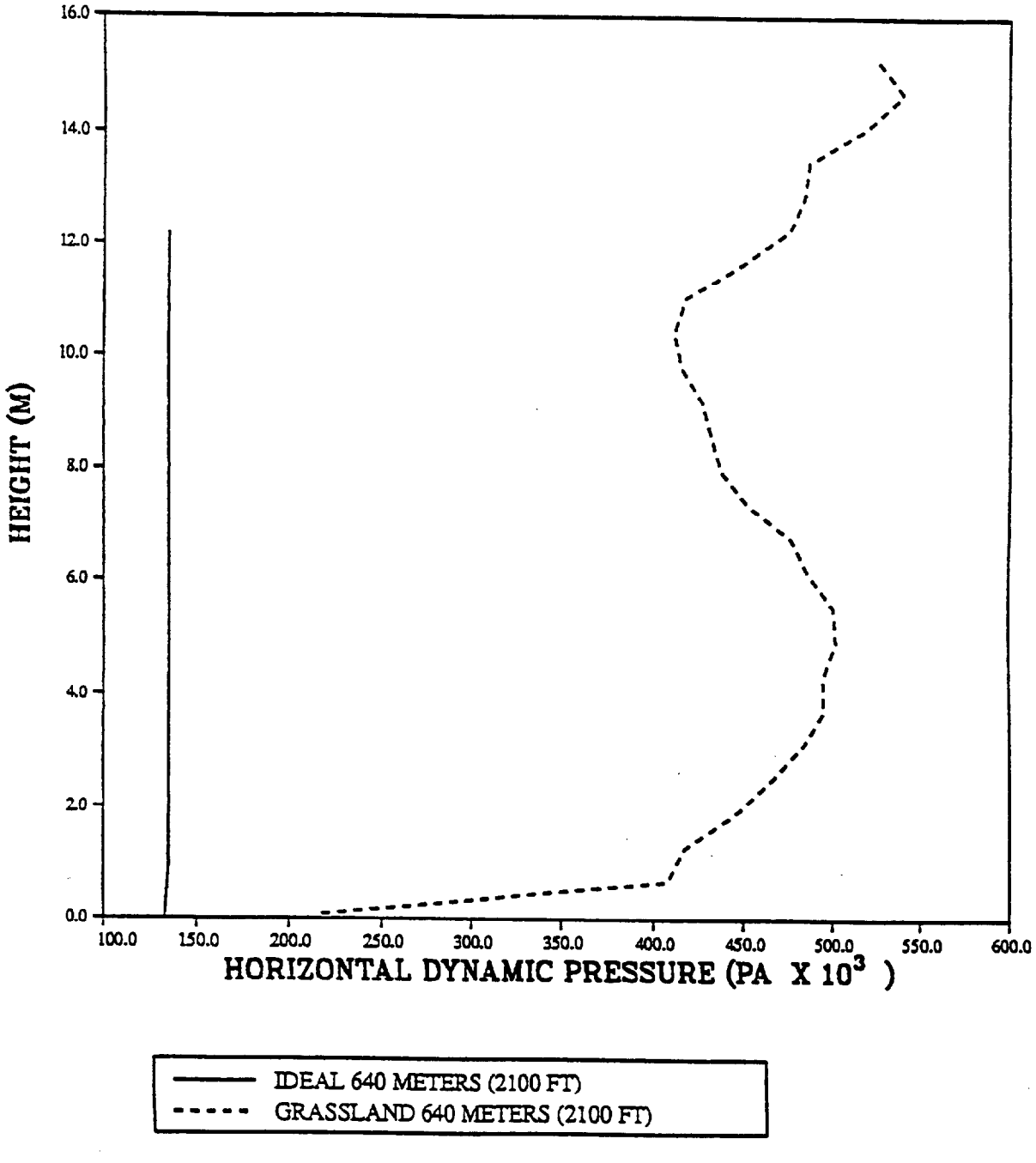

PRISCILLA
HORIZONTAL DYNAMIC PRESSURE PEAKS
VERTICAL PROFILE (25 PSI OVERPRESSURE LEVEL)

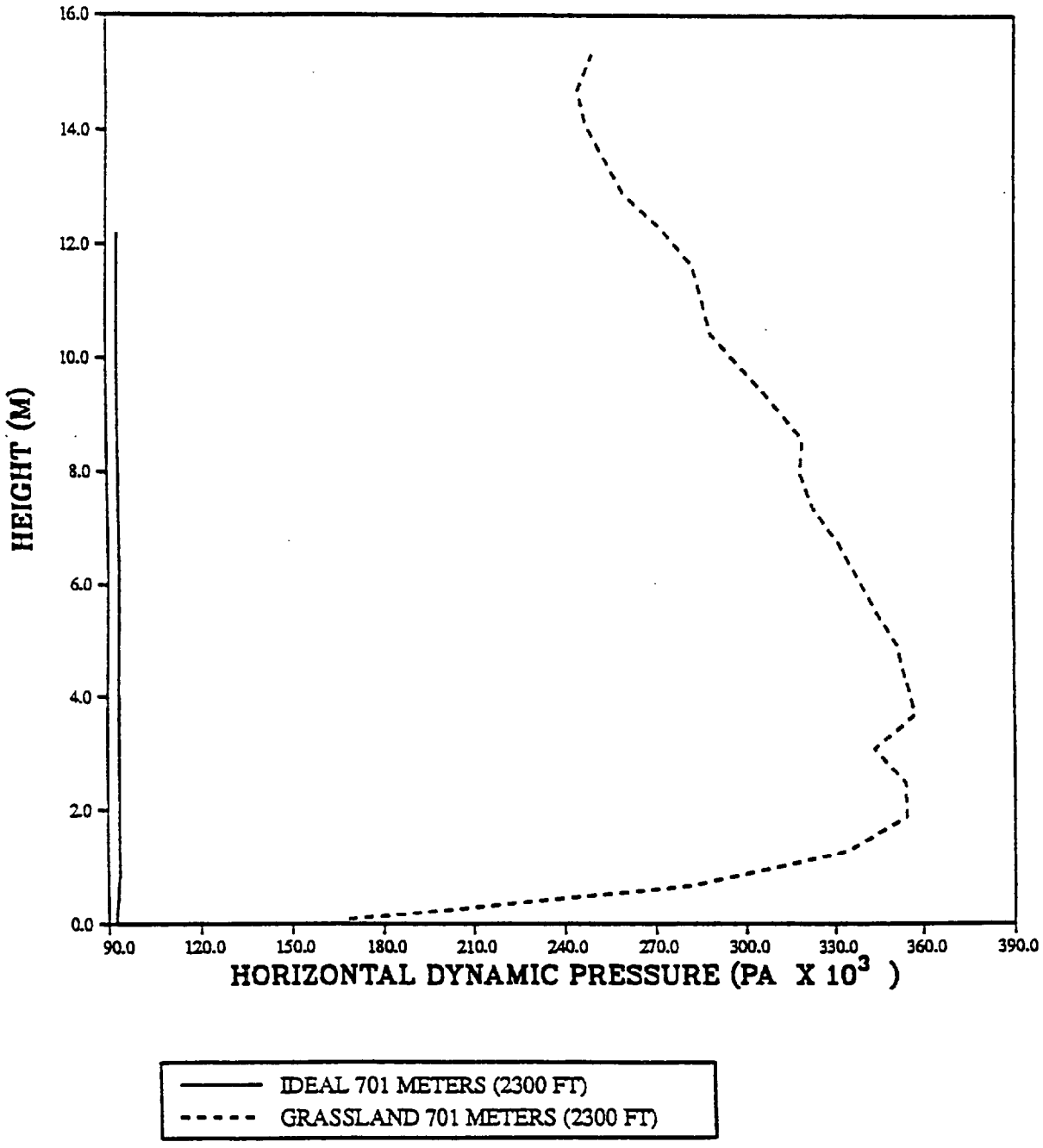

PRISCILLA
HORIZONTAL DYNAMIC PRESSURE PEAKS
VERTICAL PROFILE (20 PSI OVERPRESSURE LEVEL)

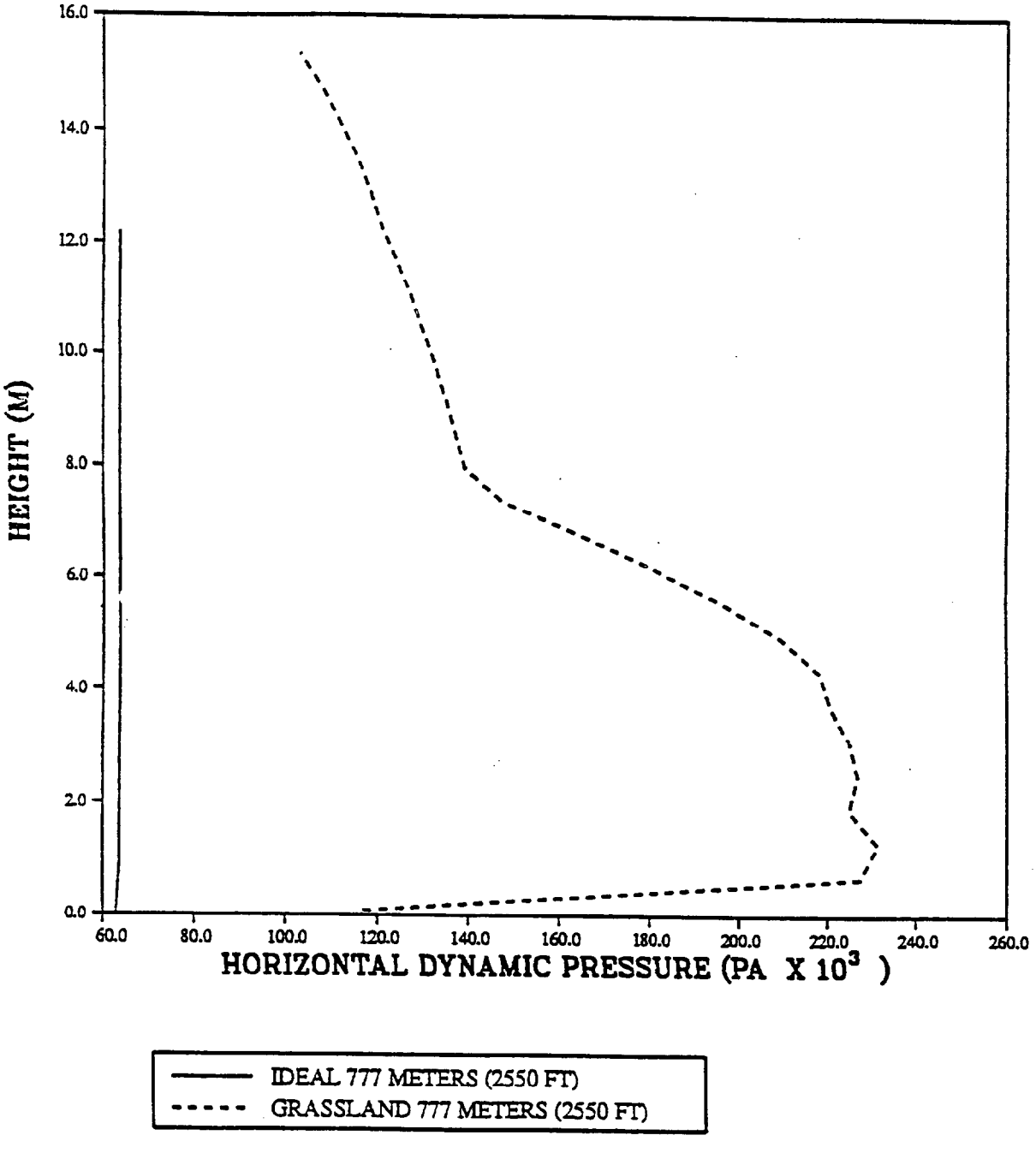

PRISCILLA
HORIZONTAL DYNAMIC PRESSURE PEAKS
VERTICAL PROFILE (15 PSI OVERPRESSURE LEVEL)

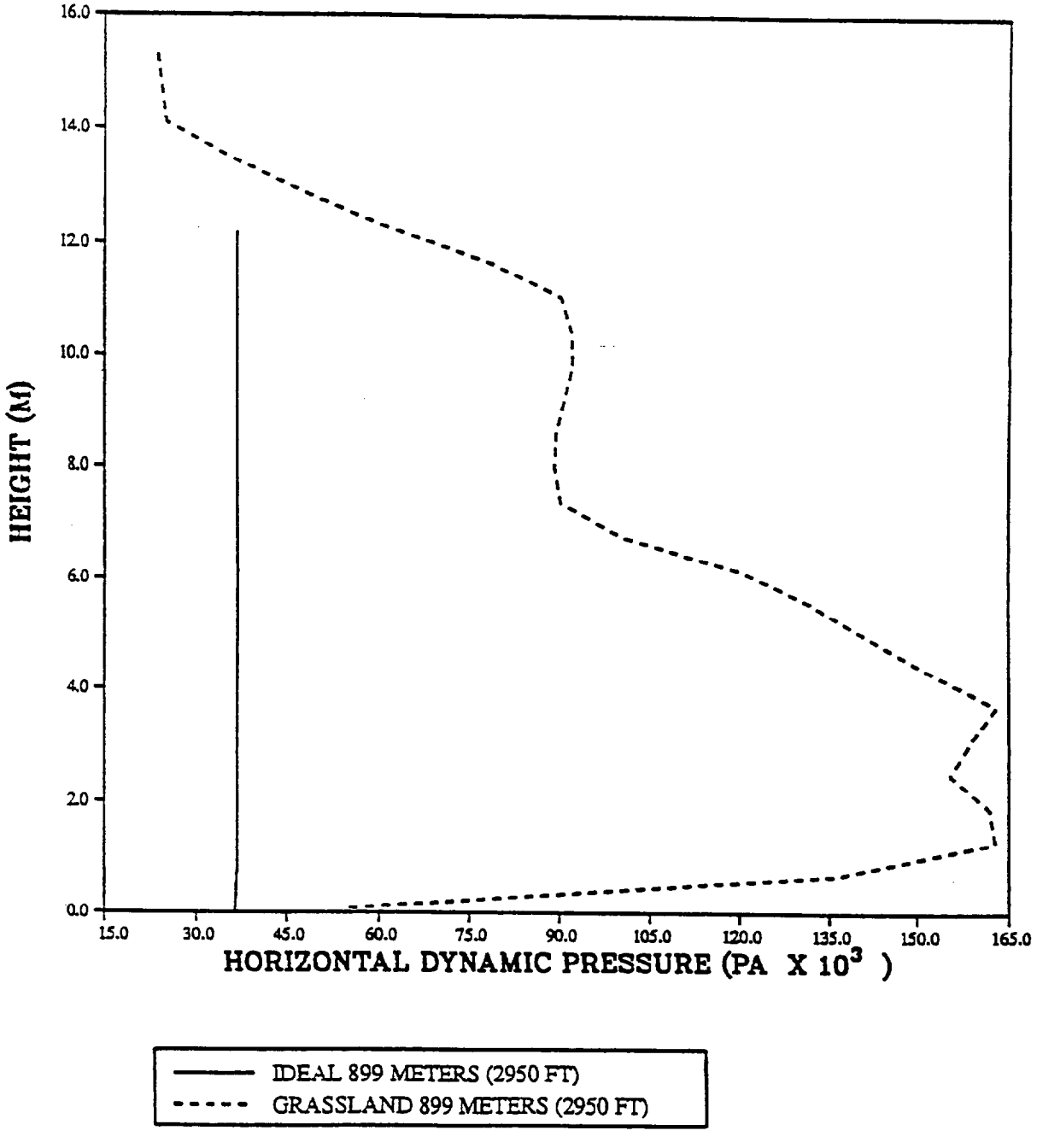

PRISCILLA
HORIZONTAL DYNAMIC PRESSURE PEAKS
VERTICAL PROFILE (12 PSI OVERPRESSURE LEVEL)

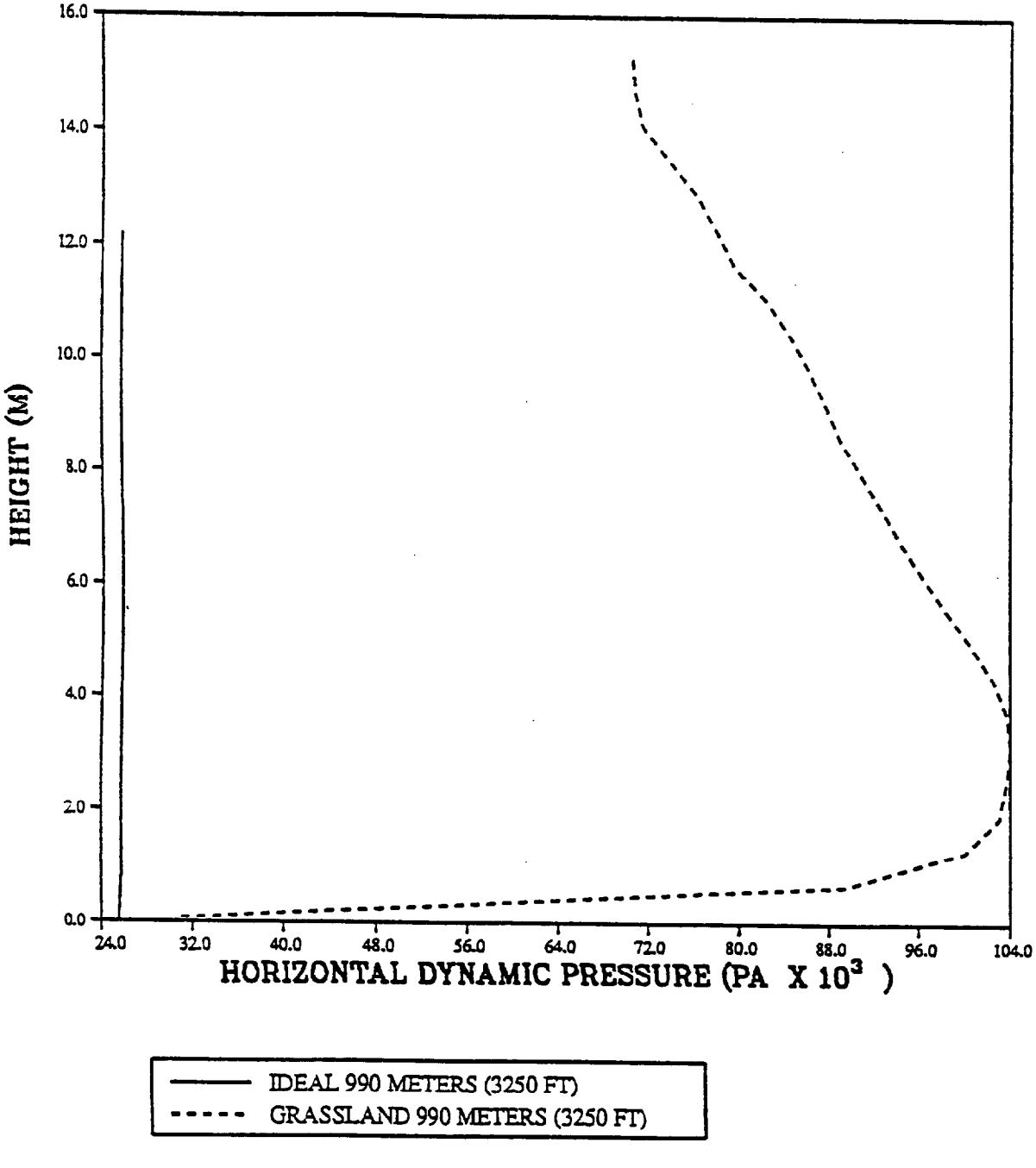

PRISCILLA
HORIZONTAL DYNAMIC PRESSURE PEAKS
VERTICAL PROFILE (10 PSI OVERPRESSURE LEVEL)

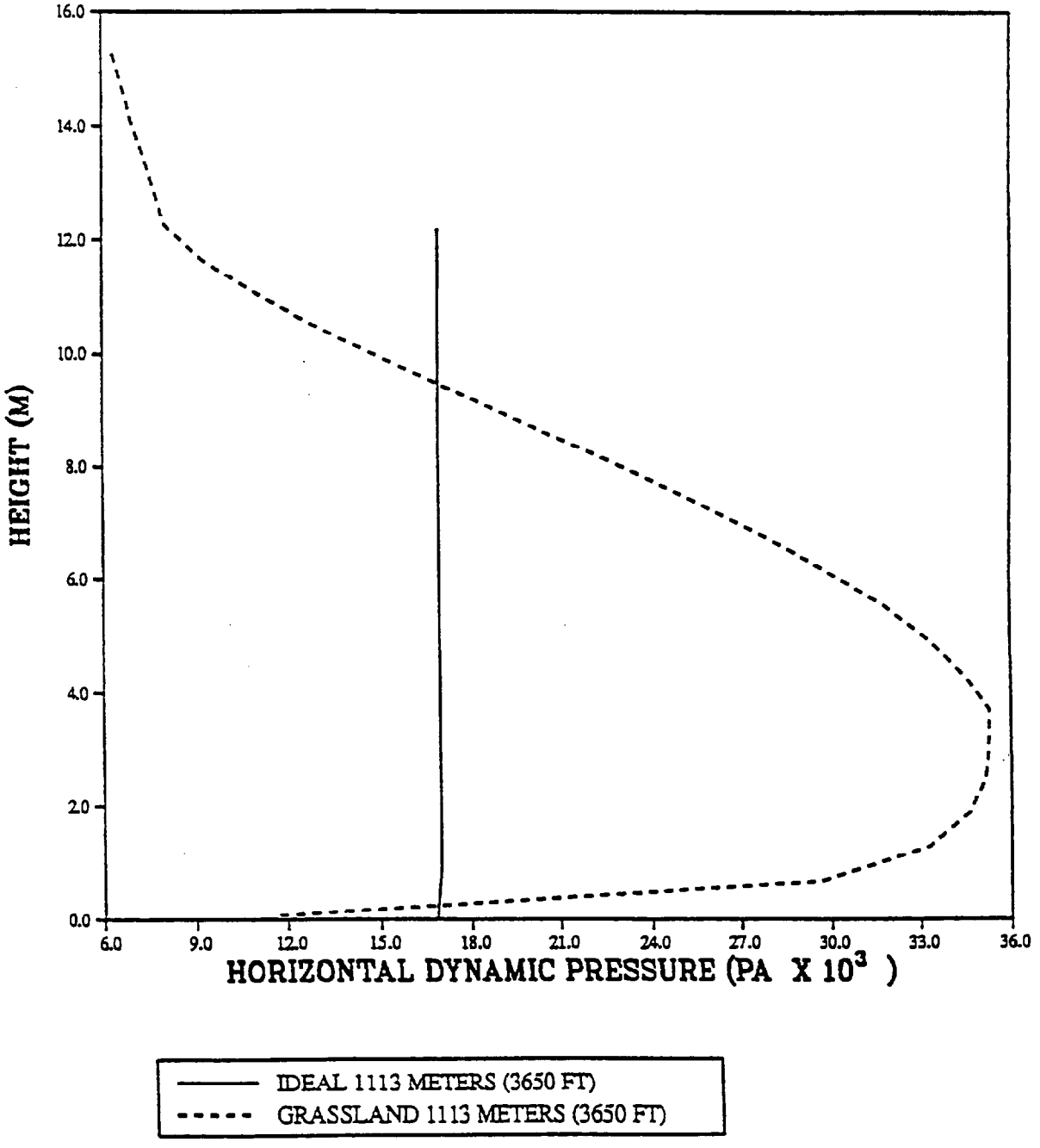

PRISCILLA
HORIZONTAL DYNAMIC PRESSURE PEAKS
VERTICAL PROFILE (8 PSI OVERPRESSURE LEVEL)

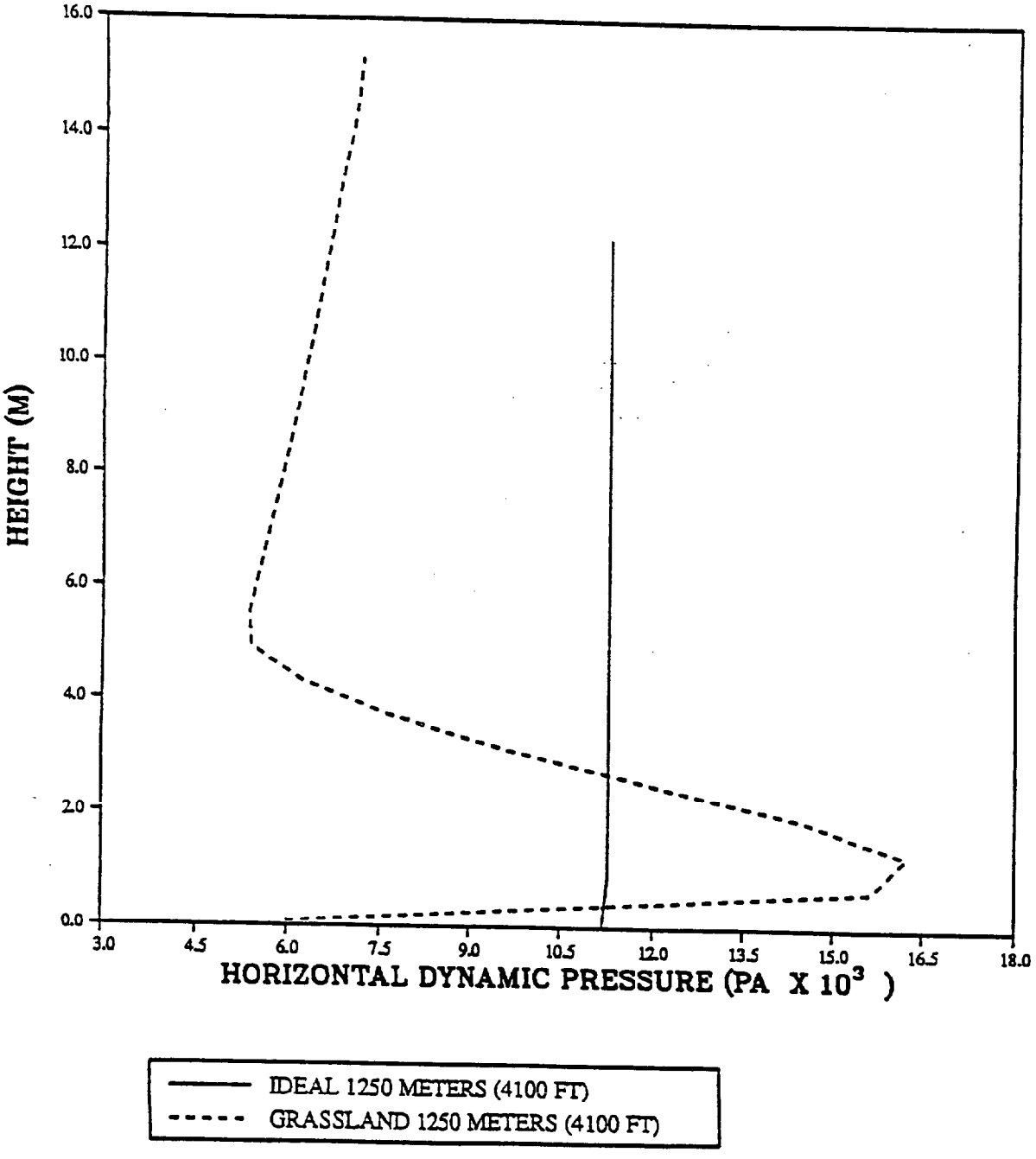

PRISCILLA
HORIZONTAL DYNAMIC PRESSURE PEAKS
VERTICAL PROFILE (6 PSI OVERPRESSURE LEVEL)

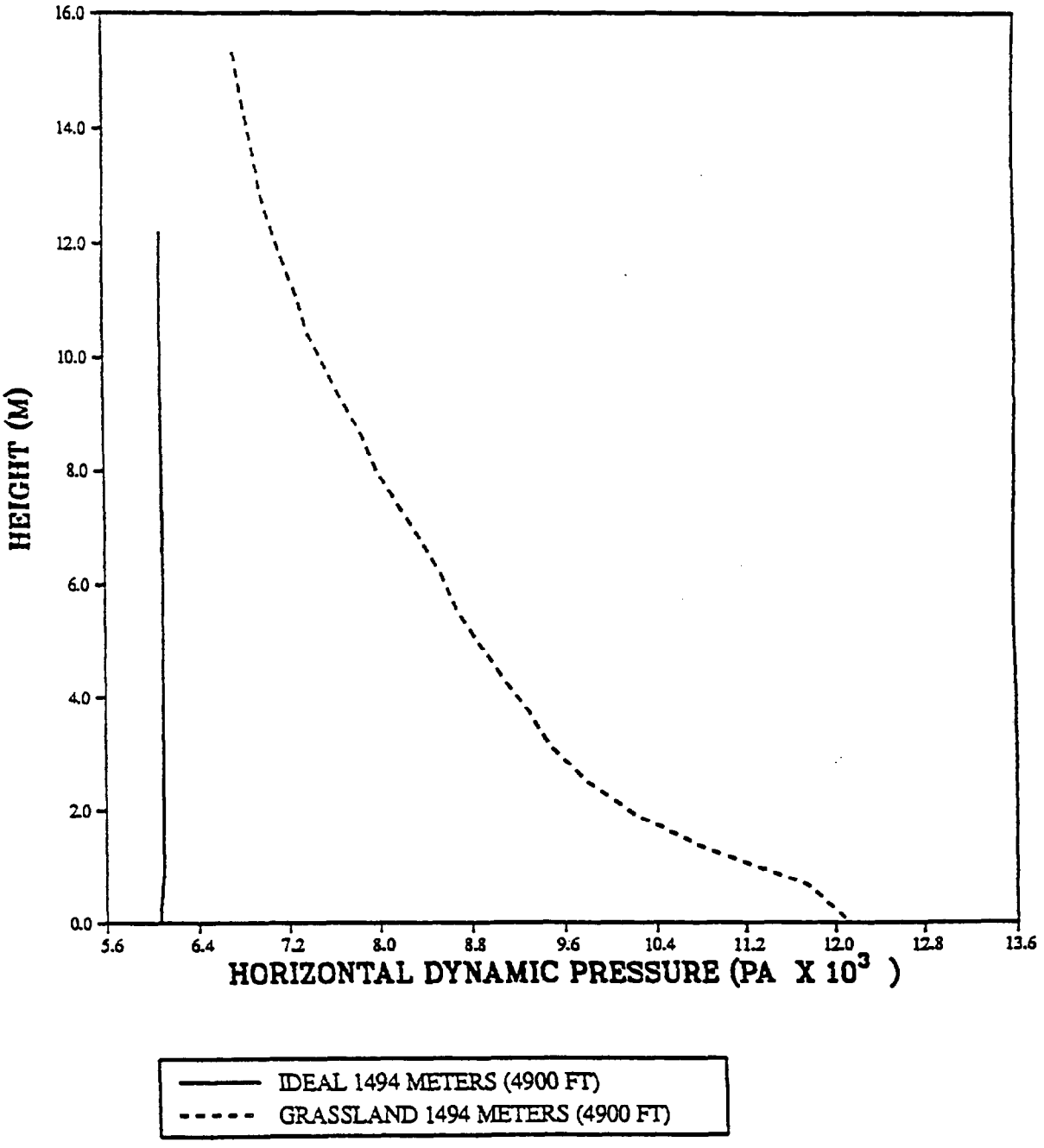

PRISCILLA
HORIZONTAL DYNAMIC PRESSURE PEAKS
VERTICAL PROFILE (5 PSI OVERPRESSURE LEVEL)

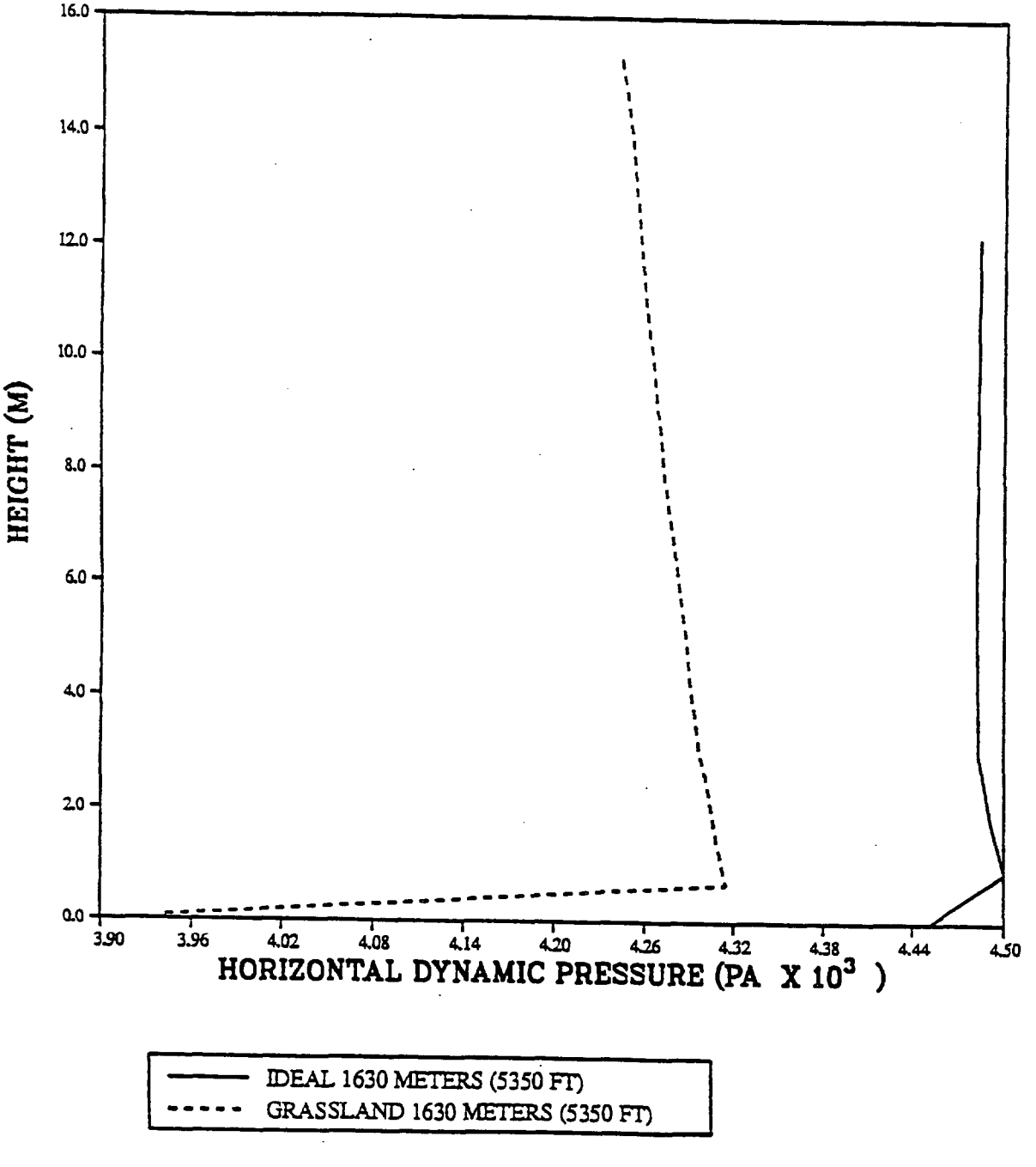

PRISCILLA
HORIZONTAL DYNAMIC PRESSURE IMPULSE
VERTICAL PROFILE (30 PSI OVERPRESSURE LEVEL).

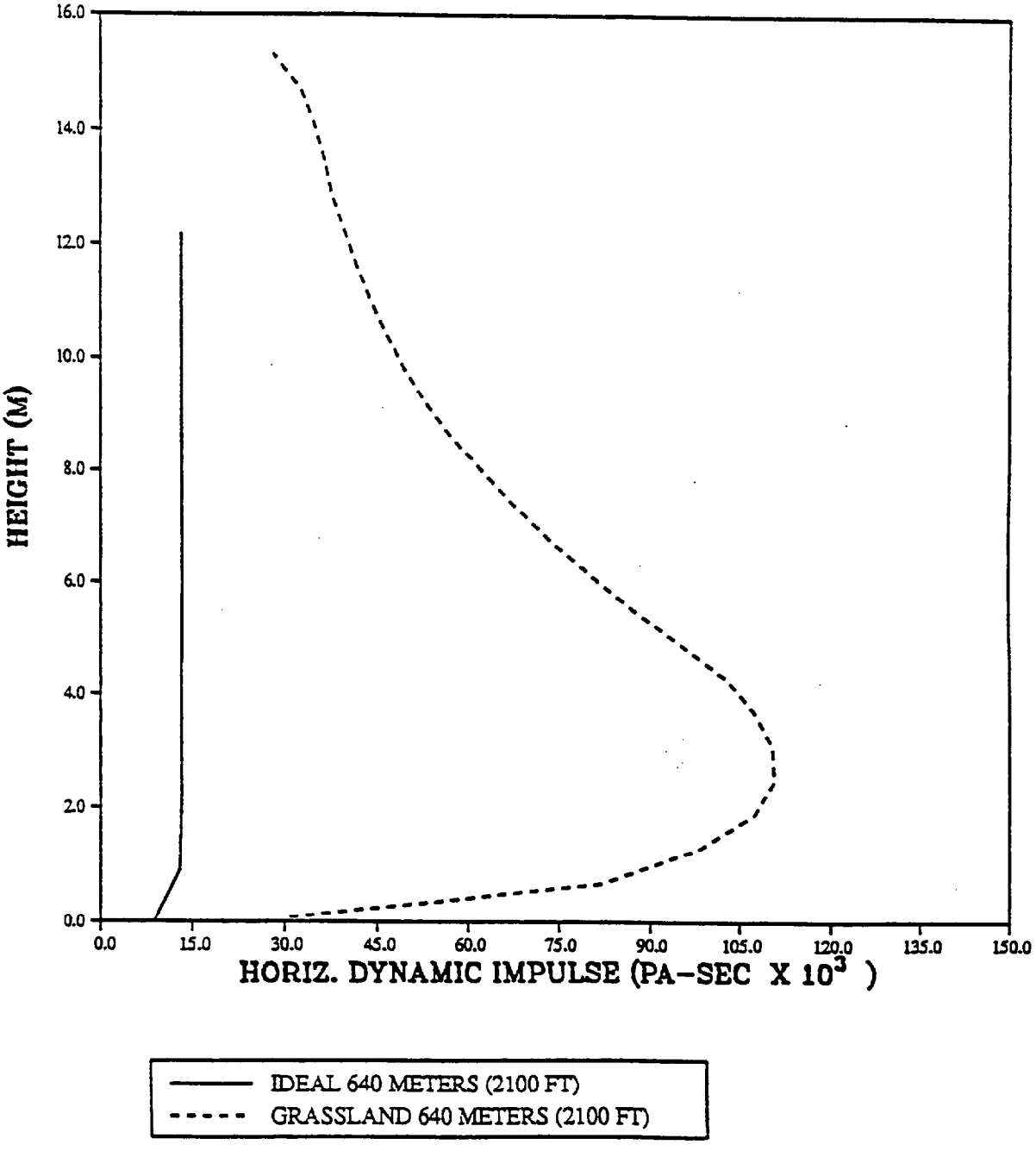

PRISCILLA
HORIZONTAL DYNAMIC PRESSURE IMPULSE
VERTICAL PROFILE (25 PSI OVERPRESSURE LEVEL).

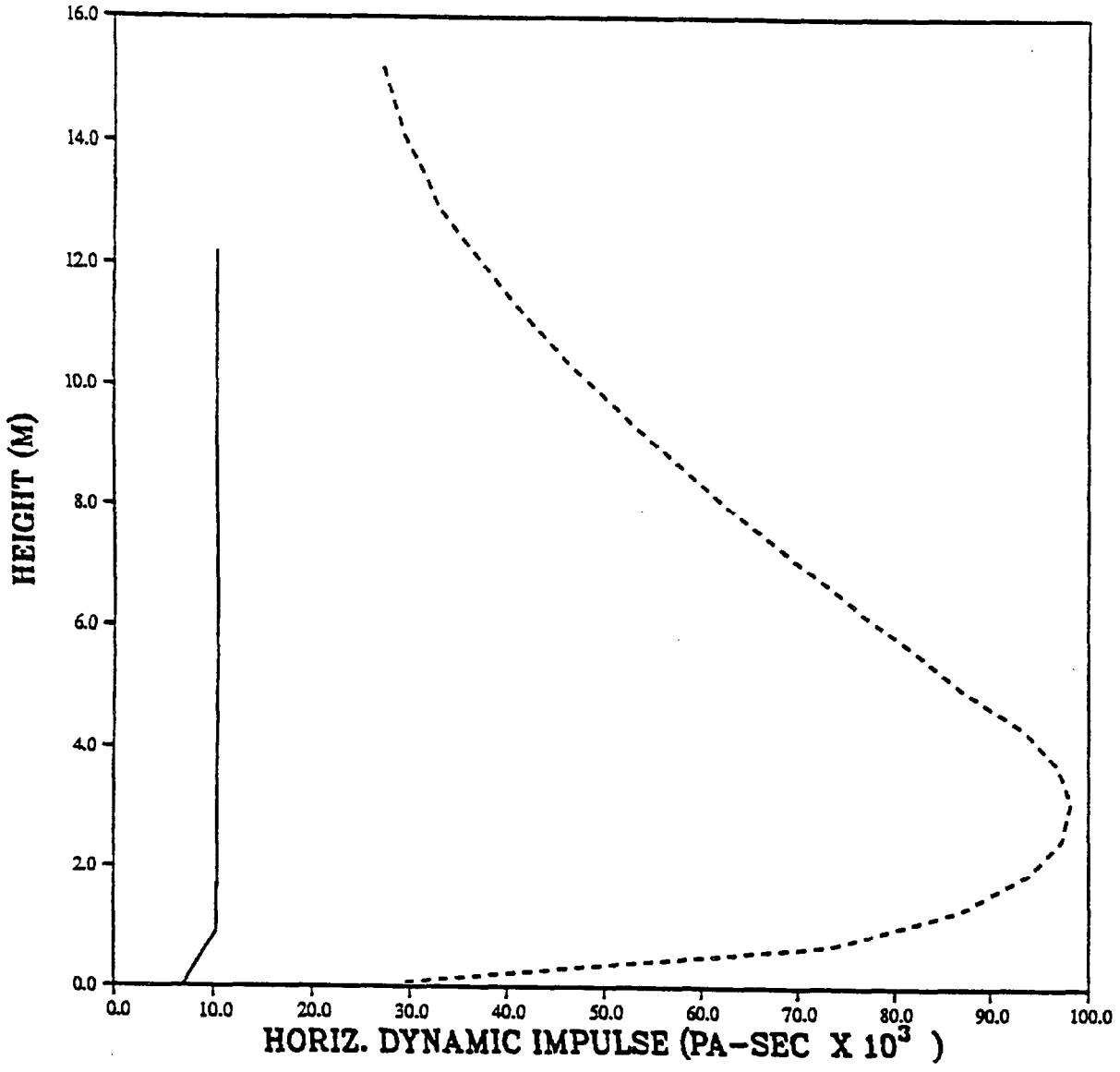

PRISCILLA
HORIZONTAL DYNAMIC PRESSURE IMPULSE
VERTICAL PROFILE (20 PSI OVERPRESSURE LEVEL).

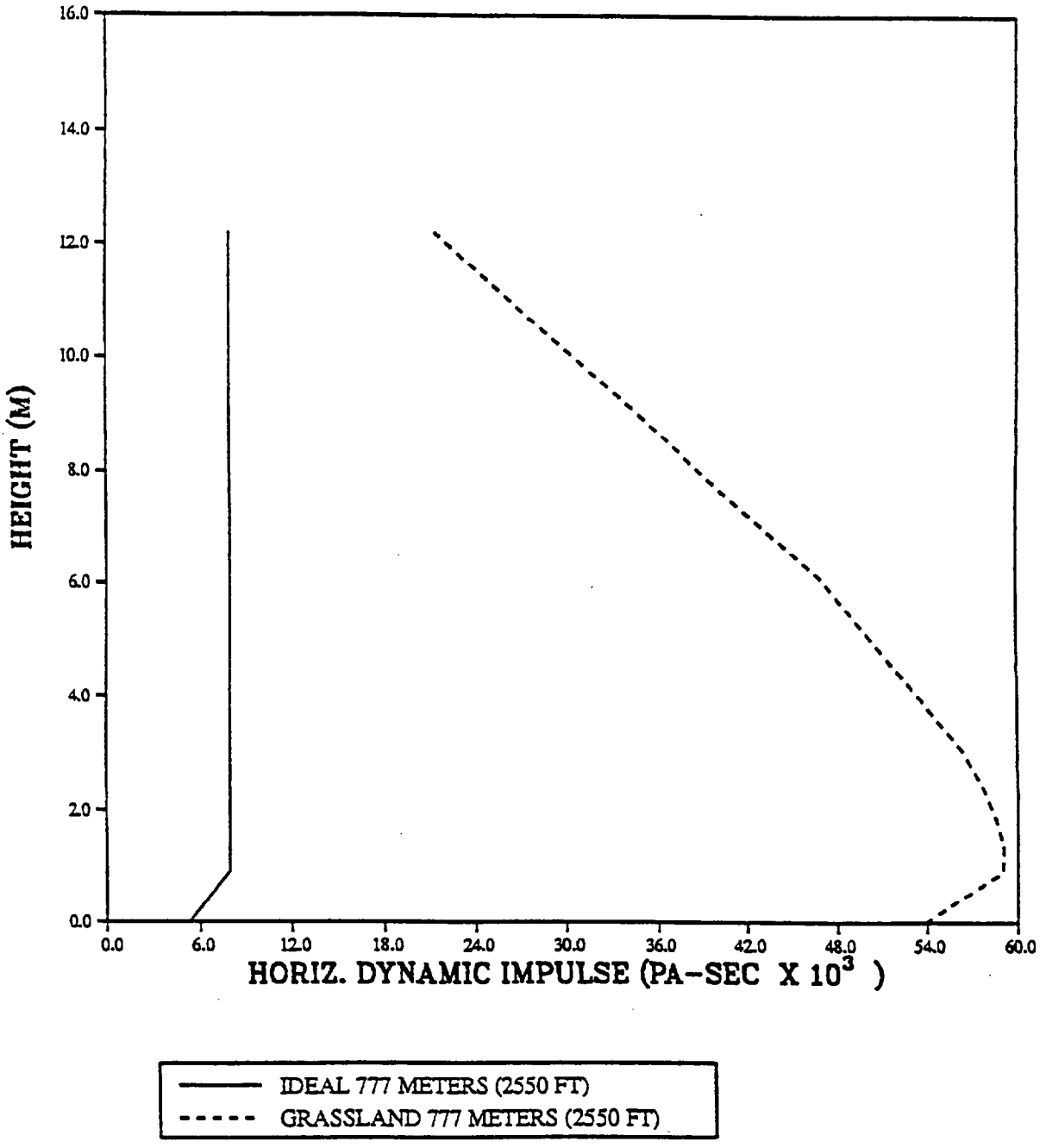

PRISCILLA
HORIZONTAL DYNAMIC PRESSURE IMPULSE
VERTICAL PROFILE (15 PSI OVERPRESSURE LEVEL)

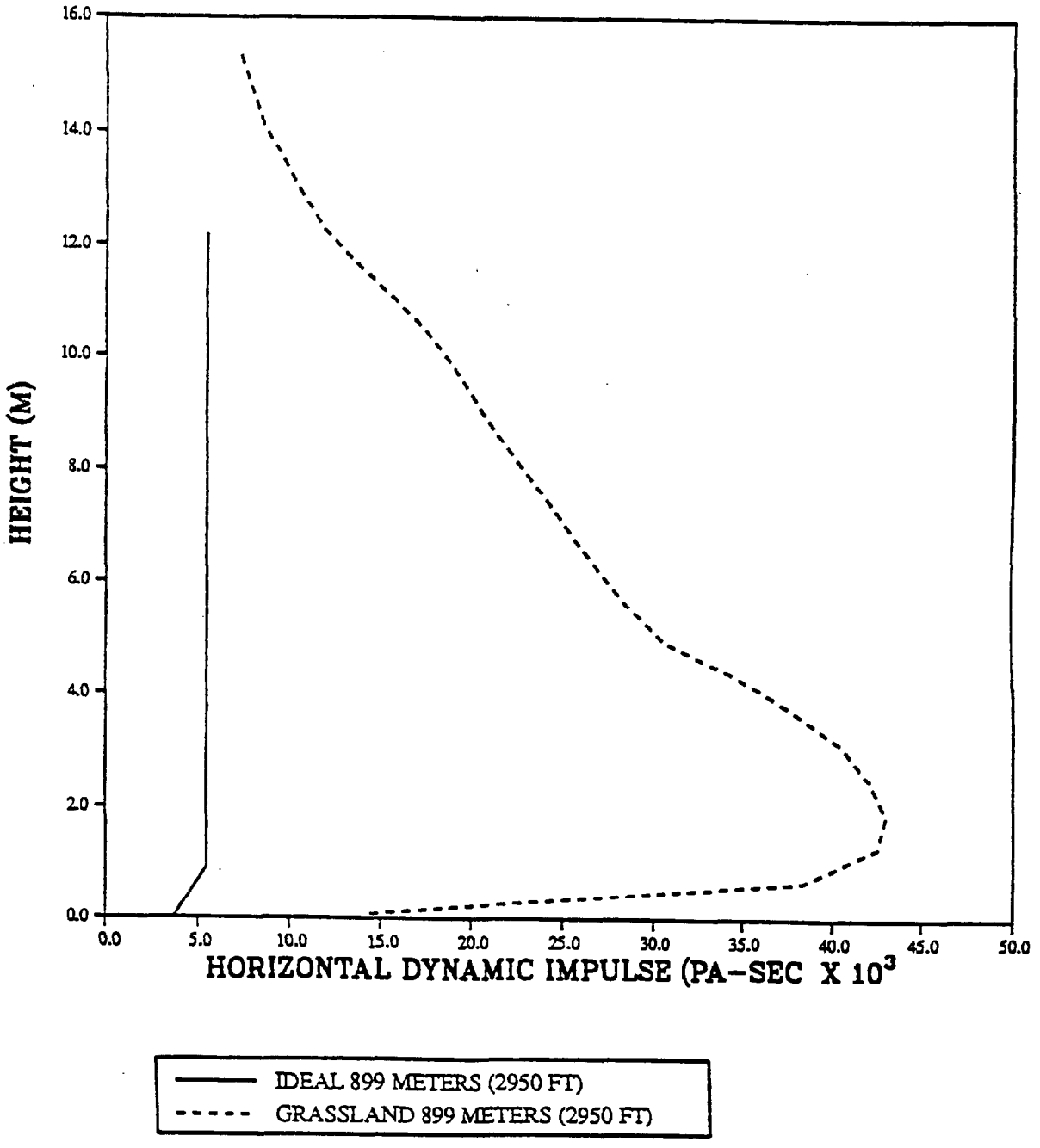

DESERT PRISCILLA
HORIZONTAL DYNAMIC PRESSURE IMPULSE
VERTICAL PROFILE (12 PSI OVERPRESSURE LEVEL)

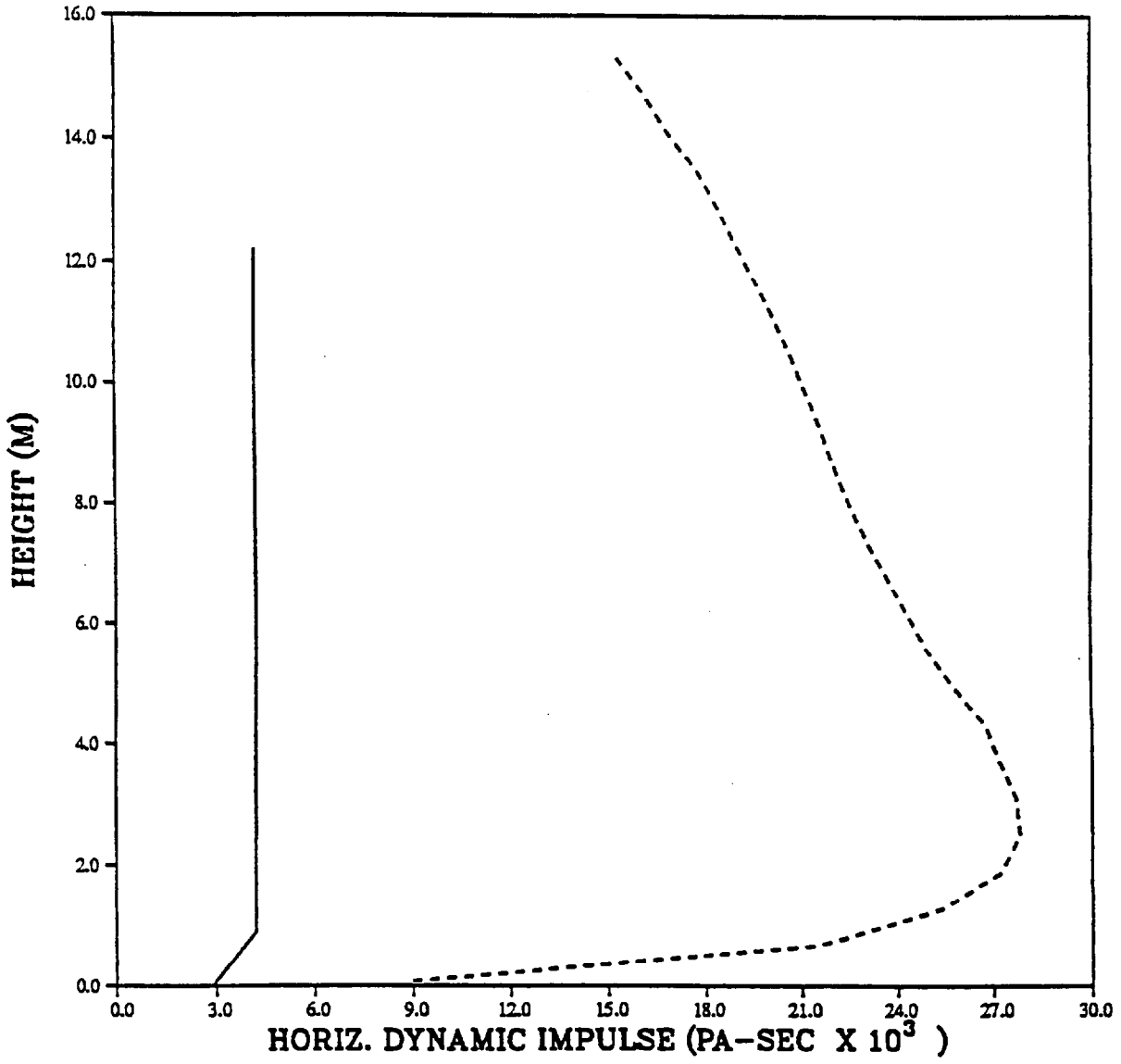

PRISCILLA
HORIZONTAL DYNAMIC PRESSURE IMPULSE
VERTICAL PROFILE (10 PSI OVERPRESSURE LEVEL)

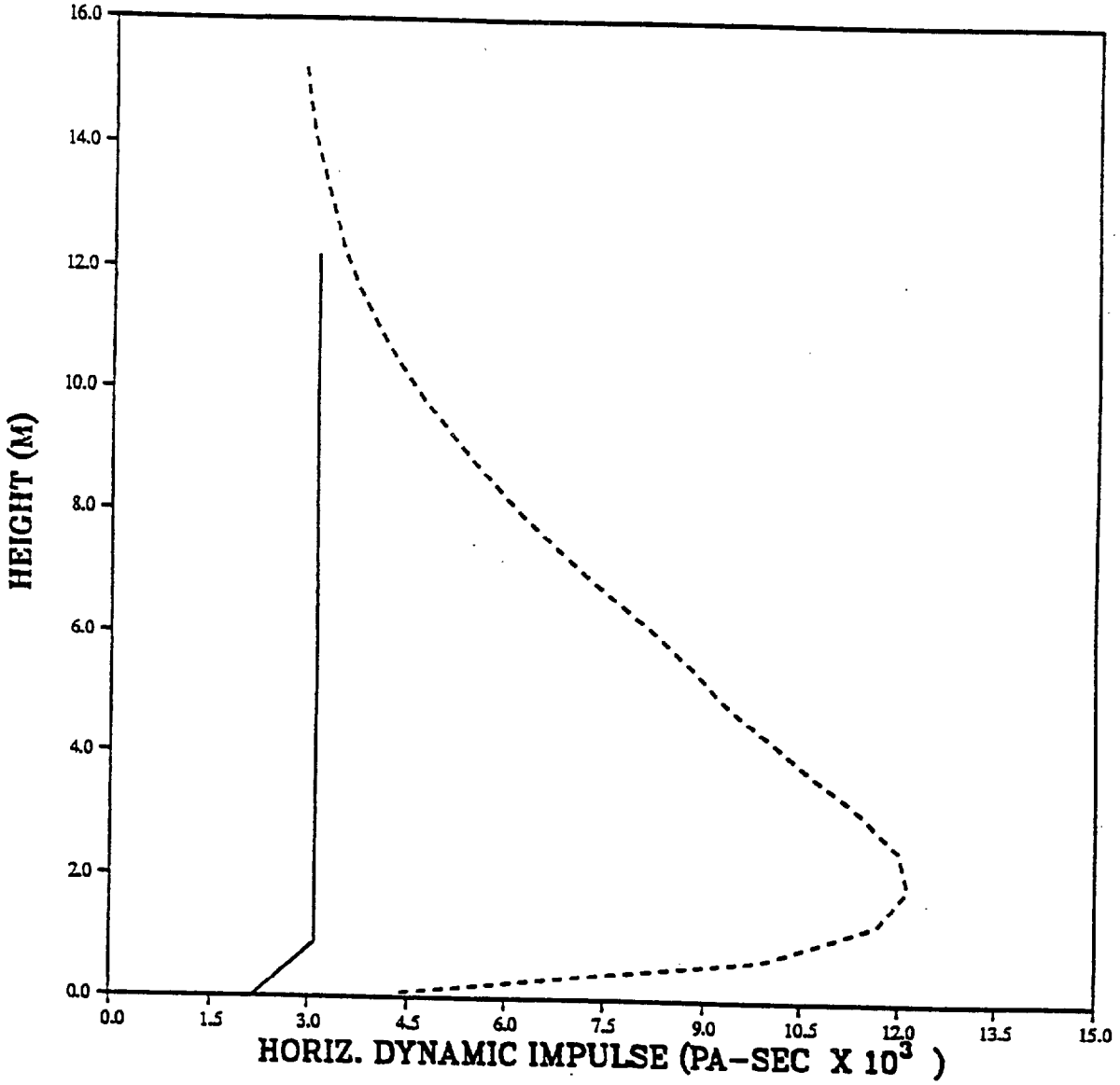

PRISCILLA
HORIZONTAL DYNAMIC PRESSURE IMPULSE
VERTICAL PROFILE (8 PSI OVERPRESSURE LEVEL)

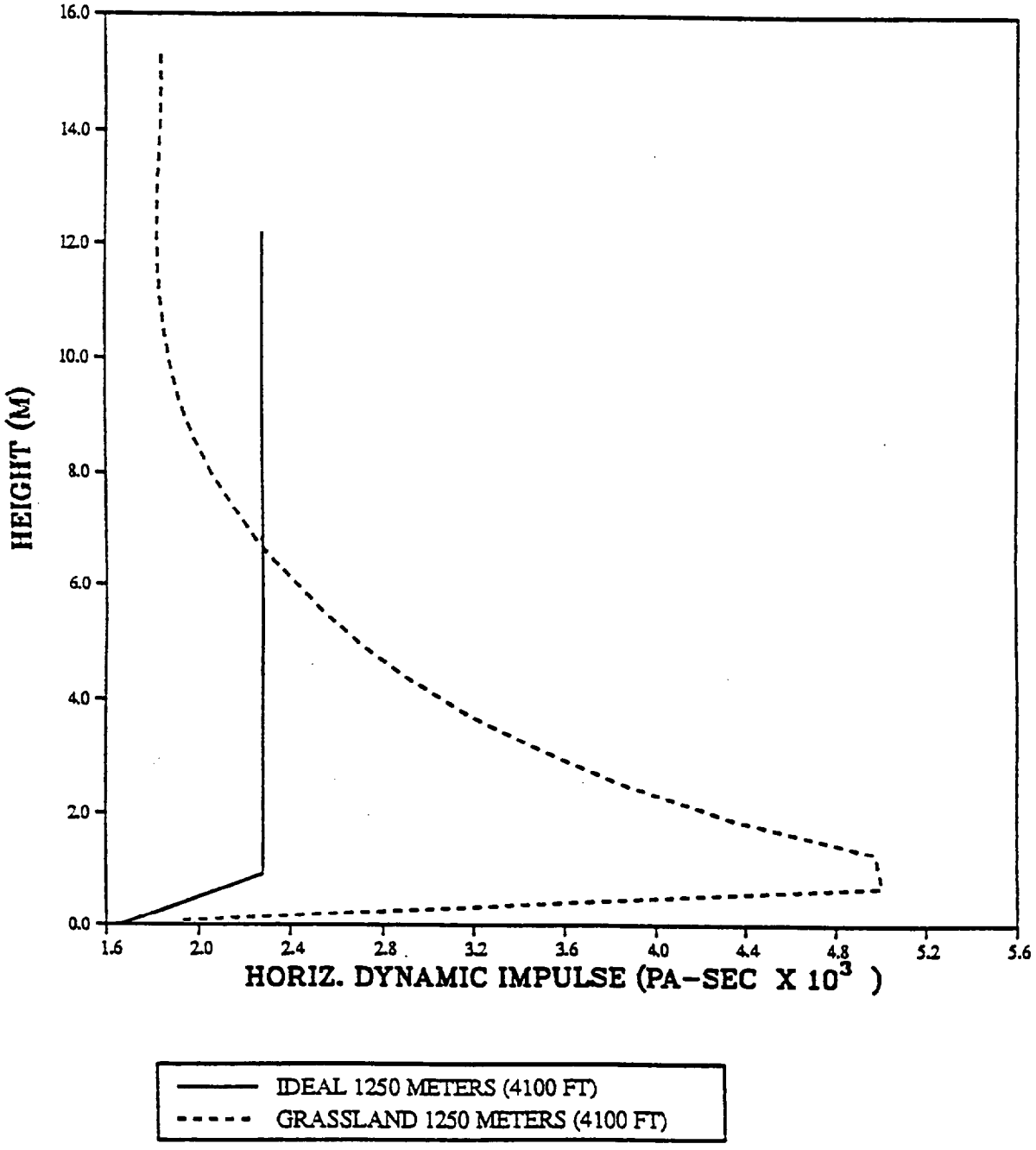

PRISCILLA
HORIZONTAL DYNAMIC PRESSURE IMPULSE
VERTICAL PROFILE (6 PSI OVERPRESSURE LEVEL)

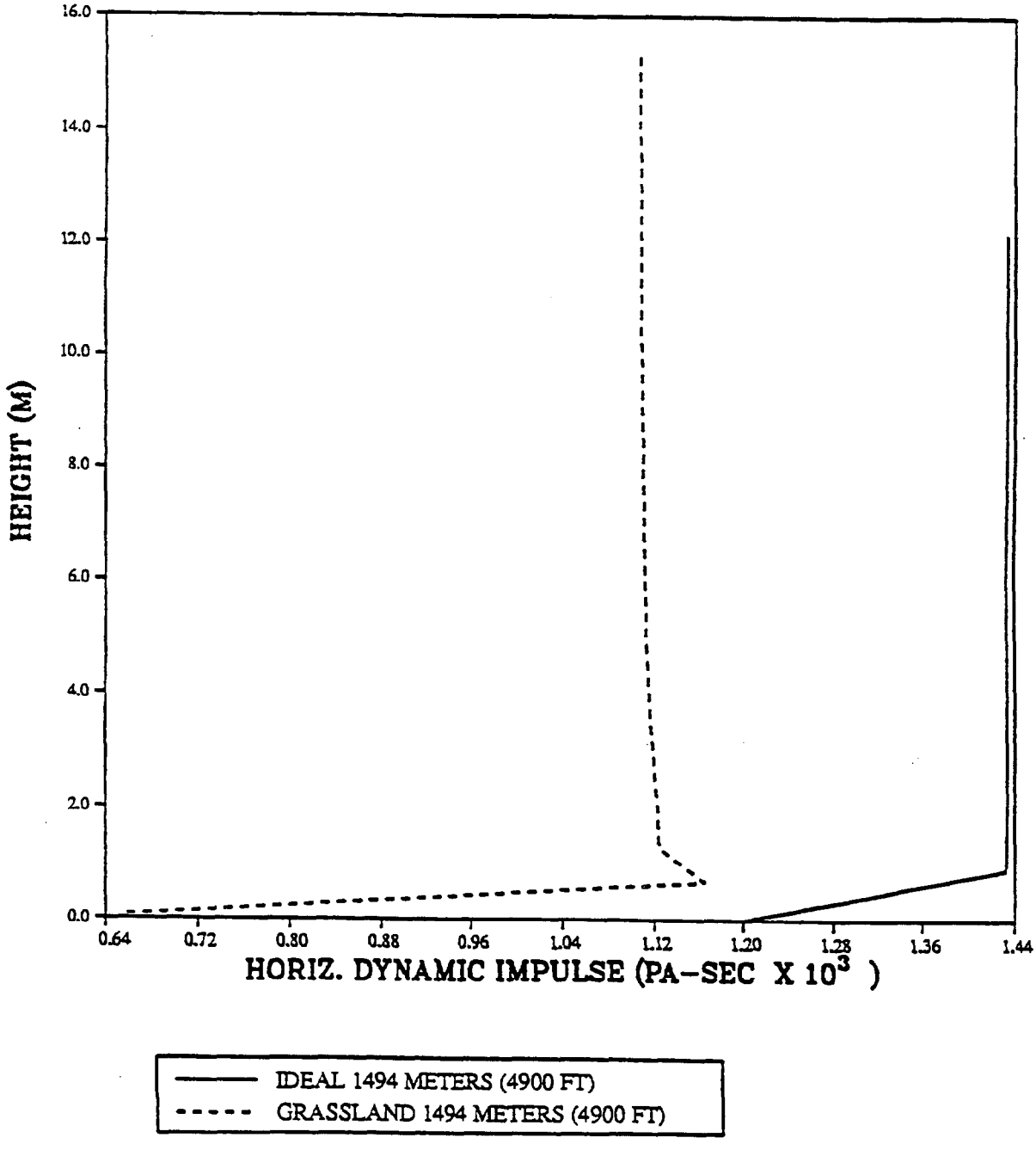

PRISCILLA
HORIZONTAL DYNAMIC PRESSURE IMPULSE
VERTICAL PROFILE (5 PSI OVERPRESSURE LEVEL)

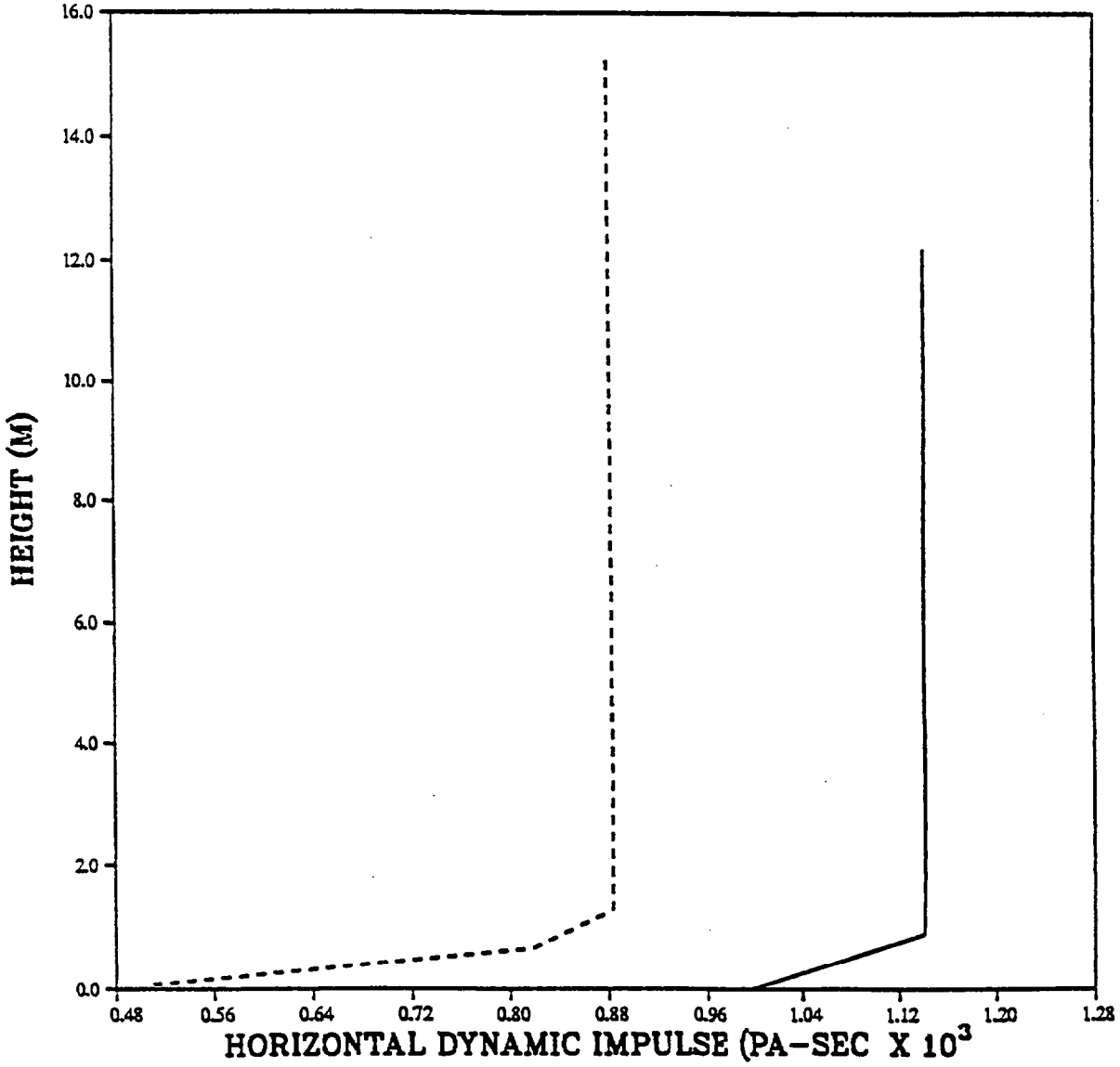

INTENTIONALLY LEFT BLANK.

APPENDIX D:

CONVERSION TABLE

Conversion factors for U.S. Customary to metric (SI) units of measurement

MULTIPLY → TO GET	BY	← BY DIVIDE
angstrom	1.000 000 X E -10	meters (m)
atmosphere (normal)	1.013 25 X E +2	kilo pascal (kPa)
bar	1.000 000 X E +2	kilo pascal (kPa)
barn	1.000 000 X E -28	meter ^{2} (m^2)
British thermal unit (thermochemical)	1.054 350 X E +3	joule (J)
calorie (thermochemical)	4.184 000	joule (J)
cal (thermochemical)/cm^2	4.184 000 X E -2	mega joule/m^2 (MJ/m^2)
curie	3.700 000 X E +1	* giga becquerel (GBq)
degree (angle)	1.745 329 X E -2	radian (rad)
degree Fahrenheit	$t_K = (t\,°f + 459.67)/1.8$	degree kelvin (K)
electron volt	1.602 19 X E -19	joule (J)
erg	1.000 000 X E -7	joule (J)
erg/second	1.000 000 X E -7	watt (W)
foot	3.048 000 X E -1	meter (m)
foot-pound-force	1.355 818	joule (J)
gallon (U.S. liquid)	3.785 412 X E -3	meter ^{3} (m^3)
inch	2.540 000 X E -2	meter (m)
jerk	1.000 000 X E +9	joule (J)
joule/kilogram (J/kg) (radiation dose absorbed)	1.000 000	Gray (Gy)
kilotons	4.183	terajoules
kip (1000 lbf)	4.448 222 X E +3	newton (N)
kip/inch ^{2} (ksi)	6.894 757 X E +3	kilo pascal (kPa)
ktap	1.000 000 X E +2	newton-second/m^2 ($N\text{-}s/m^2$)
micron	1.000 000 X E -6	meter (m)
mil	2.540 000 X E -5	meter (m)
mile (international)	1.609 344 X E +3	meter (m)
ounce	2.834 952 X E -2	kilogram (kg)
pound-force (lbs avoirdupois)	4.448 222	newton (N)
pound-force inch	1.129 848 X E -1	newton-meter (N•m)
pound-force/inch	1.751 268 X E +2	newton/meter (N/m)
pound-force/foot ^{2}	4.788 026 X E -2	kilo pascal (kPa)
pound-force/inch ^{2} (psi)	6.894 757	kilo pascal (kPa)
pound-mass (lbm avoirdupois)	4.535 924 X E -1	kilogram (kg)
pound-mass-foot ^{2} (moment of intertia)	4.214 011 X E -2	kilogram-meter ^{2} ($kg•m^2$)
pound-mass/foot ^{3}	1.601 846 X E +1	kilogram/meter ^{3} (kg/m^3)
rad (radiation dose absorbed)	1.000 000 X E -2	** Gray (Gy)
roentgen	2.579 760 X E -4	coulomb/kilogram (C/kg)
shake	1.000 000 X E -8	second (s)
slug	1.459 390 X E +1	kilogram (kg)
torr (mm HG, O°C)	1.333 22 X E -1	kilo pascal (kPa)

* The becquerel (Bq) is the SI unit of radioactivity; 1 Bq = 1 event/s.
** The Gray (GY) is the SI unit of absorbed radiation.

A more complete listing of conversions may be found in "Metric Practice Guide E 380-74," American Society for Testing and Materials.

INTENTIONALLY LEFT BLANK.

NO. OF COPIES	ORGANIZATION
2	ADMINISTRATOR ATTN DTIC DDA DEFENSE TECHNICAL INFO CTR CAMERON STATION ALEXANDRIA VA 22304-6145
1	DIRECTOR ATTN AMSRL OP SD TA US ARMY RESEARCH LAB 2800 POWDER MILL RD ADELPHI MD 20783-1145
3	DIRECTOR ATTN AMSRL OP SD TL US ARMY RESEARCH LAB 2800 POWDER MILL RD ADELPHI MD 20783-1145
1	DIRECTOR ATTN AMSRL OP SD TP US ARMY RESEARCH LAB 2800 POWDER MILL RD ADELPHI MD 20783-1145
	ABERDEEN PROVING GROUND
5	DIR USARL ATTN AMSRL OP AP L (305)

NO. OF COPIES	ORGANIZATION
2	HQDA ATTN SARD TR MS K KOMINOS DR R CHAIT PENTAGON WASHINGTON DC 20310-0103
2	HQDA ATTN SARD TT MS C NASH DR F MILTON PENTAGON WASHINGTON DC 20310-0103
1	DIR OF DEFNS RSRCH AND ENGRG ATTN DD TWP WASHINGTON DC 20301
1	ASST SECRETARY OF DEFNS ATTN DOCUMENT CONTROL ATOMIC ENERGY WASHINGTON DC 20301
1	CHAIRMAN ATTN J 5 R&D DIV JOINT CHIEFS OF STAFF WASHINGTON DC 20301
2	DA DCSOPS ATTN TECH LIB DIR OF CHEM & NUC OPS WASHINGTON DC 20310
1	EUROPEAN RSRCH OFC ATTN DR R REICHENBACH USARDSG UK PSC 802 BOX 15 FPO AE 09499-1500
1	DIR ATTN TECH LIB ADVNCD RSRCH PROJ AGCY 3701 N FAIRFAX DR ARLINGTON VA 22203-1714
2	CDR ATTN AMSEL RD AMSEL RO TPPO P US ARMY CECOM FT MONMOUTH NJ 07703-5301
1	MIT ATTN TECH LIB CAMBRIDGE MA 02139

NO. OF COPIES	ORGANIZATION
2	DIR ATTN PUBLIC RELATIONS OFC TECH LIB FED EMERG MGMT AGCY WASHINGTON DC 20472
1	CHAIRMAN DOD EXPLOSIVES SAFETY BOARD ROOM 856 C HOFFMAN BLDG 1 2461 EISENHOWER AVE ALEXANDRIA VA 22331-0600
1	DIR ATTN DT 2 WPNS & SYS DIV DEFNS INTLLGNC AGCY WASHINGTON DC 20301
8	DIR ATTN CSTI TECH LIB DDIR DFSP NANS OPNA SPSD SPTD DFTD DEFNS NUCLEAR AGENCY WASHINGTON DC 20305
3	CDR ATTN FCPR FCTMOF NMHE FIELD COMMAND DNA KIRTLAND ARB NM 87115
10	CIA ATTN GE 47 HQ DIR DB STANDARD WASHINGTON DC 20505
2	CDR ATTN AMSNA D DR D SIELING STRNC UE J CALLIGEROS US ARMY NRDEC NATICK MA 01762
1	CDR ATTN ASQNC ELC IS L R MYER CTR US ARMY CECOM R&D TECH LIB FT MONMOUTH NJ 07703-5000

NO. OF COPIES	ORGANIZATION
1	CDR ATTN SMCAR FSM W BARBER BLDG 94 US ARMY ARDEC PCTNY ARSNL NJ 07806-5000
1	DIR ATTN AIAMS YDL US ARMY MISSILE & SPACE INTLLGNC CTR REDSTONE ARSNL AL 35898-5500
1	DIR ATTN AMSMR ATL US ARMY RESEARCH LAB WATERTOWN MA 02172-0001
1	CDR ATTN HNDED FD US ARMY ENGINEER DIV PO BOX 1500 HUNTSVILLE AL 35807
1	CDR ATTN CESWF PM J US ARMY CORPS OF ENGRS FT WORTH DISTRICT PO BOX 17300 FT WORTH TX 76102-0300
1	CDR ATTN SLCRO D US ARMY RESEARCH OFFICE PO BOX 12211 RSCH TRI PK NC 27709-2211
1	DIR ATTN ATRC RPR RADDA HQ TRAC RPD FT MONROE VA 23651-5143
1	DIR ATTN ATRC WC KIRBY TRAC WSMR WSMR NM 88002-5502
1	CDR ATTN STEWS NED DR MEASON US ARMY WSMR WSMR NM 88002-5158

NO. OF COPIES	ORGANIZATION
2	CHIEF OF NAVAL OPERATIONS ATTN OP 03EG OP 985F DEPT OF THE NAVY WASHINGTON DC 20350
1	CDR ATTN RSRCH AND DATA BRANCH US ARMY NGIC 220 7TH STREET NE CHARLOTTESVILLE VA 22901-5396
1	DIR ATTN ATRC L MR CAMERON US ARMY TRAC FT LEE FORT LEE VA 23801-6140
2	CDR ATTN CSSD H MPL TECH LIB CSSD H XM DR DAVIES US ARMY STRATEGIC DEFENSE COMMAND PO BOX 1500 HUNTSVILLE AL 35807
3	CDR ATTN CEWES SS R J WATT CEWES SE R J INGRAM CEWES TL TECH LIBRARY US ARMY CORPS OF ENGINEERS WATERWAYS EXPERIMENT STATION PO BOX 631 VICKSBURG MS 39180-0631
3	CDR US ARMY NUCLEAR & CHEMICAL AGENCY 7150 HELLER LOOP, SUITE 101 SPRINGFIELD VA 22150-3198
1	DIR ATTN ATRC TRAC FLVN FORT LEAVENWORTH KS 66027-5200
1	CDR ATTN PME 117 21A NAVAL ELECTRONIC SYSTEMS COMMAND WASHINGTON DC 20360
2	OFFICE OF NAVAL RESEARCH ATTN DR A FAULSTICK CODE 23 800 N QUINCY STREET ARLINGTON VA 22217

NO. OF COPIES	ORGANIZATION
1	CDR ATTN CODE SEA 62R NAVAL SEA SYSTEMS COMMAND DEPARTMENT OF THE NAVY WASHINGTON DC 20362-5101
1	COMMANDING OFFICER CODE L51 ATTN J TANCRETO NAVAL CIVIL ENGINEERING LABORATORY PORT HUENEME CA 93043-5003
1	CIVIL ENGINEERING LABORATORY ATTN TECHNICAL LIBRARY CODE L31 NAVAL CONSTRUCTION BATTALION CTR PORT HUENEME CA 93041
1	CDR ATTN CODE E23 LIBRARY NAVAL SURFACE WARFARE CENTER DAHLGREN VA 22448-5000
1	WHITE OAK WARFARE CTR DETACHMENT ATTN CODE E232 TECHNICAL LIBRARY 10901 NEW HAMPSHIRE AVENUE SILVER SPRING MD 20903-5000
1	CDR ATTN DOCUMENT CONTROL NAVAL WEAPONS EVALUATION FAC KIRTLAND AFB NM 87117
1	AEDC ATTN R MCAMIS MAIL STOP 980 ARNOLD AFB TN 37389
1	OLAC PL TSTL ATTN D SHIPLETT EDWARDS AFB CA 93523-5000
2	AIR FORCE ARMAMENT LABORATORY ATTN AFATL DOIL AFATL DLYV EGLIN AFB FL 32541-5000
3	PHILLIPS LABORATORY (AFWL) ATTN NTE NTED NTES KIRTLAND AFB NM 87117-6008

NO. OF COPIES	ORGANIZATION
1	AFIT ATTN TECHNICAL LIBRARY BLDG 640 B WRIGHT PATTERSON AFB OH 45433
1	FTD NIIS WRIGHT PATTERSON AFB OH 45433
4	DIR ATTN R GUENZLER MS 3505 R HOLMAN MS-3510 R A BERRY W C REED IDAHO NATIONAL ENGINEERING LABORATORY EG&G IDAHO INC PO BOX 8757 BWI AIRPORT BALTIMORE MD 21240
3	KAMAN SCIENCES CORPORATION ATTN LIBRARY P A ELLIS F H SHELTON P O BOX 7463 COLORADO SPRINGS CO 80933-7463
2	DIR ATTN TH DOWLER MS F602 DOC CONTROL FOR REPORTS LIBRARY LOS ALAMOS NATIONAL LABORATORY PO BOX 1663 LOS ALAMOS NM 87545
1	DIR ATTN DOC CONTROL FOR TECH LIB SANDIA NATIONAL LABORATORIES LIVERMORE LABORATORY P O BOX 969 LIVERMORE CA 94550
1	DIR ATTN TECHNICAL LIBRARY NASA LANGLEY RESEARCH CENTER HAMPTON VA 23665
1	ADA TECHNOLOGIES INC ATTN JAMES R BUTZ HONEYWELL CENTER SUITE 110 304 INVERNESS WAY SOUTH ENGLEWOOD CO 80112

NO. OF COPIES ORGANIZATION

1 ALLIANT TECHSYSTEMS INC
ATTN ROGER A RAUSCH MN48 3700
7225 NORTHLAND DRIVE
BROOKLYN PARK MN 55428

1 AEROSPACE CORPORATION
ATTN TECH INFO SERVICES
P O BOX 92957
LOS ANGELES CA 90009

1 THE BOEING COMPANY
ATTN AEROSPACE LIBRARY
P O BOX 3707
SEATTLE WA 98124

1 CALIFORNIA RES & TECH INC
ATTN M ROSENBLATT
20943 DEVONSHIRE STREET
CHATSWORTH CA 91311

1 DYNAMICS TECHNOLOGY INC
ATTN D T HOVE
G P MASON
21311 HAWTHORNE BLVD SUITE 300
TORRANCE CA 90503

1 EATON CORPORATION
ATTN J WADA
DEFENSE VALVE & ACTUATOR DIV
2338 ALASKA AVE
EL SEGUNDO CA 90245-4896

5 DIR
ATTN DOC CONTROL 3141
C CAMERON DIV 6215
A CHABAI DIV 7112
D GARDNER DIV 1421
J MCGLAUN DIV 1541
SANDIA NATIONAL LABORATORIES
P O BOX 5800
ALBUQUERQUE NM 87185-5800

1 BLACK & VEATCH
ENGINEERS - ARCHITECTS
ATTN H D LAVERENTZ
1500 MEADOW LAKE PARKWAY
KANSAS CITY MO 64114

NO. OF COPIES ORGANIZATION

1 DIRECTOR
ATTN DR T HOLTZ MS 202-14
NASA-AMES RESEARCH CENTER
APPLIED COMPUTATIONAL AERO BRANCH
MOFFETT FIELD CA 94035

2 APPLIED RESEARCH ASSOCIATES INC
ATTN J KEEFER
N H ETHRIDGE
P O BOX 548
ABERDEEN MD 21001

1 CARPENTER RESEARCH CORPORATION
ATTN H JERRY CARPENTER
27520 HAWTHORNE BLVD SUITE 263
ROLLING HILLS ESTATES CA 90274

1 GOODYEAR CORPORATION
ATTN R M BROWN BLDG 1
SHELTER ENGINEERING
LITCHFIELD PARK AZ 85340

2 FMC CORPORATION
ATTN J DROTLEFF
C KREBS MDP95
ADVANCED SYSTEMS CENTER
BOX 58123
2890 DE LA CRUZ BLVD
SANTA CLARA CA 95052

1 SVERDRUP TECHNOLOGY INC
ATTN B D HEIKKINEN
SVERDRUP CORPORATION AEDC
MS 900
ARNOLD AFB TN 37389-9998

1 KTECH CORPORATION
ATTN DR E GAFFNEY
901 PENNSYLVANIA AVE NE
ALBUQUERQUE NM 87111

4 KAMAN AVIDYNE
ATTN R RUETENIK (2 CYS)
S CRISCIONE
R MILLIGAN
83 SECOND AVENUE
NORTHWEST INDUSTRIAL PARK
BURLINGTON MA 01830

NO. OF
COPIES ORGANIZATION

2 KAMAN SCIENCES CORPORATION
ATTN DASIAC (2 CYS)
P O DRAWER 1479
816 STATE STREET
SANTA BARBARA CA 93102-1479

1 LOCKHEED MISSILES & SPACE CO
ATTN J J MURPHY
DEPT 81 11 BLDG 154
P O BOX 504
SUNNYVALE CA 94086

1 ORLANDO TECHNOLOGY INC
ATTN D MATUSKA
60 SECOND STREET BLDG 5
SHALIMAR FL 32579

2 THE RALPH M PARSONS COMPANY
ATTN T M JACKSON
LB TS PROJECT MANAGER
100 WEST WALNUT STREET
PASADENA CA 91124

1 SAIC
ATTN N SINHA
501 OFFICE CENTER DRIVE APT 420
FT WASHINGTON PA 19034 3211

1 SAIC
ATTN J GUEST
2301 YALE BLVD SE
SUITE E
ALBUQUERQUE NM 87106

2 S CUBED
A DIVISION OF MAXWELL LABS INC
ATTN C E NEEDHAM
L KENNEDY
2501 YALE BLVD SE
ALBUQUERQUE NM 87106

1 TRW
BALLISTIC MISSILE DIVISION
ATTN H KORMAN
MAIL STATION 526 614
P O BOX 1310
SAN BERNADINO CA 92402

1 THERMAL SCIENCE INC
ATTN R FELDMAN
2200 CASSENS DR
ST LOUIS MO 63026

NO. OF
COPIES ORGANIZATION

2 MCDONNELL DOUGLAS ASTRNTCS CORP
ATTN ROBERT W HALPRIN
K A HEINLY
5301 BOLSA AVENUE
HUNTINGTON BEACH CA 92647

1 MDA ENGINEERING INC
ATTN DR DALE ANDERSON
500 EAST BORDER STREET
SUITE 401
ARLINGTON TX 07601

2 PHYSICS INTERNATIONAL CORPORATION
P O BOX 5010
SAN LEANDRO CA 94577-0599

1 R&D ASSOCIATES
ATTN G P GANONG
P O BOX 9377
ALBUQUERQUE NM 87119

1 SCIENCE CENTER
ROCKWELL INTERNATIONAL CORPORATION
ATTN DR S CHAKRAVARTHY
DR D OTA
1049 CAMINO DOS RIOS
THOUSAND OAKS CA 91358

3 S CUBED
A DIVISION OF MAXWELL LABS INC
ATTN TECHNICAL LIBRARY
R DUFF
K PYATT
P O BOX 1620
LA JOLLA CA 92037-1620

1 SUNBURST RECOVERY INC
ATTN DR C YOUNG
P O BOX 2129
STEAMBOAT SPRINGS CO 80477

1 SVERDRUP TECHNOLOGY INC
ATTN R F STARR
P O BOX 884
TULLAHOMA TN 37388

1 SRI INTERNATIONAL
ATTN DR G R ABRAHAMSON
DR J GRAN
DR B HOLMES
333 RAVENWOOD AVENUE
MENLO PARK CA 94025

NO. OF COPIES ORGANIZATION

1 BATTELLE
TWSTIAC
505 KING AVENUE
COLUMBUS OH 43201-2693

2 THINKING MACHINES CORPORATION
ATTN G SABOT
R FERREL
245 FIRST STREET
CAMBRIDGE MA 02142-1264

1 CALIFORNIA INSTITUTE OF TECHNOLOGY
ATTN T J AHRENS
1201 E CALIFORNIA BLVD
PASADENA CA 91109

1 UNIVERSITY OF MINNESOTA
ARMY OF HIGH PERF COMP RES CTR
ATTN DR TAYFUN E TEZDUYAR
1100 WASHINGTON AVE SOUTH
MINNEAPOLIS MN 55415

2 CDR
ATTN SSCNC YSD J ROACH
SSCNC WST A MURPHY
US ARMY NRDEC
KANSAS STREET
NATICK MA 10760-5018

3 SOUTHWEST RESEARCH INSTITUTE
ATTN DR C ANDERSON
S MULLIN
A B WENZEL
P O DRAWER 28255
SAN ANTONIO TX 78228-0255

1 STATE UNIVERSITY OF NEW YORK
MECHANICAL & AEROSPACE ENGNRNG
ATTN DR PEYMAN GIVI
BUFFALO NY 14260

2 DENVER RESEARCH INSTITUTE
ATTN J WISOTSKI
TECHNICAL LIBRARY
P O BOX 10758
DENVER CO 80210

2 UNIVERSITY OF MARYLAND
INSTITUTE FOR ADV COMPUTER STUDIES
ATTN L DAVIS
G SOBIESKI
COLLEGE PARK MD 20742

NO. OF COPIES ORGANIZATION

1 NORTHROP UNIVERSITY
ATTN DR F B SAFFORD
5800 W ARBOR VITAE STREET
LOS ANGELES CA 90045

1 STANFORD UNIVERSITY
ATTN DR D BERSHADER
DURAND LABORATORY
STANFORD CA 94305

ABERDEEN PROVING GROUND

1 CDR USATACOM
ATTN AMSTE-TE-F (L TELETSKI)

1 CDR USATHAMA
ATTN AMSTH-TE

1 CDR USACSTA
ATTN STEC-LI

3 DIR USARL
ATTN AMSRL-SL-CM (BLDG E3331)
AMSRL-WT-NC
R LOTTERO (2 CP)

INTENTIONALLY LEFT BLANK.